Introducing controllable 3D features into dense collagen constructs for tissue engineering applications

Thesis submitted by

Tijna Alekseeva

For the degree of

Doctor of Philosophy

UCL

2011

I, Tijna Alekseeva confirm that the work presented in this thesis is my own. Where information has been derived from other sources, I confirm that this has been indicated in the thesis.'

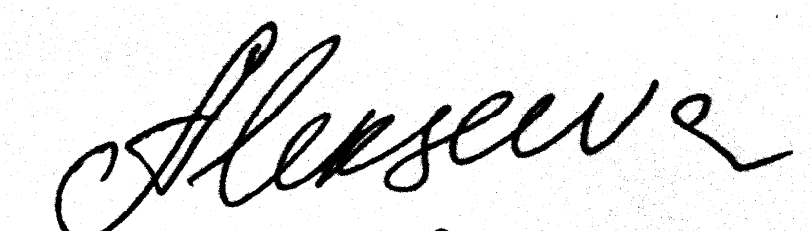

Acknowledgments

It has been a journey. A journey of discovery both scientific and self. And I would like to express my gratitude to all who were there for me during this time.

My parents, who like the North Star, were there for me always, a reassuring presence.

My supervisor, Professor Robert A. Brown, my guide and mentor, who suffered through the first, unintelligible draft and did not lose patience.

My fellow travellers on this road, who in time became my good friends, Dr. Chauvonne Thrope, Dr. Michelle Korda, Dr. Hedeer Javad, Ms. Rebecca Porter.

Thank you to Professor John Priestley, who was always helpful with particularly difficult spelling of English words and always very supportive and to my colleague, who became my best friend, Dr. Umber Cheema. They believed in me even when I did not.

I would like to say thank you to my little sister. It has been difficult time for both of us, but I could not have done it without her support.

I would like to dedicate this work to my uncle. Even in the darkest of times he remained strong and I hope that our conversations helped him in his struggle.

Abstract

Plastic compression of collagen is based on unidirectional expulsion of fluid from hydrated collagen gel. The process results in dense collagen sheet, with higher density of collagen at the fluid leaving surface (FLS) than non-FLS. Compression process is completely cell-independent and at the same time cell-friendly. However, engineered tissues should replicate not only components of tissues *in vivo* (extracellular matrix and cells) but also their complex micro-architecture. Therefore the aim of this work was to develop collagen-based scaffolds with controllable micro-architecture for biomedical and tissue engineering applications using plastic compression (PC) of collagen. The objectives of this project were: i. to test formation of progressively opening channels in the PC collagen, ii. to investigate stable and predictable PC collagen patterning, iii. to adapt PC method in a upward-flow system as a route to process automation, iv. to investigate formation of channels using in layered PC collagen constructs. Two approaches were used in this work.

Firstly, internal channels were introduced using lost fibre approach, where soluble glass fibres are incorporated in the scaffold and leave channel when dissolved. Shape and potentially progression of the channels' opening is controlled by the shape of the template. The shape of the fibres was altered from cylindrical to conical in a controlled manner and incorporated into the PC constructs, resulting in conically-shaped channels, giving predictable internal 3D structures.

The second approach relied on formation of dense collagen zone at the fluid leaving surface of the compressed collagen constructs. Formation of the densely packed collagen zone at the fluid leaving surface is essential for stable and faithful pattern formation in the process of micro-moulding. This finding has been applied in a novel upward-flow compression system to create channels using a 'roofing' technique. 'Roof' is formed by a compression of a new collagen gel on top of a patterned one; process results in open lumen channels. This appears to be due to a combination of the small dimension of the grooves in the base layer and viscosity of the collagen in the upper layer.

This work demonstrates a new, previously unknown level of subtlety by which collagen fibrils can be packed and aggregated due to directional fluid flow. The outcome of this work is important for understanding pattern formation in PC collagen *in vitro* and potentially tissue morphogenesis *in vivo.* It also introduces new generation of implantable living tissue equivalents with complex micro-architecture. The multi-well compression technique has already been implemented in semi-automative working station for biomedical applications.

Table of contents

List of tables

Chapter1

Chapter 5

Chapter 6

List of figures

Chapter 1.

Chapter 3

Fig 1. Schematic illustration of the dissolution dynamics of the conically shaped fibre. Patterned surface indicates diameter of the fibre at time 0, clear field is the diameter of the fibre at time n. As fibre dissolves, thinner end will disappear faster relative to the thicker end. That will potentially provide direction of cell ingrowth in the channel.

Fig 2. Schematic illustration of conical fibres fabrication process. Fibres, fixed onto a carrier ring, were immersed into PBS. The level of buffer was decreased stepwise over 6 hours to create a tapering cross section towards the base of the fibre.

Fig. 3 Construct assembly. (a)Schematic diagram showing assembly of the plastic compressed collagen construct with incorporated fibres. Neutralized collagen is set on top of the preformed fibres for 30 min and then compressed under load to produce dense construct with fibres, incorporated in the matrix. Plastic fibre-bearing ring (b) is inserted into a stainless-steel mould and filled with collagen solution(c). Set collagen gel is transferred onto blotting elements and compressed (d, loading not shown). Process results in a thin, tissue-like construct with incorporated conical glass fibres (e). (f) – histological image of the construct sectioned in transverse plane showing channel left by the fibre.

Fig. 4 Graph illustrating loss in fibre diameter along the fibre length(mm). Primary vertical axis - mean diameter loss over the length of phosphate based glass fibres after treatment in percent ± standard deviation (n=20). Measurements were taken at each mm over the length of the fibre, 3 mm correspond to 1 hr exposure to PBS. Note the linear fall in diameter of 25% over ~ 20mm of cumulative fibre length. * p<0.001, start and end point of treatment. Absolute diameter measurements for one specimen fibre are plotted on the secondary vertical axis and confirm diameter loss over the fibre length.

Fig. 5 (a) Reconstructed SEM image of conically shaped phosphate fibres. Fibres were fixed on a plastic ring and submersed in to PBS. Level of buffer was gradually reduced over 6 hours giving conical shaped fibres. Arrow heads indicate individual fibres, arrow shows the direction of diameter reduction. (b) SEM image of plastic compressed collagen construct with incorporated conical glass fibre. Collagen gel was set with preformed conical fibres and compressed under load. Shape of the channel is dictated by the shape of the fibre.

Chapter 4

Fig. 1 SEM image of the PC collagen surface with the impression of the nylon mesh which was used as the part of the compression process. Clear negative image of the interwoven fibres is visible (double arrow).

Fig. 2 Schematic illustration of the four experimental designs used. Simultaneous patterning of the FLS (a), the template (strip of glass fibres) is placed between the gel and absorbent prior to compression, and nonFLS (b), where glass fibres are placed on top of the gel prior to compression. Consecutive patterning, where

the gel is pre-compressed for 2.5 min and pattern is either pressed into the formed FLS (partFLS) (c), or non FLS (part nonFLS) (d) for further 2.5 min.

Fig. 3 Graphs of (a) average dimensions (width and depth) of the grooves on the surface of PC collagen constructs introduced into the FLS throughout compression, into the FLS following partial compression, into the nonFLS throughout compression and into the nonFLS following partial compression. (b) – plotted patterning coefficients (width:depth ratio) for the same experimental treatments as in (a). * - $p<0.05$ compared to FLS and part FLS, ** - $p<0.05$ compared to FLS, part FLS and nonFLS.

Fig. 4 Representative SEM images of the PC collagen constructs. (a) – surface of the construct (left) and profile of the grooves (right) on the FLS; (b) same on the nonFLS (nFLS); (c) – FLS of the partially compressed gel (partFLS); (d) – nonFLS of the partially compressed collagen (partnFLS).

Fig. 5 Representative histological images of the PC collagen constructs with patterns pressed into the FLS (a), non FLS (b), FLS of the partially compressed gel (part FLS, c) and non FLS of the partially compressed gel (part nFLS, d). Sections were stained with Sirius Red. Arrows indicate grooves, arrow heads indicate the fluid leaving surface. Insert – higher magnification of the highlighted region.

Fig. 6. Patterning coefficient of the topological features (grooves) imprinted into the FLS of acellular and cell-seeded PC constructs as an indicator of groove stability after long-term (14 days) culture. Measurements were taken at days 0, 7 and 14 *in vitro*. Topological features introduced onto the FLS were permanent and stable under culture conditions with and without resident cell remodelling of the matrix.

Fig. 7. Representative microphotographs of the PC collagen, seeded with human limbal fibroblasts, with grooves, introduced onto the fluid leaving surface (FLS), taken after 1(a) and 14 (b) days of culture. Insert – higher magnification of the highlighted region.

Fig.8 Diagram, showing proposed mechanism of pattern formation on the non-FLS. Template glass fibres placed on the gel and load applied initiating fluid flow in the direction of FLS. Fibres are initially fully immersed in the non-FLS, causing stretching of outer collagen film under the template. After template is removed, non-deformed, elastic collagen film between the pattern is released and cause pattern deformation, resulting in shallow grooves.

Fig.9 Diagram, showing proposed mechanism of pattern formation on the FLS. Template fibres are placed at the FLS of the gel, load applied and fluid flow initiated. Accumulation of collagen fibres at the FLS causes moulding of collagen around the template. Accumulation of dense collagen layer around the template cause permanent deformation of the patterned FLS even after template is removed.

Chapter 5

Fig. 1 Original method of plastic compression (PC). (a) Gels (pink), set in the double-pocket rectangular moulds (mould is seen in the background), were transferred onto the blotting elements (filter paper, stainless steel mesh) between two layers of nylon mesh. (b) Gels were then covered by the glass slide and loaded with weight for 5 minutes. (c) Process resulted in formation of the dense collagen sheet (dashed outline, construct is resting on a supportive nylon mesh) that could be cultured as a sheet or spiralled along its long axis to give a rolled construct

Fig. 2 Modified method – multi-well plastic compression (M-PC). (a) Standard tissue-culture grade 12 well-plate base served as a mould for the collagen gel casting. To ensure uniform compression, 12 holes have been made in the cover of the plate (arrows) to guide the absorbing plungers. This was replaced with purpose-made guiding plate indicated by an arrowhead (insert). (b) Spirally wound rolls (arrows) of absorbent paper were used as blotting elements and made using custom-build paper rolling machine. Assembled plungers are shown on the insert (arrows). (c) Gels (arrows) were set in the wells of the 12 well-plate and plungers (arrowheads) placed on the gels using guiding plate. (d) Depending on the number of simultaneously compressed gels, appropriate weight was applied. (e) After compression is completed, liquid is contained in the paper rolls (arrows), which are removed. (f) Process resulted in uniform dense collagen sheets in the respective wells (arrows) that can be cultured if required without further manipulations.

Fig. 3 Dynamics of fluid loss from the gels of 5.3 (a), 7.9 (b), 10.6 (c) and 13 (d) mm initial height during the first 5 minutes of the of plastic compression process. Fluid loss from the gels at each minute of the process is presented in percent of initial weight. *-statistically significant difference compared to the previous time point ($p<0.05$). Arrows indicate characteristic 'jumps' in values noted for 7.9 and 10.6 mm gels.

Fig.4 Effect of the initial height of the gel (5.3, 7.9, 10.6 and 13 mm) on fluid loss (in % of initial weight) during the first 5 minutes of plastic compression process. *-significant difference between gel heights at each time point ($p<0.05$).

Fig. 5 Change in the rate of fluid loss from the gels of 5.3 (a), 7.9 (b), 10.6 (c) and 13 (d) mm initial height during the first 5 minutes of the of plastic compression process. Rate of fluid loss from the gels at each minute of the process is presented in millilitre per minute. *-statistically significant difference compared to the previous time point ($p<0.05$).

Fig. 6 Effect of the height of the gel (5.3, 7.9, 10.6 and 13 mm) on the rate of fluid loss (in ml/min) during the first 5 minutes of plastic compression process. *-significant difference between gel heights at each time point ($p<0.05$).

Fig. 7 Change in the hydraulic resistance of the fluid leaving surface (R_{FLS}) of the gels of 5.3 (a), 7.9 (b), 10.6 (c) and 13 (d) mm initial height during the first 5 minutes of the of plastic compression process. Hydraulic resistance of the fluid

leaving surface of the gels at each minute of the process is presented in cm^{-1}. *-statistically significant difference compared to the previous time point ($p<0.05$). Arrows indicate 'jumps' in value characteristic for 7.9 and 10.6 mm gels.

Fig. 8 Effect of the height of the gel (5.3, 7.9, 10.6 and 13 mm) on the hydraulic resistance of the fluid leaving surface (R_{FLS}) (in cm^{-1}) during the first 5 minutes of plastic compression process. *-significant difference between gel heights at each time point ($p<0.05$).

Fig. 9 Representative histological images of the constructs (in triplicate, indicated by arrows), fabricated using multi-well plastic compression process from the gels of 5.3 (a), 7.9 (b), 10.6 (c) and 13 (d) mm initial height. Constructs were fixed immediately after compression. Staining-Sirius Red.

Fig. 10 (a) Histogram showing percentage of viable cells in the constructs prepared using multi-well plastic compression immediately after assembly (day 0) and after 14 days in culture. (b) Representative histological image of the cell-seeded construct after 14 days *in vitro*. Areas of cell matrix remodelling are outlined in black.

Fig.11 Diagram, illustrating the proposed mechanism of the secondary FLS formation during the multi-well compression process.

Chapter 6

Fig. 1 Schematic illustration of the multi-layered collagen construct assembly. (a) Collagen gels are set and compressed in the 12 well-format, leaving compressed collagen sheet at the bottom of the well which will act as a first layer. (b) Second volume of neutralized collagen is set on top of the first (compressed) layer. When second gel is set, process of compression is repeated, resulting in the double layered construct. Process is repeated in the same manner for fabrication of collagen constructs, consisting of more than two layers.

Fig. 2 Results of the layer separation assay. Double-layered constructs were prepared either by separately compressing two collagen gels and manually pressing them together afterwards (insert on the upper left corner) or by compressing the first layer and setting next gel on top of it prior to compression (insert on the lower right corner). The resulting constructs were subjected to mechanical agitation on a shaker plate for up to 20 minutes. Constructs, made using the first protocol separated after 2 minutes of agitation; two separate layers are shown floating in the Petri dish on the left. Constructs, prepared using second protocol remained intact after 20 minutes agitation and shown in the Petri dish on the right as a single construct. Constructs are indicated on the image by arrows.

Fig. 3 Representative SEM images of the interface area between two layers of the double-layered construct, made from 5.3 mm gels. Constructs were fabricated by compressing the first collagen gel and subsequent setting and compression of the next layer on top of the first (compressed) layer. (a) Transverse view of the construct. Top layer on the image is the second (top) layer of the construct. The

fluid leaving surface of the top layer is indicated by the downward arrows, the area of interface between the layers is indicated by the upward arrows. (b) Top view of the exposed interface area. For that, top layer was lifted to expose underlying surface. Arrows indicate collagen fibrils torn in the process, which gives the interface characteristic 'wispy' appearance. (c) Internal view of the interface between two layers. Layers were gently separated without total detachment prior to expose the interface. Dashed arrow indicates area of interest, solid arrows point at collagen fibrils, stretched between two layers.

Fig. 4 (a) Graph showing change in the thickness of the compressed constructs, made in the 12 well-format, with the incubation time; initial height of the gel – 13 mm. * - significant difference compared to time 0 ($p<0.05$). (b) Bar chart, showing relative change in the height of the compressed collagen immediately after compression and after 30 minutes incubation in PBS compared to the initial height of the gel (13 mm) in percent to confirm plastic nature of the process. Initial height of the gel is taken as a 100%.

Fig. 5 (a) Bar chart showing the thickness of the triple-layered constructs, assembled from the 13 mm gels per layer. Constructs were either fixed immediately (time 0) or incubated for 24 hours (time 24 hrs) in PBS prior to fixation. (b) Representative histological images of the constructs, fixed at time 0 and time 24 hrs. Dashed lines indicate interlayer boundaries. Dashed arrows indicate primary fluid leaving surface of the third (uppermost) layer. Solid arrows point at the secondary FLS of the first (base) layer.

Fig. 6 Graphs, showing the dynamics of fluid loss from the double-layered collagen constructs made of the 5.3 mm gels per layer during the first 5 minutes of the of plastic compression process; (a) - layer 1 , (b) – layer 2. Fluid loss from the gels at each minute of the process is presented in percent of initial weight. *-significant difference between % fluid loss from the gels at each time-point ($p<0.05$).

Fig. 7 Bar chart showing the effect of the layering of two 5.3 mm gels on fluid loss (in % of initial weight) during the first 5 minutes of plastic compression process.

Fig. 8 Graphs, showing the dynamics of fluid loss from the double-layered collagen constructs made of the 10.6 mm gels per layer during the first 5 minutes of the of plastic compression process; (a) - layer 1 , (b) – layer 2. Fluid loss from the gels at each minute of the process is presented in percent of initial weight. *-statistically significant difference compared to the preceding time-point ($p<0.05$). Arrow points at the characteristic 'jumps' in the curve.

Fig. 9 Bar chart showing the effect of the layering of two 10.6 mm gels on fluid loss (in % of initial weight) during the first 5 minutes of plastic compression process. *-significant difference between % fluid loss from the gels at each time-point ($p<0.05$).

Fig. 10 Graphs, showing the dynamics of fluid loss from the double-layered collagen constructs made of the 13 mm gels per layer during the first 5 minutes

of the of plastic compression process; (a) - layer 1 , (b) – layer 2. Fluid loss from the gels at each minute of the process is presented in percent of initial weight. *- statistically significant difference compared to the preceding time-point ($p<0.05$).

Fig. 11 Bar chart showing the effect of the layering of two 13 mm gels on fluid loss (in % of initial weight) during the first 5 minutes of plastic compression process. *-significant difference between % fluid loss from the gels at each time-point ($p<0.05$).

Fig. 12 Graphs, showing the dynamics of fluid loss from the first and tenth layers in the 10-layered constructs, made of (a) 5.3 mm gels per layer and (b) 13 mm gels per layer during the first 5 minutes of the of plastic compression process. Fluid loss from the gels at each minute of the process is presented in millilitres. *- statistically significant difference compared to the value at preceding time-point ($p<0.05$).

Fig. 13 Images, showing morphology of the 10-layered constructs, made of the 5.3 (left panel) and 13 (right panel) mm gels per layer. (a) – top view of the constructs, (b) – transverse view of the constructs,. (c) – representative histological images of the constructs. Inserts show images of the sections at a higher magnification. Arrows show the direction of the construct assembly.

Fig. 14 Representative histological images of the constructs made of 1, 2, 3, 4 and 5 layers of the cell-seeded plastic compressed collagen. Constructs were made in the 12-well format as described in the text. Each layer was made of 10.6 mm gels. Constructs were cultured for 3 weeks and fixed at the end of the culture period. Panel on the left shows low magnification images of the constructs; arrows indicate approximately position of the individual layers. Panel on the right shows images at higher magnification; dashed ovals indicate areas of cellular remodelling of the matrix. Note that interlayer boundaries are not distinguishable on the images, as well as fluid leaving surfaces in the upper or base layers.

Fig. 15 Diagramm, showing schematically formation of the interlayer bond in the double-layered PC construct. At time 0, when neutralised collagen solution (second layer) is poured on top of the compressed first layer, reswelling of the FLS area of the first (precompressed) construct leads to formation of shared interface between layers at time 30 minutes (setting time for the second gel), providing physical bond.

Chapter 7.

Fig. 1 Schematic illustration of the constructs assembly. Templates were placed on top of the collagen gels prior to compression. After compression process completion, patterned constructs were incubated for 5 min with PBS prior to template removal. Double layered construct were made by setting fresh collagen gel on top of the patterned one and compressing in the standard manner. Triple layered constructs were assembled in the same manner, but all three gels were micro-moulded. As a result, grooves were formed in the single-layered constructs; channels in the double-layered construct; in the triple-layered

constructs, channels were formed between layers one and two and two and three with the additional grooves in the upper-most layer.

Fig. 2 Schematic illustration of the template used for micro-moulding of the collagen gels in the 12 well-plate format. Image on the left shows gross appearance of the template. Image on the right shows cross-sections of the rungs in the templates of three sizes, used for patterning of the constructs.

Fig. 3 Schematic illustration of the direct cell delivery technique. Template was placed at the bottom of the well in the 12 well plate and incubated with the cell suspension for 2 hrs, to allow cells to settle on the template. At the end of the incubation period, the template was lifted and placed (cells down) on top of the collagen gel, set in the well of the 12 well plate. After gel was compressed and pattern formed template was left on the construct for 2 hrs to allow cells to attach to the surface of the collagen. The expected result was cells, confined to the bottom of the groove, after template was lifted.

Fig. 4 Graph, showing the dynamics of fluid loss from the micro-moulded constructs made of the 10.6 mm gels during the first 5 minutes of the of plastic compression process; Fluid loss from the gels at each minute of the process is presented in percent of initial weight. *-statistically significant difference compared to the previous time point ($p<0.05$). Curve for the non-moulded compressed 10.6 mm gel was added for comparison. Note the disappearance of the characteristic 'kink' from the curves of the moulded gels.

Fig. 5 Bar chart showing the effect of the micro-moulding on fluid loss (in % of initial weight) from the 10.6 mm gels during the first 5 minutes of plastic compression process compared to the non-moulded gels of the same height. *-significant difference between gels at each time point ($p<0.05$).

Fig. 6 Representative SEM images of the patterned constructs made of 10.6 mm gels. Constructs were micro-moulded using 25x75 µm template (left-hand panel), and 100x75 µm template Right-hand panel). Upper row of images shows surface of the patterned constructs with parallel grooves, indicated by arrows. Middle panel shows images of the individual grooves in transverse view, indicated by arrows. Bottom row of images shows surface of the patterned constructs, with the branching of the templating rungs from the middle and upper supportive bars on the template (shown in the inserts)

Fig. 7 Bar chart showing depth of the grooves in percentage of expected value (thickness of the template, 75 µm, taken as a 100%). Grooves were micro-moulded into the 10.6 mm gels using templates with rungs of 25, 50 and 100 µm width. *-statistically significant difference ($p<0.05$).

Fig. 8 (a) Bar chart, showing average depth and width of the grooves, made using 50x75 µm template in the 5.3, 10.6 and 13 mm gels. (b) The respective fidelity of the pattern, based on the depth to width ratio, to the moulding template. * - statistically significant difference ($p<0.05$).

Fig. 9 Representative histological images (SiriusRed staining) of the grooves (transverse view) made using 50x75 µm template in the (a) 5.3 mm gels, (b) 10.6 mm gels and (c) 13 mm gels. Inserts show grooves at high magnification. Dashed areas outline grooves, dashed arrows point at the secondary FLS, solid arrows indicate collagen fibrils accumulation in the vicinity of the groove.

Fig. 10 Bar charts showing the dimensions of the channels (depth and width), made by micro-moulding 10.6 mm gels (base layer) and casting and compressing fresh gel of the same height on top (upper layer, roof of the channel). The dimensions of the grooves in the single layer are plotted for comparison. (a) 25x75 µm template, (b) 50x75 µm template, (c) 100x75 µm template.

Fig. 11 Representative histological images (low and high magnification, inserts) of the open channels (transverse view, SiriusRed staining) made by micro-moulding 10.6 mm gels (base layer) and casting and compressing fresh gel of the same height on top (upper layer, roof of the channel). (a) 25x75 µm template, (b) 50x75 µm template, (c) 100x75 µm template. Solid arrows indicate the open area of the channel, arrow heads point at the collagen fibrils, protruding into the channels from the upper layer (the 'roof').

Fig.12 (a) Bar chart showing the dimensions (depth and width) of the grooves, made in the single-layered constructs using 100x75µm template. Dimensions of the grooves in the cell-seeded constructs, cultured for 1 week and 2 weeks are compared with the dimensions of the grooves in the acellular constructs at time 0. (b) Representative histological images (H&E staining) of the patterned cellular constructs at week 1 and 2. Dashed ovals indicate areas of cellular matrix remodelling, arrows point at the grooves in the constructs surface.

Fig. 13 (a) Images of the live HaCat cells (green), stained using live-dead protocol. Left – cells on the rungs of the template, following 2 hrs incubation with the cell suspension. Middle and right are images of the cells in the grooves, taken at time 0 and 24 hrs of culture period. Dashed lines indicate the rung of the template (left image), and grooves (centre and right images). (b) SEM images of the cells, delivered in the grooves following direct cell delivery protocol at time 0. Insert – higher magnification of the cell in the groove showing cell, attached to the collagen surface. Arrows on the image on the right point at the groove borders. Open arrows show cell filopodia attached to the collagen fibres.

Fig. 14 Histological image of the channel in the double-layered collagen construct, with the cells (HaCat), delivered using the direct cell delivery protocol, and cultured for 1 week. Layer 1 (patterned layer) was made of 10.6 mm gel, layer 2 (roof of the channel) was made of 5.3 mm gel. Dashed line indicates interface between layers, arrows point at the channel lumen.

Fig. 15 Diagram, showing proposed mechanism of pattern formation in the multi-well format. Immediately after contact with absorbent and loading, fluid starts to flow out of the gel towards the absorbent (primary flow). However, presence of the impermeable template results in faster blockage of the primary FLS due to the process of ultrafiltration. Following that event, fluid starts to leave the gel through the bottom part (secondary flow), creating secondary FLS.

This is blocked as well due to the same ultrafiltration process. Fluid, still left in the gel by this point can leave through the only unblocked surface – bottom of the grooves (tertiary flow). This potentially leads to slight lift off of the template and possibly collapse of the walls of the grooves, resulting in shallower than expected features.

Chapter 1.

Introduction.

Tissue engineering – general overview

Tissue engineering, as defined by Langer and Vacanti (1993) is 'an interdisciplinary field that applies the principles of engineering and life sciences toward the development of biological substitutes that restore, maintain, or improve tissue function or a whole organ'. Since then tissue engineering principles have been applied to provide basic knowledge and better understanding and control of fundamental functions and principles of biological tissues (Curtis and Riehle, 2001, Freed et al., 2006, Keung et al., 2010) and to supply viable alternatives to animal research (Holmes et al., 2009). Currently tissue engineering applications include, but are not limited to, bone, muscle (skeletal and cardiac), blood vessels, skin, cartilage, tendon, liver, kidney, intestines, nerve tissue (both CNS and PNS) and adipose tissue. Clearly, these aspirations cross boundaries of cell, tissue and organ replacement therapies.

The notion that cells behave differently in 3D environment, which is an appropriate mode of existence for the majority of cells in the vertebrate tissues, brought with it great shift in scaffold design strategies and cell-seeding techniques (Pampaloni, 2007). Currently, two main approaches exist in the field of TE, namely scaffold free and scaffold based TE.

Scaffold free TE approach includes single cell type delivery (either stem cells or tissue specific differentiated cells), cell sheets or microtissues (cell aggregates created in vitro under specific conditions, usually by preventing cell adhesion to the tissue culture plastic) (Kelm and Fussenegger, 2010). Cell sheet engineering, where cells are delivered embedded in their own matrix, is based on use of thermoresponsive

plastics which allow harvesting of the sheet of confluent cells together with ECM. These can be arranged in complex structures by variation of patterning techniques (Hannachi et al., 2009).

Scaffold based approaches are more common in the field of tissue engineering. Several design factors should be considered when engineering 3D constructs: substrate and extracellular matrix composition, composition and rates of tissue development, cell types, localisation and segregation, tissue shape and microarchitecture and local tissue functional requirements (Brown, 2000, Chan and Leong, 2008).

Scaffold based TE can be divided into groups based on the scaffold material – natural, synthetic or combination of both. Scaffolds can be further modified to controllably release drugs or growth factors, for example to attract host vasculature or facilitate bone healing (Chunga and Park, 2007).

Scaffolds can vary greatly in shape (eg. microspheres, sheets or foams), mechanical properties (from hydrogels to metals), surface topography (smooth or structured, nano- or micrometer scale), porosity (micrometers to hundreds of micrometers, examples in Table 1) and rate and mode of degradation (days to years, examples in Table 2) (Leong et al., 2008).

Table 1. Examples of a range of pore sizes in the biomaterials used for different tissue engineering applications (adapted from Leong et al., 2008).

Tissue regeneration	Cell size (μm)	Preferred pore diameter (μm)
Hepatocytes	20–40	20
Fibroblast	20–50	90–360
Bone	20–30	100–350

Table 2. Examples of degradation rates and mode for a variety of natural and synthetic polymers used in tissue engineering (adapted from Leong et al., 2008).

Biomaterials	Degradation time	Degradation mechanism
Natural polymers:		
Collagen	0.5-3 months	Enzymatic degradation
Chitosan	10days-1.5 months	Enzymatic degradation
Synthetic polymers:		
Poly(L-lactic acid) (PLLA)	2–12 months	Hydrolytic mechanism
Poly(glycolic acid) (PGA)	4–6 months	Hydrolytic mechanism
Poly(caprolactone) (PCL)	12-24 months	Hydrolytic mechanism

Scaffold based TE can be further divided based on the nature of the material, either synthetic or natural polymers, used for scaffold fabrication.

Synthetic polymers as scaffold material.

The advantages of synthetic polymers for TE applications include controllable and reproducible structure and chemistry, eliminated risk of transmitting disease and lack of batch-to-batch variability. Additionally, with the variety of fabrication techniques, synthetic scaffolds can be better tailored to end-users requirements with the ultimate target to tailor degradation rate to the rate of tissue regeneration and to provide appropriate mechanical properties (Yang and El Haj, 2006).

Currently, FDA approved hydrolytically degradable polymers, such as polyglycolic acid (PGA), polylactic acid (PLA), co-polymers (PLGA), polycaprolactone and polyethyleneglycol (PEG) are amongst the most widely used for fabrication of TE scaffolds (Place et al., 2009).

However, these materials remain intrinsically non-biological and cannot provide the cells with appropriate environments for their ‘correct’ function. As such, currently synthetic polymer scaffolds can be regarded as a delivery vehicle rather than a truly engineered piece of living tissue that cells can attach to and remodel. The research into overcoming these drawbacks is currently under way. Hydrophobicity

can be overcome by plasma treatment, chemical etching, peroxide or ozone oxidation (Place et al., 2009). Cell-adhesion can be improved by coating with natural ECM proteins (collagen, vitronectin, laminin, fibronectin, hyaluronic acid), or by incorporating the short peptide motifs, derived from binding regions of ECM proteins, usually well-studied Arg-Gly-Asp (RGD) integrin-binding motif from various ECM proteins including fibronectin, laminin and collagen type I (Place et al., 2009). However, currently naturally derived polymers represent more attractive alternative for tissue engineering applications.

Naturally derived polymers as scaffold material.

Naturally derived polymers are naturally non-cytotoxic, bio-compatible and cell-adhesive. A growing body of evidence shows that complex extracellular matrix (ECM)-cell interactions *in vivo* provide not only essential structural support but encompasses a multitude of other cues such as regulation of cell differentiation, adhesion, cell phenotype, cell motility and matrix production (Hynes, 2009). The drawbacks of natural polymers as TE scaffolds include a high degree of variability and possibility of microorganism or antigen transmission from the source.

Currently, natural polymers of mammalian (collagen, gelatin, fibrin, hyaluronan), invertebrate (chitosan, silk), algae (alginate) and plant (starch) origin are used for various TE applications (Yang and El Haj., 2006, Chunga and Park, 2007, Malafaya et al., 2007). Several examples exist of recombinant human ECM production, but technologies are in the early stage of development (Ramshaw et al., 2009). Commercially available Matrigel, often used as a coating agent, contains a mixture of several ECM molecules produced by mouse tumour cells, with greater representation of laminin and collagen IV, and can be regarded as a model of basal lamina.

Decellularised tissues form a group of their own and are usually favoured for retention of natural composition of ECM proteins and microarchitecture. However, these must be extensively processed to remove cellular components which could trigger immune reactions. Despite this drawback, recent successful face (Devauchelle et al., 2006) and trachea (Macchiarini et al., 2008) transplantation clearly show the importance of correct 3D micro-architecture in scaffold fabrication.

Importance of controllable 3D micro-architecture for TE scaffold.

Several design factors should be considered when engineering 3D constructs: substrate and extracellular matrix composition, composition and rates of tissue development, cell types, localisation and segregation, and tissue functional requirements, shape and micro-architecture (Brown, 2000, Chan and Leong, 2008).

The importance of controllable 3D micro-architecture in the 3D scaffold design is based on the fact that native tissues (i.e. the very thing that researchers are striving to engineer) are not uniform blocks of cells and matrix. Tissues of the human body have complex internal (blood vessels and nerves, present in every tissue) and surface (interfaces, invaginations and protrusions of the basement membrane as seen for example in skin (rete ridges), cornea (limbus) and small intestines (villae) architecture. Therefore, in order to engineer a truly bio-mimetic tissue, these micro-structures should ideally be a part of the scaffold. Moreover, these structures should be permanent and stable, as they are *in vivo* (Le Gros Clark, 1975).

It is increasingly appreciated that the topography of a tissue engineered construct at the micrometre scale is critical to controlling many cell functions (Ingber, 2005), although there is still an opinion that surface topography is not enough to elicit control over function of the engineered tissue (Pietak et al., 2008). It is well established, for example, that surface anisotropy and micro-structure have a profound

effect on cell alignment and differentiation (Clark et al., 1987, 1990, Pins et al., 2000, Teixeira et al., 2003 and 2004, Downing et al., 2004, Vernon et al., 2005). Bruder et al. (2006) demonstrated alignment of neurites cultured on replicas of pre-aligned Schwann cells. Cao et al (2010) showed that primary human vascular smooth muscle cells, cultured on the surface of a biodegradable synthetic polymer with microgrooves are aligning to the walls of the grooves and switching towards contractile phenotype upon reaching confluence; behaviour not exhibited on a planar control or by non-confluent culture. These authors showed that such morphological changes were accompanied by significant increases in contractile protein expression. Similar results were achieved by this group using immortalized rat aorta smooth muscle cells, cultured in microgrooves (Shen et al., 2006, Feng et al., 2007). Isenberg et al. (2008) demonstrated fabrication of cell-sheets with aligned vascular smooth muscle cells. Cells were cultured on a patterned thermo-responsive polyester substratum. Following cell alignment, cell sheets were released by lowering the temperature to 20°C.

Indeed, some studies show that the effects of topological features on cells extend well beyond the single layer and affect cells that are not in direct contact with the surface (Ejim et al., 1993, Papenburg et al., 2007, Sørensen et al., 2007, Guillemette et al., 2009, Then et al., 2011). Ejim et al. demonstrated alignment of fibroblasts to pre-aligned fibronectin fibres. Cell alignment persisted over several cell layers. Pappenburg et al. (2007) showed alignment of mouse myoblasts and osteoblasts to the microgrooves in the porous poly(L-lactic acid). These authors showed that cell alignment persisted over 7 days in culture and extended over multiple cell layers. Guillemette et al. (2009) showed that topological features affect multilayered cell sheets (human stromal corneal fibroblasts, human dermal fibroblasts and smooth muscle cells), such that alignment of the first layer directed morphology

and deposition of extracellular matrix in subsequent cell layers. Similar results have been reported by Sørensen et al. (2007). Authors showed that alignment of astrocytes on the microgrooves was translated to alignment of neurons cultured as a top layer. Then et al. (2011) showed that alignment of keratocytes, cultured on microgrooved polycaprolactone films, caused cells in the second layer to align at 30-40° angle to the cells in the first.

Consequently, accurate, predictable and stable topographic patterning is a pre-requisite for next generation studies investigating biomimetic 3D niches to control, for example, stem cell function and fate (Chaubey et al., 2007, Vazin and Schaffer, 2010), as well as cell-cell/cell-matrix interactions at interfaces (e.g. dermo-epidermal junction). Indeed, Nelson and Tien (2006) pointed out that simply by adding structure it may be possible to improve almost any biomaterial by creating extra cues that influence cell behaviour, making this a favourable strategy to expand the function of a tissue engineered construct.

The importance of the micro-architecture, in particular surface topography, can be easily seen from the profound effect that addition of such simple surface features as grooves have on cell behaviour. The fact that surface anisotropy can affect behaviour of cells has been known since the beginning of last century and in 1954 Paul Weiss suggested a term ‘contact guidance’ to describe his observation that neurites can be guided by scratches on the substrate (glass) (Weiss, 1954). Since then the effects of the topology (most often grooves) on the cell behaviour has been studied extensively. These studies used a variety of cell types (neurons, astrocytes, fibroblasts, macrophages, keratinocytes) and dimensions of the grooves (microns to nano) (Flemming et al., 1999, Martinez et al., 2009, Hoffman-Kim et al., 2010). The data collected up to date show that both cell type and dimensions of the features are

important factors to consider when designing a patterned scaffold (Clark et al., 1987, Clark et al., 1990, Curtis and Riehle, 2001 Kapoor et al., 2010).

Currently, the following hypotheses are proposed to explain mechanisms of the cellular alignment on the micro-grooved substrata. First is that cells minimise distortions to the cytoskeleton which would occur if they ignore, rather than follow the groove (Hamilton et al., 2009), based on the theory, put forward by Dunn and Heath (1976), that cytoskeleton microfilaments cannot bend over angles more than 4°. Second theory proposes that attachment to topographical cues (for example ridge of the groove) create mechanical stresses in the cell that directly cause alignment (Walboomers et al., 1998). Curtis and Clark (1987, 1990) showed that cells (fibroblasts) react to discontinuities in the substratum (grooves and ridges) by actin condensation at the boundaries between ridge floor and groove wall. These data were confirmed by Wojciak-Stothard et al. (1995); authors showed that this effect of topology on fibroblasts is observed within 30 minutes after cell seeding. Similar effect of the surface topology on the epithelial cells has been shown by Brunette and colleagues (Brunette, 1986, Chehroudi et al., 1989, 1990, Hamilton et al., 2009). Dalby et al. (2003) showed that such distortion in the cytoskeleton and shape of the cells on the grooved substrata cause change in the shape of the nuclei (elongation) and hypothesised that this leads to changes in the gene expression of the aligned cells due to the change in the relative position of the chromosomes and their accessibility for transcription (Dalby, 2005).

Thus, the effect of the micro-scale 3D architecture of the scaffolds on cells is indeed profound and merits investigation as a tool for incorporation into natural materials, such as collagen. In addition to engineering tissue micro-structure, these

studies can be used to further our knowledge of tissue development, both normal and pathological and for testing systems in drug discovery. On the other hand engineered natural polymer scaffolds with predictable and controllable 3D micro-architecture can represent next generation of tissue engineered implants and also serve as 'lab on a chip' models for pharmaceutical or cosmetic industries as a substitute for animal testing.

Currently, several well-described techniques had been developed to produce scaffolds with predictable surface topography both on micro- and nano-scale. These include various lithographic techniques such as photolithography and soft lithography, micro contact printing, hot embossing. However, these techniques are largely only applicable to synthetic materials; hence the majority of our knowledge on cell behaviour on the patterned surfaces is based on these substrata. Clearly these do not reflect the surface chemistry or mechanical properties of native tissues. It is, therefore, particularly important to develop appropriate techniques of micro-fabrication to introduce appropriate geometrical features onto the surface of naturally-derived materials (Nelson and Tien, 2006). From the literature search it becomes obvious that there are very few techniques available, developed to introduce predictable and stable 3D structures into the natural polymers, and none which allow survival of the cells, embedded in the bulk of polymer or which do not require some form of cross-linking to render structures permanent.

Soft lithography is probably most widely used method of patterning natural polymers, usually in the form of hydrogels. In its simplest form, hydrogel is set on a negative template, and features on its surface are cross-linked afterwards to make them stable in culture conditions. Indeed, without this extra step in construct

fabrication, pattern, made in collagen gel detiorated in culture by day 14 (Ber et al., 2005). Predictably, this changes the mechanical properties of the scaffold and prevents cell-seeding of the bulk material prior to templating. This technique has been used to pattern flow-network onto the collagen-glycosaminoglycan co-polymer membranes (Janakiraman et al., 2007), defined cavities onto collagen hydrogels (Nelson et al., 2008) and micro-grooves onto chitosan and gelatine scaffolds (Wang and Ho, 2004).

To avoid use of chemical cross-linking agents and in attempt to produce more biologically appropriate patterned surfaces, following techniques have been proposed independently by Pins (2000) and Vernon (2005).

Pins et al. reported in 2000 the fabrication of gelatin and collagen type I membranes with well-defined microgrooves by air-drying hydrated gels on negative templates and subsequent thermal dehydration at 105ºC in vacuum. These micro-patterned collagen membranes (as seen in Figure 1 a and b) have been used as an analogue of skin and intestinal basal lamina (Pins et al., 2000, Downing et al., 2005, Wang et al., 2010).

Similar method have been developed by Vernon and colleagues (Vernon et al., 2005), where fibrillar collagen gels were air-dried for 24-48 hours at room temperature on the template to produce thin lattices (as seen in Figure 1 c and d) which were peeled off after drying. These authors used the micro-grooved collagen membranes to assess alignment of human dermal fibroblasts and umbilical artery smooth muscle cells.

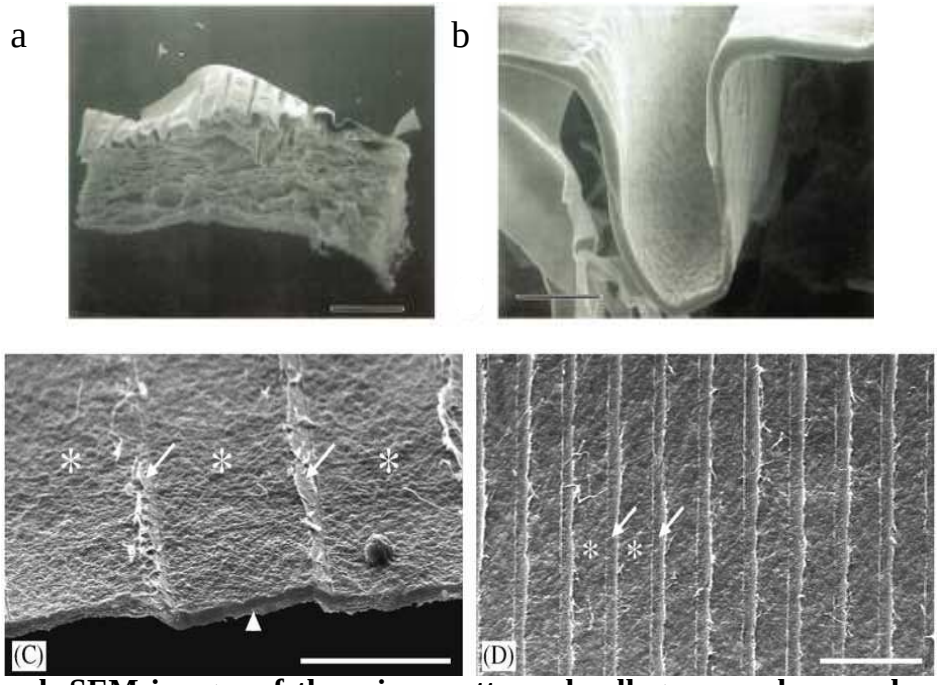

Fig. 1 a-b SEM images of the micro-patterned collagen membranes, laminated onto collagen-GAG sponge. Scale bar a-1mm, b-50 µm (From Pins et al., 2000); c-d SEM images of the micropatterned collagen lattices. Scale bar – 25 µm (From Vernon et al, 2005).

It is obvious, that this method is based on conformation of an extremely dehydrated protein layer to the underlying pattern. As such, these constructs can be used as patterned flat surfaces to study cell behaviour but hardly can be regarded as engineered tissue. Indeed, in the study by Downing et al. (2005), these lattices needed to be laminated onto a freeze-dried collagen sponge (later seeded with dermal fibroblasts) to be regarded as a skin model, as authors showed previously that fibroblasts migration into air-dry collagen lattices is severely compromised (Cornwell et al., 2004).

The study by Downing et al. (2005) can serve as an example of indirect approach to tissue engineering, where the researcher has effectively no control over the end-product – the engineered tissue. In case of a skin model, described above, the perfect scaffold was created first, with patterned surface and porous supportive bulk material. However, to serve as skin model both patterned surface and collagen sponge

need to be populated by the appropriate cell type, in this case keratinocytes and dermal fibroblasts. Cells (fibroblasts) are added to a preformed matrix (collagen sponge) and need to penetrate and populate the scaffold, process which cannot be controlled.

It is easy to see that the results here are hardly predictable and over time this population of matrix cells can (and will) change the initial matrix structure beyond control of the researcher, which in turn will distort the pattern on the surface. Similarly fabrication of scaffold with pre-formed pores by gas foaming, phase separation, freeze drying and particulate leaching (Hutmacher, 2001, Hollister, 2005, Madaghiele et al., 2008, Annabi et al., 2010) or addition of growth factors and/or endothelial cells to the matrix to create tubular structures can serve as examples of indirect approach (Nakagami et al., 2005, Finkenzeller et al., 2009, Ghanaati et al., 2010, He et al., 2011, Reckhenrich et al., 2011, Chiu et al., 2011). Both are done *in expectation* that pores will not get blocked by cells' ECM and will provide adequate oxygen supply; that cells will not change mechanical properties of the scaffold or that growth factors will attract host blood vessels and endothelial cells will arrange into tubes.

Indirect approach provides valuable information for material scientists and biologists. However, direct tissue engineering provides more controllable and predictable results. For example, as opposed to methods mentioned above, to create channels (pores) in the material of controllable dimensions, geometry and spacing, sacrificial structures can be used. The rationale behind this approach is that upon removal of the structure from the bulk material, pore (or channel) is left behind, all features of which were designed by the researcher. Golden and Tien (2007) used micro-moulded gelatin mesh to create micro-channels in collagen hydrogel. Collagen

gel was set around pre-moulded gelatin template. After collagen gel was set, template was removed (melted) by raising temperature to 37°C, leaving channels of designed dimensions in the gel. Vernon et al. (2005) used paraffin as sacrificial structure in air-dried collagen membranes for the same purpose. Collagen gels with incorporated paraffin template were air-dried and template melted, leaving channels in the collagen construct. Li et al. (2009) used sucrose fibres, embedded in poly (l-lactic acid)/chloroform base to fabricate aligned pores. Aligned micro-channels were fabricated in the compressed collagen construct by dissolution of soluble glass fibres (Nazhat et al., 2007).

Another approach to create controllable micro-channels is to layer micro-patterned sheets, so that pattern in the underlying layer is covered by the next layer of biomaterial, creating open channels. However, this approach has been generally used for synthetic polymers, such as poly-(glycerol sebacate) (Fidkowski C. et al., 2005), polydimethylsiloxane (Shin M. et al., 2004, Mata et al., 2009), poly(L-lactic acid) (Pappenburg et al., 2009), poly (lactide-co-glycolide), poly(ε-caprolactone-co-glicolide), poly(dioxanone) and Monocril® (Ryu et al., 2006). The two parts of the channels (the patterned layer and the upper cover) are held together by uncured polymer (PMDS, Mata et al., 2009), treatment of the interface by oxygen plasma (Fidkowski C. et al., 2005, Shin M. et al., 2004), solvent vapour bonding (Ryu et al., 2006) or by physically rolling patterned stacted sheets in a tube (Pappenburg et al., 2009). Although, these methods successfully create open channels, use of synthetic materials and additional steps needed to hold the patterned sheets together make these methods less attractive for engineering living tissue equivalents. Therefore, there is a need for new generation of tissue engineered constructs comprising natural polymer and cellular components of the native tissues with added topological features. The

addition of the surface topology must not interfere with the material or chemical properties of the polymer or compromise viability of the resident cells. This research offers solution to the stated problem, using collagen type I as a scaffold material.

Collagen type I in tissue engineering

Collagen type I is a perfect starting material for tissue engineering when natural polymers are used, being basic structural constituent of a mammalian body. Collagen molecules and fibres have evolved as structures of high tensile strength, equivalent to that of steel when compared on the basis of the same cross-sectional area, but three times lighter on a per-unit weight basis (Hulmes, 2008). To date 28 types of mammalian collagens and about the same number of other members of the collagen superfamily have been discovered; though the function of some is still obscure (Hulmes, 2008). Fibrillar collagens are paramount to the viability of the organism and are shared in some form by all multicellular animals, from sponges to mammals.

All collagens share the same basic characteristics and contain rigid, rod-like molecules with three subunits (alpha-chains) wound into right-handed triple helix. Collagens assemble into fibrils, arranged with well-described periodicity, so called D-banding, of 64-67 nm, resulting from the near-crystal ¼ stagger packing of collagen molecules in to fibril as shown schematically in Figure 2 (Hulmes, 2008)..

Collagen fibril, composed of collagen molecules, is 300 nm long and 1.5 nm wide with fibril diameter ranging from 20 nm in cornea to 500 nm in tendon.

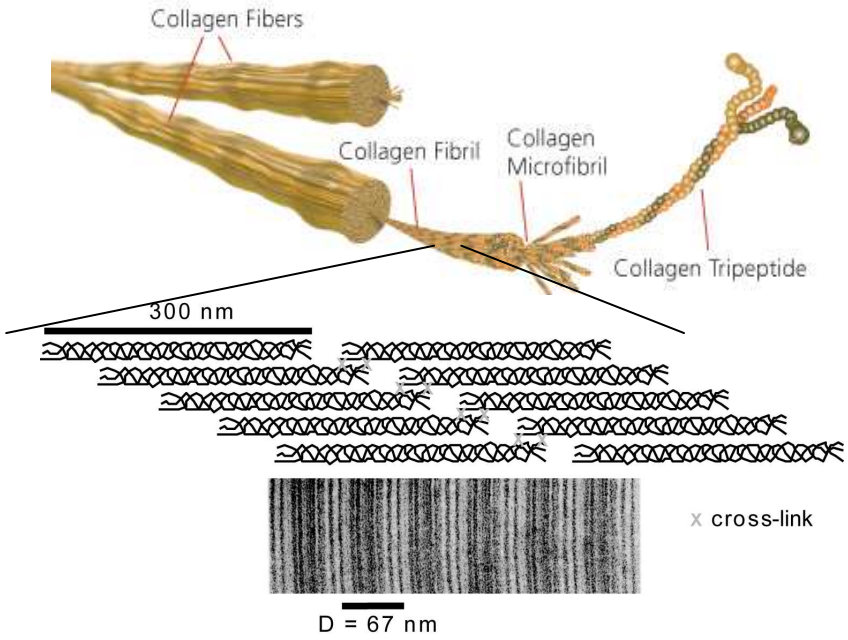

Fig.2 Schematic illustration of the collagen type I structure, showing collagen fibres, fibrils and molecules. Lower image shows collagen molecules in characteristic staggered arrangement. (From http://www.sigmaaldrich.com/life-science/metabolomics/enzyme-explorer/learning-center/structural-proteins/collagen.html and Hulmes, 2008)

Collagen type I is the most abundant form in mammalian tissues such as skin, bones, ligament, tendon, cornea, lungs and vasculature. It has long been recognised as an appropriate scaffold material for tissue engineering applications. It is intrinsically biocompatible and biodegradable, highly conserved between species, minimising the immune reactions. Collagen type I is found in high concentration in skin, bone and tendon, providing abundant sources for isolation of this polymer.

As has been mentioned above, the majority of research on collagen type I usage for TE applications is based on mammalian collagens from animal sources. Recently, several alternative sources of collagen from more primitive animal species (fish scales (Chen et al., 2011), jumbo squid (Uriarte-Montoya et al., 2010) as well as use of recombinant human collagen produced by genetically modified microorganisms, plants, silkworm and transgenic mice have been reported (Ramshaw et al., 2009). These developments can potentially substantially reduce cost and

eliminate possible problems of immunogenesity. However, substantial further work is needed in this area before these sources are practical.

Collagen scaffolds have been proposed for hard and soft tissue engineering. For hard TE applications, combination of collagen and inorganic component (e.g. hydroxylapatite, tricalcium phosphate), mimicking bone composition *in vivo*, is usually used (Habraken et al., 2007).

Acid-soluble collagen gels

The major fibrillar collagens are soluble at low pH, usually in dilute acetic acid. In commercially available acid soluble collagens N- and C-telopeptides are intact which helps to initiate fibril assembly *in vitro* and to produce long cylindrical fibres (Hulmes, 2002). The phenomenon of collagen fibril reassembly (fibrillogenesis) was first reported in the middle of last century and proposed as a model to study collagen assembly in vivo. Since then the phenomenon has been extensively studied and exploited for TE and other applications.

Self-assembly of collagen monomers from acidic solutions depends purity of initial solution, buffer composition, pH and temperature (Gross and Kirk, 1958, Wood and Keech, 1960). When pH is adjusted to around neutral and temperature is raised to physiological level, fibrils form spontaneously and present D-periodicity of native collagen fibrils. The process involves three phases: initial lag phase, rapid growth phase and plateau region. During the lag phase small number of collagen molecules associate to form nuclei; during growth phase new molecules are recruited and longitudinal and lateral interactions ensure growth in fibril length and width (Comper and Veis, 1977). Growing fibrils form a network, within which water is trapped, eventually forming a gel.

Collagen gels have been extensively researched as scaffolds for bone, cartilage, skin and adipose TE applications (Malafaya et al., 2007, Huang and Fu, 2010). One of the draw-backs of hydrated collagen gels is their inherent mechanical weakness. Several approaches have been developed to improve mechanical stability of collagen scaffolds. These can probably be divided in two groups: cell-compatible and cell-incompatible. The latter involves chemical cross-linking (Chan and So, 2005), cross-linking by thermal dehydration (Pins et al., 2000) and air-drying (Vernon et al., 2005). The former includes cell-mediated gel contraction (Bell et al., 1979, Grinnell and Lamke, 1984), photochemical cross-linking (Chan and So, 2005), high concentration collagen stock solution (Helary et al, 2010,2011) and plastic compression (Brown et al., 2005).

Plastic compression of collagen

The method of plastic compression of collagen has been originally reported by Brown et al. in 2005. The method is based on uniaxial removal of unbound water from hyperhydrated collagen gels, reconstituted from acidic solution. As a result, collagen sheets are produced which, dependent on application, can contain known number of viable embedded cells. The process is shown schematically in Figure 3.

The word ‘plastic’ refers to irreversible nature of the process, i.e. that thickness of collagen sheets does not change (i.e. re-swell) significantly in fluid once the load is removed. The main advantages of this method are: simplicity, speed and reproducibility, calculable, predictable physical and concentration parameters and compatibility with viability of a resident cell population. Thus, in contrast to other techniques, the improved mechanical properties, achieved using this method, are controlled by the researcher rather than cells, but most of all without loss of cell viability.

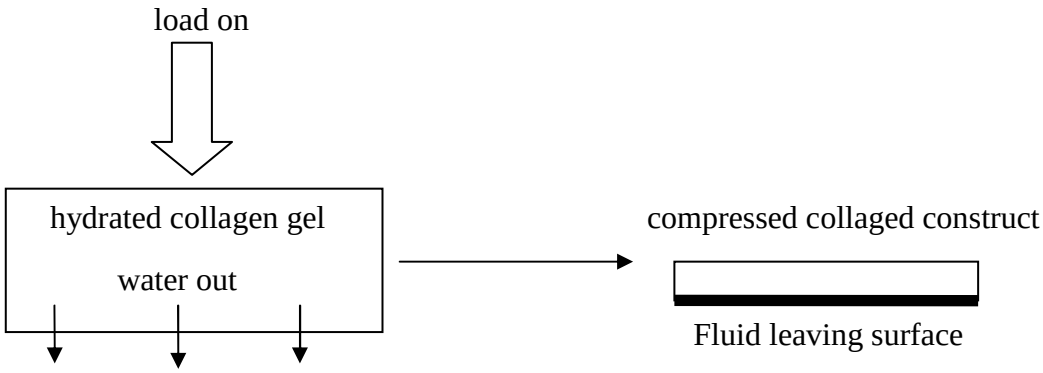

Fig.3 Schematic illustration of the plastic compression process (Brown et al., 2005) Load is applied to the hydrated collagen gel and cause unidirectional fluid flow from the gel, which results in formation of dense collagen layer with anisotropic distribution of collagen in the construct with denser area at the fluid leaving surface.

This technology has been proposed for a number of TE applications, such as tendon (Brown et al., 2005), skin (Ananta et al, 2009, Hu et al., 2010), cornea (Levis et al., 2010) , bone (Bitar et al., 2007, Buxton et al., 2008, Pedraza et al., 2010), bladder (Micol et al., 2011) and spinal cord repair (East et al., 2010). In addition it has been successfully applied to basic research in tissue interfaces and vascularisation strategies (Hadjipanayi et al., 2009a, Cheema et al., 2010), oxygen diffusion (Cheema et al., 2008, 2009) and cell behaviour in dense collagen matrices (Hadjipanayi et al., 2009b, Serpooshan et al., 2011). These have recently led to successful development of the first practical hypoxia-dependent angio-therapy Use of this material as a peripheral nerve repair conduit is currently under investigation.

Aims and hypotheses

There is still lack of techniques to pattern natural polymers and retain viability of the embedded cells. Such new types of scaffold will provide valuable platform to research tissue morphogenesis, cell-cell and cell-pattern interactions as well as drug discovery. Moreover, it can bring us closer to the ultimate goal of tissue engineering – direct fabrication of an artificial tissue, composed of native components and micro-architecture which can substitute lost or diseased host tissue.

This approach of *direct* engineering of collagen matrix has been adopted in current research. Here, our goal was to control the following parameters of the resulting constructs: distribution and viability of the embedded cells, appropriate mechanical properties compared to the starting material (weak hydrogel), control over geometry and dimensions of the internal (channels) and external (grooves) features. The target is to fabricate without cell action an engineered tissue equivalent with cells *in situ* with engineered internal and external 3D features, composed of native natural polymer, in this case collagen type I.

The goal of this work was to further advance understanding of mechanisms of PC process by creating a new generation of these constructs with predictable and stable 3D features, both internal and external, using micro-moulding technique.

The overarching hypothesis was that dense collagen constructs with a viable cell population and engineered microarchitecture (i.e. surface topology, internal microchannels and defined interfaces) will be a valuable tool for clinical and pharmacological applications as well as an easy-to-use model of basic biological processes.

The working hypothesis was that fluid flow from the collagen gel during compression process controls pattern formation by directing where and how collagen fibrils finally accumulate. Therefore, if correct, controlled deflection of the flow, using impermeable templates of known dimensions, could permanently remodel collagen matrix, giving predictable 3D features in the construct.

In order to introduce controllable 3D features (both internal and external) in to the PC collagen construct two approaches were used. Firstly, the ‘lost fibre’ technique was used to create channels in the dense collagen matrix. The main principle of the method has been reported on by Nazhat et al. (2007). In the original paper, soluble

phosphate-based glass fibres were incorporated in the construct and when fibres dissolved, open channels of uniform diameter were formed in the collagen matrix. We have hypothesised that progressively opening channels will aid in controlled tissue (such as axons) ingrowth into the implant. To achieve that goal, shape of the fibre should be changed from a uniform cylinder to a cone with steadily decreasing diameter. When construct with such conical fibres is implanted, channels will start opening faster at the thinner end than thicker, thus favouring ingrowth of tissue from one end of the channel and delaying from another. These progressively opening channels are predicted to be of particular use for nerve tissue engineering, where correct direction and timing of axon regrowth is crucial.

To engineer surface features in the PC collagen constructs we have hypothesised that by controllably deflecting fluid outflow from the gels during compression around a designed templates. This will form stable and faithful pattern on the fluid leaving surface due to collagen fibres accumulation around the template.

It is known that plastic compression produces an asymmetric layered structure in the construct, different at the two opposite surfaces, the non fluid leaving surface (non-FLS) and fluid leaving surface (FLS) respectively (Brown et al., 2005, Hadjipanayi et al., 2010). It is known, that the two differ in mechanical properties, as directional expulsion of liquid leads to the formation of much denser layer closest to the blotting elements than the opposite surface, creating a surface anisotropy which could affect the outcome of patterning.

To test this hypothesis several experimental designs have been tested. Additionally, stability of the pattern in the presence and absence of matrix remodeling cells (fibroblasts) have been tested in tissue culture conditions.

As has been mentioned before, our knowledge of cell behavior on the patterned surfaces is mainly based on synthetic materials with inadequate chemistry and mechanics. Using these novel TE scaffolds we can study cell behavior on patterns not only made of natural polymer but also in the presence of matrix cells. Therefore, this knowledge can be used to recreate morphogenesis in vitro as well as give rise to a new generation of engineered living tissues equivalents.

Automation of the process is necessary for this innovative methodology to be used to its full advantage in drug testing and engineered tissue customisation. In additions, automation will allow fabrication of the constructs with optimal speed and reproducibility. We hypothesise that as a preliminary step towards automation/mechanisation of the PC process that setting and compression of the constructs in a multi-well format would significantly decrease variability whilst enabling fabrication of multiple and multilayered constructs with controllable parameters. To test this idea, a process of multi-well plastic compression (M-PC) was developed, offering not only great control over the process of PC but also valuable knowledge of its underlying mechanisms (such as fluid loss and FLS formation). This would bring the technique closer to fully controllable by the operator.

This novel methodology allows for fabrication of multilayered constructs, consisting of interconnected layers of dense cell-seeded collagen, which was not possible using the original method. As plastic compression effectively produces a sheet of cell-seeded collagen it appears to represent a further advance for engineering thick, multilayered constructs. Hadjipanayi et al (2009) demonstrated fabrication of double-layered constructs (cellular and acellular) by separately casting collagen gels, with the first gel being set prior to addition of the second layer. The whole structure was then compressed in a single stage as per the original method. However, this

technology has its limitation, mainly due to the blocking of FLS (fluid leaving surface) by collagen fibrils, carried with the fluid and accumulated at the boundary level (Hadjipanayi et al., 2010). This results in decrease of fluid flow from the compressed gels. Formation of dense FLS zone does not permit layering using original method, as fluid from the next gel needs to pass through the underlying compressed layer. It has been shown that restriction of FLS blockage when using the original PC method can be partially overcome by separate compression of the gel on each side, so that two FLS are formed on the opposite surfaces of the gel, (Hadjipanayi et al., 2010). However, this method is also limited by the initial height of the gel and alters the final construct structure, creating greater top-bottom symmetry.

We hypothesised that as the multi-well PC system creates FLS on the top of the gel (upward fluid flow), there will be no progressive restrictions of the FLS during multilayering. Each new gel layer forms a new FLS when compressed. Theoretically, the thickness of each single layer is the main restriction, not their total number, as each layer is compressed individually through a new fluid leaving surface. By using this method, it would be possible to fabricate complex multilayered tissues with different cell-types or densities in each layer. It may also be possible to control cell infiltration between the layers, as it is known that increased stiffness of the matrix enchances motility of some cell types (Hadjipanayi, 2009).

Next, micro-moulding of the FLS has been evaluated in the multi-well format, using as a template laser-cut Kapton® masks. Kapton® is a polyimide film, developed by DuPont, and is known to be bio-compatible and support cell adhesion (Prichard, Reichert and Klitzman, 2007). The micro-moulding technique was combined with the multi-layering, in order to fabricate two-part channels. The idea was that a first layer, containing grooves, was effectively overlaid with a second layer

of collagen, which after compression would create a channel ‘roof’. Our hypothesis was that width of the grooves and viscosity of the collagen solution will prevent occlusion of the channel by the fresh, liquid collagen of subsequent (roof) layer.

Lastly, the possibility of direct delivery of the cells into the channels was evaluated with the view of creating an endothelial cell lining of the channel to potentially aid the vascularisation of the construct upon implantation.

The outcome of this work can lead to new generation of implantable constructs with complex micro-architecture comprising two vital tissue components: native, chemically or physically un-altered ECM and viable cells. Additionally, the knowledge gained in this work can help in substituting animal use in drug and cosmetics testing with 3D *in vitro* tissue replicates made using multiple compression technique as assays.

The hypotheses in this study can be investigated by testing the following objectives:

- average reduction in diameter of the soluble glass fibres along their length with time of incubation in PBS and shape of the channels in the compressed collagen constructs made using fibres with tapering cross-section
- dimensions (depth and width) of the grooves, formed during the process of plastic compression on the FLS and non-FLS and fidelity of the pattern to the template
- average fluid loss against time, rate of fluid loss and dynamics of fluid leaving surface formation during compression of the range of collagen gel heights in the multi-well format and weight and thickness of the resulting constructs

- qualitative assessment of layer separation of double-layered constructs following agitation and change in thickness of the constructs, brought in contact with fluid immediately after PC
- fluid loss from upper layer and progression of the compression process compared to the compression of the single layer in double-layered constructs
- effect of layering more than two (up to ten) gels on the construct morphology and fluid loss dynamics from the upper layer
- width and depth of the channels, produced by micro-moulding in double - layered collagen constructs
- efficiency of the cell delivery into the grooves during the micro-moulding of the gels.

Chapter 2

Materials and Methods

Methods and materials reported in this chapter have been used throughout the project. Any derivations or additions will be described in the Materials and Methods section of each Chapter.

Cells

In this project two cell-types were used as exemplary epithelial (HaCat) and matrix-embedded (corneal fibroblasts) cells respectively.

Human limbal fibroblasts (HLF).

HLF were a generous gift from Dr. Hannah Levis (Institute of Ophthalmology, UCL). The cells were obtained from cadaveric corneal rims with appropriate research consent and ethical permission from the Research Ethics Committee (UK) (Levis H., 2010). Explants were cultured on a tissue culture plastic in DMEM-Glutamax supplemented with 1% antibiotic-antimycotic (Invitrogen, UK) and 10% adult bovine serum (Sigma, UK) for up to one month. Expanded cells were cultured in DMEM supplemented with 1% penicillin-streptomycin and 10% foetal calf serum. Prior to seeding in constructs cells were lifted from tissue culture plastic with 0.05% Trypsin-EDTA, counted using hemaetocytometer and suspended in tissue culture medium.

HaCat cell line.

Spontaneously immortalized human keratinocyte line has been used for development of highly reproducible skin model (Kehe et al., 1999), and has been used in the present work to model epithelial cell effect on the surface of the construct. Cells, stored at -70ºC, were defrosted by rapidly bringing to the room temperature, resuspended in warm DMEM (4000 glucose content) supplemented with 1% penicillin-streptomycin and 10% FCS and plated in 250 mm^2 tissue culture flasks. Prior to seeding onto the constructs, cells were lifted from the tissue culture plastic

with 0.05% Trypsin-EDTA, counted using hemaetocytometer and suspended in tissue culture medium.

Collagen gel preparation

Collagen gels were neutralised using protocol from the original report on the method of plastic compression (Brown et al., 2005). The original method was based on uniaxial expulsion of fluid from hyperhydrated collagen gels under load. Gels were originally set in the double-pocket custom-made stainless steel moulds (3.2x2.3x0.9 cm) for 30 min at 37°C. After setting, gels were transferred onto the blotting elements (3 sheets of Whatman No1paper (Whatman, UK), stainless steel mesh and nylon mesh), covered with second nylon mesh and glass slide and compressed under load (120g) for 5 minutes. The process resulted in removal of >90% of water content from the gel and increase of collagen concentration in the construct up to 11% (Brown et al., 2005).

Acellular collagen gels

Acellular collagen gels we prepared by mixing rat-tail type I collagen (2.1 mg/ml protein in acetic acid (First Link, UK) with 10xMEM (Gibco) and DMEM (Sigma, UK) in proportion 80% (collagen):10% (10xMEM):10%(DMEM) and neutralized using 5M NaOH until change of colour (yellow to pink). This corresponds to pH of 7.4-7.8. All solutions were kept on ice prior to mixing. Neutralized collagen solution was kept on ice for 30 min to remove air bubbles. To initiate gel formation, the required volume of the neutralized solution was pipetted into each mould and brought to 37ºC. Gels were left to set for 30 minutes prior to compression.

Cellular collagen gels

When cell-seeded collagen gels were prepared, 80 % of acidic collagen solution was mixed with 10% 10xMEM and neutralised as before with 5M NaOH. Cells, suspended in DMEM (1% penicillin-streptomycin, 10% FCS), were added after

neutralization to prevent detrimental effect of low pH on the cells. All cell-seeded collagen constructs were prepared with $5x10^5$ HLF per gel.

Staining protocols

Live-dead staining

The effect of different treatments on cell population (embedded and surface cells) was assessed using fluorescent live/dead stains. Cellular constructs were incubated with 2 μm calcein acetoxymethyl ester (AM) and 4 μm ethidium homodimer 1 (calcein AM, Molecular Probes, UK) in sterile phosphate buffer solution (PBS) for 1 hour at 37ºC. Prior to viewing under the fluorescent microscope, samples were washed in dye-free PBS for 5 minutes. Under the microscope cells were identified and counted as live (colour green) or dead (colour red). This effect is based on the fact that cytoplasm of the live cells contains esterases that cleave membrane-permeable, non-fluorescent calcein AM and convert it to fluorescent calcein. Ethidium homodimer is membrane-impermeable (i.e. it cannot penetrate cells with the intact membrane). If cell membrane is compromised (indicative of cell death) the dye will bind to the nucleic acid of the dead cell producing red fluorescence. The percentage of live cells in the construct was calculated as follows. Images were taken of ten random fields of view and number of live (green) and dead (red) cells was counted. Percentage of the live cells in each field of view was calculated relative to the total number of cells. Data is presented as percent ± standard deviation (SD).

Hematoxylin-Eosin staining

Effect of the different culture periods (up to two weeks) on the morphology of the cellular constructs was assessed using hematoxylin-eosin (H&E) staining protocol. H&E is the most commonly used staining technique in animal histology and histopathology. The method is based on using two dyes with basic and acidic affinity. Hematoxylin is a basic dye and stains structures rich in acids (nuclei) blue; eosin is an

acidic dye and stains basic structures (cytoplasm and ECM) pink. Routine protocol was used in this study.

Sirius Red staining

Acellular constructs were stained with SiriusRed (DirectRed 80, CI number 3578, Sigma) to emphasise collagen fibres in the constructs especially with regards to fluid leaving surface and for morphological analysis. Modification of original technique was used here (Francis, 1990). The dyeing solution was prepared as follows. SiriusRed stock powder (0.5 mg) was dissolved in 45 ml distilled water and 50 ml of absolute alcohol after which 1 ml of 1% NaOH was added to the solution. Whilst stirring 20% NaCl was added to the mixture until a fine precipitate was observed. This solution was left overnight and filtered before use. Staining protocol included the following steps. Sections were dewaxed in xylene and rehydrated to water in descending alcohol series. After rinsing in 70% alcohol, sections were incubated with SiriusRed for one hour, washed in tap water, dehydrated and mounted prior to viewing.

Microscopy

Light and Fluorescent microscopy

Histologically stained sections and fluorescently labelled live and dead cells were visualized using Zeiss microscope and images taken using AxioCam digital camera (Zeiss, Germany). Image analysis was carried out using AxioVision image program.

Scanning Electron microscopy

Scanning electron microscopy allowed for high resolution quality three dimensional imaging of the surface of the samples. Samples were sputter-coated with metal alloy (here gold palladium) to ensure conductivity. The electron gun emits a beam of high energy electrons, in the range of 0-40 kV which are focused on the very

small spot on the sample by a series of magnetic lenses. The beam scans an area of the sample and emits secondary electrons from the surface which are counted by a detector, which send signals to amplifier. The image is based on the number of electrons emitted from each spot on the sample and whole image is reconstructed point-by-point by a scanning system. Samples need to be thoroughly dehydrated prior to imaging as process is carried out in the vacuum to ensure the direction of the electron beam. In this study, samples, fixed in 2% Glutaraldehyde in 0.1 M Sodium Cacodylate buffer (pH 7.4) at 4 °C overnight, dehydrated in ascending alcohol series at room temperature to Hexamethyldisilazane and left to dry overnight at room temperature. Dry samples were mounted on aluminium stubs, sputter-coated with gold palladium and viewed on a Joel scanning electron microscope (JSM 5500 LV) at voltage of 20 kV.

Statistical analysis

Appropriate statistical analysis for each study was carried out using SPSS 17 program for Windows. When two sets of data were compared *t*-test analysis was performed. Comparison of more than two sets of data was performed by first using one-way Analysis of Variance (ANOVA) to determine if there were statistically significant differences within the groups of data. If significant differences within groups of data were found ($p<0.05$) post-hoc tests were performed to determine which pairs of groups were significantly different. Levene's test for homogeneity of variance was conducted to access homogeneity of data distribution. If equal variances were assumed ($p>0.05$), Turkey's Honestly Significant Difference (HSD) post-hoc test was conducted. Otherwise, Games-Howel post-hoc test was conducted. In all cases data were considered significantly different at a confidence interval of 95% and probability (p) value <0.05. All numerical data are reported as mean ± SD.

Chapter 3

Integration of channels with controlled geometry in to the PC collagen constructs

Introduction

Regeneration of biomimetic tissue structure frequently involves guided directional ingrowth of cells and tissues in a predetermined direction for optimal spatial organisation. A key point of tissue engineering is the generation of 3D biomimetic structure and composition for any given target tissue and this can involve the need to tailor the integration processes to the recipient site location. Essential parts of functional integration are innervation and micro-vascular ingrowth from the surrounding tissue. For engineered constructs to truly become part of the host tissue, direction and guidance are important components. Rapid, directionless or even counter-direction ingrowth of nerves or blood vessels can cause actual damage in some instances. It has previously been shown that collagen constructs can be rapidly micro-channelled using soluble phosphate glass fibres via a lost fibre technique (Nazhat et al., 2007). The follow-up research showed that this modification of the dense collagen lattices leads to better perfusion of oxygen to the core of spirally rolled constructs compared to non-channelled control (Cheema et al., 2010). Cylindrical fibres of uniform diameter have been used to create these channelled constructs, and fibres dissolved at constant rate throughout the construct matrix (Nazhat et al., 2007). Therefore, in order to control the channel opening and therefore giving it desired direction, several techniques can be employed. As dissolution time of the fibres is controlled by chemical composition, one of the approaches could by to fabricate fires, consisting of fast and slow dissolving parts. When incorporated into the collagen constructs, these will dissolve slower at one end, allowing the ingrowth of cells,

whilst blocking the opening of the channel at the opposite end. However, it is technically challenging to prepare this type of blended fibres and will require thorough preliminary investigation. Another approach would be to prepare highly soluble fibres and give them conical shape as they are drawn during the process of fibre collection. The fibres are collected on a moving drum. The rotation speed of the drum is directly related to fibre diameter, whereas lateral movement speed controls spacing between the fibres. The whole process is akin to collecting a thread on the spool. Knowing that, it is easy to appreciate that with the current technology of fibre collection it is not possible to fabricate a continuous strip of conically shaped fires. The third approach is to fabricate a strip of fibres of uniform diameter and cylindrical shape and to fabricate a tapering cross-section later in a controlled manner. The resulting fibres, once incorporated into the collagen construct will dissolve in a specific direction, effectively creating dynamic, opened channels. As phosphate base glass fibres dissolve by surface hydrolysis, by changing the shape of the fibres, without changing their chemistry, the thinner end will disappear faster than thicker end, as shown schematically in Figure 1.

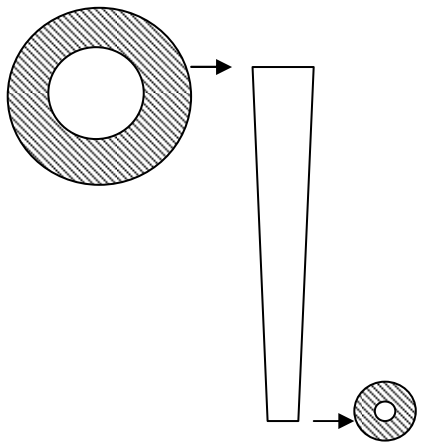

Fig 1. Schematic illustration of the dissolution dynamics of the conically shaped fibre. Patterned surface indicates diameter of the fibre at time 0, clear field is the diameter of the fibre at time n. As fibre dissolves, thinner end will disappear faster relative to the thicker end. That will potentially provide direction of cell ingrowth in the channel.

Therefore, the hypothesis is that soluble phosphate glass fibres will generate channels through constructs which open up in one direction to provide guidance over a predictable time course according to their dissolution rate. We propose that the most elegant way to achieve directional glass fibre dissolution (and so directional channel formation) is to fabricate conically shaped glass fibres. Gradual reduction of the surface area/volume of such soluble fibres would produce fibre loss and so faster channel formation in the chosen direction, by opening channel at one (thinner) end while the thicker end physically blocks counter-direction ingrowth. However, to achieve that result preliminary work is need to show that fibres with gradually changing diameter can be fabricated in a controlled manner. Another challenge is to integrate the resulting fibres into the plastic compressed collagen construct. Both will be explored in this chapter.

Phosphate based glass fibres have proved to be useful for tissue engineering as their dissolution rate can be tailored to a range of uses from hours to weeks or months (AbouNeel et al., 2005). Depending on the chemistry, phosphate glass can be pulled into fibres from 10 to 50 µm in diameter (Ahmed et al., 2004). Biocompatibility of these fibres has been shown for osteoblasts, myocytes, chondrocytes, and tendon fibroblasts and these fibres have been also proposed as reinforcing agents for cranial reconstructive surgery (Bitar et al., 2004, Bitar et al. 2005, Shah et al., 2005).

Collagen is probably the most widely used natural protein as tissue engineered scaffolds. However the mechanical properties of the native form of collagen scaffolds, i.e. hyperhydrated gels, are poor. Plastic compression is a novel method of engineering tissue-like implants, in a matter of minutes, without dependence on cell synthesis of the bulk matrix material, by rapid expulsion of liquid from the collagen-cell gel (Brown et al., 2005). Collagen scaffolds prepared by plastic compression are

mechanically strong and ideal matrix templates to test the idea of directional micro-channel formation. These can be used to improve biomimetic tissue engineering by virtue of their cell guidance and ability to improve deep perfusion even before vascularisation (Cheema et al., 2008, 2010).

In this chapter the method of the glass fibres shape modification will be described as well as the morphology of the channels in the collagen constructs, produced by incorporating conically shaped fibres made using this method. Following parameters will be investigated: (i) average reduction in diameter of the fibres along their length with time of incubation in PBS (ii) shape of the channels in the compressed collagen constructs made using fibres with tapering cross-section.

Materials and methods

Fibre preparation and construct assembly

Unidirectional glass fibres of composition ratio 0.5 (P_2O_5) : 0.25(CaO) : 0.25 (Na_2 O), average diameter of 40 μm and spacing of 70 μm were made using a fibre-drawing method described previously (Ahmed et al., 2004). Briefly, glass of composition 0.5 (P_2O_5):0.3(CaO):0.18(Na_2O): 0.3(Fe_2O_3) was melted in a furnace at 1050 ºC over a custom made fibre-drawing rig. Rotation speed of the drum allows control over diameter, and lateral displacement of the drum with time controls spacing between the fibres.

Fibres were fixed to a custom-made plastic ring (diameter 22 mm) to prevent them from adhering to each other after submersing into the buffer. The ring-mounted fibres were immersed into PBS, which acted as a solvent, to just cover the fibres as they hung vertically in the liquid. After each hour of immersion the level of PBS was reduced so that the liquid surface fell at a rate of approximately 3 mm/hr, with the hourly level reductions repeated over 6 hours. The process is shown schematically in

Figure 2. Plastic ring with the attached fibres is shown in Figure 3b. Resulting fibres were washed with 100% ethanol and air-dried before viewing and measurement by scanning electron microscopy (SEM) to calculate the rate of diameter reduction.

Construct assembly

The same fibres (still attached to the carrier rings) were used for incorporation into the plastic compressed (PC) collagen. Process is shown schematically in Figure 3a. Plastic compression process was carried out as described previously (Chapter 2). Briefly, acid-soluble type I collagen (rat tail, FirstLink, UK) was diluted with equal volumes of 10XMEM and DMEM and neutralised with 5M NaOH. The mixture was left on ice for 1 hour to remove air bubbles. Rings with conical fibres were fitted into the stainless-steel moulds and 3ml of collagen solution was set for 30 min at 37^0C (Figure 3c). The set collagen gels with fibres were transferred to the blotting paper sheets (Whatman, UK) and compressed for 5 min, as shown in Figure 3d with immediate fixation and dehydration for SEM analysis.

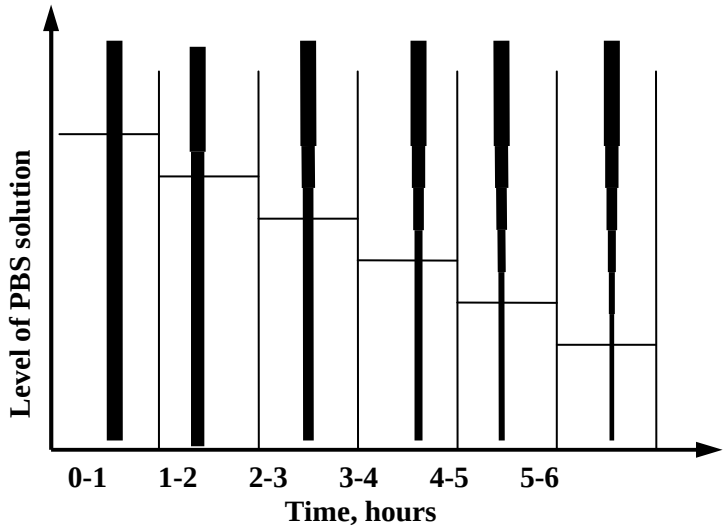

Fig 2. Schematic illustration of conical fibres fabrication process. Fibres, fixed onto a carrier ring, were immersed into PBS. The level of buffer was decreased

stepwise over 6 hours to create a tapering cross section towards the base of the fibre.

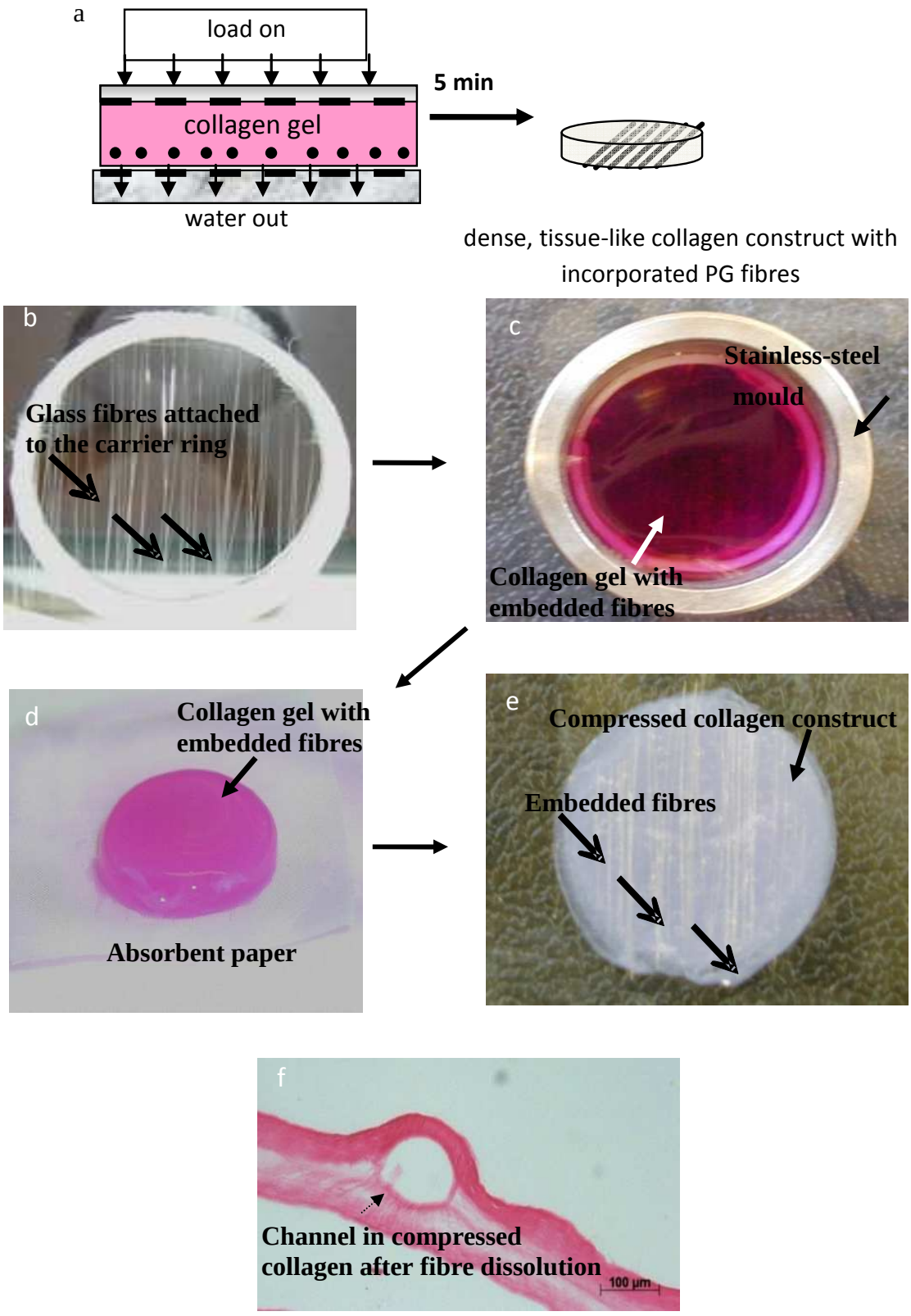

Fig. 3 Construct assembly. (a)Schematic diagram showing assembly of the plastic compressed collagen construct with incorporated fibres. Neutralized collagen is

set on top of the preformed fibres for 30 min and then compressed under load to produce dense construct with fibres, incorporated in the matrix. Plastic fibre-bearing ring (b) is inserted into a stainless-steel mould and filled with collagen solution(c). Set collagen gel is transferred onto blotting elements and compressed (d, loading not shown). Process results in a thin, tissue-like construct with incorporated conical glass fibres (e). (f) – histological image of the construct sectioned in transverse plane showing channel left by the fibre.

Imaging and image analysis

Wax-embedded constructs were sectioned in a transverse plane at a thickness of 12 µm and mounted onto glass slides. Samples were stained with Sirius Red using method described in Chapter 2. Sections were viewed by light microscope (Zeiss, Germany) and digital images taken (AxioCam, Zeiss, Germany).

For SEM imaging, constructs were treated as described in Chapter 2.

Statistical analysis

Data are presented as mean percentage change ±SD. Statistical analysis was carried out as described in Chapter 2.

Results

In this study parallel positioned soluble glass fibres were fixed on a supportive carrier and submerged in to the PBS as illustrated in Fig.1. The depth of liquid was gradually reduced by 3 mm/hr over 6 hrs. We hypothesised that by gradually reducing the length of fibre subjected in this way to the dissolution there will be a corresponding step-wise reduction in fibre diameter along its length. The reduction in the fibre diameter along its length will be a function of the glass solubility. Hence, fibre diameter will be inversely proportional to the dissolution time. To test this hypothesis the resulting fibres were subjected to SEM analysis to determine the change in diameter over the total length of the fibre. Measurements were converted into percentage change with respect to the initial untreated fibre diameter, to illustrate the dynamic of change in diameter and allow for differences in individual fibre

starting diameter. A specimen single fibre absolute diameter change is shown on the same plot. Reducing the volume of the solvent by 3 mm hourly i.e. decreasing the exposure time of the top section of the fibre (while leaving the remainder of the fibre immersed in the solvent) over 6 hrs resulted in a significantly smaller diameter at the bottom end (i.e. the longest exposure), compared to the upper end, which was effectively initial fibre diameter.

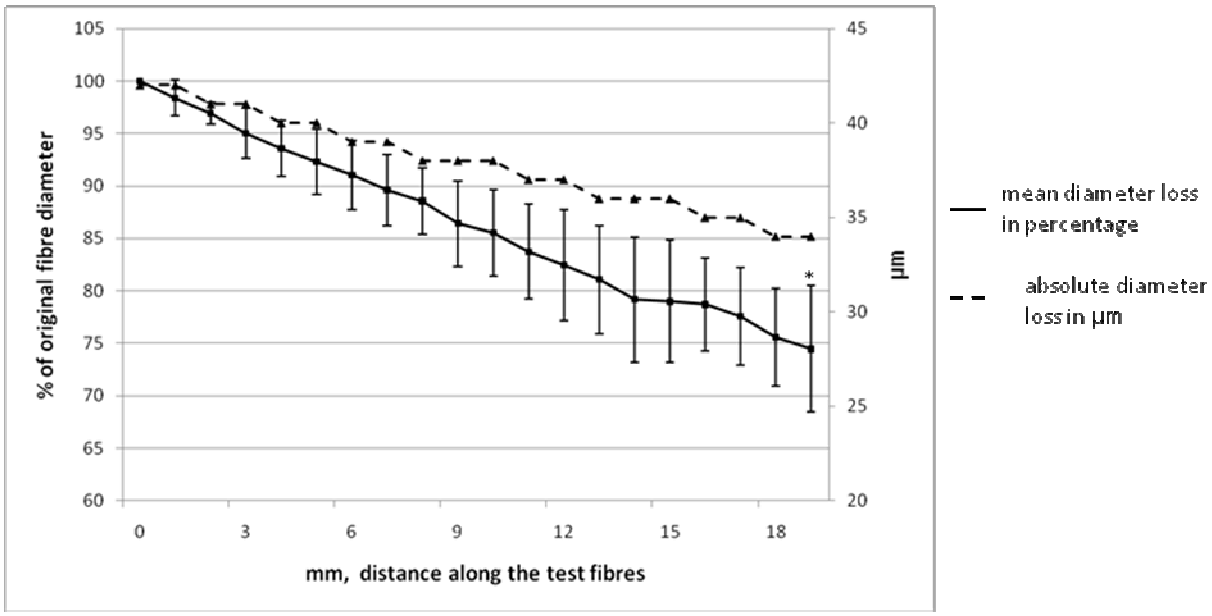

Fig. 4 Graph illustrating loss in fibre diameter along the fibre length(mm). Primary vertical axis - mean diameter loss over the length of phosphate based glass fibres after treatment in percent ± standard deviation (n=20). Measurements were taken at each mm over the length of the fibre, 3 mm correspond to 1 hr exposure to PBS. Note the linear fall in diameter of 25% over ~ 20mm of cumulative fibre length. * p<0.001, start and end point of treatment. Absolute diameter measurements for one specimen fibre are plotted on the secondary vertical axis and confirm diameter loss over the fibre length.

Gradual dissolution of the soluble glass fibres resulted in approximately 25% reduction in diameter over 2cm of fibre length, which corresponds to 6 hrs immersion in the PBS compared to time 0. (Figure 4, Figure 5a). This represented a statistically significant linear reduction in diameter along the fibre length. The mean fibre diameter at time 0 was 34.65±8.13 µm and fell to 25.8±7 µm after 6 hrs submersion. The mean loss in diameter for 20 fibres was 8.85±2.8 µm over 19.5 mm (6 hrs),

giving mean rate of change 0.5 µm per mm of fibre length or 1.5 µm per hour. For the chosen specimen fibre the total absolute loss in diameter was 9.2 µm, changing from 36 µm at time 0 to 25.8 µm after 6 hrs.

A standard plastic compression was performed to incorporate the preformed conical fibres in to the collagen construct as shown schematically in the Figure 3a. As described previously (Brown et al., 2005), process involves removal of 98% water from hyperhydrated collagen gel. Incorporation of the glass fibres into this process has been described by Nazhat et al. (2007). The process is based on setting collagen hydrogel with the fibres *in situ*. Collagen gel and incorporated fibres then undergo the process of compression, which leads to formation of collagen lattice with the fibres in the matrix. For the method described here, same process was used. Fibre bearing ring (Figure 3b), was inserted into the stainless steel mould and collagen gel was cast on top as shown in Figure 3c. Set gel was transferred to absorbent paper on a nylon mesh support and compressed (Figure 3d, load not shown) to force most of its fluid content into the absorbent layer below. Plastic compression resulted in thin (50 µm), tissue-like constructs, 22 mm in diameter, with incorporated uniaxial fibres (Figure 3e). When these dissolve, they left behind open channels as shown on histological section in Figure 3f.

The resulting constructs were processed for viewed using SEM to confirm incorporation of the fibres into the construct. Images confirmed inclusion of the fibres into the collagen matrix with the channels mirroring the shape of the fibre (Figure 5b).

a

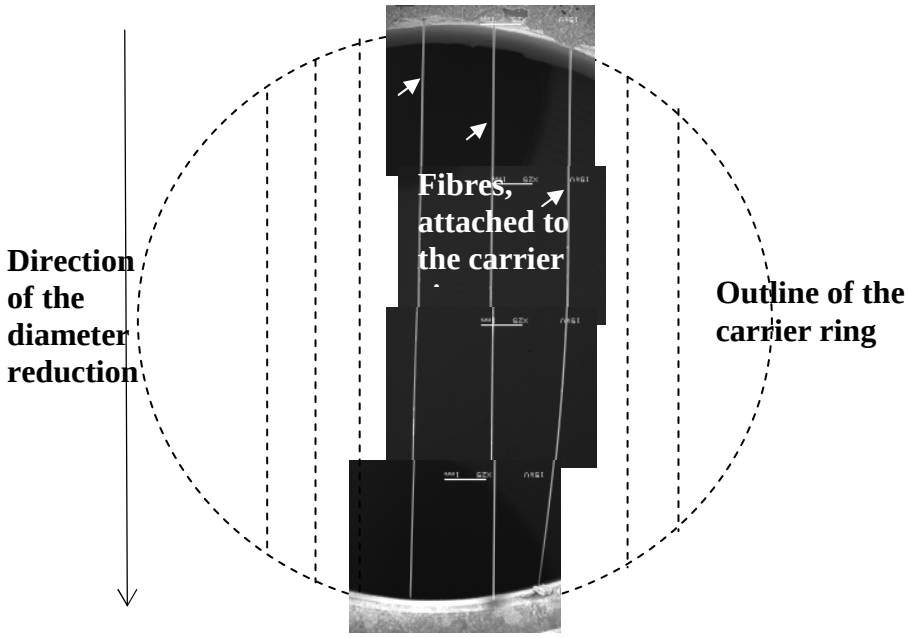

b

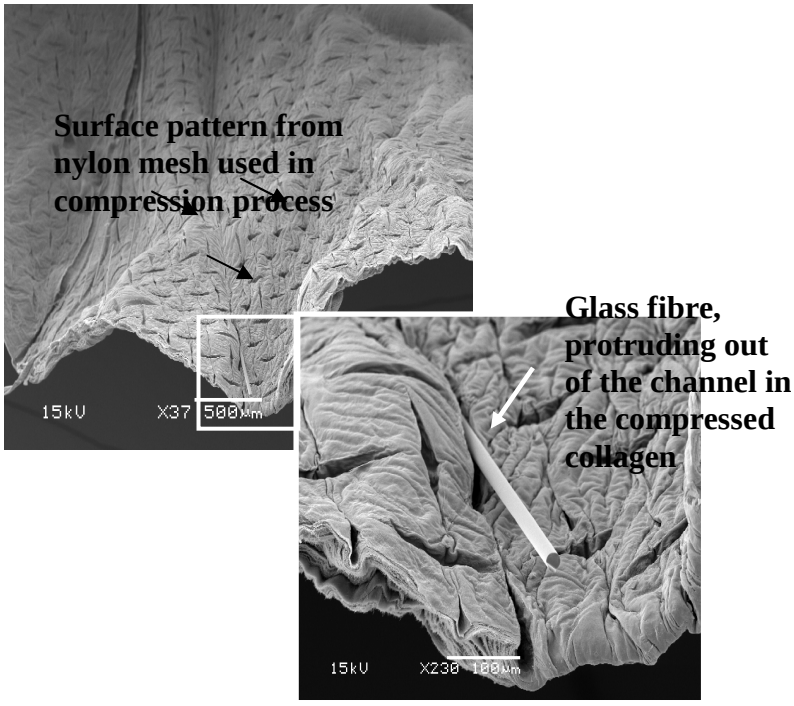

Fig. 5 (a) Reconstructed SEM image of conically shaped phosphate fibres. Fibres were fixed on a plastic ring and submersed in to PBS. Level of buffer was gradually reduced over 6 hours giving conical shaped fibres. Arrow heads indicate individual fibres, arrow shows the direction of diameter reduction. (b) SEM image of plastic compressed collagen construct with incorporated conical glass fibre. Collagen gel was set with preformed conical fibres and compressed under load.

Discussion

In this chapter it has been demonstrated that the solubility and micro-channel forming capacity of phosphate-based glass fibres can be used to generate potentially dynamic and complex structures within engineered collagen tissues. This effect can be achieved by controllably manipulating the shape of the fibres. Following parameters have been investigated: (i) average reduction in diameter of the fibres along their length with time of incubation in PBS (ii) shape of the channels in the compressed collagen constructs made using fibres with tapering cross-section. The results show that there was an inverse correlation between the time of incubation and the diameter of the fibre, so that gradual reduction in the diameter of the fibres was achieved, resulting in the tapering cross-section. When these fibres were incorporated into the plastic compressed collagen construct, formed channels reflected the shape of the fibre, so that when the latter gradually dissolves, it will not only potentially impart directional tissue ingrowth but indeed determine the shape of the resulting channel, which would be conically shaped rather than cylindrical. This could have potential effect on the oxygen perfusion dynamics through the construct. Recent report by Ahn et al. (2010) showed that shape of the pore affects oxygen diffusion in two and three dimensional scaffolds. The authors conclude that cone-shaped pores with diameter gradient support better cell viability and proliferation in the long-term culture (up to three weeks) as a result of higher oxygen concentration in the cone shaped channels compared to cylindrical.

Conical phosphate glass fibres described here show in principle that it will be possible to form micro-channels through a construct which open up in specific direction, over time. This principle could be employed to direct and control the rate of neurite and capillary ingrowth. In a separate study we have demonstrated that even in

a worst case, very rapid dissolution of high density soluble glass fibres in the presence of particularly sensitive cells (Schwann cells) in the collagen, the loss of cell viability was manageable (35%). This means that even cells adjacent to fibres would be unlikely to be damaged by SPG dissolution products.

Importantly, the demonstration that differential dissolution times will produce definable conical profile fibres is also proof of concept that the same process will occur on implantation. Given that this effect has been demonstrated *in vitro*, it is likely that the same surface area:volume dominated rate of fibre loss will produce a time-dependant channel opening (thin to thick fibre direction) *in vivo* after implantation. The simple channelling effect (without direction) has already been shown to form patent structures with continuous lumen right through the full length of such collagen constructs (Nazhat et al., 2007). This system will be tuneable, in terms of rate, direction and diameter of dynamic channelling by changing the conical pattern, glass chemistry, density of fibres and even through using a mix of fibre diameters.

The concept of directional pores is of particular importance for vascular and nerve tissue engineering as well as in the maintenance and survival of thicker implants. Progression from 2D to 3D engineered tissues accentuated the problem of oxygen and nutrients delivery to the centre of the construct and the importance of guidance has been recognised for nerve repair. Furthermore, bridging of the glial scar around spinal cord injuries is now a major clinical problem which could be solved by time and direction controlled channel formation. It seems possible to divide existing methods into two distinct groups – production of open aligned pores or use of parallel polymeric fibres (natural or artificial) embedded into the supportive material or on their own. Formation of tubular aligned pores has been demonstrated for chemically

cross-linked gelatin (Van Vlierberge et al, 2008), collagen (Van Vlierberge et al, 2008, Bozkurt et al., 2007) and agarose (Stokols and Tuszynski, 2004) using freeze-drying techniques. Microfibre templating of poly(2-hydroxyethyl methacrylate-co-methacrylic acid) and agarose hydrogels produced constructs with aligned micropores (Madden et al, 2010, Stokols et al., 2006).

Customised moulds have been used to give a construct with uniaxially aligned pores in poly(DL- lactide-*co*-glicolide) and polylactic co-glycollic acid (Krych et al., 2009, Sundback et al., 2003).

Silva et al. (2006) reported on successfully fabricating hydroxyapatite and poly(DL-lactic acid) constructs with parallel channels by either forming constructs around steel needles with known diameter or by using computer-controlled drill. Parallel aligned pores were created in alginate/hydroxyapatite composite constructs by ionotropic gelation (Dittrich et al., 2007) and laser microablation has been used to produce pores in poly(glycerol sebacate) substrate (Guillemette et al., 2010).

Simple inclusion of spider silk fibres (Allmeling et al., 2008, Huang et al., 2007), electrospun PLGA fibres (Aviss et al 2010), Bioglass® (Bunting et al., 2005), aligned PLLA filaments (Cai et al., 2005), polydioxanone fibres (Chow et al., 2007) among others have been used to align cell/tissue ingrowth. Poly(ethylene terephthalate) fibres, covered with human umbilical cord vein cells and embedded in fibrin were proposed for vascularisation of tissue engineered constructs (Hadjizadeh and Doillon, 2010).

Use of sacrificial structures for pore formation in the bulk material has been used for synthetic and natural polymers. The rationale behind using sacrificial structures is to create open pores, usually in the block scaffold, by introducing soluble materials (usually in fibrous form), which upon degradation will leave behind a

channel; alternatively block polymer (PMDS (Verma et al., 2006, Perry et al., 2007)) can be cast around a structure (fibre), which can be manually extracted after polymer hardening. Several materials have been proposed for this use. Golden and Tien (2007) used micro-moulded gelatine mesh embedded in collagen and fibrin hydrogels to create micro-channels. Vernon et al. (2005) used paraffin as sacrificial structure in air-dried collagen membranes. Li et al. (2009) used sucrose fibres, embedded in poly (l-lactic acid)/chloroform base to fabricate aligned pores. Gafni and colleagues used highly degradable biomaterial (PEG – lactic acid co-polymer). Endothelial cells, seeded on top of these fibres formed a monolayer. When these cell-covered fibres were tested *in vivo*, polymer filaments degraded leaving tubular structures of endothelial cells that became perfused vessels (Gafni et al., 2006).

It is evident that a variety of techniques can be used to either produce open aligned pores or aligned fibres, but it is still a challenge to engineer a number of parallel channels with high degree of control over direction and diameter. Here, we not only confirm previous results using a lost fibre technique but also demonstrate the possibility of making constructs with inbuilt control over vascular/nervous tissue ingrowth.

In conclusion, our results open the potential for new levels of engineering and control of implant – directionally controlled integration with host cells and tissues.

Integration of the channels in the body of the collagen construct could be viewed as one of the methods to increase construct complexity and impart micro-architecture necessary for correct tissue function. In addition to internal structure, external features (i.e. on the surface) are also potent ways to enhance construct bio-complexity. In the next Chapter the methods and mechanisms of controllable formation of such topological features will be explored.

Chapter 4

Engineering stable topological features in the PC collagen constructs

Introduction

One of the most direct approaches to manipulate cell behavior *in vitro* is to provide them with anisotropic surfaces, capable of orientating or polarizing their morphology (Curtis and Riehle, 2001). To date our knowledge of how various topographical features, from micron- to nano-scale, affect cell differentiation, proliferation and morphology is extensive in some areas but incomplete in others, in particular with regards to cell behavior on patterned surfaces of natural-polymer based scaffolds (Nelson and Tien, 2006). However, the knowledge of the cellular responses to topological features on micro- and nano-scale based on synthetic rigid substrates suggests that this is a simple and powerful tool to increase bio-complexity of implantable scaffolds.

Amongst the methods available for introducing topography onto substrate surfaces photolithography, etching, soft lithography and hot embossing are widely used (Folch and Toner, 2000, Falconett et al., 2006). However, many of these methods are designed for patterning glass, silicon, metals or rigid plastics, which are not bio-mimetic and so less useful for tissue engineering. Since much of our knowledge of cell behavior on patterns is based on these stiff, non-bio materials, recent efforts have begun to focus on the ability to produce known patterns on the bio-compatible and bio-degradable substrates with bio-mimetic stiffness, in particular those, based on the naturally derived polymers (Nelson and Tien, 2006) using variety of techniques. Photolithographic techniques are widely used to fabricate controllable patterns on the variety of surfaces. In particular soft embossing is a method of choice patterning surface of fragile materials such as hydrogels (Folch and Toner, 2000).

Both synthetic and natural materials can be micro-molded using this method and require an elastic poly (dimethylsiloxane) (PMDS) template with desired pattern as a negative mask or use of patterned PMDS as a substrate. Kobel et al. (2009) developed a method of soft embossing to micro-patterned poly(ethylene glycol) (PEG) hydrogels. Patterned template was imprinted onto partially cross-linked hydrogel and when the cross-linking was completed, features were permanently embossed onto the surface of the gel. This technique was used to create an analytical platform to study the behavior of single stem cells. Using soft lithography and micro-fabrication techniques, Mata et al. (2009) reported fabrication of three-dimensional scaffold, by stacking patterned PMDS membranes. Behaviour of mesenchymal stem cells was investigated by Lee et al. (2008) on a micro-patterned poly(l-lactic acid) substrate. Naturally derived polymers such as chitosan, gelatin and collagen hydrogels can be patterned in this manner (Wang and Ho, 2004, Nelson et al., 2008).

Soft lithography is the only available method up to date to pattern the surfaces of dense collagen membranes. Pins, Toner and Morgan (2000) used it to pattern gelatin and collagen membranes with ridges and channels by air-drying and thermal dehydration (105ºC in vacuum) of small quantities of protein solution poured onto a negative PDMS mask. This method produced thin (10-20 µm) membranes, conformed to the pattern. To fabricate thick constructs, the authors laminated patterned membranes onto collagen sponges and these were evaluated as an analog of the basal lamina in skin (Pins et al., 2000). This method was used to micro-pattern chitosan membranes with addition of selective non-adhesive regions for cell-patterning and micro-patterning of collagen films for intestinal tissue engineering (Wang et al., 2010). Vernon et al. has reported patterning of thin collagen membranes by extensive air-drying of hydrated gels (24-48 hours at room temperature) against a

negative mask with ridges and shown alignment of fibroblasts seeded on these patterned matrices (Vernon et al., 2005).

These methods of pattern formation in the natural polymer scaffolds are based on conformation of the polymeric hydrogel to the underlying patterned surface as a result of extensive air-drying and thermal dehydration. In effect, the result is a patterned membrane, surface of which is used to investigate cell behaviour. These micropatterned membranes may prove useful to investigate cell responses to the patterns on the natural polymer surface, but, on their own, can hardly be regarded as a tissue engineered construct. Indeed, as shown by Pins et al., these membranes need to be attached to a freeze-dried collagen sponges to be regarded as a skin model. Indeed, this indirect approach to the construct engineering, where the composition and micro-architecture are designed first and cellular component is added at later stages is in stark contrast to a more direct approach taken in the current study.

Using the first approach, the ideal design of the acellular construct can be compromised by the addition of the cellular population. Firstly, even distribution of the cells throughout the construct needs to be achieved. If the construct is pre-formed, with the pre-determined porosity and pores interconnections some form of physical agitation is needed to infiltrate construct with the cells, which is usually difficult to control. Even if this was successful, the mere fact of addition of the live cell population will inevitably change the morphology of this ‘ideal’ construct when cells start laying down their own matrix, therefore changing exactly those parameters that were so carefully designed in the first place. The method of plastic compression is an example of a direct approach, where the starting point of the construct fabrication is a weak hydrogel with the embedded cells. All the subsequent manipulations to increase the mechanical properties of the construct or indeed the surface topology needs to be

designed and introduced in a way that takes into account cellular activity and its effect on the end-product and, at the same time are bio-compatible, i.e. do not have detrimental effect on the embedded cells viability or function. Another example of this approach is to increase the mechanical properties of the collagen hydrogels by cell compaction as pioneered by Bell et al. (1979). However, introduction of the pattern into the collagen hydrogel surface where subsequent cell compaction of the gel is allowed will lead to the unpredictable distortion (shrinkage) of the initial template pattern. As formation of the surface topology will add to the bio-complexity of the PC constructs, the technique must be developed in a way that complies with these requirements. In this chapter a novel method of pattern formation on the surface of dense collagen constructs will be described and mechanisms of pattern formation will be discussed.

Plastic compression (PC) of collagen allows fabrication of dense, tissue-like scaffolds with cells embedded in the matrix prior to construct assembly. It uses rapid, uniaxial expulsion of water from hyper-hydrated gels to generate controlled-density 3D tissues in minutes. Cells can be seeded in to the collagen prior to compression and the process does not affect cell viability. In addition, other cell-types (eg. epithelial) can be seeded onto the surface once it is fabricated. This technology has been proposed for a number of TE applications, such as skin (Ananta et al, 2009, Hu et al., 2010), cornea (Levis et al., 2010) , bone (Pedraza et al., 2010), bladder (Micol et al., 2011) and spinal cord repair (East et al., 2010), together with basic research in tissue interfaces and vascularisation strategies (Hadjipanayi et al., 2009a, Cheema et al., 2010), oxygen diffusion (Cheema et al., 2008, 2009) and cell behaviour in dense collagen matrices (Hadjipanayi et al., 2009b, Serpooshan et al., 2011). Furthermore,

use of this material as a peripheral nerve repair conduit is currently under investigation.

When initially described it was noted that images of the surface of the PC collagen surface retain a stable embossed pattern of the nylon mesh (Fig.1) (with woven fibers of dimensions ranging from <1 to >100 µm), which was used as a support. This suggested that it will be possible to introduce controlled topological features in the surface of the constructs by impressing a negative pattern of known shape and dimensions. For the purpose of this study we chose parallel-aligned, evenly spaced glass fibers, whose diameter and spacing can be easily controlled during the manufacture process (Ahmed et al., 2004).

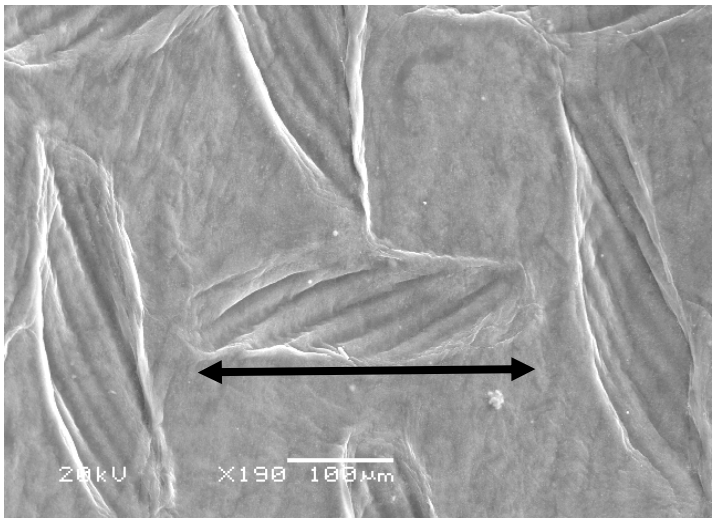

Fig. 1 SEM image of the PC collagen surface with the impression of the nylon mesh which was used as the part of the compression process. Clear negative image of the interwoven fibres is visible (double arrow).

Plastic compression produces an asymmetric layered structure in the construct, different at the two opposite surfaces, top and bottom, as the non fluid leaving surface (non-FLS) and fluid leaving surface (FLS) respectively (Brown et al., 2005, Hadjipanayi et al., 2010). It is known, that the two differ in mechanical properties, as directional expulsion of liquid leads to the formation of much denser layer closest to

the blotting elements than the opposite surface, creating a surface anisotropy which could affect the outcome of patterning. This anisotropy in collagen density (and by extrapolation matrix stiffness), as reported by Hadjipanayi et al. (2009c) between the top and bottom of the gel, could potentially affect the outcome of patterning. On this basis four different experimental setups of template patterning were used, to test the effect of matrix density and stiffness differences at each surface. In the first two setups the pattern template was introduced onto the non-FLS or FLS simultaneously with the compression, while in the latter two setups patterning was performed following partial compression, once the two surfaces had been formed.

The second part of the study aimed to test the effect of cellular remodeling on the stability of the resulting patterned topography by comparing the dimensions (width and depth) of grooves formed in acellular constructs and constructs seeded with human limbal fibroblasts (prior to patterning), over a two weeks culture period.

In this chapter development of the technique to form a stable surface topology in the compressed collagen constructs will be described. The following parameters will be investigated: (i) dimensions (depth and width) of the grooves, formed during the process of plastic compression on the opposite surfaces of the constructs (ii) fidelity of the pattern, formed on these surfaces to the dimensions of the template (iii) fidelity of the pattern on the fluid leaving surface of the plastic compressed constructs with and without embedded cells to the patterning template after two weeks in culture.

Materials and Methods.

Preparation of acellular and cellular collagen gels.

Collagen gels we prepared as described previously (see Chapter 2). For cell-seeded gels, collagen solution was mixed with 10xMEM, neutralised as before and mixed with $5x10^5$ Human Limbal Fibroblasts.

Glass fibres template preparation.

Phosphate based glass fibres were prepared as described previously (Ahmed et al. 2004). As shown by Abou Neel (Abou Neel, 2006), fibre-collecting drum, moving around its axis with rotating speed of 100 RPM and horizontally along its axis with a step of 50 Hz will result in average fibre diameter of 50±8 µm with spacing of approx. 100 µm between the fibres. Fibres of diameter of 70±12 µm were used when stability of the pattern was determined in the cell-seeded constructs.

To form a mask for patterning study, resulting fibres were lifted from the drum by placing two strips of adhesive tape perpendicular to the direction of the fibres on the drum with spacing of 2 cm (short axis of the mould, used to form collagen gel). Each pattern mask contained 20 fibres per collagen gel on average. When used in sterile conditions fibres were sterilised with UV light irradiation for 30 minutes on each side.

Experimental designs and constructs patterning.

In order to determine a way to introduce stable topographical features onto PC collagen constructs and investigate the mechanisms of such patterning, the following experimental set-ups were investigated:

1. Simultaneous PC and patterning:

    1a. PC+ Pattern on the FLS

    1b. PC+Pattern on the non-FLS

2. Consecutive PC and patterning:

    2a. PC, Pattern on the FLS

    2b. PC, Pattern on the non- FLS

Schematic presentation of experimental set-ups is shown in Figure 2.

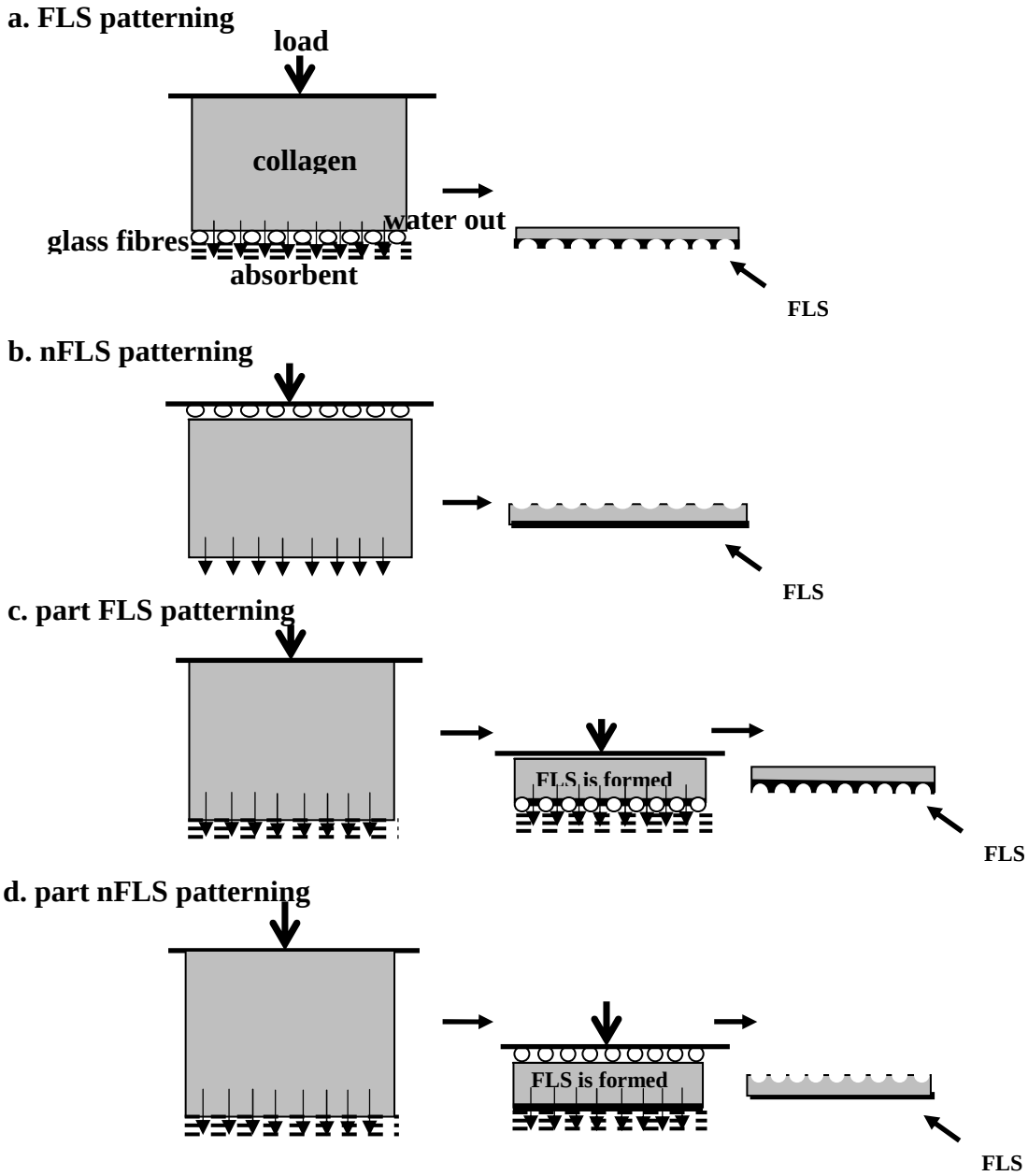

Fig. 2 Schematic illustration of the four experimental designs used. Simultaneous patterning of the FLS (a), the template (strip of glass fibres) is placed between the gel and absorbent prior to compression, and nonFLS (b), where glass fibres are placed on top of the gel prior to compression. Consecutive patterning, where the gel is pre-compressed for 2.5 min and pattern is either pressed into the formed FLS (partFLS) (c), or non FLS (part nonFLS) (d) for further 2.5 min.

For set-up 1a (Figure 2a), a strip of glass fibres (3 cm) was placed on three layers of filter paper (Whatman 1, Whatman, UK). The set collagen gel was transferred onto the fibres, covered by a glass slide and compressed under load for 5 min, as per standard protocol (Brown et al., 2005).

In protocol 1b (Figure 2b), collagen gel was placed in the same manner onto the blotting elements and glass fibre pattern was positioned on top of the gel, which was then compressed as above.

For protocol 2a and b (Figure 2 c and d), gels were pre-compressed on the filter paper for 2.5 min. In protocol 2a, the partially compressed gel was lifted from the filter paper and (as in 1a) placed on a patterning template with the glass fibres facing FLS. In 2b, the glass fibre template was placed on top of pre-compressed gel (i.e. non FLS).

All constructs after assembly were left in PBS overnight and fixed the following day in either 10% neutral formalin solution for histological examination or 2.5% glutaraldehyde for SEM imaging.

Imaging and image analysis

Wax-embedded constructs were sectioned in a transverse plane at a thickness of 12 µm and mounted onto glass slides. Acellular samples were stained with Sirius Red (see Chapter 2), cellular constructs were stained using standard hematoxilin and eosin (see Chapter 2).

For SEM imaging, constructs were treated as described in Chapter 2.

Dimensions of the grooves made using different experimental designs

It has been shown that the method of collagen PC normally creates two different structures at the fluid leaving surface and opposite surface with different mechanical properties (Brown et al., 2005, Hadjipanayi et al., 2010). In other words, collagen

structure is asymmetrical along the principle axis of fluid movement. Our hypothesis was that this asymmetry will leave the two surfaces with different abilities to accept and retain the pattern. To test this, width and depth measurements of each microgroove produced using four experimental designs were compared. Width was measured as the distance between two points in the opposite sides in the widest part of the groove; depth was measured as the perpendicular distance from the 'width' line to the deepest point in the groove base. Therefore template fibre radius (25 µm) was the expected groove depth as this was measured to the width (diameter) line. Expected groove width was the diameter of the template fibre - 50 µm on average. Total of 30 grooves (10 grooves per construct) were measured for each condition of each treatment.

To assess pattern fidelity a patterning coefficient was calculated as the ratio of depth to width for each measured groove. Coefficients of 0.5 represent near perfect fidelity based on the fibre dimensions where groove width equals fibre diameter (50 µm), groove depth – fibre radius (25 µm).

Statistical analysis

Statistical analysis was performed as described in Chapter 2.

Results

Dimensions of the grooves made using different experimental designs

Figure 3a summarises the width-depth measurements for the 4 treatments as measured on histological images. It is clear that groove widths were significantly reduced and groove depths significantly increased where template was pressed into the FLS either simultaneously or consecutively with compression. Groove dimensions (Figure 3a) impressed into the FLS (i.e. template was between the gel and absorbent layer, treatment 1a, Figure 2a) produced grooves of 55±11µm mean width (expected

value - 50 µm) and 25±7µm mean depth (expected value – 25 µm). These correspond with the mean diameter and radius of the glass fibres, used as the patterning mask, as predicted. Similar results were obtained when gels were partially pre-compressed, with the template pressed into the preformed FLS (design 2a, Figure 2c). Mean groove width and depth were 50±12µm and 19±8µm respectively.

SEM images (Fig. 4 a and c) show a well defined pattern of continuous parallel grooves on the fluid leaving surface of these forms of compressed collagen constructs. Interestingly, images in cross-section show that grooves in the fluid leaving surface are not confined to the uppermost layer of collagen but also affects underlying collagen matrix. This effect is absent on the images of the patterned nonFLS surfaces.

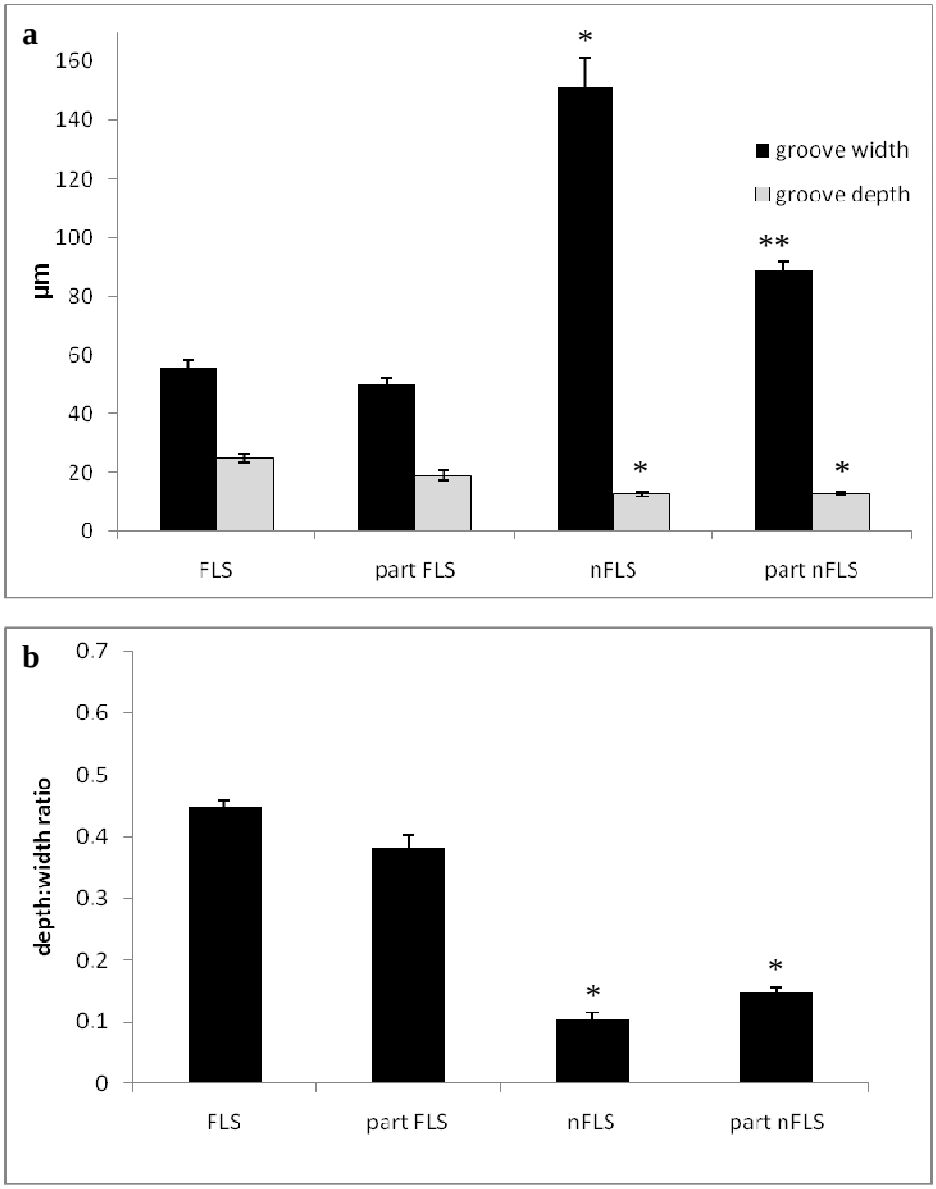

Fig. 3 Graphs of (a) average dimensions (width and depth) of the grooves on the surface of PC collagen constructs introduced into the FLS throughout compression, into the FLS following partial compression, into the nonFLS throughout compression and into the nonFLS following partial compression. (b) – plotted patterning coefficients (width:depth ratio) for the same experimental treatments as in (a). * - $p<0.05$ compared to FLS and part FLS, ** - $p<0.05$ compared to FLS, part FLS and nonFLS.

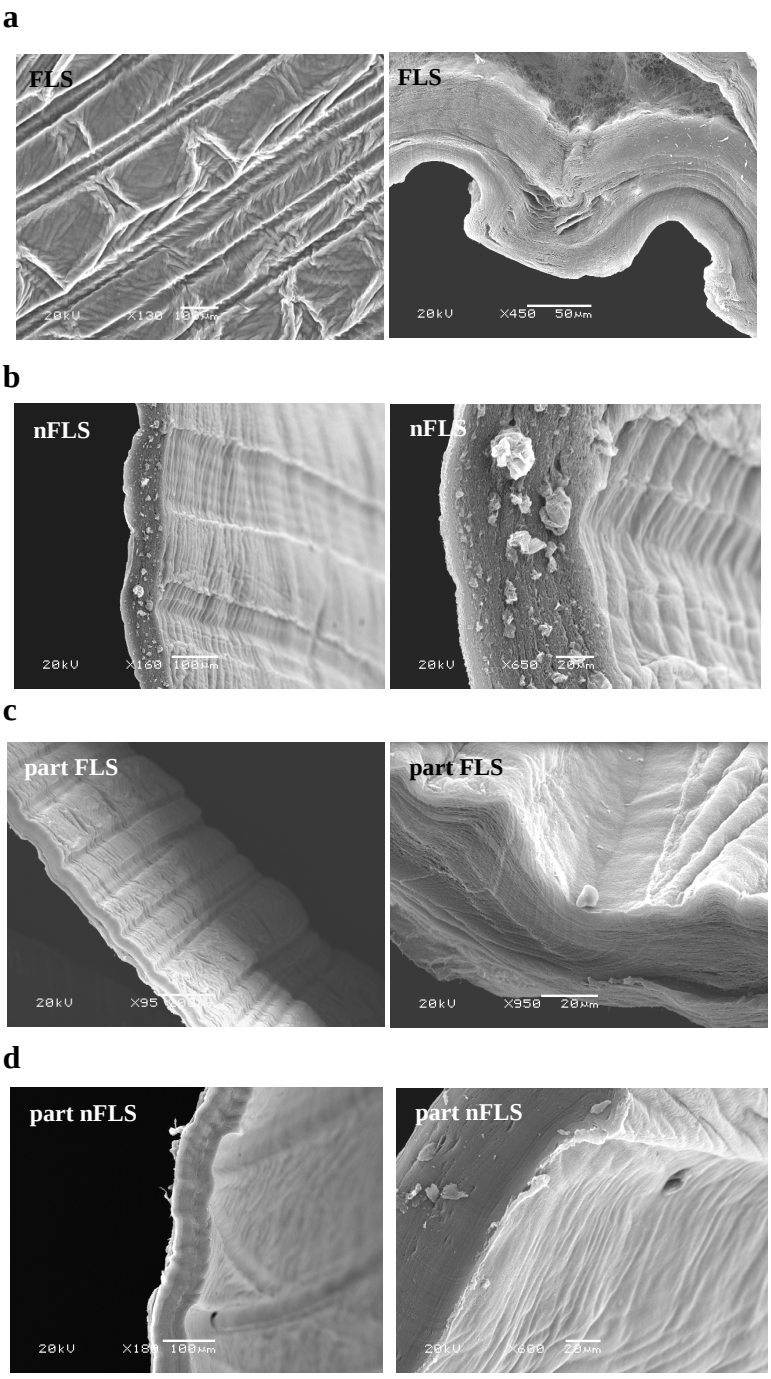

Fig. 4 Representative SEM images of the PC collagen constructs. (a) – surface of the construct (left) and profile of the grooves (right) on the FLS; (b) same on the nonFLS (nFLS); (c) – FLS of the partially compressed gel (partFLS); (d) – nonFLS of the partially compressed collagen (partnFLS).

Histological images of the transverse sections of the constructs (Figure 5 a and c) confirmed that the profile of the grooves corresponded with that of the cylindrical fibre.

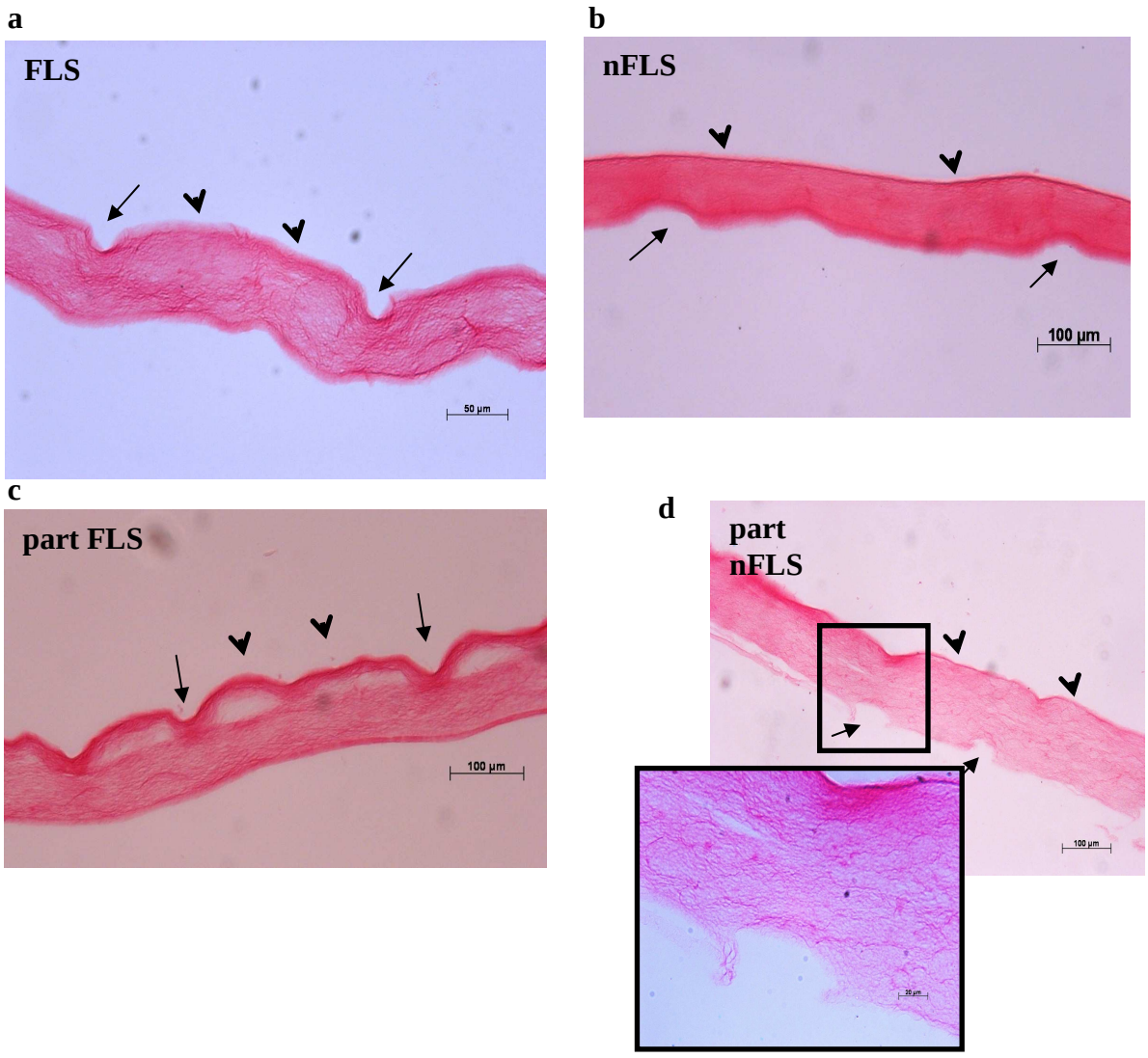

Fig. 5 Representative histological images of the PC collagen constructs with patterns pressed into the FLS (a), non FLS (b), FLS of the partially compressed gel (part FLS, c) and non FLS of the partially compressed gel (part nFLS, d). Sections were stained with Sirius Red. Arrows indicate grooves, arrow heads indicate the fluid leaving surface. Insert – higher magnification of the highlighted region. Please note: discoloured regions in (c) are artefacts of staining.

When fibres were placed on top of the gel prior to compression (treatment 1b, Figure 2b), the resulting grooves were 151±50µm wide (expected value - 50 µm) and

10±2.7µm deep (expected value - 25 µm) (Figure 3a). SEM images of the surface of the gel show parallel running marks left by the template fibres (Figure 4b) and histological images confirm formation of wide, shallow grooves (Figure 5b). Similar patterns were produced where the template was impressed into the non fluid leaving surface (top) of pre-compressed gels (treatment 2b, Figure 2d). In this case, dimensions of the measured grooves were 89 ±14µm wide (expected value - 50 µm) and 13±3.5 µm deep (expected value - 25 µm). The 70% increase in width between grooves with and without pre-compression was statistically significant (Figure 3a). Again SEM images showed shallow impressions of parallel tracks in the non-fluid leaving surface (Figure 4d), confirming the histological images (Figure 5d).

Fidelity of the grooves to the patterning template

The difference between FLS and nonFLS treatments was most evident when fidelity of the groove pattern to the glass fibre template was compared. Average pattern coefficient for the 4 treatments is shown on Figure 3b.

Patterning of the fluid leaving surface both simultaneously and consecutively with compression resulted in pattern with good fidelity in both cases (fidelity coefficient of 0.45±0.05 and 0.38±0.07 respectively). However coefficients for the non FLS treatments were 0.1±0.06 and 0.15±0.04 respectively, 4 to 5 times less than expected.

Thus, FLS patterns were excellent replicates of the template in size and depth but nonFLS grooves were as much as 3 times wider and 2.5 fold less deep. Clearly, there was a consistent and extensive remodelling of the initial impression in nonFLS treatment. In this the groove floor appears to have recoiled back almost to the surface, resulting in the shallow grooves. However, the increased width of the grooves

suggests that the elastic rebound was confined to the spaces between the grooves and not the floor of the groove.

Pattern stability in tissue culture conditions

To determine stability of the grooves in culture, constructs with and without cells were cultured for up to 14 days. For cell-seeded constructs cells were introduced prior to gelling and compression as per standard plastic compression protocol (Brown et al., 2005). Constructs with and without embedded cells were cultured over time to assess for possible effects of the reswelling of the constructs and cell remodelling on the pattern.

Constructs were produced by patterning on the FLS simultaneous to the compression (Fig.2a), as these had the grooves with the highest patterning coefficient. As shown in Figure 6 there was no significant difference in mean patterning coefficient of grooves generated in cell-seeded constructs, over 14 days of culture (patterning coefficient ranging from 0.47 (day 0) to 0.5(day 14, not significant), suggesting that active cellular remodelling had not altered the groove 3D profile/geometry. Importantly, in acellular constructs mean patterning coefficient remained stable (0.48 from day 0 to day 14 with no significant change) over 2 weeks of culture (as measured at day 0, 7 and 14), indicating minimal passive remodelling (e.g. re-swelling) of the constructs.

Histological cross-sectional images of the cellular constructs taken on days 1 and 14 (Fig 7 a, b) confirmed the presence of stable grooves, while showing signs of collagen matrix remodelling (seen as matrix-sparse areas) by the resident cells at the end of the culture period, giving the construct a characteristic ‘lacy’ appearance.

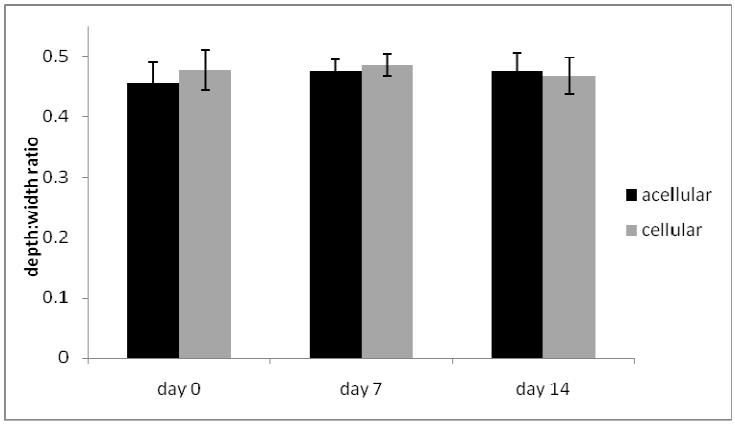

Fig. 6. Patterning coefficient of the topological features (grooves) imprinted into the FLS of acellular and cell-seeded PC constructs as an indicator of groove stability after long-term (14 days) culture. Measurements were taken at days 0, 7 and 14 *in vitro*. Topological features introduced onto the FLS were permanent and stable under culture conditions with and without resident cell remodelling of the matrix.

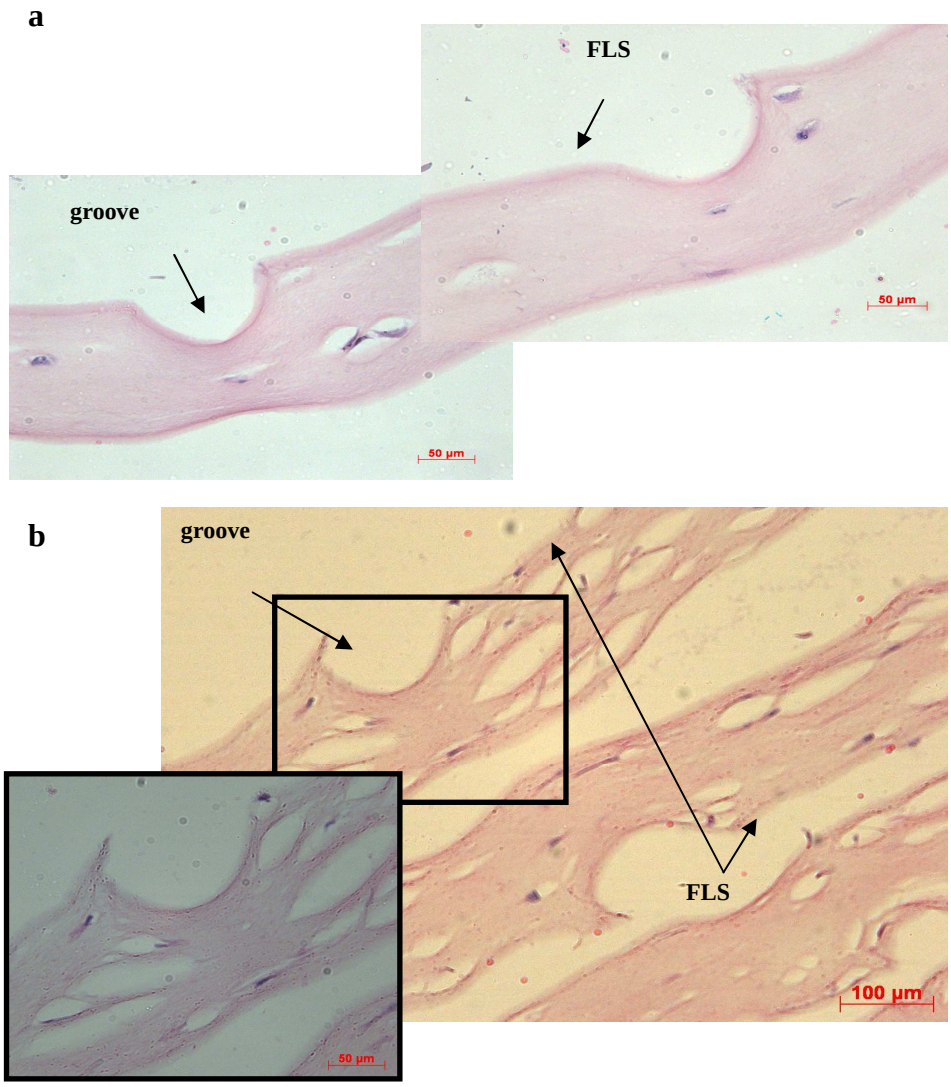

Fig. 7. Representative microphotographs of the PC collagen, seeded with human limbal fibroblasts, with grooves, introduced onto the fluid leaving surface (FLS), taken after 1(a) and 14 (b) days of culture. Insert – higher magnification of the highlighted region.

Discussion

In this chapter the stability and mechanisms by which topography is impressed into dense collagen gels during fluid outflow has been investigated. Following parameters have been assessed: (i) dimensions (depth and width) of the grooves, formed during the process of plastic compression on the opposite surfaces of the constructs (ii) fidelity of the pattern, formed on these surfaces to the dimensions of the template (iii) fidelity of the pattern on the fluid leaving surface of the plastic compressed constructs with and without embedded cells to the patterning template after two weeks in culture.

In the process this has allowed to develop predictable, stable surface patterning technique. The fact that 3D pattern can be introduced stably at all into these dense collagen materials is not surprising. The collagen gel compaction process involves a plastic (i.e. largely non-reversible) deformation as fluid is forced out from the collagen fibril network in one direction. The same non-elastic (plastic) deformation also occurs at the micron scale around any solid structure pressed into the surface or contained within the gel during compaction. It also explains the formation of stable channels running through the bulk of the material where embedded glass fibres dissolve (Nazhat et al., 2007). However, the fluid flow out of such gels is predominantly uniaxial and the eventual collagen distribution is asymmetric with greatest density at the fluid leaving surface (Brown et al., 2005, Hadjipanayi et al., 2010). It is now clear that micro-scale topography formation can be significantly influenced by these local factors. This makes it important to understand why and where micro-pattern formation is stable (i.e. remains long after compression) and how accurately the impressed pattern reflects the pattern used as the embossing template (i.e. degree of fidelity).

Micro-patterning in native extracellular matrix has considerable biomimetic advantage over more common experimental patterned surfaces made in synthetic polymers or rigid substrates such as glass, metal or silica. In addition, the present technique is an attractive alternative to existing methods of surface patterning of soft hydrogels where cell-lethal cross-linking is an essential part of the process, so cells must be added later where this is possible.

It is increasingly appreciated that the topography of a tissue engineered construct at the micrometre scale is critical to controlling many cell functions. It is well established, for example, that surface anisotropy and micro-structure have a profound effect on cell alignment and differentiation (Clark et al., 1987, 1990, Pins et al., 2000, Teixeira et al., 2003 and 2004, Downing et al., 2004, Vernon et al., 2005). Indeed, some studies show that the effects of topological features on cells extend beyond the single layer and affect cells that are not in direct contact with the surface (Mudera et al., 2000, Sørensen et al., 2007, Guillemette et al., 2009, Then et al., 2011). Consequently, accurate, predictable and stable topographic patterning is a pre-requisite for next generation studies investigating biomimetic 3D niches to control, for example, stem cell function and fate (Vazin and Schaffer, 2010), as well as cell-cell/cell-matrix interactions at interfaces (e.g. dermo-epidermal junction). Indeed, Nelson and Tien (2006) pointed out that simply by adding structure it may be possible to improve almost any biomaterial by creating extra cues that influence cell behaviour, making this a favourable strategy to expand the function of a tissue engineered construct.

It is possible that development of techniques to controllably pattern surface of naturally derived polymer constructs together with the knowledge of the effect of topography (in particular grooves) on the cells can have similar implications as a shift

from a monolayer approach to tissue engineering to understanding of the importance of the complex three-dimensional scaffolds. The ability to add that same structures to tissue-like cell-rich collagen matrix represents an ideal evolution. However, it is key to understand the mechanisms and effectiveness of this micro-patterning. Although in this study cells were not seeded on the surface of the construct, it has been shown by Hadjipanayi (2010) that one-two micrometer deep grooves on the surface of PC collagen construct can have profound effects on keratinocyte distribution. Hadjipanayi showed that such shallow grooves (width 30-50 μm, depth 1-1.5 μm) corresponded to the accumulation keratinocyte multi-layers which were only formed over the grooves.

Techniques of surface micro-patterning, which have been developed up to date most often require use of photolithographic methods. In particular, soft lithography has been method of choice when pattern is introduced onto a surface of fragile materials, such as hydrogels. This method is based on conformation of the patterned material to the negative template. The main drawback of this method is that stability of the resulting features requires extra treatments, which are often non-compatible with the viability of the resident cells. Soft lithography has been used to successfully pattern collagen-glycosaminoglycan co-polymer membranes (Janakiraman et al., 2007), collagen hydrogels (Nelson et al., 2008), chitosan and gelatine scaffolds (Wang and Ho, 2004). However as these materials are mechanically weak, cross-linking with glutaraldehyde is required which is not compatible with the resident cells, thus rendering this method less than desirable when fabricating bio-compatible construct. Moreover, although cross-linking increases mechanical strength of these constructs to some degree, it is not adequate compared to the native tissues.

An alternative method has been reported by Pins et al. in 2000. This includes fabrication of gelatine and collagen type I membranes with well-defined microgrooves by air-drying the polymer solution on negative templates and subsequent cross-linking by thermal dehydration at 105ºC in vacuum, a treatment that effectively resulted in thin, extremely dehydrated protein membrane, conformed to the pattern. These micro-patterned collagen membranes have been used as an analog of skin and intestinal basal lamina and provided valuable information about cell reaction to the patterned surface of natural polymers (Pins et al., 2000, Wang et al., 2010). Culture of the human keratinocytes on these microgrooves surfaces showed enhanced stratification in the grooves compared to flat surfaces. Further investigation showed that keratinocyte stratification and differentiation increased in the channels with high depth to width ratio. The most pronounced difference was found with grooves of 200 µm depth and 50 µm width (Downing et al., 2004). The dimensions of these grooves were close to the structures, found in the native epidermis. *In vivo*, dermal pappilae and rete ridges of the epidermal skin are lined with the clusters of epidermal stem cells. These amplifying cells migrate up the basal layer and produce post-mitotic cells which in turn migrate to the surface of skin where they are eventually sloughed off. Authors remark that although this effect is well known, the underlying mechanisms are still unclear and engineering precise micro-topography will help to understand these. Indeed, by staining the membranes with the grooves of different depth to width ratio with the marker of terminal differentiation – involucrin, authors found greater expression of the marker in the grooves with the greatest aspect ratio. This led to conclusion that deep and narrow grooves promote keratinocytes differentiation and the formation of the stratified layer. Examination of the cells proliferation found little evidence of the mitotic activity in the cells in the grooves. The authors attributed this

to the absence of the fibroblasts in the underlying scaffold – freeze-dried collagen sponge. This can easily be overcome in the current system, as cells can be embedded in the collagen matrix prior to the construct assembly.

Topological features on the surface of the collagen constructs have a pronounced effect on the cell-types more conventionally used in the field to demonstrate alignment of the cells to the grooves. In the study by Vernon and colleagues (2005), fibrillar collagen gels were air-dried for 24-48 hours at room temperature on the template and peeled off after drying. The resulting collagen membranes had well-defined pattern of parallel grooves. Authors used these micro-grooved collagen membranes to assess alignment of human dermal fibroblasts and umbilical artery smooth muscle cells. Cells showed strong alignment of the nuclei and cytoplasmic actin filaments (f-actin) parallel to the direction of the grooves after 6 days in culture, similar to the results found on the patterned stiff surfaces, such as quartz (Dalby et al, 2003). Indeed, these results agree with the data reported by Kureshi et al (2010), where alignment of fibroblasts to the grooves in the FLS has been shown.

These results are important not only from the point of view of utility of such micro-grooved dense collagen substrates for tissue engineering purposes. An additional aspect of these observations is the response of the cells to such features on the surface of the material that is less stiff than conventional micro-grooved substrata (glass, quartz, metal) and by itself presents cells with random nano-cues in the form of collagen fibres. Alignment of the cells to micro-scale grooves shows that micro-scale features are more potent to influence cell behaviour on such bio-conductive materials. As such, further investigation into the mechanisms of such alignment to the pattern in

the natural polymers may provide answers as to the mechanisms of the cell alignment *in vivo* which are more appropriate compared to those gained from the cell alignment on stiff, non-biomimetic materials.

Currently, the following hypotheses exist that explain mechanisms of the cellular alignment on the micro-grooved substrata: (a) cells minimise distortions to the cytoskeleton which would occur if they ignore, rather than follow the groove (Hamilton et al., 2009) and (b) attachment to these topographical cues (for example ridge of the groove) create mechanical stresses in the cell that directly cause alignment (Walboomers et al., 1998). Dalby et al. (2003) showed that such distortion in the cytoskeleton and shape of the cells on the grooved substrata cause change in the shape of the nuclei (elongation) and hypothesised that this leads to changes in the gene expression of the aligned cells due to the change in the relative position of the chromosomes and their accessibility for transcription. Thus, the effect of the micro-scale grooves on cells is indeed profound and merits investigations of these phenomena on the biological materials, such as dense collagen constructs.

In this study we have investigated a key observation, that patterning appears to be more effective when the embossing template is pressed into the fluid leaving surface (FLS). Because, in plastic compression, the fluid is forced out in one direction a single FLS is formed. Hence the initial fluid out-flow generates a profound top-bottom anisotropy in the collagen sheet, along with multiple lamellae (Brown et al., 2005, Hadjipanayi et al., 2010). It has been demonstrated that PC process resembles ultra-filtration where FLS rapidly accumulates a densely packed layer of collagen fibrils whereas non-FLS has lower collagen density (Hadjipanayi et al., 2010). It has been shown previously that collagen fibril density correlates closely with local

mechanical stiffness of the material (Hadjipanayi et al., 2009). These local differences can explain the differences in the fidelity of the pattern made in the FLS and non-FLS and speculate as to the mechanisms of pattern formation on these opposing surfaces.

Groove dimensions (width and depth) describe two main attributes of the pattern and were used to monitor the nature of the produced pattern relative to the known average diameter of the template. In addition a patterning coefficient was developed and used to assess pattern fidelity. For this the ratio measured was depth of each groove by its maximum width. Because of the way depth was measured the nominal maximum coefficient was 0.5. Hence comparison of actual pattern coefficient with this theoretical ideal means that fidelity of different grooves, from different templates could be compared; in this case a value of 0.5 would equal a perfect copy of the template.

Patterns formed in the FLS during plastic compression were far more predictable than those formed in the non-FLS. In effect the full diameter and a curvature of the fibre (including a lip) could be retained in grooves in the FLS. Similarly predictable patterns were obtained for template patterns pressed into the preformed FLS. Pattern coefficient confirmed high pattern fidelity for both FLS patterning treatments. Importantly, though, the pattern coefficient, or fidelity, was much less than ideal where the non-FLS was patterned. This was due to non-FLS grooves being very shallow (approx. 20 % of the fibre diameter) and almost double the template fibre width. This large width to depth discrepancy suggests that grooves in the non-FLS underwent a form of elastic recoil after the fibres were withdrawn. We hypothesise that this is a consequence of the elastic properties of the ‘skin-like’ surface film of packed collagen fibrils which surrounds the original collagen gel when it is cast (i.e. present on the gel-air casting interface) (Karamichos et al., 2006). On the

non-FLS this ordered fibrillar structure will not be substantially changed (i.e. compacted) in collagen density, due to the highly asymmetric fluid movement during compression. Hence, pushing the template fibres into the surface, when embossing the non-FLS, stretches the film around the template, so that borders of the groove are formed, but elastic recoil of the film removes all but a few micrometres of its original depth, while moving the borders further apart. Interestingly, the total wall length of the wide shallow groove corresponds well with 157 µm circumference of the glass fibre template, indicating that the floor of the groove was not elastic. However, the floor was raised dramatically, suggesting that the non-deformed collagen film between the grooves was elastic and has reshaped the groove when template was removed by raising its floor as demonstrated schematically in Figure 8.

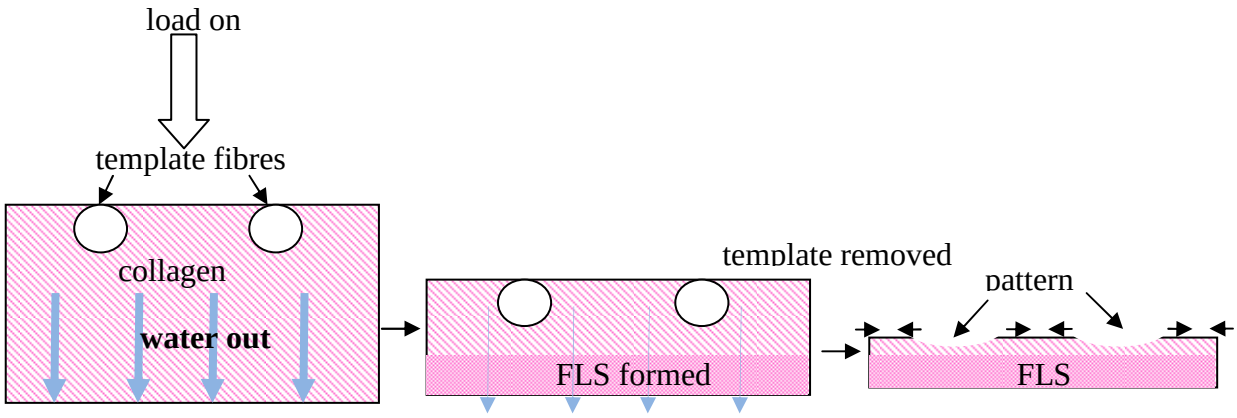

Fig.8 Diagram, showing proposed mechanism of pattern formation on the non-FLS. Template glass fibres placed on the gel and load applied initiating fluid flow in the direction of FLS. Fibres are initially fully immersed in the non-FLS, causing stretching of outer collagen film under the template. After template is removed, non-deformed, elastic collagen film between the pattern is released and cause pattern deformation, resulting in shallow grooves.

Another possibility would be deformation of the grooves in the process of template removal due to surface tension between the glass fibres and collagen. However, to prevent this, constructs were incubated in the PBS prior to the template removal to release these local adhesions.

For plastic compression to produce predictable patterns in a one-step process it is critical that there is a rapid fluid flow out of the collagen fibril mesh and around the impervious (template) surface, as developed in method 1a. It now seems likely that this rapid fluid efflux not only compacts collagen fibrils locally into the dense FLS but also remodels them around the embossing template. An alternative system for gel compaction by rapid directional fluid outflow which also aligns collagen fibrils parallel to the flow within the gel body has recently been described (Kureshi et al., 2010). In the present FLS patterning example, such induced collagen fibril alignment would be expected to be circumferential around the glass fibres, in the direction of deflected flow. It is proposed that this local remodelling of fibril orientation contributes strongly to pattern stability and fidelity by eliminating elastic recoil. The proposed mechanism is shown in Figure 9.

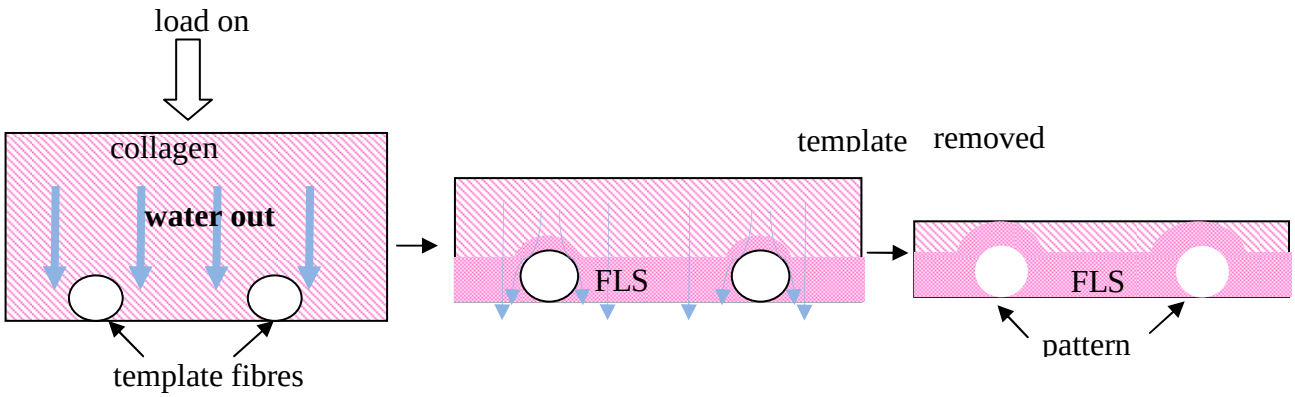

Fig.9 Diagram, showing proposed mechanism of pattern formation on the FLS. Template fibres are placed at the FLS of the gel, load applied and fluid flow initiated. Accumulation of collagen fibres at the FLS causes moulding of collagen around the template. Accumulation of dense collagen layer around the template cause permanent deformation of the patterned FLS even after template is removed.

This concept suggests that a large part of the PC micro-patterning is due to controlled fibril remodelling, similar to fibrous material moulding, for example in the manufacture of felt goods. The process will be therefore referred to as pattern micro-moulding.

Although it has been shown that density of the collagen fibrils at the FLS is greater than the non-FLS, it is still capable of plastic deformation as illustrated by the results of pattern formation in the partially formed FLS. In this case pattern fidelity was as high as in the case of forming fluid leaving surface, although the stability of such features was not investigated.

The suggestion that this process is one of remodelling/moulding is supported by the observation that micro-patterns, moulded into the FLS were stable in all respects over two weeks in culture. Interestingly, over that period cells seeded into the collagen bulk material had already begun to remodel their local collagen matrix to give new, open structures, which is consistent with previous *in vitro* remodelling reports (Brown et al., 2005, Bitar et al., 2008). This implies considerable 3D stability and tissue engineering utility for micro-moulded grooves.

In conclusion, this study has clarified the mechanisms by which faithful, less faithful and very low-fidelity micro-patterns are formed in the surface of dense collagen materials. This is key knowledge as it opens the way to more detailed and controlled engineering of tissue-like native collagen constructs, with cells in situ. Such processing in turn represents a considerable biomimetic advantage over previous patterned substrates partly due to its use of native protein, partly its cell content and partly its level of fine control. As in the case of original PC collagen compaction process pattern micro-moulding by this technique is rapid and cell compatible. In addition, since this is essentially a physiological material, these findings may indicate how fluid flow through natural, living tissues can sculpture the fine local patterns which are known as bio-nano/micro morphology.

Understanding of the mechanisms of stable pattern formation on the surface of bio-mimetic construct appears to be a useful tool for a variety of TE applications, and

as such merits development of scaling-up method. In the next Chapter multiple construct fabrication will be reported together with some basic mechanisms of plastic compression.

Chapter 5

Scaling-up of plastic compression method

Introduction

The original method of plastic compression (PC) of collagen, as reported by Brown et al. (2005), was based on application of mechanical loading and capillary uniaxial flow to remove fluid from hyperhydrated collagen gels. Brief photographic description of the method is shown in Figure 1. Gels are set in the custom-made rectangular mould (Figure 1a), transferred onto the blotting elements between two layers of nylon mesh, covered with a glass slide and fixed load to compress, typically for 5 min (Figure 1b). As a result dense collagen sheets, consisting on average of 11% collagen and 89% water, are fabricated (Figure 1c). This technology allows for control over resulting collagen construct density (by reducing/increasing total fluid removal) and, with further processing, fibril diameter and fibril alignment as shown by Cheema et al. (2007). An important point to make here is that this technique does not rely on cellular remodelling (contraction) of the matrix or other cell-dependent manipulations. However, the process is cell-friendly with average post-compression cell viability for several cell types such as dermal fibroblasts, mesenchymal progenitor stem cells and Schwann cells being above 80%. As a result, this technology allows for true engineering of tissues, where matrix and cells are building blocks of *de novo* tissues.

As with all useful developments, there are points where the original technology needs to be extended. To this end, a prototype machine was developed to automate the process of PC. The core original methodology was retained, i.e. collagen gels were set in standard moulds, compressed by applying load and blotting liquid

into a moving conveyer belt of absorbent paper to produce and finally collect compressed collagen constructs.

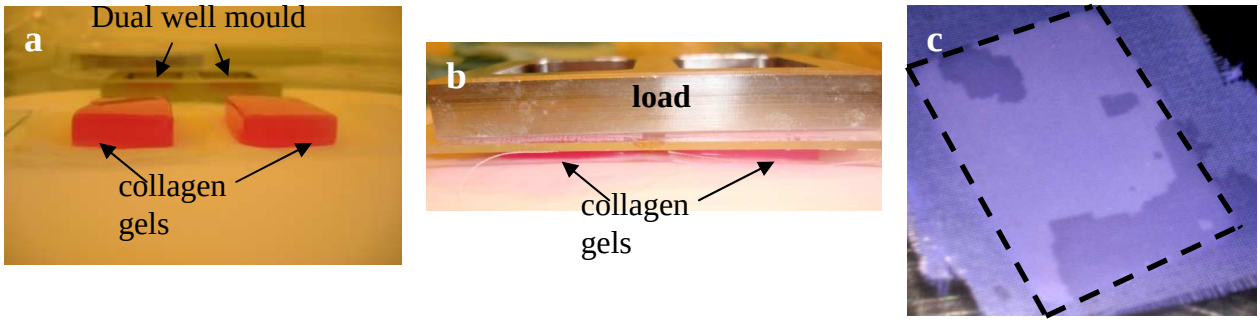

Fig. 1 Original method of plastic compression (PC). (a) Gels (pink), set in the double-pocket rectangular moulds (mould is seen in the background), were transferred onto the blotting elements (filter paper, stainless steel mesh) between two layers of nylon mesh. (b) Gels were then covered by the glass slide and loaded with weight for 5 minutes. (c) Process resulted in formation of the dense collagen sheet (dashed outline, construct is resting on a supportive nylon mesh) that could be cultured as a sheet or spiralled along its long axis to give a rolled construct

In this chapter an alternative route to scaling up a process is evaluated where multi-well format is employed to allow simultaneous fabrication of multiple constructs in a controlled manner – multi-well plastic compression (M-PC). The same principle of uniaxial capillary fluid flow from the collagen gel into the absorbent under load is used. Here, the load is applied directly to the fluid leaving surface (FLS) of the gel by the absorbent material.

M-PC of collagen allows for fabrication of multiple constructs simultaneously with possibility to vary certain parameters of each individual construct. Possible variables include initial collagen height (proportion to volume), number and type of cells seeded in or on the construct etc. This not only saves time on compressing individual constructs but also reduces variability between samples and minimises contamination risk. Effectively, all constructs can be assembled and cultured in the same mould, essentially standard tissue culture multi-well plate. Moreover, this

system presents a further opportunity for investigation of basic underlying mechanisms of the process (such as fluid loss and FLS formation), bringing the technique closer to fully controllable by the operator.

It has been shown, that fluid movement and mass compaction in PC can be described to some extent by Darcy's law of fluid flow through a porous membrane under pressure (Hidjapinayi et al., 2010).

The general formula is:

$$Q=AxΔP/μxR$$

where Q is the rate of flow (in ml/min), A is surface area (in cm^2), P is pressure gradient over the surface, μ is the dynamic viscosity coefficient of water at 20 ºC ($1.002x10^{-3}$ Ns/m^2) and R is the hydraulic resistance of fluid leaving surface (FLS). From this equation change in hydraulic resistance of FLS with time during the process of M-PC has been calculated for the range of gel heights. As FLS in itself is a 3D structure in the construct and its formation is essential for patterning of the surface (see Chapter 4) it is important to be able to monitor and control its formation.

In this chapter development of the multiple PC technique will be described as well as basic characteristics of the constructs, produced using this technique. Following parameters will be investigated: (i) average fluid loss against time, rate of fluid loss and dynamics of fluid leaving surface formation during compression of the range of collagen gel heights, (ii) end time-point of full compression for the same gel heights, (iii) reproducibility of the method between sets as a function of the resulting constructs weight, thickness and total volume of the fluid, lost from the gels of each height, and (iv) effect on long-term culture of cell-seeded constructs, compressed in this manner.

Materials and Methods

Multi-well compression kit

Standard tissue-culture 12-well plates (well diameter 22mm, Orange Scientific, UK) were used as the collagen gel casting mould. The original multi-well plate cover, with 12 hand-made holes corresponding in diameter and location with the wells, acted as a guide and support for the absorbing elements (plungers). This was later replaced with a purpose made plate (Figure 2a). The fluid-removing elements consisted of a spirally wound roll of Whatman chromatography paper (d=21mm) and two discs of Whatman filter paper (Whatman UK), cut to size of the well to rest on the collagen gel. Each roll was 125cm in length, 4cm in height (as supplied by the manufacturer) and 2.1cm in diameter, average weight 4.4±0.3 g. A customised paper rolling machine was designed and built by TAP Biosciences (Royston, UK) to give a constant speed and length of paper rolling, and as a result, paper rolls of uniform weight and absorption (Figure 2b).

In order to provide compressive load together with capillary action to drive fluid flow from the collagen gel, a range of fixed mass loads was used. These rested on top of each plunger and allowed for simultaneous compression of 1, 3, 6 and 12 gels. Each gel was subjected to 1042±1.6 Pa (35.8 g (fixed mass load) + 4.4±0.3 (average weight of Whatman paper roll)) initial load. Figure 2 (c-f) shows photographic report of compression of 6 gels. Gels were set in the 12 well-plate. A paper roll was placed on top of each gel (c) and loaded with weights (d). After compression, liquid-containing rolls (e) were removed, leaving the constructs in their respective wells, ready for culture if required.

Preparation of acellular and cellular collagen gels

Collagen was neutralized as described before in Chapter 2. To eliminate neutralising of multiple batches and to allow for solution degassing (i.e. to prevent

bubbles in the gels), collagen was neutralised in 25 ml bulk batch and kept on ice in 100ml specimen containers until needed.

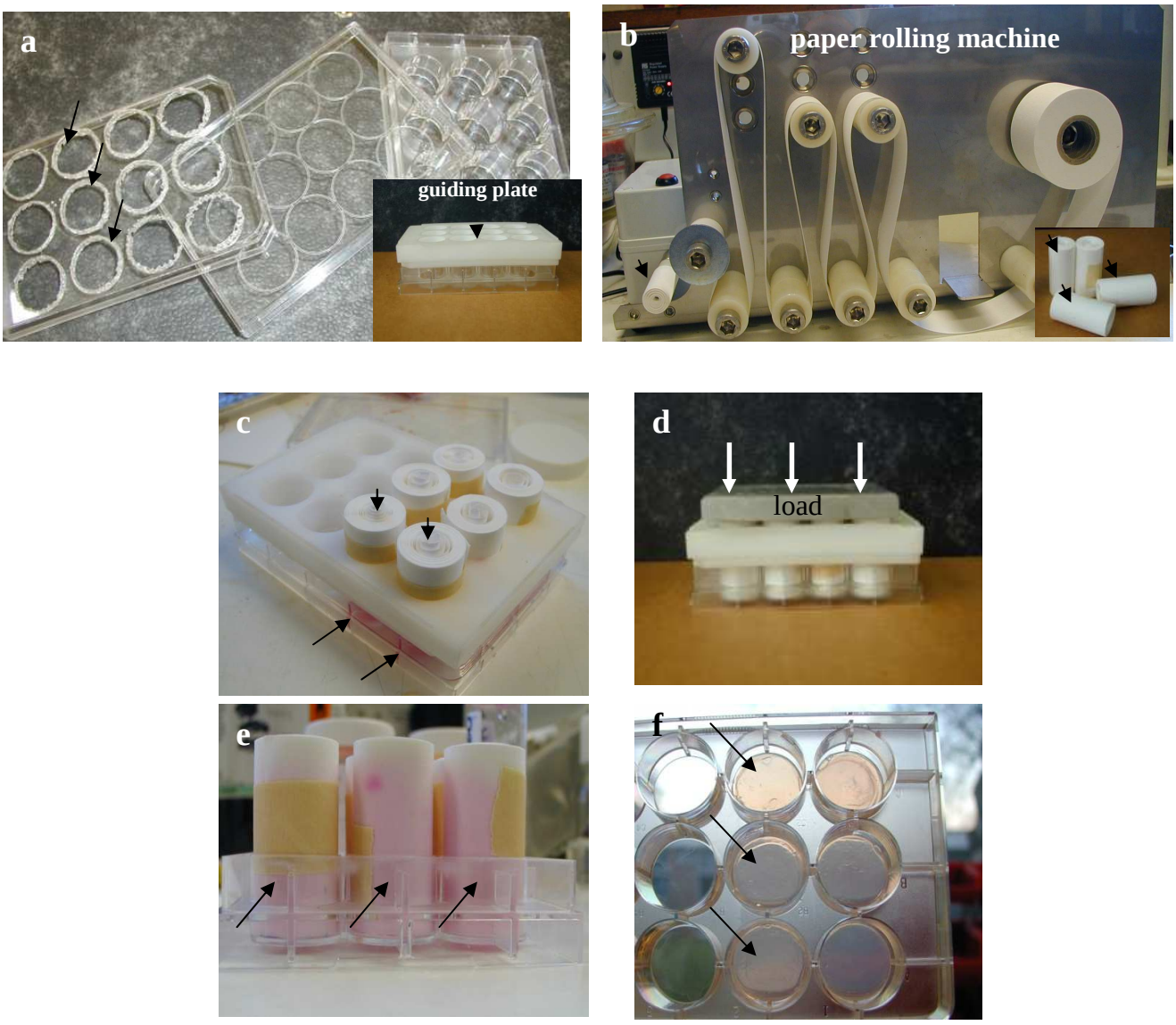

Fig. 2 Modified method – multi-well plastic compression (M-PC). (a) Standard tissue-culture grade 12 well-plate base served as a mould for the collagen gel casting. To ensure uniform compression, 12 holes have been made in the cover of the plate (arrows) to guide the absorbing plungers. This was replaced with purpose-made guiding plate indicated by an arrowhead (insert). (b) Spirally wound rolls (arrows) of absorbent paper were used as blotting elements and made using custom-build paper rolling machine. Assembled plungers are shown on the insert (arrows). (c) Gels (arrows) were set in the wells of the 12 well-plate and plungers (arrowheads) placed on the gels using guiding plate. (d) Depending on the number of simultaneously compressed gels, appropriate weight was applied. (e) After compression is completed, liquid is contained in the paper rolls (arrows), which are removed. (f) Process resulted in uniform dense collagen

sheets in the respective wells (arrows) that can be cultured if required without further manipulations.

The required volume of cold, neutral collagen solution was poured into each individual well and allowed to warm up to 37° C, which initiated setting (30 min) prior to compression. Given a constant surface area for the 22 mm well diameter (i.e. 379.9 mm^2), a range of gel volumes was investigated (2, 3, 4 and 5 ml). Gel volumes (ml) were converted into heights using basic formula

$$h=V/\pi r^2$$

for ease of future references and to make data transferrable to other systems (e.g. 24 or 96 well plate). Gel volumes (ml) and corresponding gel heights (mm) are presented in Table 1. Subsequent description will refer to the height of the gels as cast with a constant cross-section.

Table 1. Volumes and corresponding heights of the gels cast in the mould with constant surface area (379.9 mm^2).

Gel volume, ml	Gel height, mm
2	5.3
3	7.9
4	10.5
5	13

Cellular constructs were prepared as described before (Chapter 2). Cell suspension (500 000 human limbal fibroblasts (HLF)/gel) was mixed with neutral collagen solution and 6x5 ml (13mm) of cell-containing collagen gels were set in 12 well plate. Set collagen gels were compressed simultaneously using the system described above. Compressed constructs were cultured in the same plate for 2 weeks

and processed for routine histology (see Chapter 2). Cell viability was determined using live-dead staining assay (see Chapter 2).

Measurement of fluid loss and time of compression

Absorbent paper rolls were weighed on the electronic balance to two decimal points every minute for the first 5 minutes after compression then 5 min until no measurable change of weight was noted. For example, if after 10 minutes of compression weight of the paper roll did not change compared to the previous reading after 5 minutes, time-point of 5 minutes was taken as time of full compression. Weight gain in the absorbent was recorded as fluid loss from the collagen gel during compression. Weight of water removed from gel was calculated as

$$\Delta W = \text{Weight } t_n - \text{Weight } t_0$$

where Weight t_n is the weight at time point n and Weight t_0 is initial weight of paper roll (4.4±0.3g). Rate of fluid loss from the gels of different heights was calculated as

$$Q = \text{Weight } t_{n+1} - \text{Weight } t_n / \text{Time}_{n+1} - \text{Time}_n$$

Measurement of the hydraulic resistance of FLS (R_{FLS})

It has been shown that in the progress of the plastic compression process the hydraulic resistance of the fluid leaving surface is increasing due to the transport of the collagen fibrils with the leaving fluid and their accumulation at the point of fluid exit – fluid leaving surface (FLS). As plastic compression can be partially described by Darcy's law of fluid flow through the porous substrate, R_{FLS} can be calculated at each time-point of PC process in the multi-well format based on the rate of fluid flow, calculated as described previously. The formula used for these calculations takes into account the changing pressure, applied to each gel, as liquid, absorbed in the paper roll will add to the weight of the initial load (1042±1.6 Pa). In its final form the formula reads as follows:

$$R_{FLS} = AxP / \mu xQ$$

where R is the hydraulic resistance of fluid leaving surface (FLS), Q is the rate of flow (in ml/min), A is surface area (in cm^2), P is pressure over the surface (in N), μ is the dynamic viscosity of water ($1.002x10^{-3}$ Ns/m^2). Pressure was calculated for each time point based on the fluid loss data (as water lost from the gels is absorbed in the paper, changing its weight and consequently pressure applied to the gel). R FLS was calculated per surface area in cm^2 and expressed in cm^{-1}.

Measurement of intra-plate variance

In order to assess method variability the following parameters of the resulting constructs, produced between 3 plates (n=12 for each gel height), were compared for each height used: mean amount of fluid expelled from the gel at the point of full compression±SD, weight of the fixed constructs±SD and thickness of the resulting constructs±SD. Mean amount of fluid expelled from the gel at the point of full compression was derived from the fluid loss data recorded as described above. Resulting PC constructs (i.e. when no subsequent fluid loss was recorded) were fixed immediately in 10% neutral buffered formaldehyde solution and weighed on the electronic scale. Constructs were then paraffin embedded sectioned (12 μm) and stained with Sirius Red (see Chapter 2). For each volume 6 gels were compressed simultaneously in one plate, 3 different plates were used.

Statistical analysis

Data analysis was performed as described in Chapter2.

Results

Dynamics of fluid loss from collagen gels during compression

Process of plastic compression can be described in terms of percentage fluid loss from the compressed gel at set time points and the progress of the process can be

tracked minute by minute using this data. Fluid loss was measured by weighing the adsorbing paper at set time-points. To determine time-point of full compression for every gel height (5.3, 7.9, 10.6 and 13 mm), roll of absorbent paper was weighted every 5 minutes until no change in weight was noted. When this was achieved, previous time-point was noted as time of full compression. Times of compression for every gel height together with percentage fluid loss relative to the initial gel weight and absolute amount of fluid lost from the gels at the point of compression are summarized in the table 2. It is evident that height of the gel is in direct correlation with the time of compression. Gels of initial height of 5.3 mm were compressed (i.e. no further fluid loss was detected) after 5 minutes, 7.9 after 10 minutes, 10.6 after 20 minutes and 13 mm gels were compressed after 25 minutes (i.e. reading at 30 minutes and 25 minutes did not differ). Gels of all height have lost >90% initial weight at corresponding time points of full compression as summarised in Table 2.

To map the progress of the plastic compression and determine effect of the gel height on the process, first five minute were investigated closely by measuring the weight of the absorbing paper roll every minute.

Data presented in percent were used to track the progress of compression for each gel height by comparing percent fluid loss between time-points. Absolute numbers were converted into a percentage fluid loss where initial weight of the gels was taken as 100%.

Table 2 Time-points of full compression and respective values of percentage fluid loss at these time-points for collagen gels of different heights and constant surface area (379.9 mm^2)

Gel height, mm	Time of compression, min	Percentage of total fluid loss, %±SD
5.3	5	93.6±3
7.9	10	92.5±1.4
10.6	20	93±2.3
13	25	94.4±1.5

The effect of the height on fluid loss at each minute of the process was determined by comparing percent fluid loss between gels of different heights at each minute of observation.

In order to track the progress of the process, data acquired by measuring the weight loss from the gel of each height (5.3, 7.9, 10.6 and 13 mm, corresponding volumes of collagen 2, 3, 4 and 5 ml, diameter of the mould 22 mm) was analysed using one-way ANOVA.

Figure 3a shows progression of the compression process of the 5.3 mm gels. Water loss after the first minute of compression (55±11%) differed significantly from all the subsequent measurements ($p=0.0001$). It is of note that during the first minute of compression gels of this height have lost half of the original weight, i.e. water content. The loss of the remaining fluid was observed during subsequent four minutes of compression, i.e. rate slowed down considerably. During the second minute further 76±10% of the initial weight was lost, which differed significantly from minute 1 ($p=0.00034$). Water loss at minute 3 (85.9±8%) was not significant compared to minute 2. By the minute 4 of compression the gels of this height (5.3 mm) lost on

average 90.6±5.4% of weight; further compression (at minute 5) resulted in loss of 93.6±3% (significantly greater than at minutes 1, 2 and 3 ($p<0.005$), but not 4) of fluid content of the gel. Measurement at minute 10 showed no change in the weight loss hence compression was completed at 5 minutes.

Figure 3b shows progression of the compression process of the 7.9 mm gels. During the first minute of compression gels of this height lost on average 35±5% of the initial fluid content, significantly less than at all further time-points. At minute two mean weight loss from the gels of this height was 46±4% (approximately 10% increase), a significant increase compared to minute one ($p=0.0002$). At minute 3 fluid loss from the gels of this height amounted to 55±3.6% (similarly, approximate increase of 10%), a significant increase from minute two ($p=0.00028$). Further compression resulted in a loss of 75±4% at minute 4, a significant increase compared to minute 3 ($p=0.0001$) and 82±2% at minute 5, significant increase compared to minute 4 ($p=0.013$). Surprisingly, approximate increase of 20% of fluid loss was noted between minutes 3 and 4, followed by 10% increase by minute 5.

Compression for further 5 minutes led to 92.5±1.4% fluid loss at minute 10 (significant increase compared to minute 5, $p=0.00028$) after which time point no further weight loss was recorded, i.e. gel was compressed after 10 minutes.

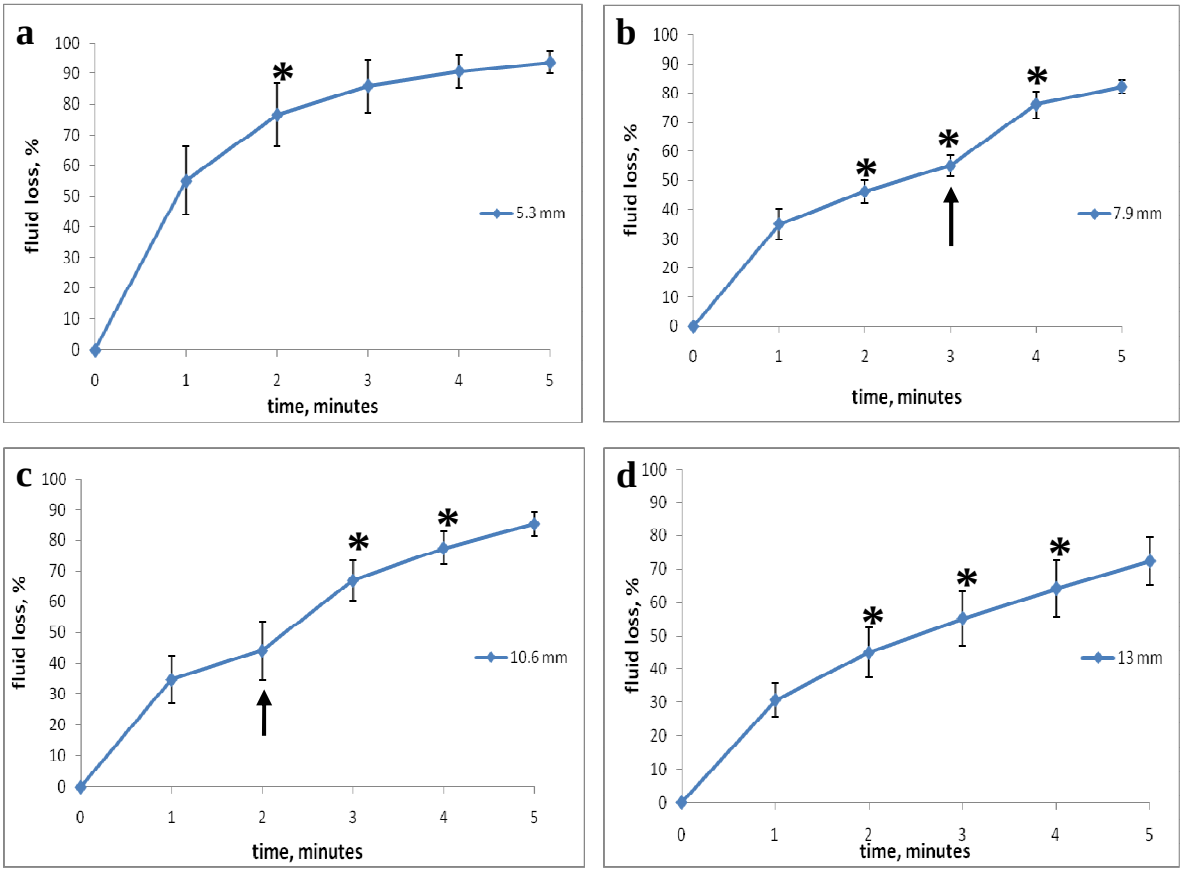

Fig. 3 Dynamics of fluid loss from the gels of 5.3 (a), 7.9 (b), 10.6 (c) and 13 (d) mm initial height during the first 5 minutes of the of plastic compression process. Fluid loss from the gels at each minute of the process is presented in percent of initial weight. *-statistically significant difference compared to the previous time point ($p<0.05$). Arrows indicate characteristic 'jumps' in values noted for 7.9 and 10.6 mm gels.

Figure 3c shows progression of the compression process of the 10.6 mm gels. During the first minute of compression gels of this height lost on average 34.7±8% of the initial weight. At minute two, weight loss of 44±9.6% was recorded for the gels of this height (approximate increase of 10%). At minute three, 66.9±6.5% of the initial weight was lost, a significant increase of compared to minute two ($p=0.0007$). Interestingly, for the gel of this height approximate increase in fluid loss of 20% was noted at this time point (minute 3) compared to minute 2, similar to the sudden increase at minute 4 for the 7.9 mm gels. Further compression resulted in the loss of 77±5%, an approximate increase of 10% compared to the previous reading at minute

3 (significant increase, p=0.03) at minute 4. This was followed by a loss of 85±4% of fluid at minute 5. After further 5 minutes of compression, at minute 10 these gels lost on average 89±3.5% of initial weight and at minute 15, 92±2.7% of fluid was lost from the gels. Compression for further 5 minutes resulted in the loss of 93±2.3% of fluid content at minute 20, at which time-point gels were compressed as further compression did not show change in weight of absorbent.

Figure 3d shows progression of the compression process of the 13 mm gels. During the first minute of compression 31±5% of fluid content was lost from the gels of this height. During the second minute further 45±7% was lost, a significant increase compared to minute 1 (p=0.0001). At minute 3, 55.2±8% of weigh loss was recorded, giving a significant increase compared to minute 2 (p=0.0007). At minute 4, 64±8% of fluid was lost from the gels, a significant increase from minute 3 (p=0.03). Weight loss at minute 5 was 72.7±7%. During the compression of the gels of this height the increase in percentage fluid loss at each time point compared to the previous was consistent 10% as opposed to the sudden 20% increase at minutes 3 and 4 noted in the gels of 7.9 and 10.6 mm respectively. Compression for further 5 minutes resulted in 89±4% weight loss at minute 10, significantly greater than at minute 5 (p=0.0001). At minute 15, an average of 93.2±3% of fluid content was lost from the gels of this height followed by further loss of 93.9±2.3% loss at minute 20. At minute 25, total of 94.4±1.5% of fluid was lost from the gels of this height, after which point no more change in weight of absorbent was recorded, i.e. gels were compressed.

To determine the effect of gel height on the percentage weight loss at each time point, data for each gel height was compared at minutes 1, 2, 3, 4, 5, 10, 15, 20 and 25. Results are presented graphically in Figure 4.

During the first minute of compression fluid loss from the gels of the initial height of 5.3 mm (55±11%) was significantly greater than from 7.9 (35±5%, p=0.002), 10.6 (34.7±8%, p=0.0008) and 13 mm (31±5%, p=0.0001) gels. There were no significant differences between fluid loss at this time-point between other gel heights.

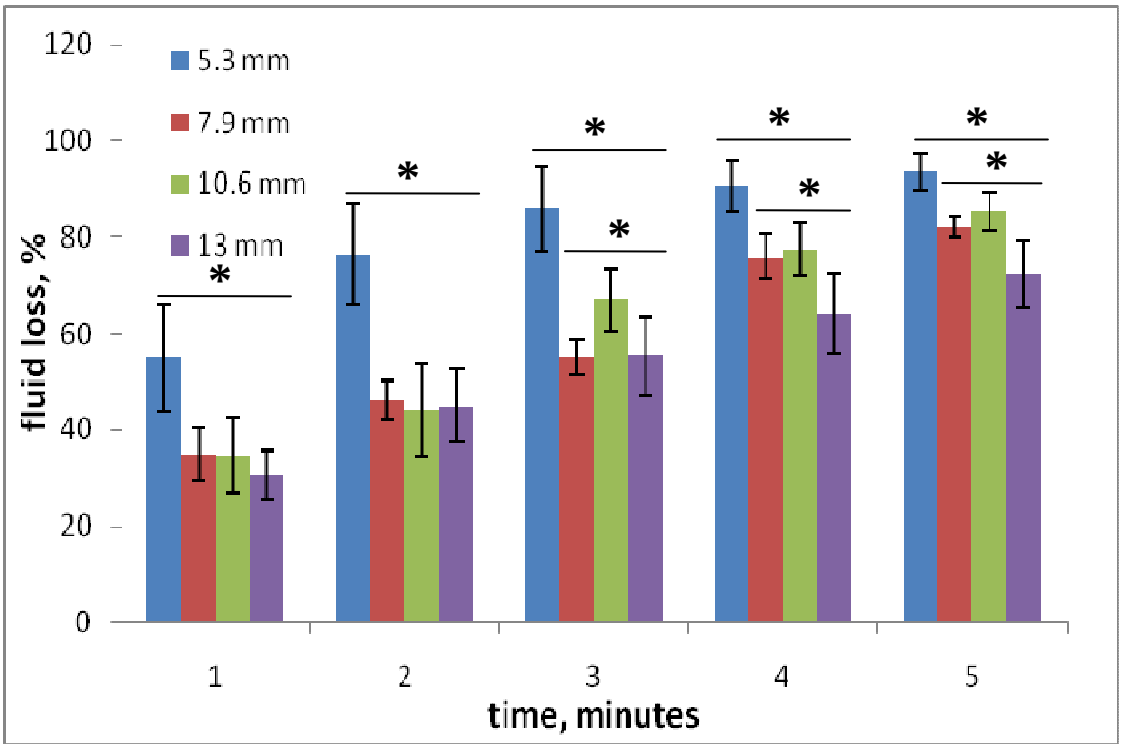

Fig.4 Effect of the initial height of the gel (5.3, 7.9, 10.6 and 13 mm) on fluid loss (in % of initial weight) during the first 5 minutes of plastic compression process. *-significant difference between gel heights at each time point (p<0.05).

During the second minute of compression the same trend continued. At this time point 76±10% loss of the initial weight was noted for the 5.3 mm gels, which was significantly greater than the value for 7.9 mm gels (46±4%, p=0.001), 10.6 (44±9.6%, p=0.001) and 13 (45±7%, p=0.001) mm gels. Differences between other gel heights were insignificant.

At the third minute 85.9±8% of the initial weight was lost from 5.3 mm gels, 55±3.6% from 7.9 mm gels, 66.9±6.5% from 10.6 mm gels and 55.2±8% from 13 mm gels. The weight loss at this time point from the 5.3 mm gels was significantly greater than from all other gel heights ($p<0.0001$). There was significantly greater percent fluid loss from the 10.6 (66.9±6.5%) mm gels compared to 7.9 (55±3.6%, $p=0.003$) and 13 (55.2±8%, $p=0.006$) mm gels.

The weight loss during the fourth minute of compression had an average of 90.6±5.4% from 5.3 mm gels, 75±4% from 7.9 mm gels, 77±5% from 10.6 mm gels and 64±8% from 13 mm gels. At this time-point significantly greater weight loss was recorded for 5.3 mm gels compared to other gel heights ($p<0.0001$). Percent fluid loss from the 13 mm gels (64±8%) was significantly lower than from 7.9 (75±4%, $p=0.0004$) and 10.6 (77±5%, $p=0.0005$) mm gels.

By the fifth minute of compression gels have lost on average 93.6±3% (5.3 mm), 82±2% (7.9 mm), 85±4% (10.6 mm) and 72.7±7% (13 mm) of the initial weight. At this time point significantly greater weight loss was recorded for 5.3 mm gels (93.6±3%, $p<0.001$) compared to other gel heights and significantly lower weight loss for 13 mm gels (72.7±7%, $p<0.001$) compared to other gel heights.

Rate of fluid loss

Fluid loss from the gels of each height at the time-points investigated was re-analysed in terms of rates of fluid loss (see Methods section of this chapter). The results are shown in Figure 5 (a-d).

The rate of fluid loss from the 5.3 mm is shown in Figure 5a. The rate of fluid loss in the initial minute of compression (min 0-1), was 1.1±0.22 ml/min. Comparison with the rate of fluid loss at each consecutive periods (1-2, 2-3, 3-4 and 4-5 minutes)

showed that it was significantly higher ($p<0.0001$) than at any other time-point of compression period. Rate of fluid loss at minutes 1-2 was 0.4±0.2 ml/min, almost 1/3 of that during the first minute. At minute 2-3 the rate fell further to 0.18±0.06ml/min, significantly lower than during the previous minute ($p=0.0085$). During minutes 3-4 and 4-5 there was further decrease in the rate of fluid loss to 0.11±0.07, 1/10 of the initial rate, and 0.1±0.05 ml per minute respectively, which was not significant compared to min 2-3.

The rate of fluid loss from the 7.9 mm is shown in Figure 5b. The rate of fluid loss during the initial minute (0-1) was significantly higher compared to all subsequent time-point (1.22±0.2 ml/min, $p<0.0001$). During the next minute (1-2), the rate fell significantly to 0.39±0.16 ml/min ($p<0.0001$). During min 2-3 the rate of fluid loss fell further to 0.3±0.1ml/min, although not significantly compared to the previous minute of compression. At minutes 3-4 and 4-5 the rate of fluid loss slowed significantly compared to min 2-3 ($p=0.0001$) to 0.23± 0.017 and 0.21±0.02 ml/min respectively

Further compression at minutes 5-10 led to further decrease in the rate of fluid loss from the 7.9 mm gels to 0.035±0.02 ml/min, although this was not significant compared to the previous time-point (min 4-5).

The rate of fluid loss from the 10 mm is shown in Figure 5c. The rate of fluid loss during the initial minute (min 0-1) of compression (1.4±0.3 ml/min) was significantly higher than during the subsequent time-points ($p<0.05$). During the second minute of compression (min 1-2) rate of fluid loss was 0.5±0.1 ml/min, significantly lower than in the previous minute ($p=0.0005$).

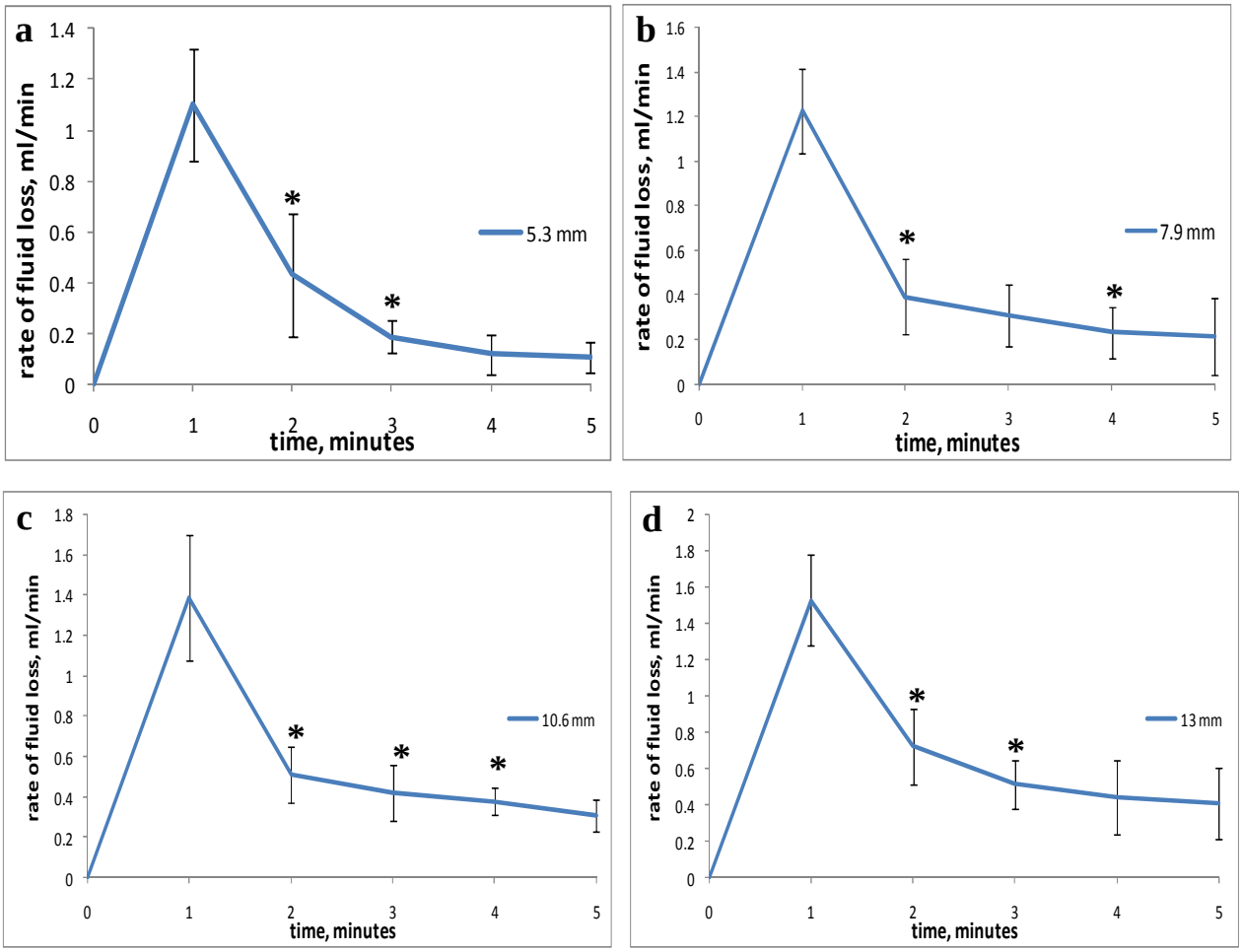

Fig. 5 Change in the rate of fluid loss from the gels of 5.3 (a), 7.9 (b), 10.6 (c) and 13 (d) mm initial height during the first 5 minutes of the of plastic compression process. Rate of fluid loss from the gels at each minute of the process is presented in millilitre per minute. *-statistically significant difference compared to the previous time point ($p<0.05$).

During min 2-3 rate of fluid loss fell further to 0.42±0.12ml/min, which was significantly lower than during the previous minute ($p=0.03$). During the min 3-4 and 4-5 the rate of fluid loss from 10.6 mm gels was 0.37±0.06 and 0.31±0.07 ml/min respectively. Rate at min 3-4 was significantly lower then at min 2-3 ($p=0.001$). Further compression led to significantly slower rate of fluid loss during min 5-10 (0.028±0.01 ml/min) compared to min 4-5. At min 10-15 and 15-20 rate of fluid loss fell insignificantly to 0.026±0.01 and 0.016±0.005 ml/min respectively.

The rate of fluid loss from the 13 mm is shown in Figure 5d. Similar to the previous gel height, rate of fluid loss during the first minute (min 0-1) was

significantly higher than at later time-points ($p<0.0001$) at 1.53±0.2 ml/min. The rate of fluid loss during the second minute (min 1-2) was significantly lower compared to min 0-1 at 0.72±0.2 ml/min. At min 2-3 of compression the rate fell further to 0.5±0.1 ml/min, which was significantly lower compared to min 1-2 ($p=0.03$). At min 3-4 rate of fluid loss fell insignificantly to 0.44±0.2ml/min, and at min 4-5 the rate fell further to 0.4±0.19 ml/min, which was also not significant. Further compression (min 5-10) led to significant ($p=0.002$) drop in the rate of fluid loss compared to min 4-5, and was 0.16±0.04 ml/min. During further compression (min 10-15) there was significant ($p<0.001$) drop in the rate of fluid loss at 0.037±0.02ml/min. The rate of fluid loss during min 15-20 and 20-25 fell further to 0.027± 0.01 and 0.02± 0.01 ml/min but did not differ significantly compared to the previous time periods.

The effect of the gel height (5.3, 7.9, 10.6 and 13 mm height corresponding to 2,3,4, and 5 ml of collagen, diameter of the mould 22 mm) on the rate of fluid loss during the process of plastic compression is presented graphically in Figure 6.

There was a significantly lower rate of fluid loss from 5.3 mm compared to 10.6 ($p=0.02$) and 13 mm ($p=0.001$) gels but not 7.9 mm gels. The rate of flow at min 0-1 from the 7.9 mm gels was significantly lower compared to 13 mm gels ($p=0.005$).

During the second minute of compression rate of fluid flow from 13 mm gels was significantly higher than from 5.3 ($p=0.0008$), 7.9 ($p=0.001$) and 10.6 ($p=0.0004$) mm gels.

Similarly, during the third minute of compression the rate of flow from 13 mm gels was significantly higher than from 5.3 ($p=0.0001$), 7.9 ($p=0.002$) and 10.6 ($p=0.004$) mm gels. Rate of fluid loss from 10.6 mm gels was significantly higher than for 5.3 and 7.9 mm gels ($p<0.0001$). Rate of fluid flow from 5.3 and 7.9 mm gels did not differ significantly.

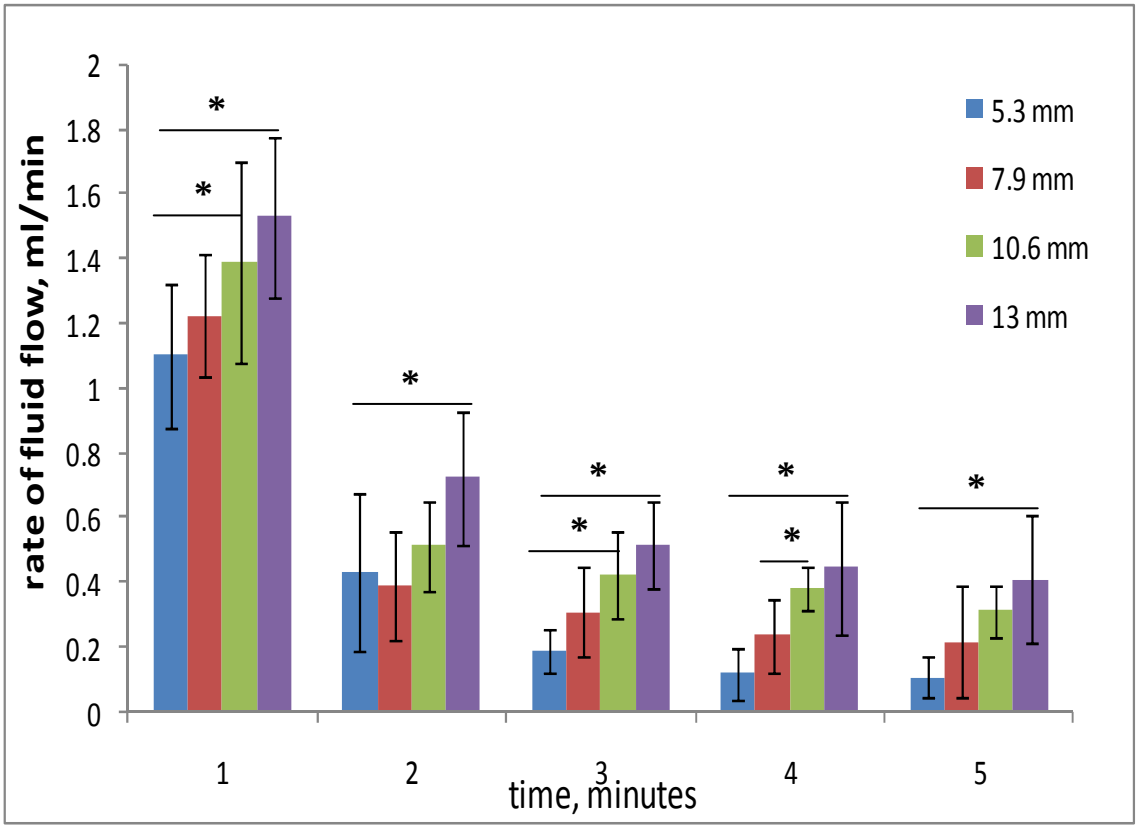

Fig. 6 Effect of the height of the gel (5.3, 7.9, 10.6 and 13 mm) on the rate of fluid loss (in ml/min) during the first 5 minutes of plastic compression process. *- significant difference between gel heights at each time point ($p<0.05$).

At minute 4 of compression the rate of fluid flow from 5.3 mm gels was significantly lower compared to all other gel heights ($p<0.001$), which is not surprising as gels at this height have lost 90% of the weight due to fluid loss by min 4. Similarly, rate of flow from 7.9 mm gels was significantly lower compared to 10.6 and 13 mm gels ($p<0.001$). There was no significant difference between 10.6 and 13 mm gels.

During the fifth minute of compression the rate of fluid loss from 5.3 mm gels was, predictably, significantly lower than from all other gel heights as these gels are fully compressed by the end of minute 5 ($p=0.0001$). There was no significant difference between the rates of fluid loss at this time-point between 7.9, 10.6 and 13 mm gels.

At minute 10 of compression the rate of fluid loss from the 13 mm gels was significantly higher than from 10.6 mm gels ($p<0.001$). During further compression (min 10-15 and 15-20 (10.6 gel is compressed) there was no significant differences between the rate of fluid loss from the gels.

Dynamic of change in FLS resistance during compression.

As has been shown previously, during the process of plastic compression accumulation of the collagen fibrils close to the fluid leaving surface (FLS) is the phenomenon behind the deceleration of fluid loss from the collagen gels. As plastic compression can be partially described by Darcy's law of fluid flow through porous substrate, it is possible to quantify the growing resistance of fluid leaving surface (R_{FLS}) for each gel height. Knowing the rate of water loss from the gels and taking into consideration increase in applied pressure over time (as liquid absorbed by the paper will add to the loading weight), R_{FLS} values were calculated for each gels height at each time-point.

For the 5.3 mm (Figure 7a) gels the resistance of FLS during the first minute of compression increased to $7.5x10^4 \pm 1.55\ x10^4\ cm^{-1}$. During the second minute value increased significantly (Games-Howell post-hoc test, $p=0.002$) to $10.5x10^4 \pm 1.4\ x10^4\ cm^{-1}$. Further compression increased the resistance to $11.8x10^4 \pm 1.2x10^4\ cm^{-1}$ during min 3, $12.5x10^4 \pm 0.77x10^4\ cm^{-1}$ during min 4 and finally $12.9x10^4 \pm 0.5x10^4\ cm^{-1}$ during min 5, these values did not differ significantly.

Compression of the 7.9 mm gels (Figure 7b) resulted in the rise in R_{FLS} during the first minute of compression to $8.3x10^4 \pm 1.3x10^4\ cm^{-1}$.

During the second minute of compression the resistance of FLS grew significantly to $11.08x10^4 \pm 0.8\ x10^4\ cm^{-1}$ compared to the min 1. Further compression resulted in further significant increase in the R_{FLS} to $13.29x10^4 \pm 0.9\ x10^4\ cm^{-1}$ during

the third minute, $18.6x10^4 \pm 1.2\ x10^4$ cm^{-1} during min 4 and $20.27x10^4 \pm 0.55\ x10^4$ cm^{-1} during min 5. Following 5 minute period of compression (min 5-10) resulted in further significant increase of the R_{FLS} bringing the value to $23.1x10^4 \pm 0.38\ x10^4$ cm^{-1} ($p=0.0001$) when the gels of this height were compressed.

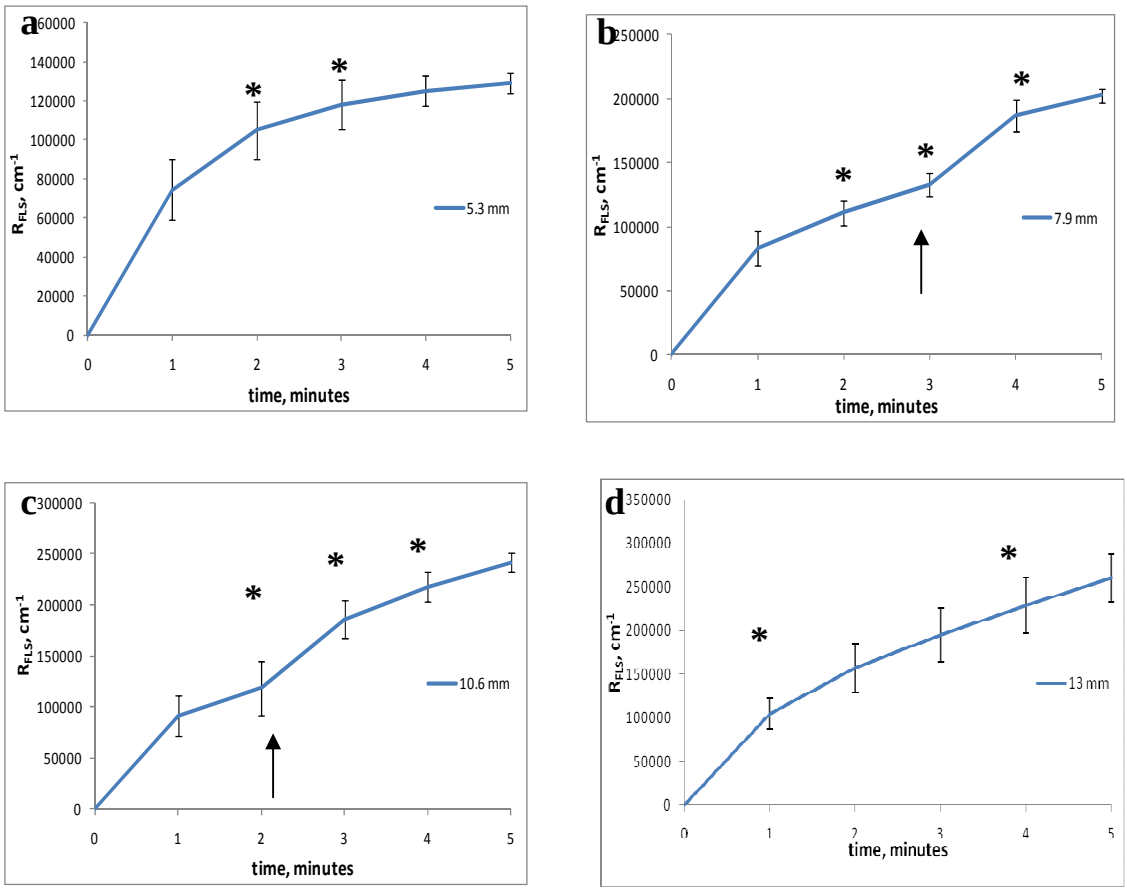

Fig. 7 Change in the hydraulic resistance of the fluid leaving surface (R_{FLS}) of the gels of 5.3 (a), 7.9 (b), 10.6 (c) and 13 (d) mm initial height during the first 5 minutes of the of plastic compression process. Hydraulic resistance of the fluid leaving surface of the gels at each minute of the process is presented in cm^{-1}. *- statistically significant difference compared to the previous time point ($p<0.05$). Arrows indicate 'jumps' in value characteristic for 7.9 and 10.6 mm gels.

Compression of the 10.6 mm (Figure 7c) gels resulted in increase of the hydraulic resistance of the fluid leaving surface in the first minute of compression to $9.14x10^4 \pm 2.1x10^4$ cm^{-1}. During the second minute, R_{FLS} grew to $11.8x10^4 \pm 2.6x10^4$ cm^{-1}. By minute three the resistance grew further to $18.6x10^4 \pm 1.9x10^4$ cm^{-1}, which was significantly greater ($p=0.0001$) compared to the previous minute. During the

next minute (min 4) value increased significantly (p=0.0001) to $21.8x10^4 \pm 1.5x10^4$ cm^{-1}. By the fifth minute of compression, R_{FLS} grew again significantly to $24.2x10^4 \pm 0.9x10^4$ cm^{-1}. Further compression led to non significant increase in the resistance of FLS. During min 5-10 of compression value rose to $25.3x10^4 \pm 0.9x10^4$ cm^{-1}, at min 10-15 R_{FLS} was $26.3x10^4 \pm 0.8x10^4$ cm^{-1} and finally by the time of full compression at min 15-20 R_{FLS} for the gels of this height was $26.7x10^4 \pm 0.7x10^4$ cm^{-1}.

During the first minute of compression of the 13 mm the hydraulic resistance of the FLS (Figure 7d) rose to $10.5x10^4 \pm 1.8x10^4$ cm^{-1}. During the second minute R_{FLS} grew significantly to $15.7x10^4 \pm 2.8x10^4$ cm^{-1}. At minute three of compression the R_{FLS} was $19.5x10^4 \pm 3x10^4$ cm^{-1}, insignificant increase compared to minute two. During minute 4 the value rose to $22.8x10^4 \pm 3.1x10^4$ cm^{-1} and by minute 5 grew significantly again (p=0.001) to $26.01x10^4 \pm 2.7x10^4$ cm^{-1}. Further compression (min 5-10) led to the last significant increase in the value (p=0.034) to $32.8x10^4 \pm 1.7x10^4$ cm^{-1}. Between min 10-15 R_{FLS} grew to $34.3x10^4 \pm 1.2x10^4$ cm^{-1}, between min 15-20 to $34.5 \pm 0.8x10^4$ cm^{-1} and finally at the time-point of compression for the 13 mm gels the R_{FLS} value was $34.7x10^4 \pm 0.4x10^4$ cm^{-1}.

To investigate the effect of the gel height on the increase in hydraulic resistance of FLS, the values for different gel height were compared at each time-points of compression. Data is presented graphically in Figure 8.

At minute one R_{FLS} of the 13 mm gels was significantly higher (p=0.0001) than any other gel height (5.3, 7.9 and 10.6mm).

At minute two of compression same result was obtained, the value of R_{FLS} of the 13 mm gels was significantly higher compared to other gel heights.

At minute three R_{FLS} of the 13 mm gels was significantly higher than that of 5.3 and 7.9 mm gels. The value for 5.3 mm gels was significantly lower compared to other gel heights. R_{FLS} of 7.9 mm gels was lower compared to 10.6 and 13 mm gels.

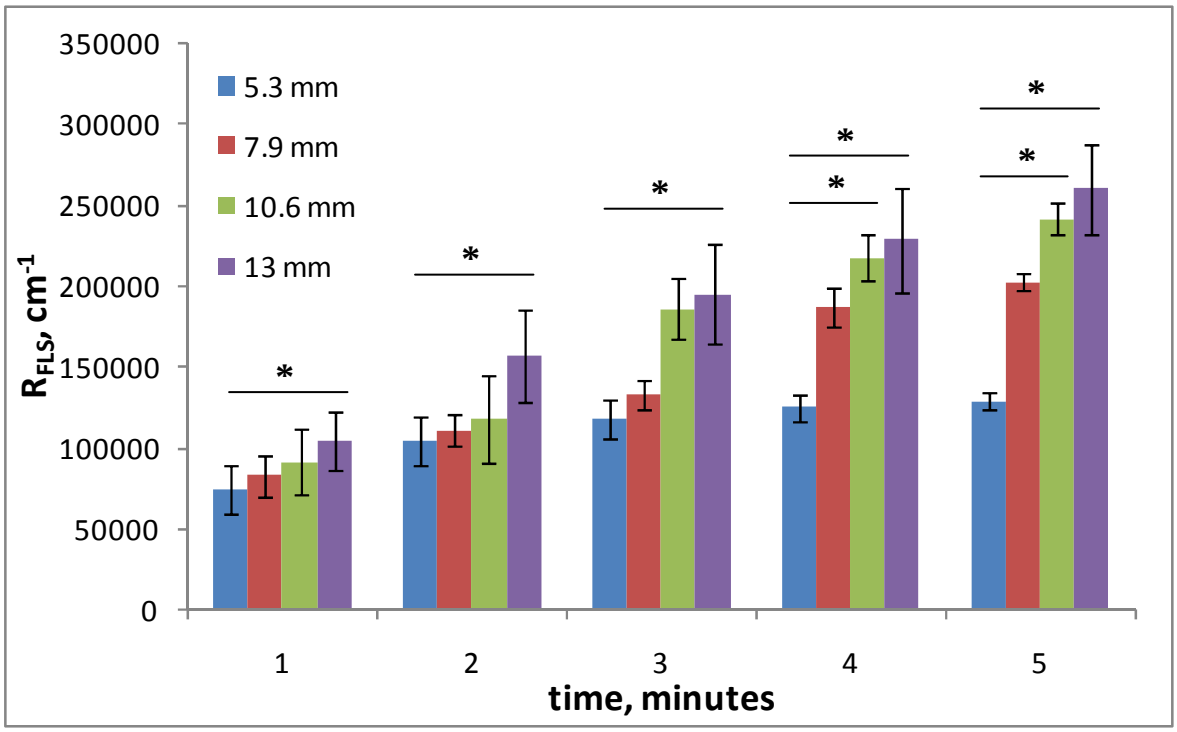

Fig. 8 Effect of the height of the gel (5.3, 7.9, 10.6 and 13 mm) on the hydraulic resistance of the fluid leaving surface (R_{FLS}) (in cm^{-1}) during the first 5 minutes of plastic compression process. *-significant difference between gel heights at each time point ($p<0.05$).

Predictably, by minute 4 of compression R_{FLS} of the 5.3 mm gels was lower compared to other gels. Also not surprisingly value for 7.9 mm gels was lower than that for 10.6 and 13 mm gels. Both shorter gels are nearing the time-point of full compression and fluid flow out of the gels of these heights slowed considerably and as a result transport and deposition of the collagen fibres at the FLS also decreased. The same trend continued during minute 5 of compression.

During min 5-10 of compression resistance of the FLS in the 7.9mm gels was significantly lower compared to 10.6 and 13 mm gels. Value of R_{FLS} in the 13 mm gels was significantly higher compared to 7.9 and 10.6 mm gels. Same was true at min 10-15 and 15-20 where R_{FLS} of the 13 mm gels was significantly higher than this

of 10.6 mm gels. The results show that gel height affects the hydraulic resistance of the fluid leaving surface.

Parameters of the resulting constructs and variability

Constructs, fabricated using M-PC, were fixed immediately, weighed and processed for routine histology to determine thickness. Immediate fixation can affect physical properties of the collagen; the data produced in this study were used only to determine values of standard deviation as an indicator of variability.

Mean values of total fluid loss±SD (in ml), weights±SD (in g) and thickness±SD (in µm) of the 12 constructs, prepared in three different 12 well plates, as measured immediately after compression of the constructs, are summarised in Table 3. There was no significant variation between the total volume of lost fluid, weights or thickness of the constructs prepared from the same gel height with values of SD within 10% of the mean.

The constructs, fabricated from 5.3 (0.01 ± 0.001 g) and 7.9 (0.03 ± 0.01 g) mm gels weighted significantly less than those resulting from compression of 10.6 (0.17 ± 0.013 g) and 13 (0.2 ± 0.01 g) mm gels ($p=0.001$).

Constructs made of 5.3 mm initial gels were significantly thinner (26.6±3 µm) compared to the constructs resulting from compression of 7.9 (37±2.7 µm, $p=0.002$), 10.6 (57.3±4.7 µm, $p=0.001$) and 13 (63.6 ± 5.4 µm, $p=0.001$) mm gels. Compression of the 13 mm gels resulted in the significantly thicker constructs compared to other gel heights ($p<0.001$).

Figure 9 shows representative histological images of the constructs (triplicates), made from the gels of 5.3 (a), 7.9(b), 10.6(c) and 13(d) mm initial height, confirming uniformity of the constructs made using multi-well plastic compression.

Table 3. Parameters of the constructs (total fluid loss, weight and thickness) fabricated from the gels of different initial heights and constant surface area (379.9 mm^2).

Gel height, mm	Mean total fluid loss ml±SD	Mean weight g±SD	Mean thickness μm±SD
5.3	1.9±0.07	0.01 ± 0.001	26.6±3
7.9	2.85±0.06	0.03 ± 0.001	37±2.7
10.6	3.7±0.09	0.17 ± 0.013	57.3±4.7
13	4.7±0.1	0.2 ± 0.01	63.6 ± 6.4

Assessment of cell viability.

To determine utility of the method for cell culture experiments, cellular gels were set in the 12 well-format and compressed. Resulting constructs were cultured in the same wells for 14 days. Viability of the resident cells was assessed at day 0 (to determine possible detrimental effects of the upward compression) and day 14 (to assess possible long-term damage). As can be seen from the Figure 10a, there was neither (i) immediate nor (ii) long-lasting negative effect on cell viability with the percentage of viable cells being 87±10% at day 0 and 90±5.3% at day 14. Figure 10b shows histological image of the cellular construct after 14 days in culture with the evidence of cellular matrix remodelling, which gives constructs characteristic ‘lacy’ appearance, with cells residing in the voids.

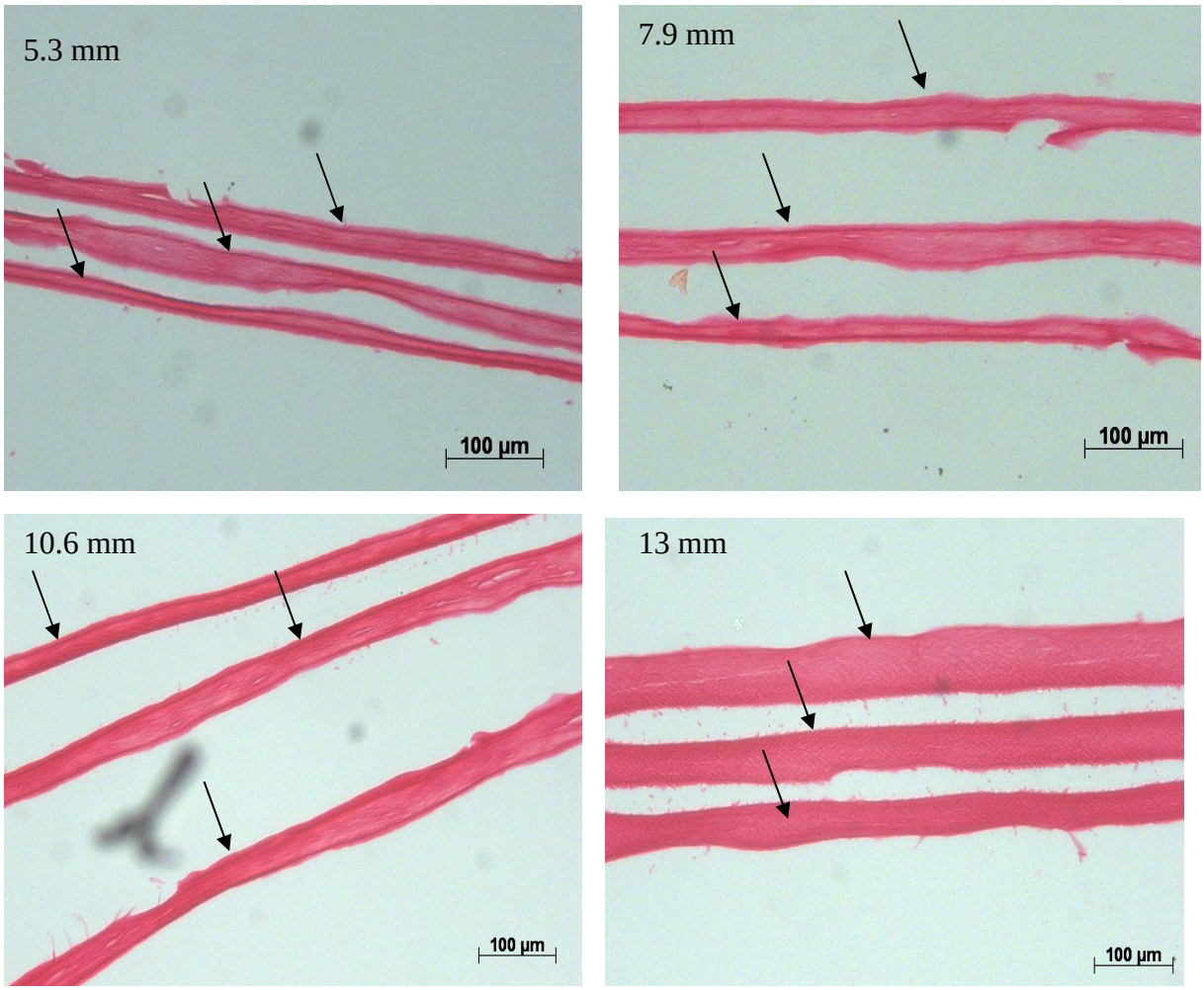

Fig. 9 Representative histological images of the constructs (in triplicate, indicated by arrows), fabricated using multi-well plastic compression process from the gels of 5.3 (a), 7.9 (b), 10.6 (c) and 13 (d) mm initial height. Constructs were fixed immediately after compression. Staining-Sirius Red.

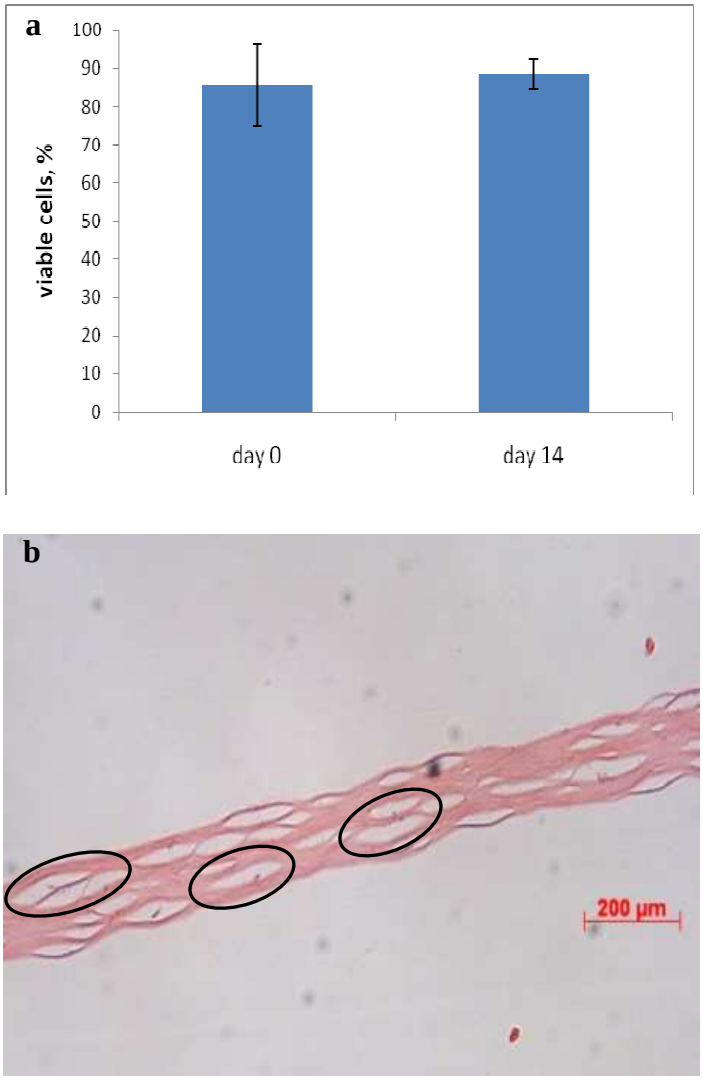

Fig. 10 (a) Histogram showing percentage of viable cells in the constructs prepared using multi-well plastic compression immediately after assembly (day 0) and after 14 days in culture. (b) Representative histological image of the cell-seeded construct after 14 days *in vitro*. Areas of cell matrix remodelling are outlined in black.

Discussion

In this chapter multi-well plastic compression (M-PC) of collagen has been developed and characterised as a route to scaling-up of the process. Basic concept of the technology, described in the original paper by Brown et al (2005), involves uniaxial rapid expulsion of >98% of interstitial fluid from hyper-hydrated collagen gels under load. The same principle of unidirectional fluid removal was used in the

spin-off method, described here but with setting and compressing of the collagen gels in a multi-well format, making use of the standard tissue culture multi-well plates. In this instance 12 well-plate format was used, though various formats (eg 6, 24 or 96 well-plates) can be used. This technique allows for simultaneous fabrication of multiple constructs in controlled manner, potentially reducing inter-construct variability as well as handling of the constructs by the operator. This last point is particularly important for cell-seeded samples as constructs can be set, compressed and cultured in the same sterile container.

In this chapter the technique has been evaluated based on the basic characteristics of the constructs, produced using this technique. Following parameters were investigated: (i) average fluid loss against time, rate of fluid loss and dynamics of fluid leaving surface formation during compression of the range of collagen gel heights, (ii) end time-point of full compression for the same gel heights, (iii) reproducibility of the method between sets as a function of the resulting constructs weight, thickness and total volume of the fluid, lost from the gels of each height, and (iv) effect on long-term culture of cell-seeded constructs, compressed in this manner.

The new method allows for simultaneous standardised compression of different collagen volumes in triplicates in the same well-plate. Rolls of absorbent paper were used as the absorbent plunger with discs of filter paper in contact with the gel to ensure even liquid distribution and absence of marks on the surface of the gel from the paper roll. Simply by measuring the change in the weight of absorbent over time as an indicator of the amount of fluid lost from the gels, it was possible not only to characterise the new process in terms of the time of full compression for the gels of different heights. It has also been shown, that the process progression greatly depends on the height of the gel for any given surface area.

There was no linear relationship between the height of the gel and compression time, i.e. by doubling the height of the gel (5.3 to 10.6 mm) does not mean that the time-point of full compression is achieved in double the time. Indeed, where smaller gels were compressed in 5 minutes, gels of twice the height were compressed in 20 minutes. These results are in perfect agreement with the current report (Hadjipanayi et al., 2010) where the authors showed that the higher the volume to surface area ratio, the longer it takes to fully compress the gel due to the following phenomenon. As the hyperhydrated collagen gels effectively comprise a network of the interconnected fibrils, suspended in large volumes of water, when liquid is removed from a single exit surface (fluid leaving surface, FLS) this effectively functions as an ultrafilter, retaining cells, fibrils and large molecules. It is a well described phenomenon, that such filters become blocked with time to the point where surface permeability falls near to zero. Such caking of the filter membrane is a major problem in the industries such as water purification. Therefore, the higher the gel (and, consequently, the amount of fibrous protein) the faster this 'filter' will become blocked and therefore longer time is required to remove the residual fluid.

The detailed mechanism of the FLS blockage has been demonstrated recently (Hadjipanayi et al., 2010). It is known that during plastic compression of collagen, deposition of protein layers on the exit surface leads to formation of microlamellae in the bulk of the constructs (Brown, 2005). Further investigation by Hadjipanayi et al. showed that this is a key to the falling permeability of the FLS during the compression. In this study carbon particles were mixed with the neutralized collagen solution, and a collagen gel was set in the mould with extremely high height to fluid leaving surface area ratio (3.5 ml of collagen was set in the barrel of the 2ml syringe) and was allowed to compress under its own weight. The set-up effectively

exaggerates the height to surface area effect and produces ‘slow motion’ compression which is easy to measure.

Particle deposition on the FLS and compaction over time was monitored. This indicated that different layers of collagen move independently, so that the area of the gel furthest from the FLS changed very little (based on carbon particles position) with time. Thus, each new collagen-lamella was added onto the filter cake on top of the previous layer of collagen, but at process completion any uncaked lamellae remained as separate outside the mass of collagen, concentrated at the fluid leaving surface. Therefore, effectively from the moment plastic compression was initiated new layers were added to the FLS, such that water has to to pass through growing number of dense layers until it becomes blocked. This hypothesis has been tested in the standard plastic compression condition, where process was unconfined (gels are removed from the setting mould prior to compression) and the height of the gels was very small compared with the fluid leaving surface area, in contrast with the new multi-well system described here.

Taking into account these two factors it is possible to explain the characteristic ‘jumps’ in the curves of average fluid loss for the 7.9 and 10.6 mm gels by the formation of the additional, secondary fluid leaving surface at the bottom of the gels. Compression of the collagen gels in the multi-well format can be described as pressure system, where fluid movement relieves the building pressure. As a consequence, when one out-let (primary FLS) becomes blocked, a secondary FLS formation is likely in the areas where it was not favourable initially, for example at the bottom of the gel, as illustrated schematically in Figure 11. The time-points of the ‘jumps’ (third minute of the process for the 7.9 mm gels and second minute for the 10.6 mm gels) would represent the time-point of the secondary FLS formation. It

appears that in the case of the 5.6 mm gels secondary FLS was not formed. In the case of the 13 mm gels, formation of the secondary FLS, if it is formed, must have taken place during the first minute of compression. The formation of the additional fluid leaving surface presents an interesting opportunity to engineer the internal structures in the compressed collagen gels using the new system. As height of the gel is a ratio of volume to the surface area this is applicable to other formats (6, 24, 96 well plates). Knowing the ratio and the desired internal structure of the construct it is possible to fabricate a uniformly compressed construct (such as resulted from compression of the 5.6 mm gels) or a construct with two dense fluid leaving surfaces as in the case of the 13 mm gels. By terminating the process at certain known time-points great degree of internal anisotropy can be engineered. For example, as in case of the 7.9 mm gels, terminating the process before the third minute of compression can potentially result in the construct with the decreasing top-bottom internal gradient of collagen density.

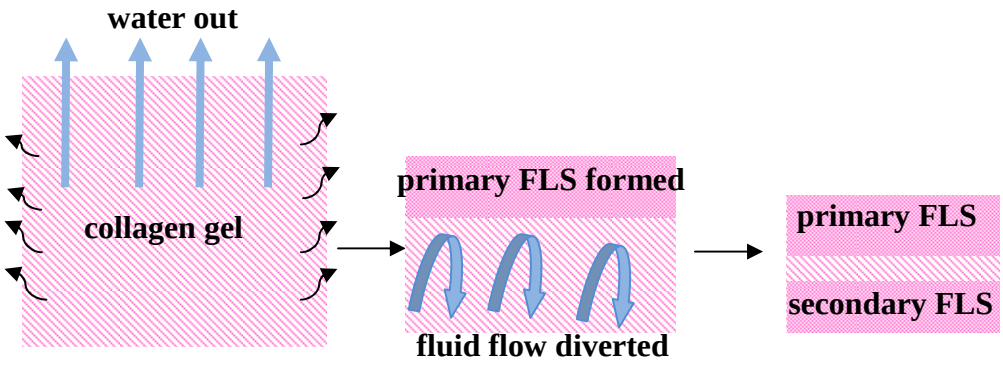

Fig.11 Diagram, illustrating the proposed mechanism of the secondary FLS formation during the multi-well compression process.

Interestingly, the effect of the gel height on the process of compression in the multi-well format was also evident when the rate of the fluid loss from the gels was analysed. The higher initial rate of the fluid flow from the gels with higher volume to surface area ratio suggests that in this system fluid is expelled from the gels not only

through the fluid leaving surface (primary and secondary) but also though the sides of the gels. This is indeed not surprising. Geometrically, gels, set in the well-plate, can be described as cylinders. As such, the surface area of the side of the cylinders in quite substantial compared to the area of the principle fluid loss (the top and bottom) of the cylinder. As an example, surface area of the side of the 13 mm high gel is 898mm^2; sum area of both top and bottom in this system is (2x380 mm^2) 760 mm^2, giving a total of 1658 mm^2. Compared to the smallest gel height, used in this study, surface area of the side is 366 mm^2, and sum area of top and bottom, as before, 760 mm^2; total area of the gel is 1126 mm^2.

Indeed, it appears that this additional fluid leaving route adds significantly to the rate of fluid flow when the height of the gels is equals or greater as radius of the FLS, as this phenomenon is not present when gels of smaller height are compressed. The sides of the gels were not usually taken into account as a route of fluid flow when collagen gels are compressed following the standard protocol due to traditionally small height (7.4 mm) to fluid leaving surface area (672 mm^2) ratio (thin rectangular block). The surface area of the side of such a gel is 784 mm^2, giving a total surface area of the gel (and potentially routes for fluid outflow) of 2128 mm^2. It appears that compression of gels which surpass a certain crucial ratio of height to FLS area is not possible in the standard conditions as it leads to the significant deformation of the compressed gels (Hadjipanayi et al., 2010). This fact highlights another advantage point of the new system, where no substantial change in shape was noted between the constructs.

The method of multi-well plastic compression allows for monitoring of the process of compression as it happens at the set time points. In this study, monitoring of the process minute by minute for the first five minutes showed that the events,

occurring during the first minute of compression, govern the whole process. During the first minute of compression same amount of fluid (approximately 1 ml) was lost from the 5.3 mm gels (2 ml of neutralised collagen solution) and 7.9 mm gels (3ml of collagen solution). Based on initial collagen concentration (2 mg/ml, as supplied by the manufacturer), when this amount of fluid left the gel, 1.6 mg of collagen has been deposited on the fluid leaving surface and this amount considerably slowed down the rate of fluid flow during the remainder of the process. Therefore, it is possible to estimate the critical collagen concentration at a fluid leaving surface is 4.2×10^{-3} mg per mm^2. When this is achieved, the permeability of the fluid leaving surface falls substantially. This constant can be used for other formats (6, 24, 96 well plates) if the same starting conditions are used (initial collagen concentration, absorbent, applied pressure), bringing further degree of control and understanding of the plastic compression process.

Collagen gels consist of two components – fluid and protein, which are mobile during the plastic compression. Movement of the fluid component can be measured directly by measuring changing weight of absorbent at set time-points. However, direct monitoring of the translocation of the protein component is challenging, although this data would help in understanding the anisotropy in the compressed gels due to blockage of the FLS. Quantitative assessment of the dynamics of the FLS formation during compression as well as protein accumulation at the FLS when process is completed, gives greater control over the internal structure of the construct. This can prove valuable for example when micro-moulding features into the FLS as stability of these greatly depends on formation of a dense layer of protein on the fluid leaving surface, as discussed in the previous chapter. One of the ways to directly quantify the dynamics of a growing layer of collagen in the vicinity of fluid leaving

surface would be to fix compressed gels at set time points and measure the thickness of denser collagen layer in the bulk of the compressing collagen gels from histological images. Alternatively, an indirect approach was taken in this study. It has been shown that the process of plastic compression can to some degree be described by the Darsy's law of fluid flow through the porous media under pressure (Hadjipanayi et al., 2010, Serpooshan et al., 2011). Using this equation, it is possible to calculate growing hydraulic resistance at the fluid leaving surface during compression of the gels of different height.

The hypothesis under test was that given equal fluid leaving surface area, pressure (force) applied to generate fluid flow, amount and quality of absorbent and collagen concentration, the hydraulic resistance of FLS will be greater in taller gels as bigger volumes of water travel through the body of the gel carrying larger amounts of collagen with it, resulting in quicker blocking of the leaving surface leading to higher resistance. The data obtained in this study support this hypothesis, however in the view of the additional points of fluid exits (sides and bottom surface) it is difficult to distinguish between the hydraulic resistance of the primary FLS (in contact with the absorbent) and others. Further experiments are needed to pin-point the time-points of the additional FLS formation together with histological examination of the constructs, as suggested previously.

Growing hydraulic resistance on the fluid leaving surface is explained by the transport of the protein content of the gel during compression which results in the gradual blocking of the FLS, as has been discussed previously. As such, this value describes the layer of collagen, closest to the fluid exit point, distinguishing it from the collagen in the bulk of the construct. Therefore, if the resistance of the FLS, achieved at the point of full compression for the gels of different heights can be

converted into the absolute amount of collagen, it would be possible to characterise compressed collagen gels by two values: the amount of protein on the FLS and in the main body of the construct. As the value of FLS resistance at the first minute of compression for 5.3 mm gels corresponds to the critical collagen concentration (as discussed previously), it is possible to convert R_{FLS} values into milligrams of collagen. Following these calculations, when the 5.3 mm gels are fully compressed, 90% (2.58 mg) of the protein content has been deposited at the FLS, giving constructs with near homogeneous density if collagen throughout the construct. Therefore, when constructs with homogeneous distribution of the protein are required, gels of this volume to surface area ration should be used. In the gels with higher ratio, formation of the secondary FLS must be taken into account but generally these will have more complex heterogeneous densities. Therefore, when the height of the gel is doubled, protein is distributed equally between the primary and secondary FLS (approximately 40%). Therefore, formation of the secondary fluid leaving surface when gels are compressed using this new system is a significant phenomenon, affecting the collagen distribution throughout the resulting construct. It offers an interesting possibility of micro-moulding of the both surfaces of the construct which was not possible using the standard PC method.

To conclude, it has been shown in this study that the main characteristics of the M-PC process are well within those for the original method. Loading pressure used here, even allowing for gradual increase in the weight of absorbing paper rolls, is within defined limits specified previously by Hadjipanayi et al. (2010). Time of compression is longer in M-PC due to smaller fluid leaving surface area and semi-confined set-up, compared to the standard protocol. The amount of fluid lost from the gels of the heights investigated is also within the range set for the original method

(90+%, Brown et al., 2005). Thickness of the fixed constructs corresponds well with the data obtained for the original method (up to a 70 µm) (Brown et al., 2005). Viability of resident cells is also within range defined for original PC method and constructs can be cultured up to 2 weeks without detrimental effect. Morphology of the constructs at the end of culture period was comparable with constructs made using the original PC method and showed signs of matrix remodelling (as discussed in the previous chapter).

The multi-well plastic compression method has several considerable advantages, compared to the original method. Simultaneous compression of multiple gels offers considerable saving on time of single construct fabrication. The process is easy to monitor and control, resulting constructs do not require additional handling and can be cultured in the same plate if needed. More importantly, given the reproducibility of the constructs produced within the set, use of M-PC will potentially give an operator greater control over properties of resulting constructs, depending on desired end-result. Additionally, the new system allows for precise control over the morphology of the resulting constructs, offering a choice of the isotropic or anisotropic distribution of the protein in the body of the construct by varying the volume to surface area ratio within the limits, defined in this study.

The key advantage of the new system is that fluid from the gels is removed in the upward direction, so that the principle fluid leaving surface is now always on top of the last compressed gel. In other words each new gelling layer has a brand new (unblocked) FLS. This makes possible to explore the repetitive fabrication of multi-layered constructs, which was not possible (or technically challenging) using the standard system. In this case water was removed downwards through the same FLS for all repeating layers (Hadjipanayi et al., 2009a, Ananta et al, 2009). In such a

system, if new layer is cast on top of the previously compressed one, the fluid content of the upper gel needs to flow though its own forming FLS and through the dense underlying compressed gel. Certainly, making triple-layered compressed constructs in such a system would allow minimal compression of layer 3. The new method circumvents this obstacle, as each newly set collagen layer will be compressed on top of the previous one with the new FLS forming on top of each layer. The next chapter is dedicated to investigating mechanisms of multi-layered construct formation and testing this fluid flow hypothesis using the upward flow multi-well format.

Chapter 6

Fabrication of the multilayered PC collagen constructs using M-PC method

Introduction

Following development and evaluation of multi-well plastic compression (M-PC) method as described in the previous chapter, the possibility of creating multilayered constructs, using this method, was investigated. The evolution of separate layers with distinct function in multi-cellular organisms appears as early as the hydra (Cnidaria). In the human body almost every tissue consists of spatially defined layers and cell types, differing from tissue to tissue in number and complexity.

Taking this into account is paramount for engineering tissues, both for *in vivo* or *in vitro* use. However, until recently, the majority of research was done on the assumption that a single-layered bulk of matrix (natural or synthetic) and cells would be sufficient. For example, in the well researched area of skin engineering, FDA approved products used in clinic to treat diabetic ulcers and burns started as single sheets of decellularised extracellular matrix or cell-compacted collagen hydrogels with only recent development of one or two cellular layers (Shevchenko et al., 2010, Groeber et al., 2011). However, human skin consists of spatially and functionally defined layers with specialised cell populations in each layer. It is not surprising, then, that allografts are still the gold standard when treating diabetic ulcers and burns. A number of techniques have been developed recently for layer or sheet tissue engineering. These generally either involve layering of cell-sheets (which are poor in matrix) or layering of biomaterials (Yang et al., 2005).

As plastic compression effectively produces a sheet of cell-seeded collagen it appears to represent a further advance for engineering thick, multilayered constructs. Hadjipanayi et al (2009) demonstrated fabrication of double-layered constructs (cellular and acellular) by separately casting collagen gels, with the first gel being set prior to addition of the second layer. The whole structure was then compressed in a single stage as per original method. However, this technology has its limitations. One of the restrictions of PC is the rate, and final extent, of compression (i.e. thickness of the resulting construct, water content and collagen concentration). These parameters are closely related to formation of the fluid leaving surface (FLS) area and the initial height of the gel, as demonstrated in the previous chapter. It is known that decrease of flow rate during compression is mainly due to the blocking of FLS by collagen fibres, carried with the fluid and accumulated at the boundary level (Hadjipanayi et al., 2010). It has been shown that restriction of FLS blockage when using the original PC method can be partially overcome by partial compression of the gel on each side, so that two FLS are formed on the opposite surfaces of the gel, (Hadjipanayi et al., 2010). However, this method is also limited by the initial height of the gel and alters final construct structure, creating greater top-bottom symmetry.

The advantage of multilayered M-PC is that there are no progressive restrictions of FLS. Each new gel layer forms a new FLS when compressed. Theoretically, the thickness of each single layer is the main restriction, not their total number, as each layer is compressed individually. Also, as stressed in the previous chapter, this model gives an opportunity to fabricate multiple constructs simultaneously (6 to 96, depending on the well-plate format used). Additionally, by using this method, it is possible to fabricate complex multilayered tissues with different cell-types or densities in each layer. It may also be possible to control cell

infiltration between the layers, as it is known that increased stiffness of the matrix enhances motility of some cell types (Hadjipanayi, 2009).

As has been shown in the previous chapter, it is possible to control the amount of collagen accumulated at the FLS and hence control the speed or even direction of cell infiltration between the layers, by selecting the initial height of the gel with a matched compression time.

In this chapter use of multi-well plastic compression for fabrication of multilayered collagen constructs will be described as well as basic characteristics of the process and the constructs, produced using this technique. The following parameters will be investigated: (i) qualitative assessment of layer separation following agitation and morphology of the interlayer interface, (ii) change in thickness of the constructs, brought in contact with fluid immediately after PC as an indicator of interlayer integration mechanisms, (iii) effect of double-layering of the gels on the fluid loss from the upper layer and progression of the compression process of the same layer compared to the compression of the single layer (iv) effect of layering more than two (up to ten) gels on the construct morphology and fluid loss dynamics from the upper layer, and (v) effect of cellular activity on the morphology of the interfaces in the multilayered cell-seeded constructs at the end of culture period.

Materials and Methods

Preparation of acellular and cellular collagen gels

Collagen was neutralised as described before (Chapter 2). Cellular constructs were prepared as described before (Chapter 2).

To investigate influence of resident cells on multilayered constructs, 1, 2, 3, 4 and 5 layered constructs were made, each layer consisting of 10.6 mm (4 ml) of cell-

containing collagen solution. Constructs were cultured in the same plate for 3 weeks (n=3 for each condition).

Fabrication of multi-layered constructs using M-PC (multi-layered M-PC)

A schematic illustration of the construct assembly is shown in Figure 2. Multi-well plastic compression was performed as described in the previous chapter. Briefly, standard tissue-culture 12-well plates were used as the casting mould. Rolls of absorbent paper (d=21mm, average weight 4.4±0.3 g) acted as the fluid-removing elements. Each gel was subjected to 35.8 g + 4.4±0.3 g (1042±1.6 Pa) initial load. After compression of the first layer (Figure 1a), fresh collagen solution was poured on top of the first (compressed) layer, set in the same manner and compressed following same protocol (Figure 1b).

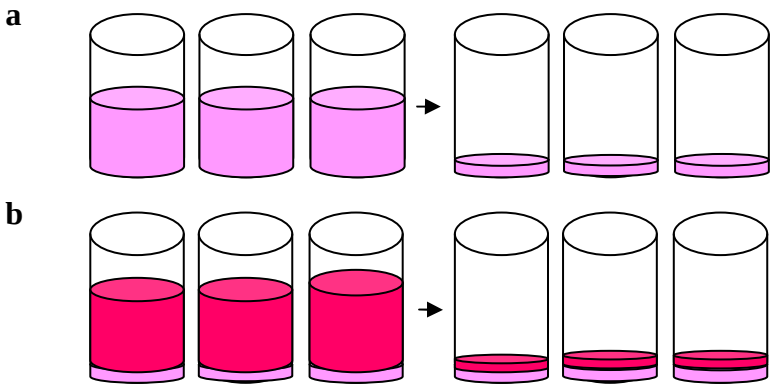

Fig. 1 Schematic illustration of the multi-layered collagen construct assembly. (a) Collagen gels are set and compressed in the 12 well-format, leaving compressed collagen sheet at the bottom of the well which will act as a first layer. (b) Second volume of neutralized collagen is set on top of the first (compressed) layer. When second gel is set, process of compression is repeated, resulting in the double layered construct. Process is repeated in the same manner for fabrication of collagen constructs, consisting of more than two layers.

Layer separation assay

Two-layered constructs (n=3), each layer consisting of 13 mm gel were prepared as described above. To investigate the nature of the interlayer connection,

these constructs were compared with two layered constructs (13 mm initial gels, n=3), where each layer was compressed simultaneously in separate wells and then pressed together with the load (43 g) for 5 min. Both types of constructs were submerged in 10 ml of PBS and agitated on a shaker plate for 20 minutes or until layers separated.

Measurement of fluid loss

Fluid loss from each layer during multi-layered construct assembly was monitored in the same manner described in the previous chapter. Data were collected for following constructs: 2 layers of 5.3mm, 10.6 mm and 13mm initial gel height (n=6 for each gel height), 10 layers of 5.3 mm gels and 10 layers of 13 mm gels (n=3 for each gel height). Data is presented as mean fluid loss±SD.

Post-compression change in construct thickness

Single layered constructs (n=3), made from 13 mm gels, were cut into quarters, which were either fixed immediately (t_0), or left in PBS for 0.5, 1, 1.5 hrs prior to fixation. A separate experiment was performed in the same manner with fixation at t_0, 2, 2.5 and 3 hrs. Constructs, made of three layers (13 mm gels in each layer) were cut in half. Each half was either fixed at t_0 or left in PBS for 24 hrs and fixed at the end of this period. Fixed samples were wax-embedded and sectioned at 12 µm thickness in transverse plane. Sections were stained using SiriusRed staining protocol (see Chapter 2) and used for image analysis.

Histology and image analysis

Cellular constructs were fixed after 3 weeks in culture and processed as described in Chapter 2. Thickness of the whole construct and individual layers was compared with the thickness of single layered construct. Data is presented as mean thickness of the construct±SD

SEM

Two-layered constructs (n=3), assembled from 5.3 mm initial gel height per layer were processed as described in Chapter 2.

Statistical analysis

Data were analysed as described in Chapter 2.

Results

Interlayer integration

It is essential requirement of the fabrication of the multi-layered contracts that layers do not separate following mechanical agitation. To qualitatively evaluate interlayer integration of two-layered constructs, gels of 13 mm initial height per layer were prepared following two experimental designs. The first treatment consisted of separately compressing two collagen sheets. The process is shown schematically in the Figure 3, insert on the left. These constructs were compared to the double-layered constructs, made of 13 mm gels compressed following the multiM-PC method, where first gel was compressed and second gel was set and compressed on top of the first one. Process is shown schematically on the Figure 2, insert on the right.

Constructs, prepared following both protocols, were then submerged in 10 ml of PBS and agitated on a shaker plate until layer separation. Double-layered constructs, made using the first treatment (manual layering) became separated after 2 minutes of agitation. Constructs, made using the second treatment did not separate following agitation for 20 minutes, at which point process was terminated. Main picture in the Figure 2 shows two dishes with the manually assembled construct on the left and multi-layered construct assembled using the multi-layered M-PC method on the left after 20 minutes of agitation.

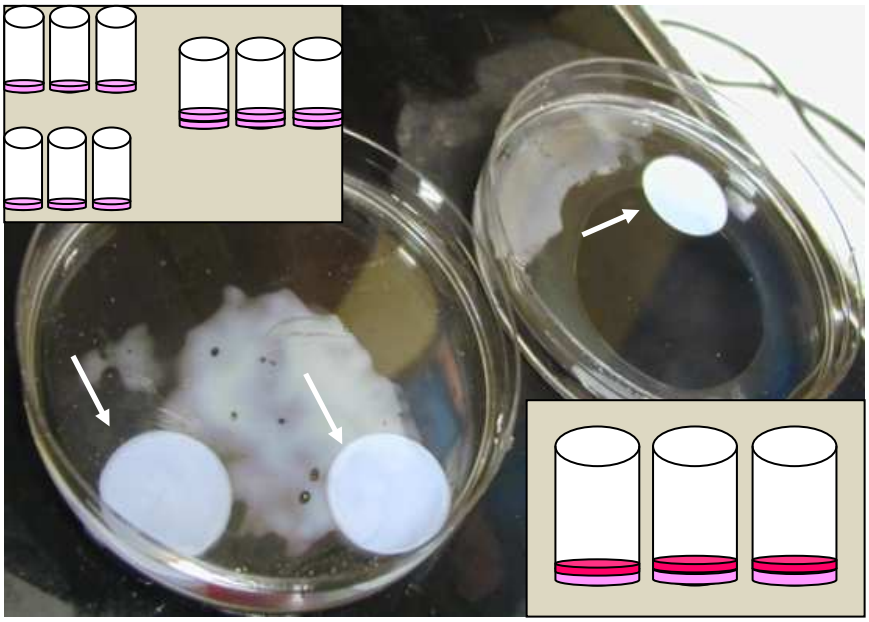

Fig. 2 Results of the layer separation assay. Double-layered constructs were prepared either by separately compressing two collagen gels and manually pressing them together afterwards (insert on the upper left corner) or by compressing the first layer and setting next gel on top of it prior to compression (insert on the lower right corner). The resulting constructs were subjected to mechanical agitation on a shaker plate for up to 20 minutes. Constructs, made using the first protocol separated after 2 minutes of agitation; two separate layers are shown floating in the Petri dish on the left. Constructs, prepared using second protocol remained intact after 20 minutes agitation and shown in the Petri dish on the right as a single construct. Constructs are indicated on the image by arrows.

Dish on the left contains two separated layers, whereas construct on the right is intact. These data indicate resistance of the multi-layered constructs to mechanical agitation.

The interface between layers of the double-layered constructs, made using multi-well plastic compression method from 5.3 mm gels, was visualised using SEM. The inter-layer interface post-compression was exposed by tearing the constructs the transverse plane and partially separating the layers. Figure 3a shows a representative SEM image of the intact bi-layer with a visible FLS (fluid leaving surface), indicated on the image by arrows, at the upper layer and the interface between the layers and indicated by arrowheads. Interestingly, it appears from the image that FLS of the

bottom layer is less dense compared to the upper layer. When layers were manually separated as shown in Figure 3b, interface surface of the bottom layer had 'wispy' fibrous appearance compared with the FLS of the upper layer. The internal structure of interlayer space, shown in Figure 3c, consisted of the fibrilar structures connecting the two layers.

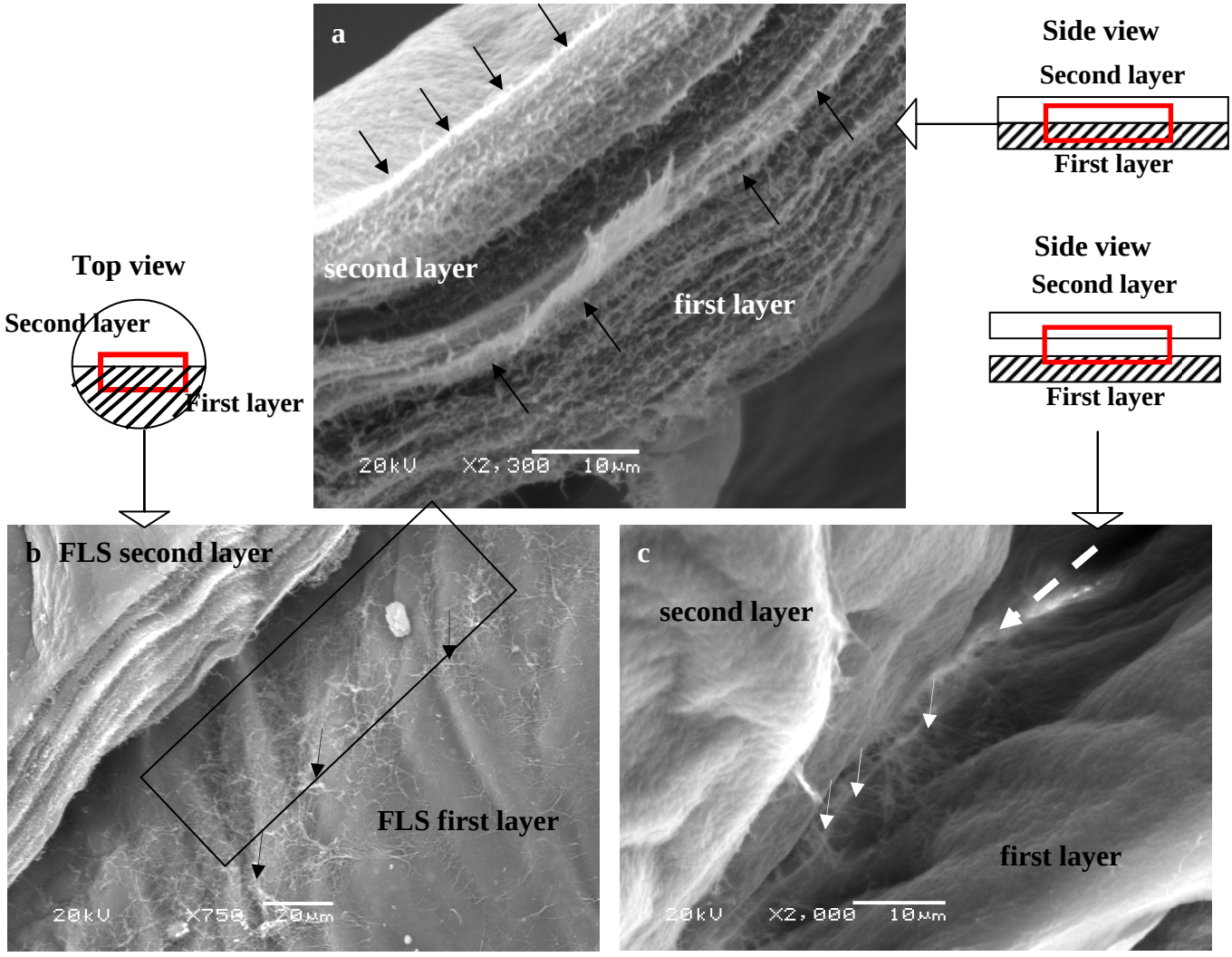

Fig. 3 Representative SEM images of the interface area between two layers of the double-layered construct, made from 5.3 mm gels. Constructs were fabricated by compressing the first collagen gel and subsequent setting and compression of the next layer on top of the first (compressed) layer. (a) Transverse view of the construct. Top layer on the image is the second (top) layer of the construct. The fluid leaving surface of the top layer is indicated by the downward arrows, the area of interface between the layers is indicated by the upward arrows. (b) Top view of the exposed interface area. For that, top layer was lifted to expose

underlying surface. Arrows in the highlighted area indicate collagen fibrils torn in the process, which gives the interface characteristic 'wispy' appearance. (c) Internal view of the interface between two layers. Layers were gently separated without total detachment prior to expose the interface. Dashed arrow indicates area of interest, solid arrows point at collagen fibrils, stretched between two layers.

These results suggest that interlayer connection must take place whilst upper gel is still in liquid form (prior to fibril assembly) as collagen fibrils, connecting the upper layer to the lower, pre-compressed layer could only have come from the second compressed gel. The interconnection between layers also suggests interlayer fluid movement, as these connecting fibrils stretch between layers one and two, so they must have been drawn in the FLS of the layer one at some point in the construct assembly.

Dynamics of change in constructs' thickness after compression

Plastic compression results in high degree of dehydration of the constructs (>90% of fluid content is removed) immediately after process is completed. This can potentially result in some degree of fluid reuptake if constructs are brought in contact with liquid afterwards. If true, it could affect interlayer integration, as the next layer of neutralised collagen is poured on top of the previously compressed one prior to gelation. To assess the effect of construct incubation on the thickness as an indirect measure of fluid reuptake, constructs made of 13 mm gels were either fixed immediately after assembly (thickness at time 0) or left in PBS for up to 3 hours in total and fixed at 0.5 hours intervals, giving measure of the thickness at 0.5, 1, 2, 2.5 and 3 hours of incubation. Constructs were fixed at these time points, stained with SiriusRed and thickness measured from the resulting images. Initial thickness (at time 0) of the constructs, made of the gels of 13 mm height was 60.8±5 µm.

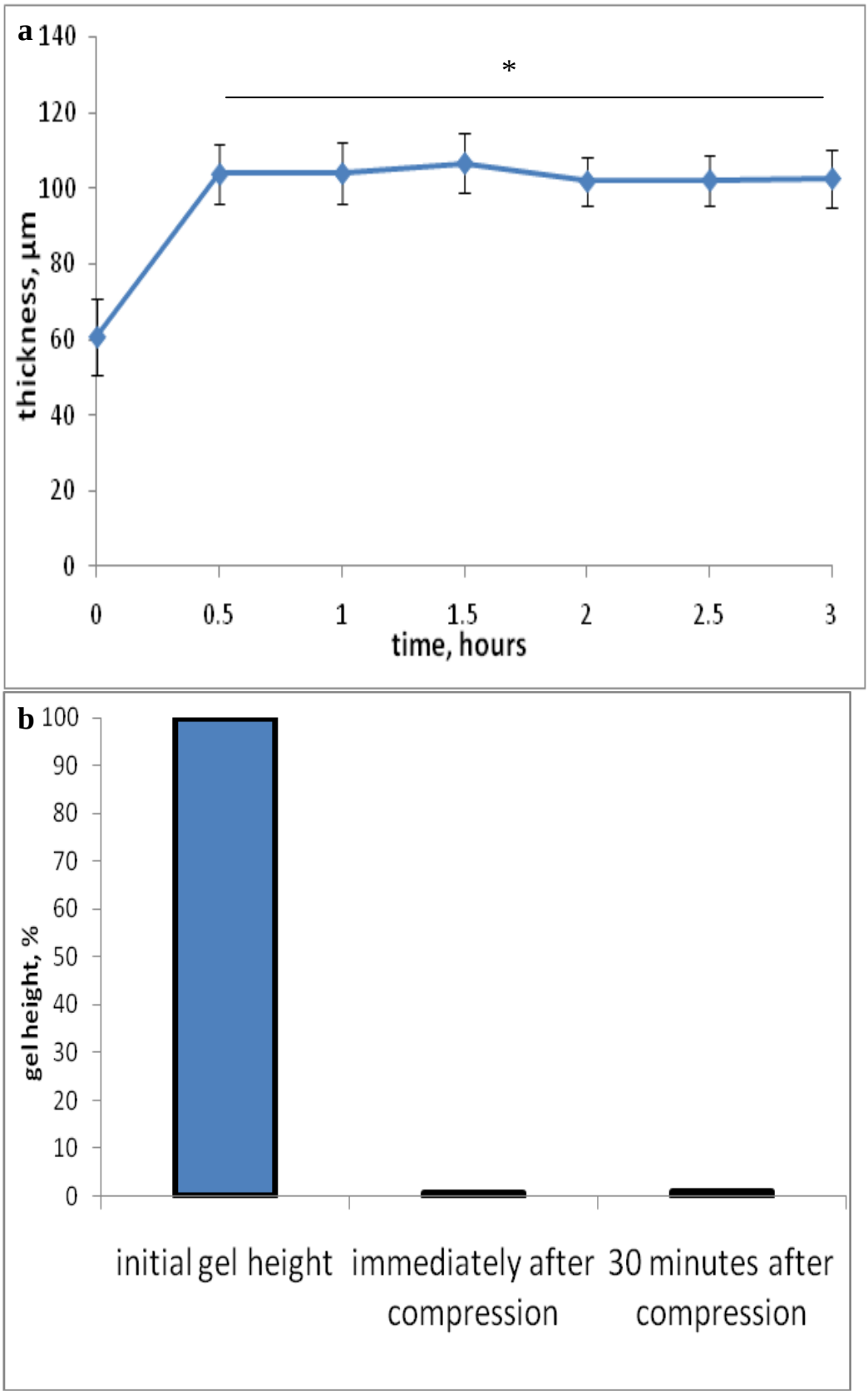

Fig. 4 (a) Graph showing change in the thickness of the compressed constructs, made in the 12 well-format, with the incubation time; initial height of the gel – 13 mm. * - significant difference compared to time 0 ($p<0.05$). (b) Bar chart, showing relative change in the height of the compressed collagen immediately

after compression and after 30 minutes incubation in PBS compared to the initial height of the gel (13 mm) in percent to confirm plastic nature of the process. Initial height of the gel is taken as a 100%.

After incubation in PBS for 0.5 hours, thickness of the constructs increased significantly ($p=0.001$) to 103.8±7.9 µm. There was no significant increase in the thickness of the constructs at subsequent time points. Data is shown graphically in Figure 4a.The results indicate that significant reuptake of fluid takes place in the 30 minute interval after compression. However, this increase in the thickness of the compressed construct is not significant compared to the initial height of the gel (44 µm compared to 13 000 µm initial height) and does not compromise the term of 'plastic compression'.

Relative change in the initial gel height (taken as a 100%) after compression and after 30 min of incubation is shown in the Figure 4 b. It can be seen from the graph, that although there is an increase in construct thickness after 30 min incubation, it is insignificant compared to the initial gel height (100% - initial height (13 mm), 0.6% immediately after compression (60 µm) and 0.92% (104 µm) after 30 min incubation). To evaluate the effect of this change on the thickness of multilayered constructs, 3-layered constructs were fabricated from 13 mm initial gel height and either fixed immediately or following incubation in PBS for 24 hrs. Qualitative evaluation (Figure 5a) showed that overall thickness of the construct made of three layers and fixed immediately was 267.9± 8.2 µm, where average thickness of the layers 1 and 2 was 102 µm, and of the layer 3 (compressed last) was 64 µm. After 24 hours, overall thickness of the construct increased to 309 ± 17.1 µm due to reswelling of the third layer, an increase of approximately 15%. Figure 5b shows representative histological images of the constructs stained with Sirius Red. When constructs were fixed immediately after assembly several distinct features can be seen on the image

such as primary and secondary fluid leaving surfaces in each layer, indicated by the arrowheads and unequal thickness of the layers.

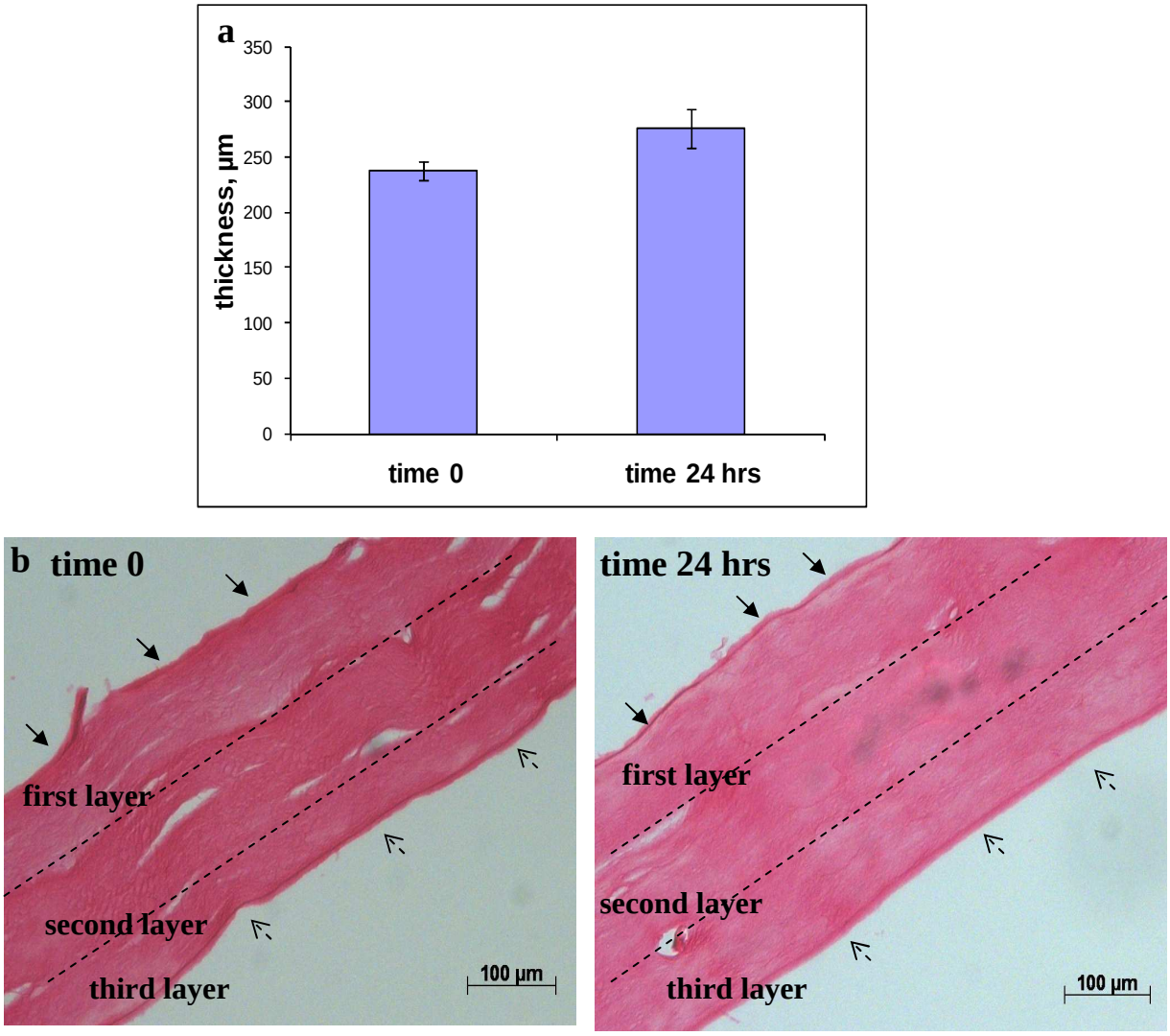

Fig. 5 (a) Bar chart showing the thickness of the triple-layered constructs, assembled from the 13 mm gels per layer. Constructs were either fixed immediately (time 0) or incubated for 24 hours (time 24 hrs) in PBS prior to fixation. (b) Representative histological images of the constructs, fixed at time 0 and time 24 hrs. Dashed lines indicate interlayer boundaries. Dashed arrows indicate primary fluid leaving surface of the third (uppermost) layer. Solid arrows point at the secondary FLS of the first (base) layer.

This morphology is indeed in agreement with previous finding. Reswelling of the layers one and two took place during the setting of the gels, which became upper layers. However, the uppermost layer had been fixed immediately and so did not

reswell, giving the discrepancy in the layer thickness. In addition it is clear that interlayer boundaries became less evident. However the primary FLS of the third (last) layer was still visible, as well as a secondary FLS at the base of layer 1, which was compressed first. These findings suggest that reswelling continues for at least 24 hours after process of compression is completed, although the increase in the thickness of the construct was not statistically significant.

Effect of multi-layering on dynamics of fluid loss from collagen gels during compression

As has been shown in the previous chapter, process of plastic compression can be described in terms of percentage fluid loss from the compressed gel at set time points and the progress of the process can be tracked minute by minute using this data. Fluid loss was measured by weighing the adsorbing paper at set time-points (every 5 minutes) until no change in weight was noted to determine the time-point of full compression. Absolute values of fluid loss from the gels (in ml) were converted into percent fluid loss; initial weight of the gel was taken as 100%. This method was used to study the effect of multi-layering on the dynamics of fluid loss from the gels of 5.3, 10.6 and 13 mm initial height. Double-layered constructs were made of 5.3, 10.6 and 13 mm gels in each layer.

To map the progress of the plastic compression in each layer and determine the effect of multi-layering on the process, the first five minute were investigated closely by measuring the weight of the absorbing paper roll every minute. Compression profile of the second layer was mapped separately, by comparing percentage fluid loss at each minute to the value at the previous time point. Data were then compared between the layers at each time-point to determine effect of double-layer compression on the fluid loss. Times of full compression and total fluid loss in

present of initial fluid content for layered 5.3, 10.6 and 13 mm constructs are summarised in Table 1. These parameters did not differ between layers 1 and 2 for all gel height investigated.

Table 1 Time-points of full compression and respective values of percentage fluid loss at these time-points for collagen gels of different heights, compressed as layers in multi-layered constructs. Surface area-379.9 mm^2

Layer number	Height of gel, mm	Time of full compression, min	Total fluid loss, %
Layer 1	**5.3**	**5**	**92.5±4**
	10.6	**20**	**93±2.3**
	13	**25**	**94.4±1.5**
Layer 2	**5.3**	**5**	**92.3±3.3**
	10.6	**20**	**93.4±1.5**
	13	**25**	**94.2±2.8**

In order to track the progress of the compression process, data acquired by measuring the weight loss from the gel of each height in each layer, diameter of the mould 22 mm) was analysed using one-way ANOVA. Where ANOVA analysis showed significant differences between the time-points ($p<0.05$), appropriate post-hoc test (Tukey HSD or Games-Howell) was performed to show significantly different time-points (minutes of compression). Data for each gel height and number of layers (5.3 (two and 10 layers), 10.6 (two layers) and 13 mm (two and 10 layers) were analysed in two ways. Firstly, in order to map the progression of the compression process, data for total fluid loss at each time-point of compression for each individual gel was compared with the value at the previous time-point (e.i. minute 2 to minute 1, minute 3 to minute 4 etc.). This analysis showed progression of the compression process for each compressed layer and helped to identify possible influences of multilayering on the progression of the process. Secondly, data collected at each time-point were compared between the layers (i.e. between layer 1 and 2 at minute 1, layer

1 and 2 at minute 3 etc.). This enabled identification of the time-points where process of multilayering resulted in significant differences in total fluid loss between layers. Both ways of data analysis allowed for better understanding of the multilayering process and its effects on fluid loss from the sequentially compressed collagen gels.

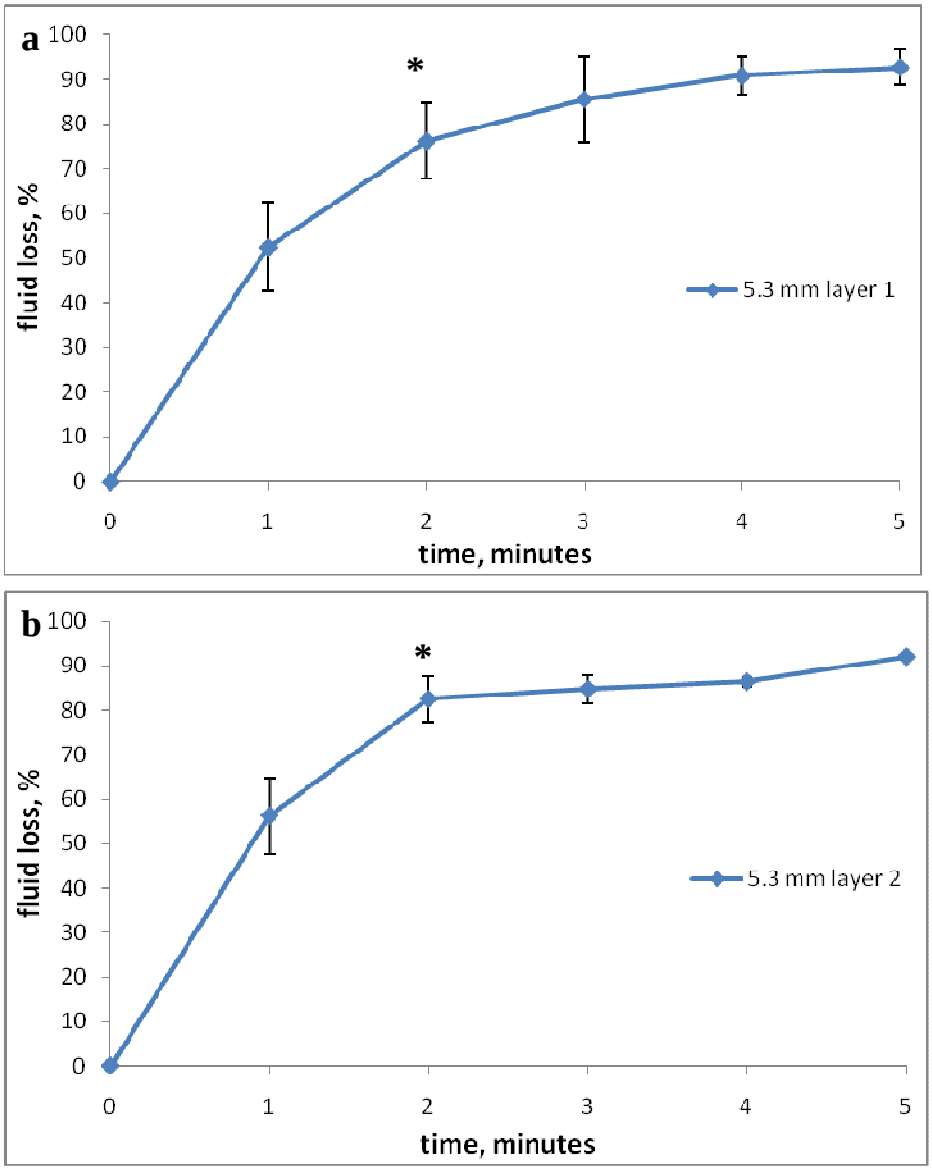

Fig. 6 Graphs, showing the dynamics of fluid loss from the double-layered collagen constructs made of the 5.3 mm gels per layer during the first 5 minutes of the of plastic compression process; (a) - layer 1 , (b) – layer 2. Fluid loss from the gels at each minute of the process is presented in percent of initial weight. *- significant difference between % fluid loss from the gels at each time-point ($p<0.05$).

Fluid loss from the first layer of the double layered construct, consisting of two 5.3.mm gels is shown in Figure 6a and did not differ from the corresponding values obtained previously (see Results, Chapter 5,).

Weight loss data from the second 5.3 mm gel (second layer is cast and compressed on top of the compressed first layer, Figure 1a) showed that total fluid loss at the first minute of compression (56.25±8.5%) differed significantly from all the subsequent measurements ($p<0.0001$). At minute 2, 82.5±10% of the initial fluid was lost (an approximate increase of 26%) which differed significantly from minute 1 ($p<0.0001$). Fluid loss at minute 3 (84.75±3.2%) was not significant compared to minute 2. By minute 4 of compression 86.37±5% of the weight was lost from the 5.3 mm gel, compressed as a second layer; further compression (at minute 5) resulted in loss of 92.3±3.3% of fluid content of the gel. Measurement at minute 10 showed no change in the weight loss. Data are shown graphically in Figure 6b.Time of compression did not differ between layer 1 and 2, both layers were compressed after 5 minutes. The general dynamics of the fluid loss from the second 5.3 mm high gel followed the same trend as during the compression of the single layer.

Fluid loss from the layers 1 and 2 made of 5.3 mm gels at each time point of compression (minutes 1 to 5) did not differ between the layers (Figure 7). Total fluid loss at minute 5 of the process was 92.5±4% from layer 1 and 92.3±3.3% from layer 2 (Table1). These data show that compression of the gel of 5.3 mm initial height on top of the construct, made by compressing gel of the same initial height has no effect on percentage fluid loss from the top layer.

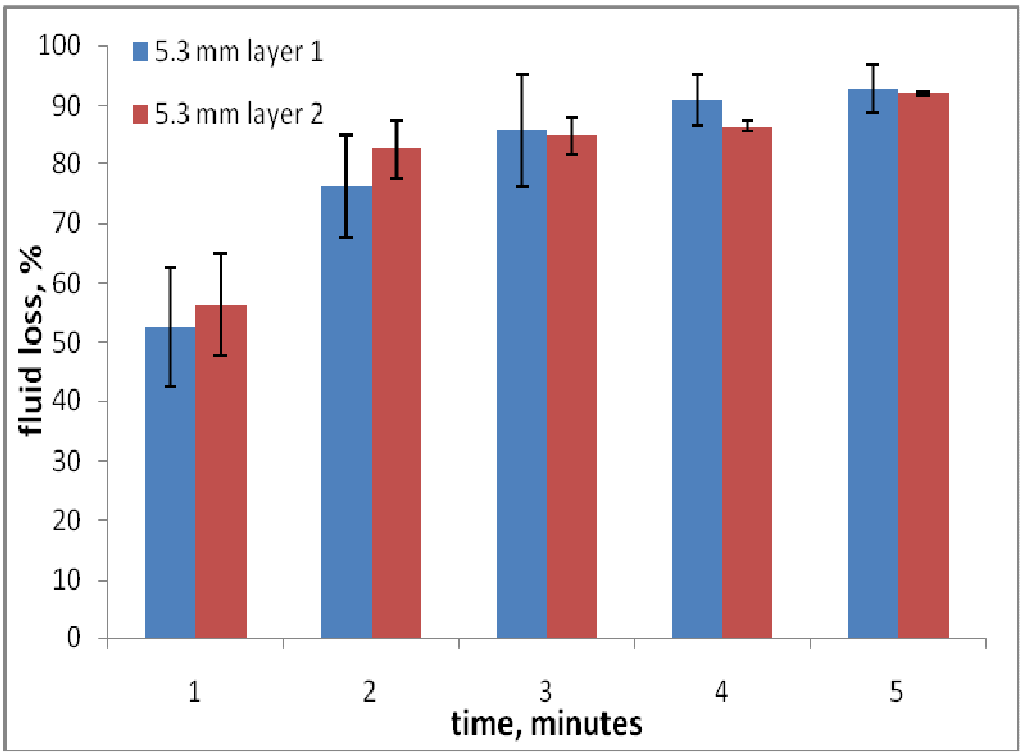

Fig. 7 Bar chart showing the effect of the layering of two 5.3 mm gels on fluid loss (in % of initial weight) during the first 5 minutes of plastic compression process.

Fluid loss from the first layer of the double layered construct, consisting of two 10.6 mm gels (Figure 8a) did not differ from the corresponding values obtained previously (see Results, Chapter 5,).

Fluid loss at each minute of compression (minutes 1 to 20) of the second 10.6 mm gel, compressed on top of the construct, made by compressing gel of the same initial height, is shown in Figure 8b. During the first minute of compression gels of this height lost on average 35±6.2% of the initial fluid content, significantly less than at all further time-points. At minute two mean weight loss from the gels of this height was 56.4±3.7% (approximately 20% increase), a significant increase compared to minute one ($p=0.0001$).

Interestingly, during the compression of the first layer, there was an approximate increase of 10%, from 37±3.9 at minute 1 to 45.5 ±2.5% at minute 2, indicating different dynamics of fluid flow when 10.6 mm gel was compressed on top of pre-compressed gel of the same height.

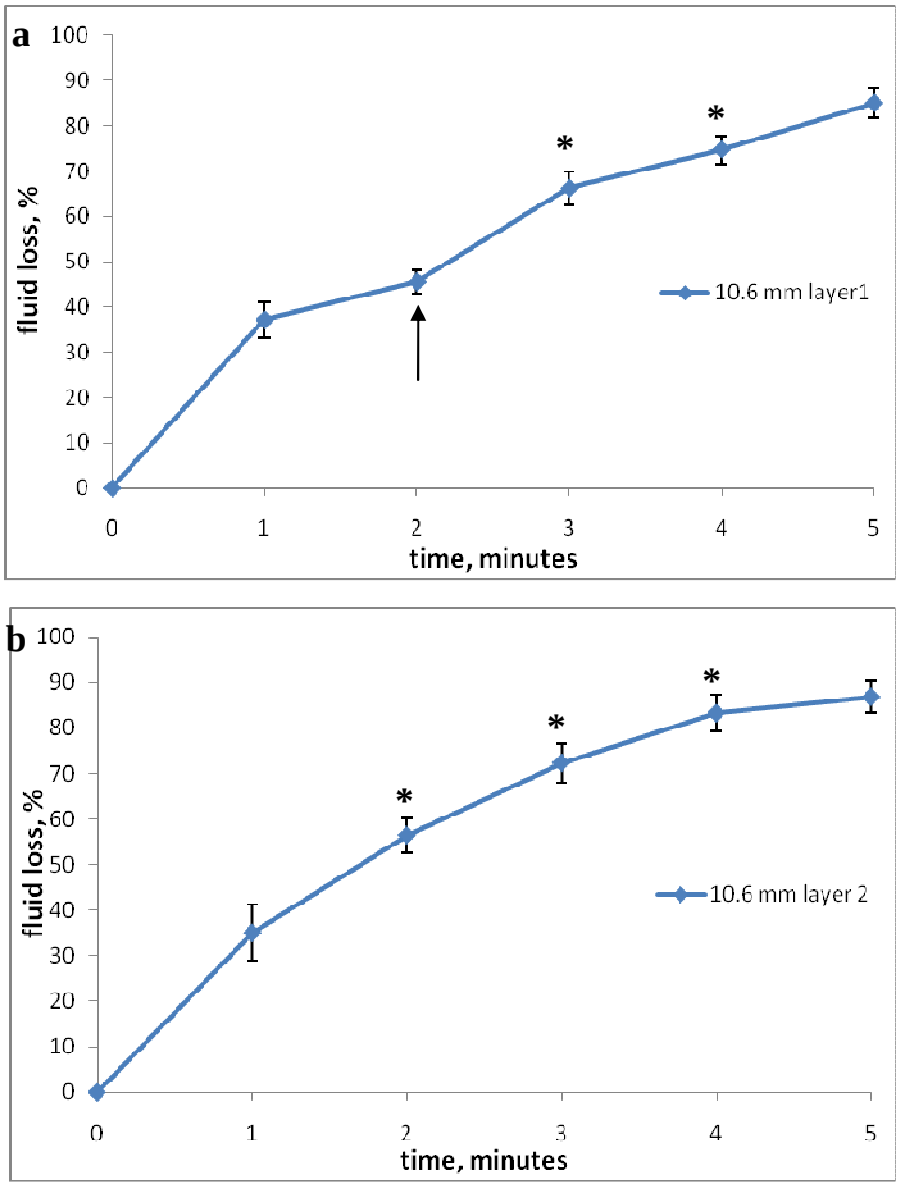

Fig. 8 Graphs, showing the dynamics of fluid loss from the double-layered collagen constructs made of the 10.6 mm gels per layer during the first 5 minutes of the of plastic compression process; (a) - layer 1 , (b) – layer 2. Fluid loss from the gels at each minute of the process is presented in percent of initial weight. *- statistically significant difference compared to the preceding time-point ($p<0.05$). Arrow points at the characteristic 'jumps' in the curve.

At minute 3 fluid loss from the second layer gels of this height amounted to 72.3±4.3%, a significant increase from minute two ($p=0.001$). Further compression resulted in a loss of 83±5% at minute 4 (increase of 10%, similar to this of the first layer), a significant increase compared to minute 3 ($p<0.0001$) and 86±3.4% at minute 5. Compression for further 5 minutes led to 89.2±2.4% fluid loss at minute 10. After further 5 minutes of compression 92.8±3% of fluid was lost from the second 10.6 mm layer at minute 15 and at minute 20, total fluid loss from the second layer was 93.4±1.5%. Compression for further 5 minute did not show change in the weight of the absorber, compression was completed at minute 20.

These results indicate that compression of the second 10.6 mm gel on top of the compressed gel of the same initial height does not affect time of compression or total fluid loss but has an effect on the dynamics of the process, resulting in a loss of characteristic ‘jumps’ in the curve

Figure 9 shows fluid loss from the layers 1 and 2 made of 10.6 mm gels at each time point of compression (minutes 1 to 20). At minute 2 fluid loss from the first layer was 45.5±2.5% and significantly greater ($p=0.005$) from the second layer 56.4±3.8%, a mean increase of 10.9%. Fluid loss at minute 3 was again significantly greater from the second layer ($p=0.014$). At this time-point 66.2±3.6% of the initial fluid content was lost from the first layer and 72.3±4.3% from the second layer, a mean increase of 6.1%,. This trend continued during minute 4 of compression, when significantly greater percentage of fluid lost from layer two (83±5%, $p=0.001$) compared to layer 1 (74.7±3.1%), a mean increase of 8.3%.

There were no significant differences between the fluid loss from the first and second layers made of 10.6 mm gels during further compression. These data show that compression of the 10.6 mm gel on top of the pre-compressed construct made of the gel of the same initial height affects fluid loss from the upper gel during first 4 minutes of compression, resulting in greater percentage fluid loss from the upper layer.

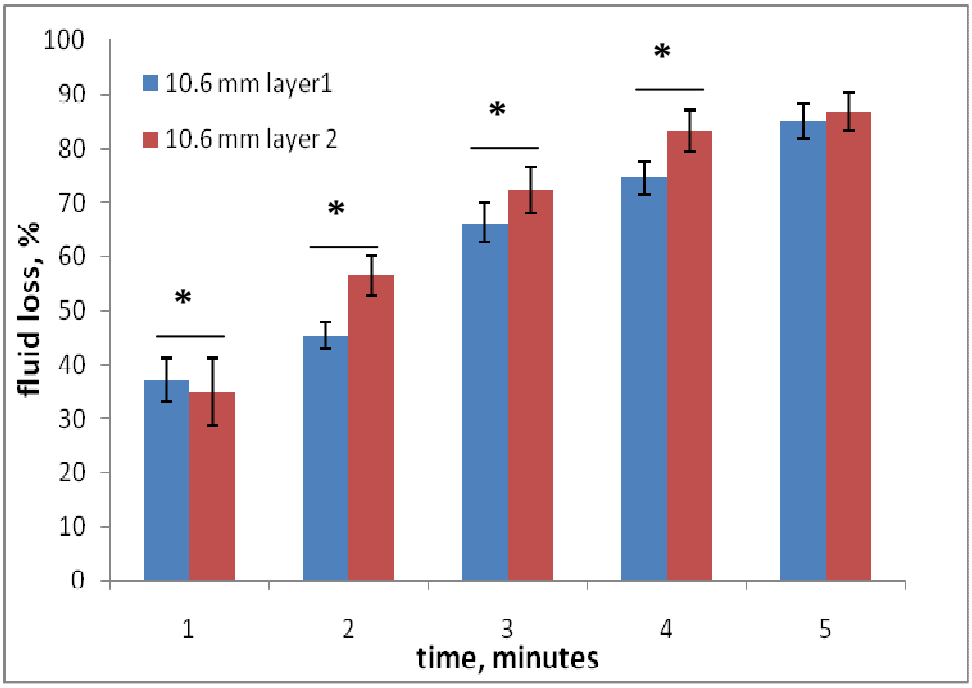

Fig. 9 Bar chart showing the effect of the layering of two 10.6 mm gels on fluid loss (in % of initial weight) during the first 5 minutes of plastic compression process. *-significant difference between % fluid loss from the gels at each time-point ($p<0.05$).

The compression profile of the first layer made of 13 mm gels (Figure 10a) did not differ from the data reported in the previous chapter (see Chapter 5, Results).

Figure 10 b shows weight loss data from the gels of 13mm initial height, compressed on top of pre-compressed gel of the same initial height. Compression profile of the second layer in this case did not differ from this of the single layer, with significant increases in loss of the initial fluid content at minutes 2 (48±5.5%, $p<0.0001$), 3 (62±7.4%, $p=0.003$), 4 (73.7±7.5%, $p=0.0003$) and 10 (89.6±6%, $p=0.002$). These data indicate that compression of the gel of this height on top of the pre-compressed gel of the same height (13 mm) does not affect dynamics of fluid loss from the upper layer.

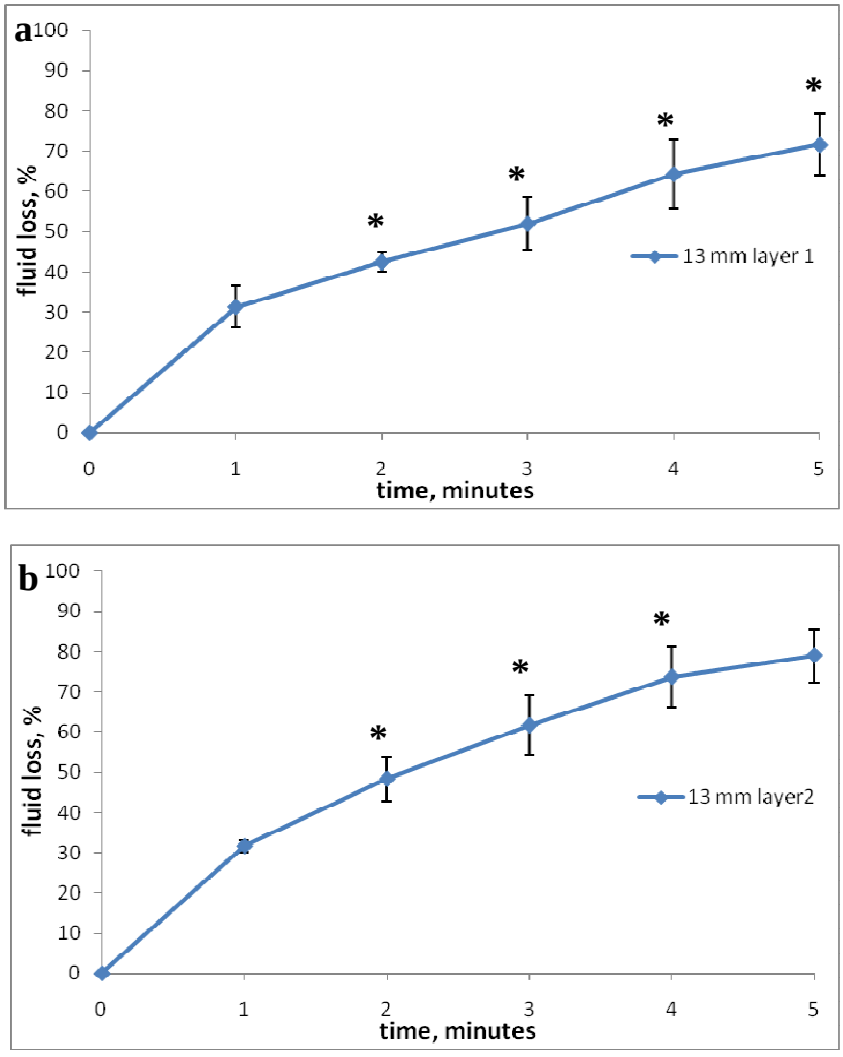

Fig. 10 Graphs, showing the dynamics of fluid loss from the double-layered collagen constructs made of the 13 mm gels per layer during the first 5 minutes of the of plastic compression process; (a) - layer 1 , (b) – layer 2. Fluid loss from

the gels at each minute of the process is presented in percent of initial weight. *-statistically significant difference compared to the preceding time-point (p<0.05).

Data on percentage fluid loss from the top layer during the compression of 13 mm gels at each time point (minutes 1, 2, 3, 4, 5, 10, 15, 20 and 25) is presented graphically in Figure 11

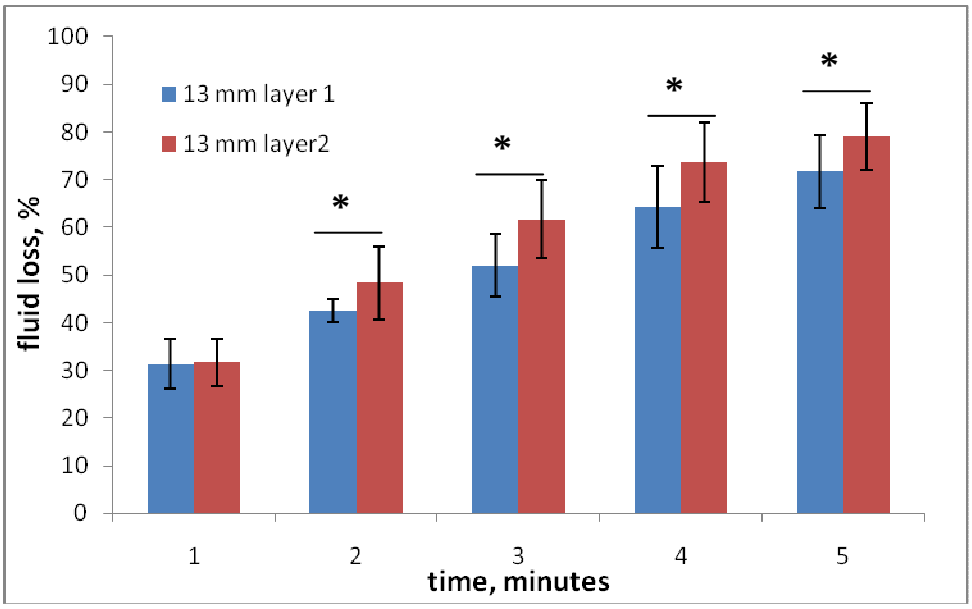

Fig. 11 Bar chart showing the effect of the layering of two 13 mm gels on fluid loss (in % of initial weight) during the first 5 minutes of plastic compression process. *-significant difference between % fluid loss from the gels at each time-point (p<0.05).

At the first minute of compression there was no significant difference between the total fluid loss from the first and second layer (31.3±5% and 32±1.5% respectively). However, at minute two fluid loss from the first layer was significantly less (42.5±2.5%) compared to layer two (48±5.5%, p=0.02), giving a mean reduction of 5.5%. Same was true for the fluid loss at minute three, where total 52±6% of fluid was lost from the first layer and 62±7.4% from the second (p=0.001), mean reduction in total fluid loss of 10%. Same trend continued at minute 4 of compression, when 9.7% less fluid was lost from layer 1 (64±8.5% and 73.7±7.5% respectively, p=0.001) and minute 5, when fluid loss from layer 1 was reduced by 8% (71±7% and 79±6.7% respectively, p=0.001) of compression. There was no significant difference

between two layers during further compression. These data indicate that compression of the 13 mm gel on the pre-compressed construct made of the gel of the same initial height affects fluid loss from the top layer during the initial 5 minutes of compression, resulting in increased percentage of the fluid loss from the upper layer.

Effect of multiple layering (10 layers) on the fluid flow from the upper layer

As has been shown in the previous chapter initial height of the gel (given constant surface area) affects the progression of the plastic compression process and has effect on the collagen-water content of the resulting construct. When initial height of the gel was 5.3 mm fluid flow from the gels seemed not to lead to the formation of near impermeable layer of collagen on the fluid leaving surface, possibly leading to more uniform distribution of the protein content throughout the body of the construct and indeed more permeable FLS. This conclusion was made based on the fact that it did not reach maximum hydraulic resistance compared to the gels of greater initial height. Formation of FLS in the 13 mm gels, with higher initial collagen and water content, will potentially result in more pronounced anisotropy in collagen distribution, due to the greater hydraulic resistance of the FLS and formation of the secondary FLS at the bottom of the gel. This fact needs to be taken into account when multi-layered constructs are assembled, as these differences are likely to affect interlayer fluid distribution.

In order to determine the effect of multiple (10 layers) layering on the interlayer water flow, fluid loss in millilitres was measured from the first and tenth layer of the constructs made of 5.3 and 13 mm gels in each layer. Collagen gels were layered in the same manner as when double layered constructs were fabricated, i.e. after first gel was compressed, fresh volume of neutralised collagen solution was set on top of the first compressed layer and process repeated. In this instance 10 gel

layers were compressed on top of each other in this manner. Fluid loss from the first and tenth layers was measured as before by weighing the roll of absorbing paper every minute for the first 5 minutes of compression. To determine effect of layering up to 10 gels on the time of full compression, after the first 5 minutes rolls were measured every 5 minutes until no change in the weight of the absorber was noted. Progression of the process during the compression of the tenth layer was tracked as before, fluid loss at each minute of the first 5 minutes of compression was compared with the value of the previous minute. Fluid loss from the first and tenth layer at each minute of compression was also compared to determine the effect of multi-layering on fluid loss at each minute. As the aim of this study was to determine effect of multi-layering on interlayer water distribution, data is presented in millilitres rather than percentage weight loss.

Figure 12a shows fluid loss from the tenth layer of the construct, consisting of 5.3 mm gels. General progression of the compression followed the same trend as compression of the single layer. However, statistical analysis showed significantly greater fluid loss from layer 10 compared to layer 1 at each time-point ($p<0.05$).

The amount of fluid was lost from the gel at minute one was 1.6±0.1 ml, significantly smaller than at all subsequent time points. During the second minute, 2±0.12 ml was lost from the tenth layer of the construct. This volume of the absorbed fluid was equal to the initial volume of the collagen gel (gel height, 5.3 mm is equal to the volume of 2 ml), giving a fluid loss at this time-point of 100%. Increase in the weight of the absorbing paper roll continued until minute 5 of compression. At minute 3, 2.3±0.11 ml (excess of 15% of the initial gel volume) of fluid had been absorbed, followed by further 2.35±0.12ml (excess of 17.5% of the initial gel volume) at minute 4 and finally 2.4±0.005 ml (excess of 20% of the initial gel volume) at minute 5.

Therefore, although layering and compression of ten gels of this height (5.3 mm) did not have an effect on the total time for nominal compression of gels of this height (compression was complete after 5 minutes), the total fluid absorbed into the paper roll at this stage indicates a certain degree of interlayer fluid filtration.

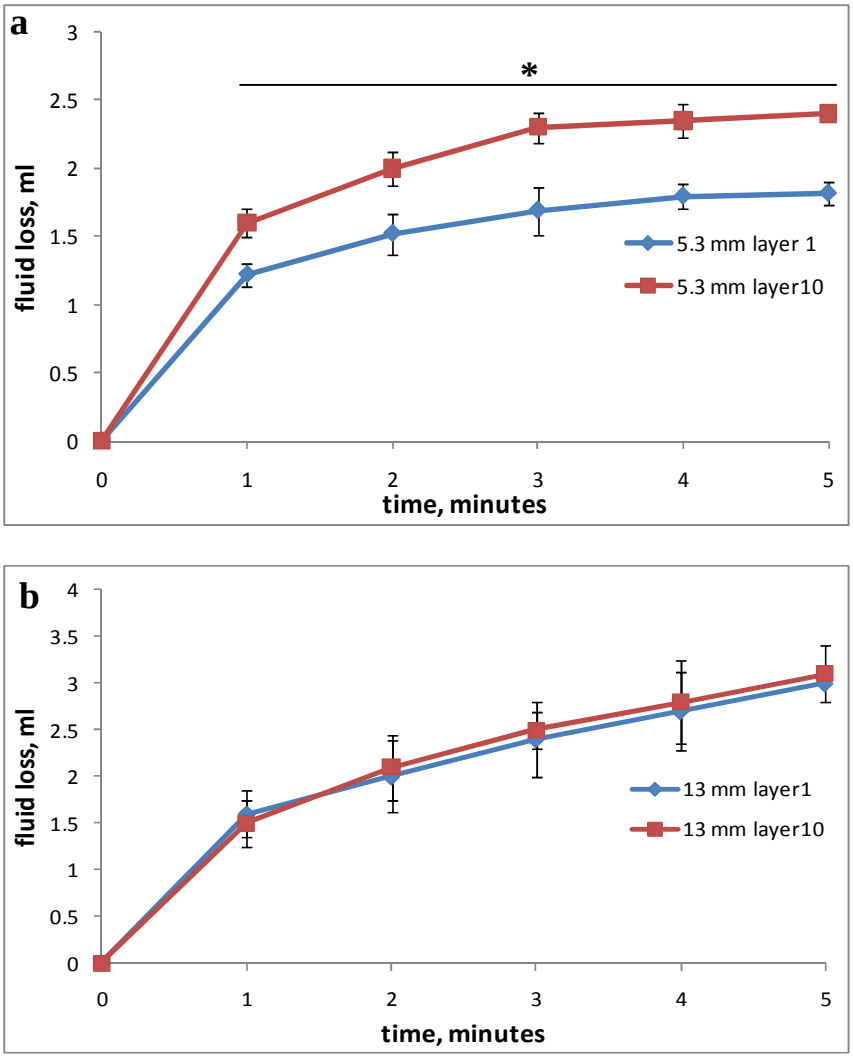

Fig. 12 Graphs, showing the dynamics of fluid loss from the first and tenth layers in the 10-layered constructs, made of (a) 5.3 mm gels per layer and (b) 13 mm gels per layer during the first 5 minutes of the of plastic compression process. Fluid loss from the gels at each minute of the process is presented in millilitres. *- statistically significant difference between layers at each time-point ($p<0.05$).

The effect of multi-layering (10 layers) of the 13 mm gels on the progression of the compression process of the last gel was determined by comparing values of the fluid loss at each minute of compression to the value at the same time point for layer

1. Statistical analysis showed no differences between fluid loss from the uppermost layer compared to layer 1. Results are shown graphically in Figure 12b.

The data show that progression of the process followed the same trend as compression of the single gel of this height (13 mm). Interestingly, layering of ten gels of 13 mm height resulted in full compression of the upper layer at 20 minutes, compared to 25 for the first layer. These data indicate that compression of ten 13mm gel did not alter the general progress of compression process but led to a shorter compression time.

There were no significant differences between the values of fluid loss (in ml) from layers 1 and 10 during the first 5 minutes of compression. The differences in the volume of fluid lost from the layers became significant at minutes 10, 15 and 20 of compression, effectively at the end stages of the process. At minute 10 of compression, 4.1±0.54 ml was lost from layer 1 and 3.6 ±0.5 ml from layer 10 (mean decrease of 12%, $p=0.02$). At minute 15, 4.3 ±0.4 ml of fluid was absorbed from layer 1 and 3.9±0.35ml from layer 10 (mean decrease of 9.3 %, $p=0.007$). At minute 20, 4.6±0.42 ml of fluid was lost from layer 1 and 4.4±0.2 ml layer 10 (mean decrease of 5%, $p=0.03$). The last (10^{th}) layer was effectively compressed after this time point; fluid loss from the first layer continued for a further 5 minutes, bringing total fluid loss at minute 25 to 4.7±0.41ml. These data indicate that compression of ten 13 mm gels on top on each other led to interlayer fluid flow, affecting compression of the upper layer in the later stages of process. In particular, this interlayer fluid flow appears to affect the rate of fluid loss from the upper most layer during the final stages of compression. Rate of fluid flow from the first layer confirmed the data reported in the previous chapter, falling steadily from 0.22 ml/min during minutes 5-10 down to

0.02 ml/min during 20-25 minutes. Rate of fluid loss from the 10th layer remained constant during these time points at approximately 0.1 ml/min.

The resulting constructs, consisting of ten layers made of either 5.3 or 13 mm gels were fixed and processed for histological examination immediately after the last layer was compressed. Representative images of the constructs, stained with SiriusRed are shown in Figure 13. Overall, the layers did not show signs of separation and were easy to handle as a coherent stack (Figure 13, a and b). Some limited areas of separation can be seen on the images, in particular between the layers compressed as first 2-3 layers which could be an artefact of mechanical damage during removal of the constructs from the wells.

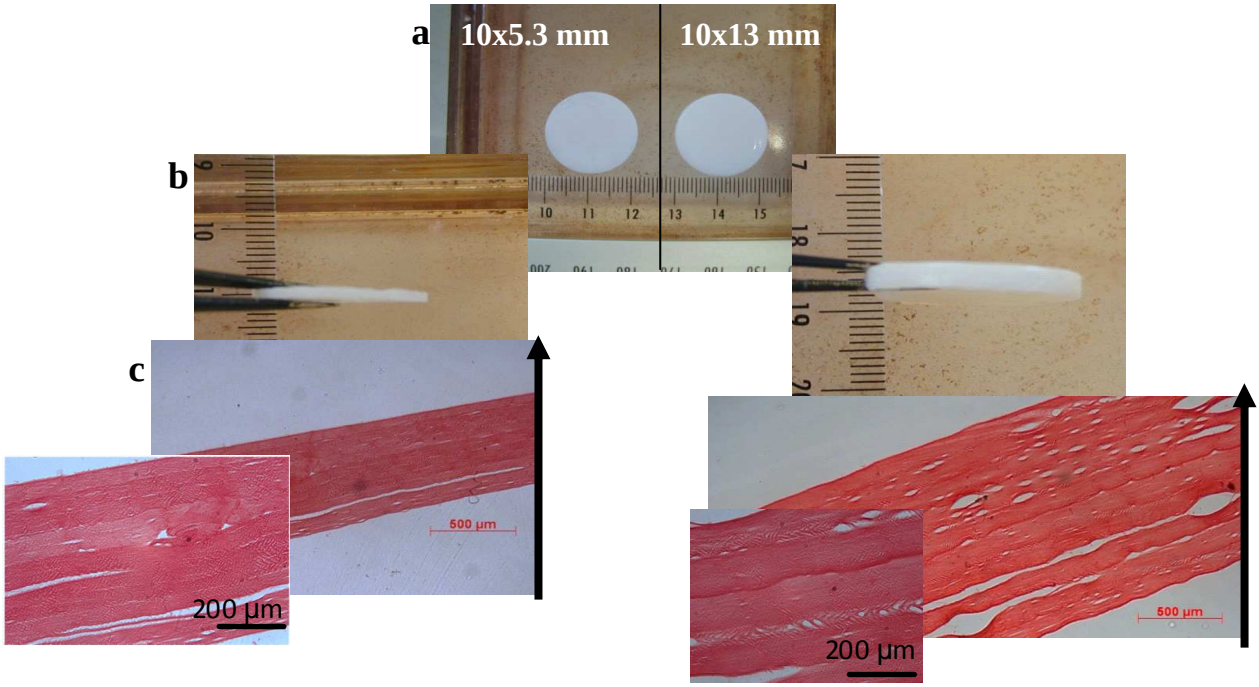

Fig. 13 Images, showing morphology of the 10-layered constructs, made of the 5.3 (left panel) and 13 (right panel) mm gels per layer. (a) – top view of the constructs, (b) – transverse view of the constructs,. (c) – representative histological images of the constructs. Inserts show images of the sections at a higher magnification. Arrows show the direction of the construct assembly.

Thickness of the 10-layered constructs, made of 5.3 mm gels (Figure 13 c, left panel), was 697± 20 µm with an average thickness of individual layers of 67.7±7.2

μm. Thickness of the constructs, made from 13 mm gels (Figure 13 c, right panel), was 1470±36 μm with an average thickness of individual layers of 137.3±12 μm.

Effect of the resident cells in the multi-layered constructs

One of the main advantages of the plastic compression is high viability of the resident cells at the end of the process. However, it is well documented that fibroblasts remodel collagen lattices in the course of culture period (Brown et al., 2005, Bitar et al., 2008). Therefore, effect of culture conditions and activity of the resident cells on layer integration is an important factor to consider. To evaluate these effects, 2-, 3-, 4- and 5-layered constructs were fabricated from 10.6 mm gels using multi-well plastic compression and cultured for 3 weeks. Each layer contained $5x10^5$ cells, bringing the total number of cells in the five-layered construct to $2.5\ x10^6$ cells per construct. Constructs were fixed and stained using H&E method (Chapter 2) at the end of culture period. Morphology of the constructs was evaluated and thickness of multilayered constructs compared with the single-layered cellular constructs, cultured for the same period of time.

Figure 14 shows representative of low and high magnification images of one- , two- , three- , four- , and five- layered cell-seeded constructs. It can be seen from the images that neither long-term culture, nor resident cell activity led to layer separation. High magnification images show well-integrated layers in all cases. In fact, it became almost impossible to identify the individual layers. The compact areas where the fluid leaving surfaces had initially been formed in the top and bottom layers were also not visible at this time point, either due to cell remodelling or continuing passive fluid uptake.

Although cell viability was not assessed in this study, there were clear signs of cell matrix remodelling in the multi-layered constructs, similar to those in the single layered construct (Figure 14, dashed outlines). Cells were evenly distributed

throughout the constructs, although there appeared to be more cell-free areas in the middle layers of the 4- and 5-layered constructs.

Average thickness of the single-layered, cellular constructs, made by compressing cell-seeded gels of 10.6 mm initial height, was 75±11 µm. As has been shown in Chapter 5, thickness of the acellular construct made of the same gel height and fixed immediately after compression was 57.3±4.7 µm, giving an increase of approximately 20 µm (30%). This increase in thickness was most probably due to the combination of two factors. Firstly, passive re-uptake of liquid by the compressed collagen construct, similar to that described earlier for the constructs made by compression of the 13 mm high gels. Secondly, these cell-seeded constructs were cultured for 3 weeks, and therefore it is possible that certain input into the increase in thickness was due to cell matrix remodelling. Indeed, it can be seen in Figure 14 that constructs had characteristic 'lacy' appearance with the voids contributing to the increased constructs thickness. This increase in thickness (compared to the acellular constructs, fixed immediately after compression) was statistically significant ($p=0.002$).

Compression of the second cellular gel of the same height on top of the first one led to increase in total thickness of the construct, bringing the value to 166±13 µm. Interestingly, compared to the thickness of single layer there was small (7%) increase compared to the predicted value (75x2=150 µm). This slight increase in thickness, compared to the predicted value (based on the thickness of single-layered constructs) was a recurrent feature in this study.

Thus, addition of the third layer led to further increase in the thickness of the construct, giving on average 273±7.2 µm (predicted value – 225 µm, an increase of 20%).

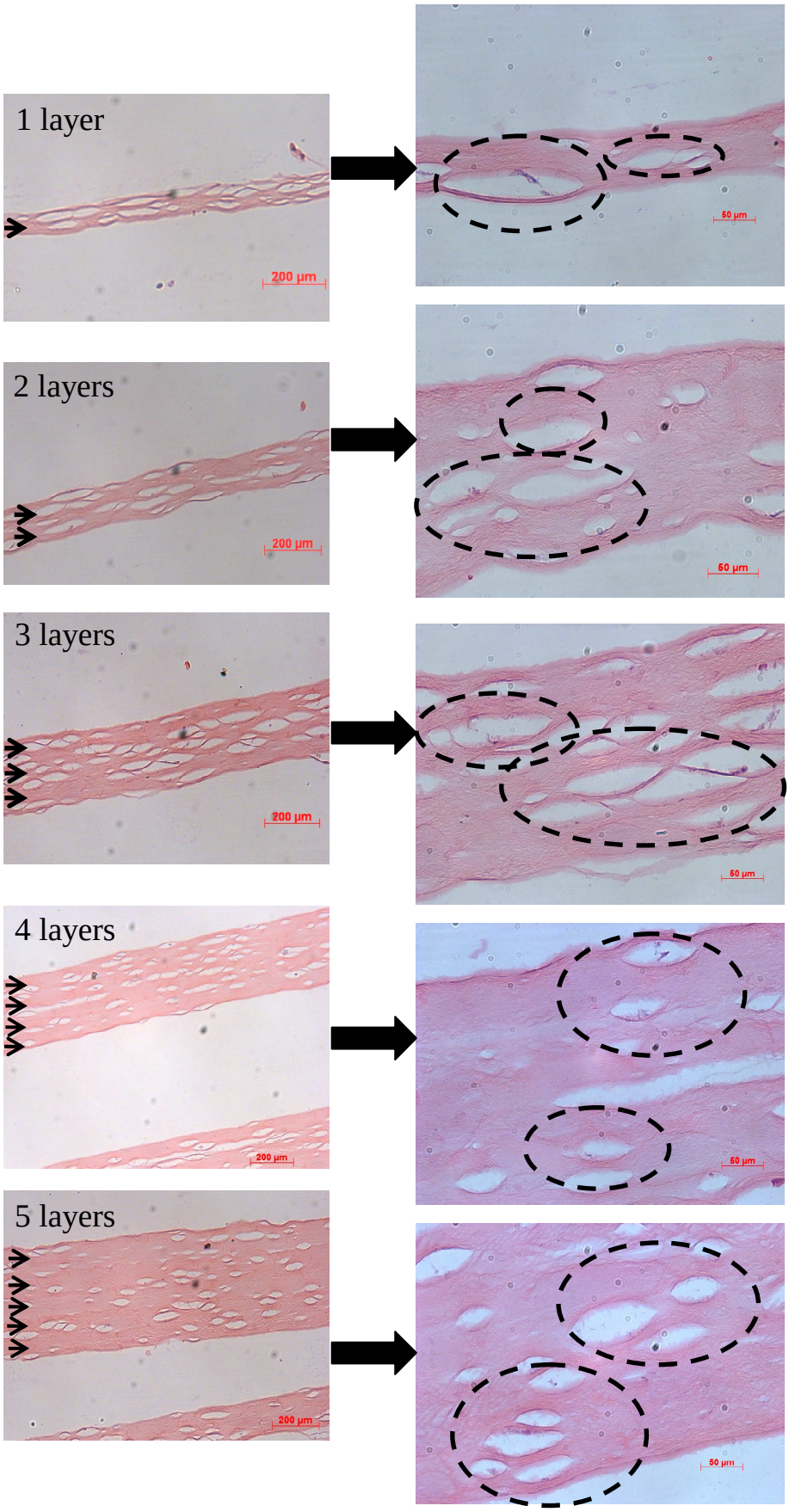

Fig. 14 Representative histological images of the constructs made of 1, 2, 3, 4 and 5 layers of the cell-seeded plastic compressed collagen. Constructs were made in the 12-well format as described in the text. Each layer was made of 10.6 mm gels. Constructs were cultured for 3 weeks and fixed at the end of the culture period. Panel on the left shows low magnification images of the constructs; arrows indicate approximately position of the individual layers. Panel on the right shows

images at higher magnification; dashed ovals indicate areas of cellular remodelling of the matrix. Note that interlayer boundaries are not distinguishable on the images, as well as fluid leaving surfaces in the upper or base layers.

When fourth layer was added to the construct, total thickness increased to 364±7.9 µm. Predicted thickness of this construct was 300 µm, giving again an increase of 21%.

Finally, addition of the fifth layer increased total thickness of the construct to 433±13.6 µm. Predicted value for this construct was 375 µm, giving an increase of 15 %.

The slight discrepancy between predicted and actual thickness of the cellular constructs, which consisted of more than two layers, could be explained by both inter-layer fluid movement during layering (detectable by comparison with the layered constructs, fixed at time 0) and cumulative effect of the cell activity (remodelling) in the layers. However, as the question asked in this study was the effect of the matrix remodelling cells on layered constructs integrity *in vitro*, the phenomenon of increased thickness was not investigated and can be proposed for future work.

Discussion

Every tissue in the human body can be considered to consist of separate layers with specialised cells residing in each layer. Thus, in order to engineer functional complex tissues, such as skin, it is important to develop techniques allowing reconstruction of this composite architecture. Various methods of sheet layering, either cell- or biomaterial based, have been developed recently. Technologies, allowing for formation and harvesting of cell-based multilayered constructs include the use of magnetic nanoparticles to arrange cells into multi-layers and later to harvest these using magnetic force (Ito et al., 2005, Akiyama et al., 2009). This technology

has been used to layer keratinocytes, myoblasts, fibroblasts and HUVECs. Another method of scaffold-free fabrication of multilayered cell-sheets is based on culturing cells to confluence on thermo-responsive polymer. Subsequently, cell sheets can be harvested and layered (Ohashi et al, 2007, Tsuda et al., 2007).

However, these methods were developed to fabricate *cell* layers and are unsuitable for engineering matrix-rich tissues, such as dermis, where cells are enmeshed in the collagen-rich matrix.

Scaffold-based multilayered constructs can employ either synthetic or natural polymers, or combination of both. Srouji et al (2008) reported development of an electrospun multilayered construct comprised of epsilon-polycaprolacton and collagen, by essentially stacking thin discs of electrospun polymer on top of each other. However, the authors did not remark on interlayer integration or separation.

Yang et al (2009) report layer-by-layer construct fabrication using only the epsilon-polycaprolacton, where each layer of electrospun polymer was followed by deposition of cell suspension prior to deposition of the next layer. In this study it was reported that 18-layered construct can be assembled. Novel technique of centrifugal casting of hylauronan-based synthetic ECM to produce multilayered constructs has been described by Mironov et al (2008), where layers of polymers are deposited (cast) on the walls of rotated mould under centrifugal forces. Similarly, the authors do not report on layer integration or separation in culture using this technique. Tubular multilayered constructs can be assembled using an acoustic focusing technique (Mazzoccoli et al, 2010). In this study, Mazzoccoli used ultrasound to deposit PEGDA matrix on the walls of the mould but in the absence of cells.

Multilayered corneal equivalent was constructed using layer-by-layer assembly of cell-seeded low-density collagen gels on the transwell membrane and

used for drug permeation studies (Reich, Bednarz and Mueller-Goymann, 2004). Another method of engineering multilayered constructs is organ printing, where cell-containing hydrogels are deposited on a substrate in spatially controlled manner. This technology is still in a developing state, suffering from drawbacks in printing technology and hydrogel chemistry. Moon et al (2010) report using a bio-printing technique for multilayered deposition of cells, suspended in hydrated collagen matrix, though each layer was 16.2µm thick, (i.e. approximately one cell diameter). Inter-layer integration and density of the matrix were not reported; hence durability and stability of such constructs are dubious.

The area of *direct* engineering of complex tissues is relatively new. It is now appreciated that architecture of the construct as well as cellular distribution are essential not only for biomedical application of engineered tissue, but also to understand the degree of structural involvement in tissue formation in vivo (e.g. during embryogenesis). The method of layer fabrication of the relatively thick tissues, reported here utilises the multi-well plastic compression method described in previous chapter. As can be seen, this method is easy to use, creating the opportunity to layer dense (tissue equivalent) collagen sheets, potentially containing different cell types or cell densities and distributions, including cell-free (e.g. to study inter-layer cell migration).

The following parameters had been investigated in this Chapter: (i) qualitative assessment of layer separation following agitation and morphology of the interlayer interface, (ii) change in thickness of the constructs, brought in contact with fluid immediately after PC as an indicator of interlayer integration mechanisms, (iii) effect of double-layering of the gels on the fluid loss from upper layer and progression of the compression process of the same layer compared to the compression of the single

layer (iv) effect of layering more than two (up to ten) gels on the construct morphology and fluid loss dynamics from the upper layer, and (v) effect of cellular activity on the morphology of the interfaces in the multilayered cell-seeded constructs at the end of culture period.

The layer separation assays showed that interlayer connection of the constructs prepared using the new system was resistant to the mechanical agitation, whereas constructs, assembled by pressing together two separately compressed constructs (i.e. held together by surface tension) separated almost immediately. Therefore, we concluded that the interlayer connection was not a result of simple surface contact between the two layers in the process of constructs assembly. Further investigation of the mechanisms of interlayer integration suggested following mechanism. It is known that air-dried, dehydrated collagen lattices reswell to some degree when rehydrated (Vernon et al., 2005). As the process of plastic compression leads to formation of a more dehydrated zone of collagen on the fluid leaving surface, if this area comes into contact with the fluid (i.e. the lower surface of the next, upper layer of collagen), it will take up fluid and reswell, potentially dragging collagen fibrils across the interface with it. In addition, it is known that assembly of the fibrils in the neutralised collagen solution continues for some time after the gel starts to form (Comper and Veis, 1977). If reswelling of the base layer and lag phase of the upper collagen gel coincide, small volumes of the collagen from the upper layer will be drawn into the FLS area of the bottom layer. Therefore, some of the collagen fibrils from the upper layer will be intertwined with the FLS of the base layer, producing trans-interface. The proposed mechanism is described schematically in the Figure 15.

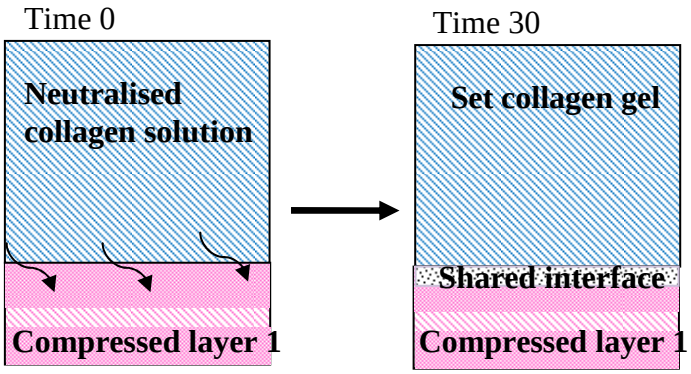

Fig. 15 Diagram, showing schematically formation of the interlayer bond in the double-layered PC construct. At time 0, when neutralised collagen solution (second layer) is poured on top of the compressed first layer, reswelling of the FLS area of the first (precompressed) construct leads to formation of shared interface between layers at time 30 minutes (setting time for the second gel), providing physical bond.

To test this theory, reswelling properties of the single layered construct have been investigated and indeed a small but significant increase in layer thickness was found in the first 30 minutes following the compression. (NB: The reswelling phenomenon does not contradict the plastic nature of the compression process, as even when hydrated compressed collagen sheets do not regain the initial dimensions of the uncompressed gels. In addition, it is likely that this is a local reswelling, probably limited to the FLS) Therefore, reswelling of the base layer, which is compressed first, coincides with the setting time of the upper gel. Furthermore, morphology of the interface area has identified collagen fibrils, which span between the bottom of the second layer and the top of the first.

Further evidence in favour of the proposed theory has been gained from the triple layered constructs fixed immediately and following incubation. In the first case two bottom layers had increased thickness compared to the uppermost layer, i.e. first two layers reswelled as a result of contact with the next collagen gel in the liquid form, whereas uppermost layer did not. If the constructs were incubated all thee layers were of uniform thickness. Interestingly, the primary FLS of the uppermost layer and

secondary FLS of the bottom layer were easily detectable on the histological images at both time-points. However, at the interface between layers these features were less pronounced at time 0 and disappeared completely after 24 hours. This can be an effect of the reswelling process as well as a consequence of the secondary FLS formation (and resulting fluid flux) during the compression of the top layers. In conclusion, we now understand layer integration and have proposed a mechanism by which it is possible to control the interlayer bonding in the plastic compression process.

Several methods have been reported by other groups, where complex hierarchy of native tissues is recreated by assembly of multi-element constructs. These methods usually involve separate fabrication of several modules and subsequent construction of the final construct from these individual parts. The final assembly of the individual parts can be done by employing capillary forces (Du et al., 2008, 2010) or physically moulding the elements so that they can be connected (eg. forming protrusions on the bottom of one module that match the shape of the grooves on the surface of the second module) (Yeh et al., 2006). However, these techniques have been used to assemble weak hydrogels or rigid synthetic polymers and require additional steps in construct assembly. The interlayer connection described here is, on the other hand, part of the construct assembly process and allows for engineering of a living tissue model using natural polymer and living cells *in situ.*

This intimate connection between the layers implies some degree of shared fluid flow, in particular during compression of the upper layers. Indeed, the analysis of fluid loss from the second construct layers (at each collagen gel height) showed differences compared to single layer compression of same respective gel heights. The most noticeable difference was in compression of the 10.6 mm gels, where the

characteristic ‘jumps’ in the compression profile disappeared in the second layer. This could be due to earlier formation of secondary FLS (see Chapter 5) at the bottom of the upper gel, as fluid was drawn into the bottom layer, so that fluid from the upper layer started to filter though the base layer earlier in the compression process.

This interlayer fluid exchange became even more pronounced when the number of layers increased to ten. When layers were made of 5.3 mm gels (height of the gel, at which only primary FLS is formed, as discussed in the previous chapter) the amount of fluid, collected into the absorbent during compression of the uppermost, tenth, layer was 30% greater than expected. It is likely to be a result of accumulation (and filtration) of the fluid from the underlying layers to the surface of the construct. As discussed previously, after process of PC is completed, 5-10% of the initial fluid content is still present in the construct. It is possible, that some of this fluid content is forced out of the layers with each additional compression of the top layers, which is only applicable to the gels of this height. As has been discussed in the previous chapter, secondary FLS is likely not to form during compression of these gels. Therefore, fluid, still present in the compressed layers, can potentially leave through the unblocked bottom surface. Accumulation of this expelled fluid could lead to the increase in fluid loss from the uppermost layer. However, this had no obvious effect on the morphology of the resulting construct, or interlayer connection.

For comparison, when gels of 13 mm height were compressed in this manner (10 layers), the amount of fluid, collected from the upper-most layer was smaller, than from the single-layered constructs, made from the gel of this height and time point of full compression was achieved faster. As have been shown in previous Chapter, compression of these gels leads to formation of two FLS, at the top and bottom of the gel. Firstly, this could prevent fluid, still left after compression, from leaving the

layers. Secondly, if reswelling is indeed only confined to FLS zones of the layers, each compressed collagen sheet will draw fluid from the top (with the primary FLS) and bottom (with the secondary FLS) layers. Cumulatively, this can lead to somewhat reduced fluid content of the uppermost, tenth layer, and as a result, smaller fluid loss during compression and shortened compression time.

It is possible that the partial separation of the bottom layers of this constructs can be attributed to this interlayer fluid exchange, but it can also be explained by the mechanical separation due to handling of the constructs. Further experimental work is needed to establish the precise mechanisms of the interlayer fluid exchange. One possible approach would be to use labled soluble marker molecules, different in each layer, to monitor their migration between layers during the process of construct assembly.

The ultimate aim of plastic compression is direct tissue engineering (i.e. increasing construct functionality whilst retaining viability of the resident cell), with the ability to grow functioning constructs in culture after fabrication. To this end, the effect of the resident cell population on the morphology of the multilayered construct was evaluated with the particular focus on interlayer separation was evaluated. The viability of the cells was not tested here, as it has been shown in the Chapter 5 that compression in the multi-well format does not affect this parameter. All tested constructs showed a high degree of cell-matrix remodelling (Brown et al., 2005, Bitar et al., 2008) and no signs of layer separation. Moreover, no interlayer boundaries were detectable histologicaly as the culture proceeded. One of the concerns when fabricating multi-layered thick constructs is appearance of necrotic areas due to poor oxygen and nutrients diffusion. However it is known from the previous study by Cheema et al (2008) that very little cell death occurs deep in collagen multilayers

even at higher cell densities than use here. Indeed, oxygen diffusion deep into the constructs was very rapid and sufficient for good fibroblasts viability. Therefore, we conclude that layering of multiple collagen sheets results in well integrated constructs with increased thickness. Increasing thickness of the constructs should not pose a danger of cell death due to oxygen deprivation.

In conclusion, fabrication of the multilayered constructs, using multi-well plastic compression has been evaluated in this study. Possible mechanism if interlayer connection has been proposed together with the mechanisms of fluid exchange between layers. Multilayered constructs, both cellular and acellular can be fabricated using this technique with high degree of interlayer integration and reproducibility. In addition, results of this Chapter confirm low variability between the constructs, made using multi-well compression, reported on in Chapter 5.

Multi-layered constructs are certainly attractive for many tissue engineered application such as, for example, skin tissue engineering. This particular area requires revascularisation and reinnervation of the implanted engineered tissue, which, in turn, would benefit from preformed channels in the construct. As the process of multi-well plastic compression shares its main characteristics with the original PC method, the possibility of micro-moulding topographical features into the FLS of compressed collagen constructs, using the method described in Chapter 4 will be evaluated in the following chapter. In addition, the intriguing possibility to fabricate instant channels in the double-layered constructs by ‘putting roof on the groove’ will be tested.

Chapter 7

Engineering micro-channels into the multi-layered PC collagen constructs

Introduction

Increasing the thickness of the engineered construct brings with it a problem of oxygen and nutrients delivery to the resident cells. Several strategies exist to overcome this obstacle, some of which are reviewed in Chapter 3. Current strategies involve either particulate leaching method, where soluble particles or fibres are embedded into the biomaterial and later removed by dissolving and leaving behind a pore. Second most used method is moulding the biomaterial around the structures (essentially future pores) with later extraction of the latter. It is now known that it is possible to introduce directional pores into the PC collagen constructs by effectively combining the two approaches. Neutralised collagen solution is set around soluble glass fibres and compressed. After incubation in the aqueous environment fibres are dissolved leaving behind unidirectional pores of known diameter and geometry (see Chapter 3). However, the described method of PC collagen micro-channelling has certain limitations. First, the thickness of the resulting construct is limited by formation of FLS. Second, after the construct assembly, glass must be dissolved, either *in vitro* or *in vivo*, adding time to the process. Third, although it has been shown that soluble glasses have minimal negative effect on cell viability *in vitro* (Nazhat et al., 2007, Cheema et al., 2010), *in vivo* effects are still not fully investigated. In this chapter an alternative method of micro-channelling of the PC collagen constructs will be described.

As has been shown in Chapter 4, micro-moulding of FLS results in stable patterning. One of the aims of the current research was to evaluate this methodology

in the M-PC format. Laser-cut Kapton® masks have been used as template in this work. Kapton® is a polyimide film, developed by DuPont, and is known to be bio-compatible and support cell adhesion (Prichard, Reichert and Klitzman, 2007). Dimensions of the grooves (width and depth), produced by using masks of different dimensions in the M-PC format have been assessed for a range of collagen gel heights.

Following the evaluation of method efficiency, the micro-moulding technique was combined with the multi-layering (see Chapter 6), in order to fabricate a two-part channel. The idea was that a first layer, containing micro-moulded grooves was effectively overlaid with a second layer of collagen, which after compression would create a channel 'roof'. The practicality and efficiency of this method in the double - layered constructs has been assessed in this chapter by investigating the physical dimensions (width and depth) of the resulting channel. These were compared with the dimensions of the groove in the single-layered constructs. Continuity of the resulting channels was assessed by serial sectioning of the resulting constructs and dimensions of the channel examined in the adjourning sections. Lastly, the possibility of direct delivery of the cells into the channels was evaluated with the view of creating an endothelial cell lining of the channel to aid the vascularisation of the construct upon implantation.

In this chapter micro-moulding of the single and multi-layered collagen gels, compressed in the multiple PC format, will be described as well as basic characteristics of the constructs, produced using this technique. The following parameters were investigated: (i) average fluid loss against time of compression of the collagen gels with the templates of different dimensions; end time-points of full compression with the templates of the same dimensions and effect of micro-moulding

on fluid loss from the compressed gels compared with the non-moulded gels (ii) width and depth of the grooves, made using the templates of different dimensions in the gels of the same height (iii) width and depth of the grooves made using the same template on gels of different heights (iv) width and depth of the channels, produced by micro-moulding double -layered collagen constructs, (v) effect of the embedded cells on the depth and width of the grooves, micro-moulded into single-layered constructs, in culture and (vi) efficiency of the cell delivery into the grooves during the micro-moulding of the gels.

Methods and Materials

Preparation of acellular and cellular collagen gels

Collagen was neutralized as described before (Chapter 2). Cellular constructs were prepared as described before (Chapter 2).

Fabrication of M-PC constructs with topological features

Topological features (grooves) were micro-moulded into the FLS of the collagen constructs using method described in Chapter 4, adapted for the use in the multi-well format. Figure 1 shows the schematic illustration of the process. Collagen gels were set in the 12-well plate (see Chapter 5). Prior to compression, Kapton® masks were placed onto the surface of the gels and compressed as described in Chapter 5.

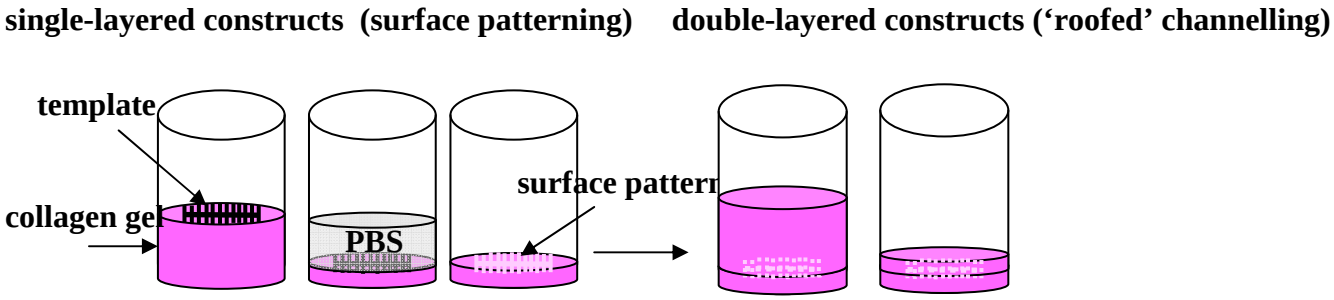

Fig. 1 Schematic illustration of the constructs assembly. Templates were placed on top of the collagen gels prior to compression. After compression process

completion, patterned constructs were incubated for 5 min with PBS prior to template removal. Double layered construct were made by setting fresh collagen gel on top of the patterned one and compressing in the standard manner. Triple layered constructs were assembled in the same manner, but all three gels were micro-moulded. As a result, grooves were formed in the single-layered constructs; channels in the double-layered construct.

Kapton® masks were custom-made by TAP Biosciences (Royston, UK) based on the designs, shown schematically in Figure 2. Each rectangular mask (15x15 mm) had a double-ladder shape with 16 rungs. The rungs were supported by 3 bars, one middle bar and 2 outer perimeter bars (500 μm wide). Three groups of masks with different rung widths were made: 25 μm (n=3), 50 μm (n=3) and a 100 μm (n=3) with the uniform depth of 75 μm.

The rungs had a rectangular cross-section. Total area of the 100 μm template was 44.1 mm^2 (11.6 % of the total area of the gel (379.9 mm^2)); total area of the 50 μm template – 33.3 mm^2 (8.8 % of the total surface area); total area of the 25 μm template – 27.9 mm^2 (7.3% of the total area of the gel).

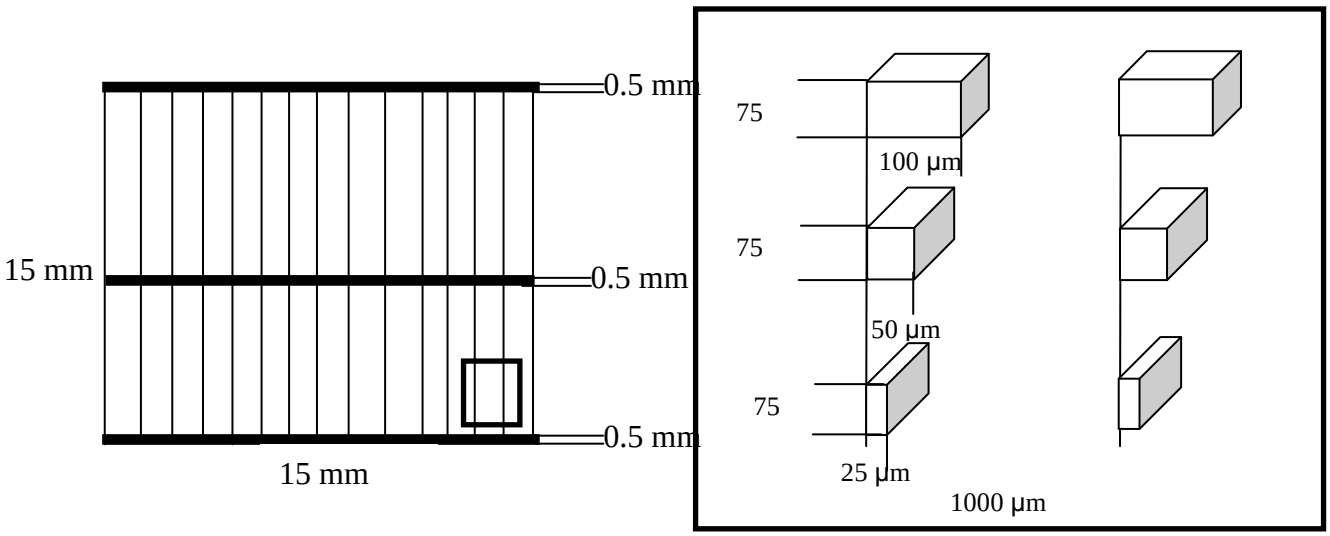

Fig. 2 Schematic illustration of the template used for micro-moulding of the collagen gels in the 12 well-plate format. Image on the left shows gross appearance of the template. Image on the right shows cross-sections of the rungs in the templates of three sizes, used for patterning of the constructs.

Efficiency of the PC collagen micro-moulding using these templates was assessed in two experimental designs. First, influence of the masks dimensions (i.e. various widths of the rungs) on the resulting features was evaluated. Collagen gels of the 10.6 mm height were compressed with the masks of each dimensions (n=6 for each treatment). Second, influence of the gel height on topography fidelity was assessed. Masks with rung dimensions of 50x75 μm were used on 5.3 and 13 mm gels (n=6 for each treatment). After compression, 3 ml of PBS was added in to the wells for 5 minutes prior to mask removal to prevent pattern deformation due to surface tension. Constructs were either fixed immediately or incubated for 1 week in PBS to determine stability of the features with time.

Assembly of the multilayered constructs with topological features (template channelling).

Figure 1 shows schematic illustration of the double-layered construct assembly. Collagen gels, set in the 12-well plate format (10.6 mm) were compressed with 25, 50 and 100 μm masks. After compression, 3 ml of PBS were added in to the wells for 5 minutes prior to template removal to prevent distortion of the features. Liquid was drained from the wells and second layer of neutralised collagen solution of the same height was added and process repeated. Double-layered constructs were assembled without adding topology onto the second layer.

Measurement of fluid loss and time of compression during micro-moulding

The effect of micro-moulding on the progress of plastic compression was investigated for all template dimensions. As the compression profile of 10.6 mm gels contained a distinct feature – i.e. formation of the second FLS at minute 2 of the process (see Chapter 5, Figure 3c), gels of this height were chosen to investigate the effect of micro-moulding on the compression curve and the time for full compression

with templates of each width dimension. Fluid loss at each minute of compression (first 5 minutes of the process) was also compared with corresponding values for single-layered 10.6 mm gels without topological features (data from Chapter 5). Measurements of fluid loss were performed as described in Chapter 5.

Development of cell-delivery technique

To evaluate the possibility of direct cell delivery into the grooves during the construct assembly, the following technique was tested. Cell-suspension (HaCat cells, $1x10^6$ cells per ml) was pipetted onto the autoclaved 100 μm masks, placed on to the bottom of the 12 well-plate and incubated at 37ºC for 2 hours to allow cells to settle. Total of 2 ml of cell suspension was used to give total coverage of the bottom of the well.

Collagen gels were set in the 12 well-format as before. Prior to compression, masks were placed onto the gels cell-side down (i.e. facing the FLS). Gels were than compressed as usual. After compression, masks were left on the gels for 2 hours prior to removal. Figure 3 shows schematic illustration of the method. Gels were either left single-layered, or second layer was added after masks were removed.

Light microscopy

Wax-embedded constructs were processed as described before (Chapter 2).

SEM

For SEM imaging, constructs were processed as described in Chapter 2.

Live-dead assay

Cell viability was determined using live-dead staining assay (see Chapter 2). Number of cells in the grooves was calculated from the images and compared to the initial number of cells on the masks as an indirect indicator of delivery method efficiency.

Statistical analysis

Data were analysed as described in Chapter 2.

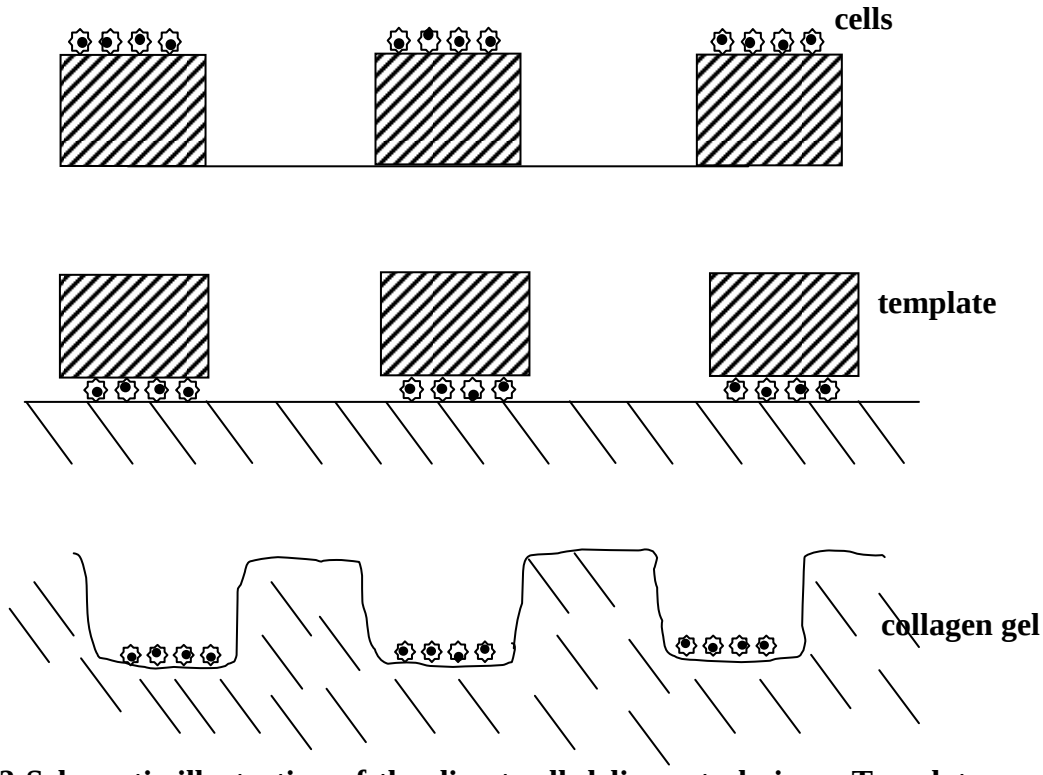

Fig. 3 Schematic illustration of the direct cell delivery technique. Template was placed at the bottom of the well in the 12 well plate and incubated with the cell suspension for 2 hrs, to allow cells to settle on the template. At the end of the incubation period, the template was lifted and placed (cells down) on top of the collagen gel, set in the well of the 12 well plate. After gel was compressed and pattern formed template was left on the construct for 2 hrs to allow cells to attach to the surface of the collagen. The expected result was cells, confined to the bottom of the groove, after template was lifted.

Results

Effect of the micro-moulding on the dynamics of fluid flow during multi-well plastic compression process

As discussed in Chapter 4, process of micro-moulding of the collagen gels during the process of plastic compression is based on the deflected flow of fluid from the collagen hydrogels around an impermeable template, resulting in thin collagen lattices with the patterned surface. Total surface area of the 100 µm template was 44.1 mm^2 (11.6 % of the total area of the gel (379.9 mm^2)); total area of the 50 µm template was 33.3 mm^2 (8.8 % of the total surface area); total area of the 25 µm

template was 27.9 mm^2 (7.3% of the total area of the gel). The question asked here was if loss of the small percentage of available FLS will affect the dynamics of fluid flow from the compressed gels. In order to answer this question fluid flow from the gels of 10.6 mm initial height at each minute of compression was measured by weighing the absorbent paper roll each minute for the first 5 minutes of compression. The effect of micro-moulding on total fluid loss and nominal compression time was determined by weighing the paper roll every 5 minutes until no change in the value was recorded.

Gels of this height were chosen for this test as compression curve of the 10.6 mm gels has a distinct feature that can potentially be attributed to the formation of the secondary fluid leaving surface (see Chapter 5).

Progress of the compression process with the templates of each dimension was determined by comparison of the percentage fluid loss from the gels at each minute of compression. The data was analysed as follows. Firstly, the effect of each template on the fluid loss from the gel was determined. This was done by comparing the value at each minute of compression with the previous one (i.e. minute 2 to minute 1 etc.).

Second part of the analysis was done by comparing the values at each minute between the treatments.

The first part of the analysis showed the effect of the micro-moulding on the progression of the process, whereas the second part indicated when the influences of the templating became significant compared to the compression without the template.

The analysis of the percentage fluid loss from the micro-moulded gels showed similar general trend regardless of the dimensions of the template. Data is shown graphically in Figure 4. The recurring feature of the compression curves for all micro-moulded 10.6 mm gels was the disappearance of the distinctive ‘jump’ at

minute 2, observed when gels of this height were compressed without the moulding template. At minute 2 of compression, gels micro-moulded with the 100 µm template lost 62.5±2.5 % of weight. Gels, compressed with 50 µm lost 60.8±5.4 % of fluid content. Compression with the 25 µm template led to 59.2±3.2% fluid loss at this time-point. Increase was significant compared to minute 1, p=0.01 for all template dimensions. Mean fluid loss from the gels, compressed without the template at this time-point was 44.1±9.6%, giving an increase of approximately 16% with the addition of the templates.

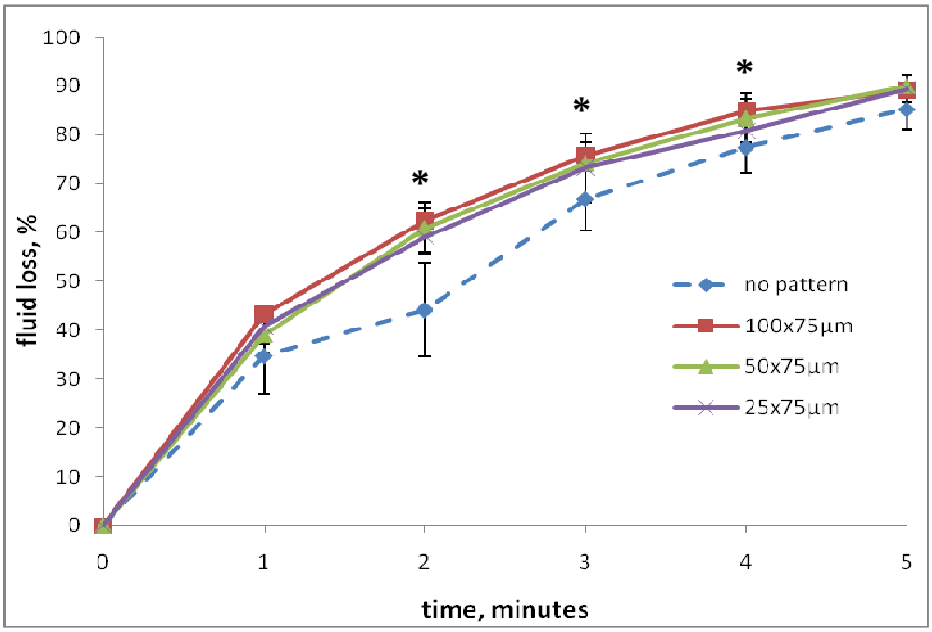

Fig. 4 Graph, showing the dynamics of fluid loss from the micro-moulded constructs made of the 10.6 mm gels during the first 5 minutes of the of plastic compression process; Fluid loss from the gels at each minute of the process is presented in percent of initial weight. *-statistically significant difference compared to the previous time point (p<0.05). Curve for the non-moulded compressed 10.6 mm gel was added for comparison. Note the disappearance of the characteristic 'kink' from the curves of the moulded gels.

During the third minute fluid loss from the gels, compressed with the 100 µm template was 75.8±2.6%, with the 50 µm template – 74.1±1.44% and with 25 µm – 73.3±7%, significant increase compared to minute 2 (p=0.02 for all template dimensions). At minute 4, gels compressed with the 100 µm template lost 85±2.5% of

fluid content. Gels, compressed with 50 µm lost 83.3±5.1 % of initial weight. Compression with the 25 µm template led to 80.8±2.4% fluid loss at this time-point (significant increase compared to minute 3, p=0.01 for all template dimensions). During the fifth minute of compression, weight loss from the 10.6 mm gels compressed with the 100 µm template was 89.2±1.2%, with the 50 µm template – 90±2.3% and with 25 µm – 89.5±2.8%.

The effects of micro-moulding on the total fluid loss and the nominal compression-point were determined by the weight loss from the gels during further 5 minutes of compression (minutes 5 to 10). The total fluid loss from the gels compressed with the 100, 50 and 25 µm templates (92±1.2, 92.5±2 and 92±3% respectively) did not differ significantly between different template dimensions.

However, there was a difference in the nominal compression point of the micro-moulded gels compared to those without a template. The nominal compression time-point for the gels of 10.6 mm initial height, as determined in Chapter 5, was 20 minutes. When gels of the same height were compressed with the impermeable template no change in the weight of absorbent paper was noted after 10 minutes of compression, effectively reducing the compression time by 50%.

Analysis of the fluid loss at each minute during the first five minutes of compression between the gels, compressed with the 100, 50 and 25 µm templates, showed no significant differences between the values, indicating that the dimension of the template does not affect the fluid loss from the gels at the time-points investigated.

Figure 5 shows the percentage fluid loss from the micro-moulded gels and the gels, compressed without the template as a bar chart. Fluid loss from the non-moulded gels at minute one of compression was significantly less (34.7±7.7% compared to an average of 40%, an approximate decrease of 5%) compared to the

gels, compressed with the templates of all dimensions (p=0.02). Same was true at minute 2.

Fluid loss from the non-moulded gels at this time-point was 44.1±9.6% compared with the average of 60.8±1.6% from the compressed with the templates of all dimensions, a decrease of 16% (p=0.002 for all template dimensions). This trend continued at minute 3 of compression, when 66.9±6.5% of initial fluid loss was recorded from non-moulded gels and an average of 74.4±1.3% from the moulded gels, a decrease of 7%. The difference between the moulded and non-moulded gels was significant (p=0.02). Fluid loss from the non-moulded gels at minute 4 and 5 did not differ significantly.

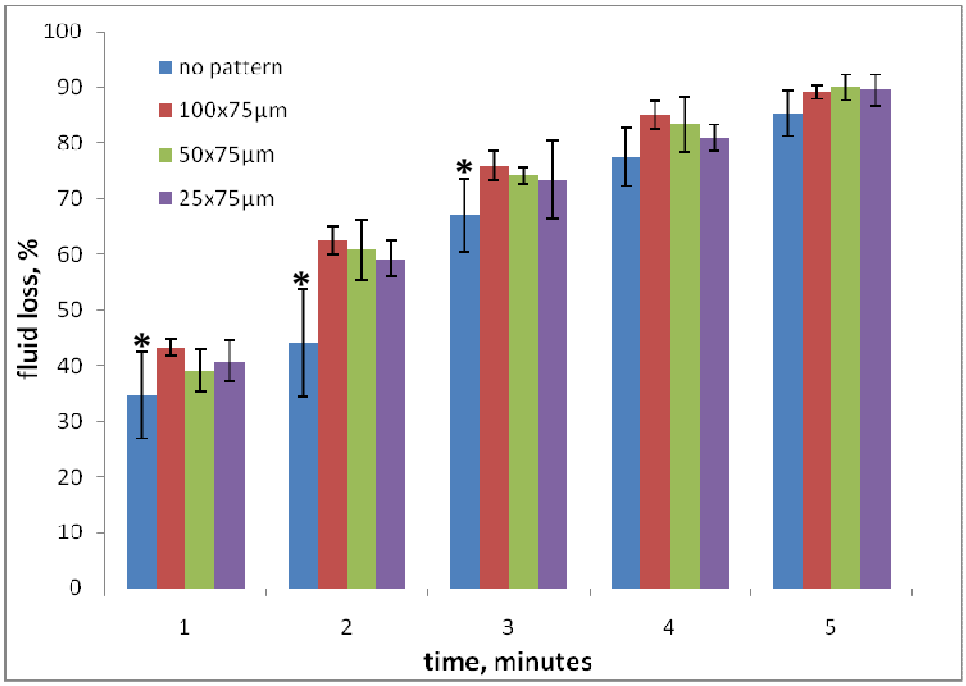

Fig. 5 Bar chart showing the effect of the micro-moulding on fluid loss (in % of initial weight) from the 10.6 mm gels during the first 5 minutes of plastic compression process compared to the non-moulded gels of the same height. *- significant difference between non-moulded and moulded gels at each time point (p<0.05).

Both analyses showed that compression of the 10.6 mm gels with the impermeable templates led to higher percentage fluid loss at minutes 1 to 3 compared

to the non-moulded gels. These changes in the fluid flow suggest formation of an extra fluid leaving surface during the first minute of compression as a result of the introduction of the impermeable template and deflected fluid flow from the gel which can lead to the earlier blockage of the primary FLS. This in turn results in disappearance of the distinctive 'jump' in the compression curve at minute 2 as at this point secondary FLS is already formed in the micro-moulded gels.

Effect of the template dimensions on the parameters of the resulting grooves

In order to evaluate the effect of different template dimensions on the parameters of the resulting grooves, templates with the rungs of 25, 50 and 100 µm width and uniform 75µm height were used. Each template was used to mould gels of 10.6 mm height. The process of micro-moulding of the single-layer collagen gels in the 12 well-plate format is described schematically in Figure 1. As had been shown in Chapter 4, features, moulded into the fluid leaving surface of the plastic compressed gels exhibited high fidelity to the moulding template and were stable in tissue culture condition. Therefore, in this study all template masks were moulded onto the FLS. Resulting constructs were processed for routine histology, sectioned and stained. Depth and width of the grooves, made by using the template of each dimensions was assessed from the resulting images. Width of the grooves was measured as length of the line drawn through the widest part of the groove. Depth was measured as length of the line drawn perpendicular to the surface of the construct from the bottom of the groove. The expected dimensions (width and depth) of the grooves were 25x75, 50x75 and 100x75 µm, based on the dimensions of the moulding template.

Moulding of the 25x75 µm template onto the FLS of the 10.6 mm collagen gels resulted in the grooves of 22.9±2.3 µm width (92% of the expected value). The depth of the grooves, made using the template of this dimensions was 22.1±2.8 µm,

which was only 29% of the expected value of 75 µm. Therefore, although the width of the grooves was very close to the expected value, the depth was compromised. Similar results were obtained when the template of 50x75 µm was used. The width of the resulting grooves was 46.7±4.7 µm, which was 94% of the expected value. However, measured mean depth of the grooves was 25.1±3.8 µm, only 33% of the expected value of 75 µm. Therefore, when this template was used, close fidelity to the width of the template was achieved, but not the depth. The histological and SEM images show the 10.6 mm constructs moulded with the template of 50x75 µm with the resulting grooves of 46.7±4.7 µm width and 25.1±3.8 µm depth. As can be seen from Figure 6 (right-hand panel), use of the template produced parallel grooves in the collagen construct, indicated on the upper image by the arrows. Next image in the panel shows transverse view of the individual groove in the FLS of the construct, showing impression of the template in the collagen, as a result of collagen fibrils moulding around the template.

When the template of 100x75 µm dimensions was used to micro-mould the fluid leaving surface of the 10.6 mm gels following dimensions of the grooves have been achieved. The mean width of these grooves (96.6±5.9 µm), as with the templates of other dimensions, was very close to the expected value of 100 µm (97% of the expected value). More surprisingly, the depth of the grooves (34.3±4.8 µm) was also closer to the expected value of 75 µm (45%) compared to the templates of other dimensions. Although depth fidelity was still poor it had increased from almost 1/3 to ½ of expected value. SEM images of the grooves, made by using the mask of this dimension can be seen in Figure 6 (left-hand panel of images).

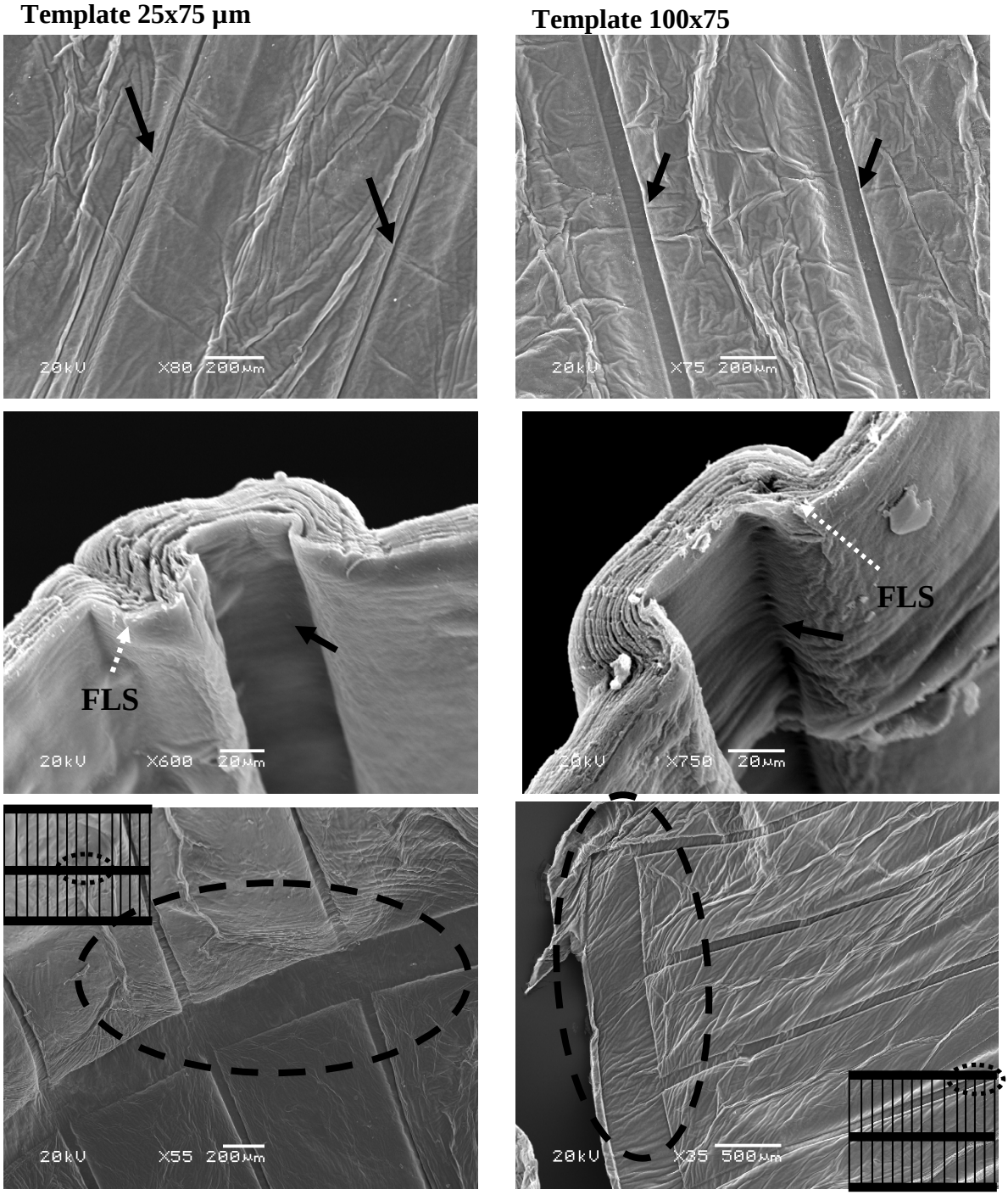

Fig. 6 Representative SEM images of the patterned constructs made of 10.6 mm gels. Constructs were micro-moulded using 25x75 µm template (left-hand panel), and 100x75 µm template Right-hand panel). Upper row of images shows surface of the patterned constructs with parallel grooves, indicated by arrows. Middle panel shows images of the individual grooves in transverse view, indicated by arrows. Bottom row of images shows surface of the patterned constructs, with the branching of the templating rungs from the middle and upper supportive bars on the template (shown in the inserts).

As can be seen from the bottom row of images in Figure 6 areas where templating bars diverged at 90° from the supportive bars on the template were patterned with excellent resolution. Therefore, complex, branching pattern (e.g. blood vessels) can be produced by micro-moulding of the collagen gels with the specially designed template. This provides an important advantage of this method of pattern generation, especially combined with the 'roofed' channel formation, as complex patterns in the compressed collagen constructs cannot be produced using other methods, such as lost fibre technique.

Analysis of the depth of the grooves, made by using templates of 25, 50 and 100 µm width and uniform 75µm height (Figure 7), showed that using the template with the widest rungs results in significantly deeper grooves in the collagen construct ($p=0.01$ compared to 25 and 50 µm templates). These results show that use of the templates of the examined dimensions in the 12 well format produces constructs with the grooves that strongly conform to the width of the template but not the depth, with the relatively deeper grooves produced by using the widest template.

As pattern on the FLS of the compressed gels is a result of the deflected fluid flow and deposition of the collagen fibres, these results suggest that formation of the pattern in case of the narrow and wide templates is somewhat different and will be discussed later.

Effect of the initial gel height on the grooves dimensions

As has been shown, formation of the pattern on the fluid leaving surface of the plastic compressed collagen gels depends on fluid flow from the gels and moulding of the collagen fibrils, Therefore, the absolute amount of fluid and protein in the gels can potentially affect the resulting pattern. To test this hypothesis, gels of the initial height of 5.3, 10.6 and 13 mm were micro-moulded with the template of 50x75 µm and the

dimensions of the resulting grooves compared between the gel heights. The fidelity of the resulting grooves to the template was also evaluated based on the patterning coefficient, calculated as described in Chapter 4. Patterning coefficient (a measure of fidelity = expected value:actual dimensions) was calculated by dividing groove depth by width and compared to this of the template, which was 1.5 for the 50x75 µm template.

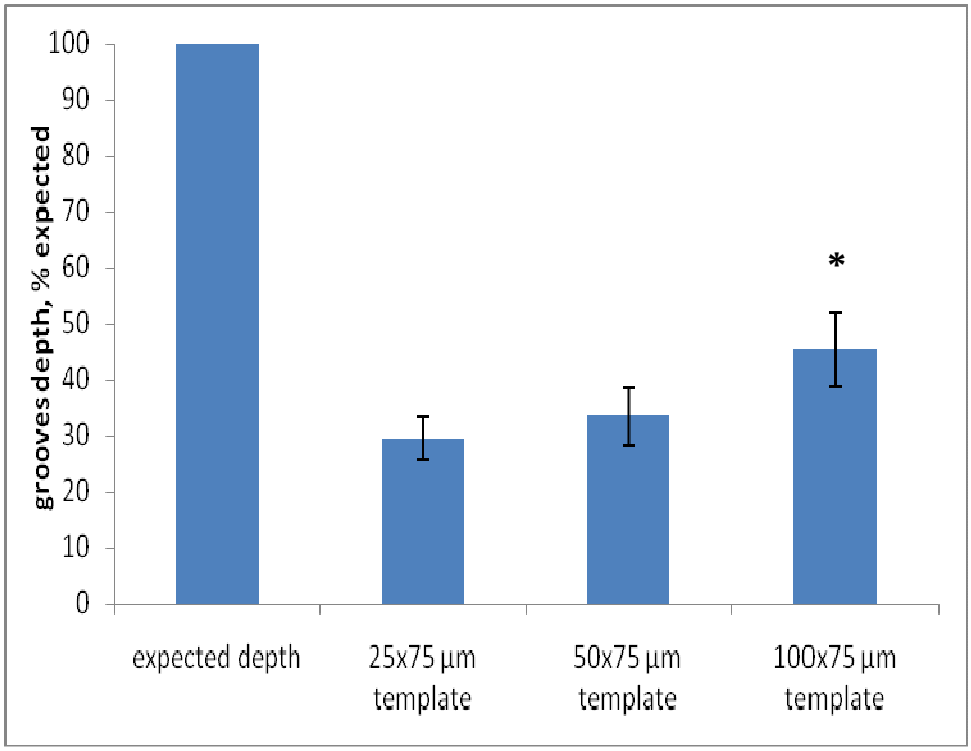

Fig.7 Bar chart showing depth of the grooves in percentage of expected value (thickness of the template, 75 µm, taken as a 100%). Grooves were micro-moulded into the 10.6 mm gels using templates with rungs of 25, 50 and 100 µm width. *-statistically significant difference ($p<0.05$).

The width of the grooves, achieved by using 50x75 µm template was 48.5±3.2 µm when 5.3 mm gels were used, 46.7±4.7 µm in the 10.6 mm gels and 45.7±5.2 µm in the 13 mm gels. Differences between values were not statistically significant. Mean depth of the grooves in the gels of different initial height was 25.2 ± 4 µm in the 5.3 mm gels, 25.1±3.8 µm in the 10.6 mm gels (33% of the expected value in both cases)

and 27.8 ± 3.9 µm (37% of the expected value) in the gels of 13 mm initial height. Although differences were not significant, marginally deeper grooves were achieved when 13 mm gels were used.

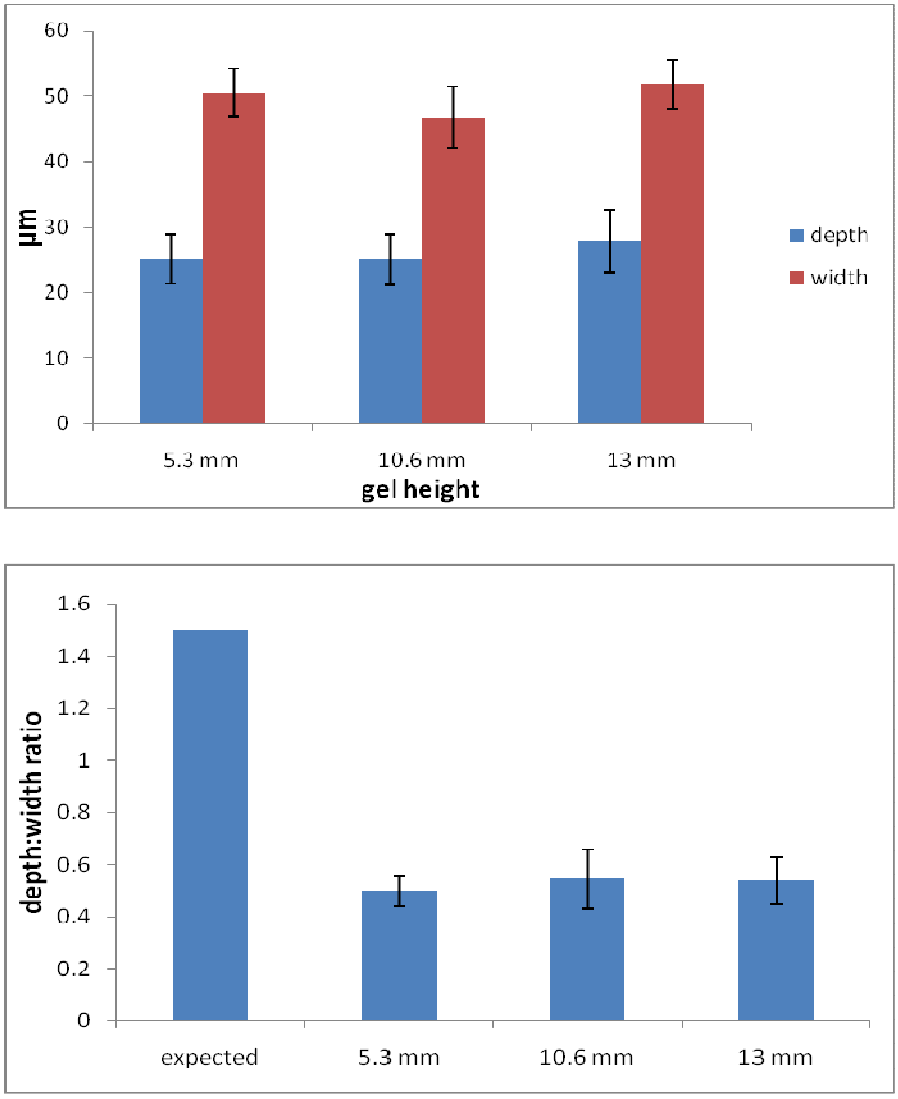

Fig. 8 (a) Bar chart, showing average depth and width of the grooves, made using 50x75 µm template in the 5.3, 10.6 and 13 mm gels. (b) The respective fidelity of the pattern, based on the depth to width ratio, to the moulding template. * - statistically significant difference ($p<0.05$).

All gel heights showed little fidelity to the template based on the patterning coefficient due to the compromised depth of the resulting pattern. Thus, patterning coefficient for the 5.3 mm gels was 0.5±0.05, for the 10.6 mm gels – 0.54±0.1 and

0.54±0.09 for the 13 mm gels, compared to the expected value of 1.5 based on the dimensions of the template. Based on these results, the dimensions of the pattern did not depend on the initial height of the gel. In all cases the width of the grooves was within 90% of the expected value; however depth of the grooves was less than half of the expected value. This has a negative effect on the fidelity of the pattern to the template.

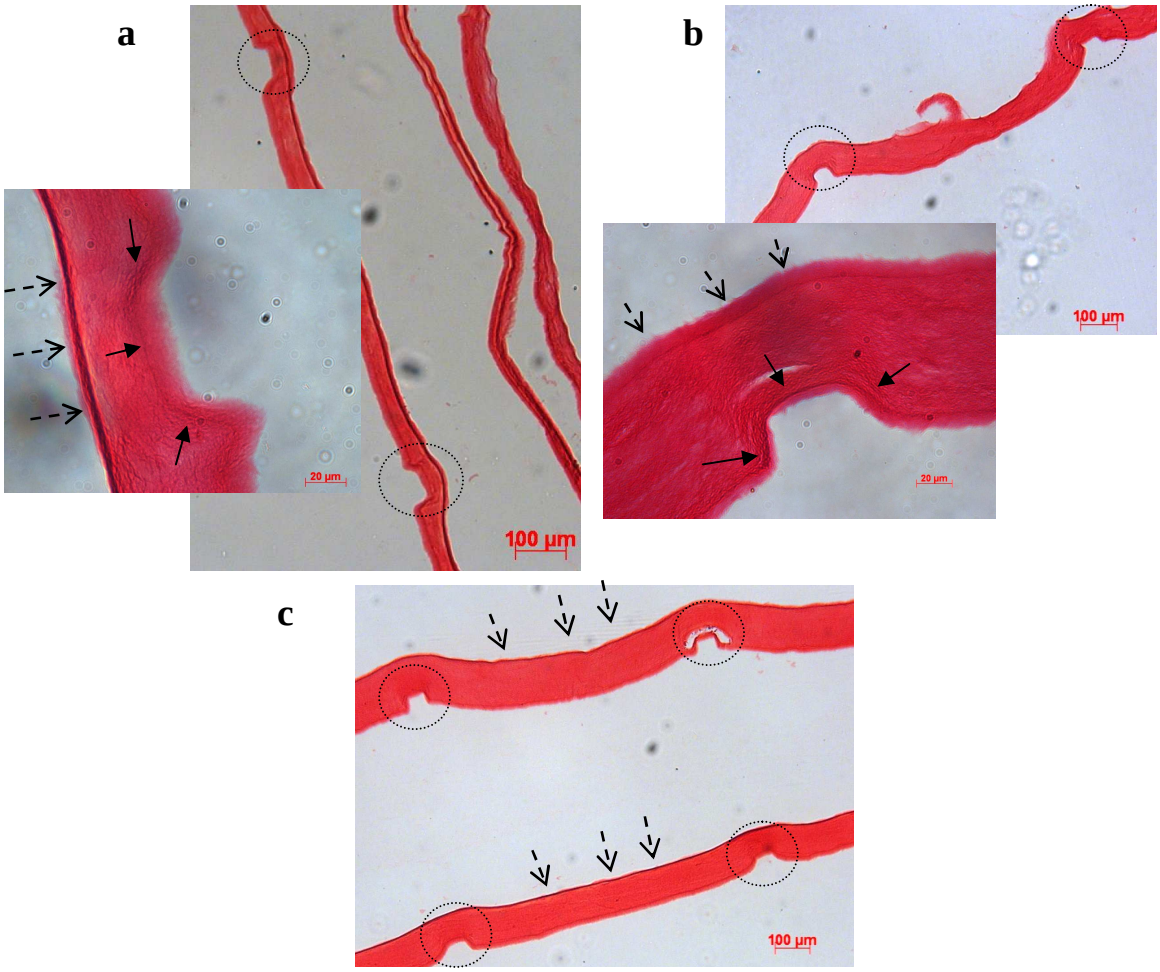

Fig. 9 Representative histological images (SiriusRed staining) of the grooves (transverse view) made using 50x75 µm template in the (a) 5.3 mm gels, (b) 10.6 mm gels and (c) 13 mm gels. Inserts show grooves at high magnification. Dashed areas outline grooves, dashed arrows point at the secondary FLS, solid arrows indicate collagen fibrils accumulation in the vicinity of the groove.

Dimensions of the'roofed' channels

The method of multi-well plastic compression and combination of the micro-moulding technique and multi-layering (as described in the previous chapter) provides an exciting opportunity of fabrication of layered collagen constructs with the channels of controlled dimensions and geometry. These channels will consist of two parts, where base layer of collagen contains the grooves, which will form the base and the walls of the channel and the upper layer of collagen will act as a roof.

The hypothesis under test was that the upper layer collagen solution will be too viscous to fill the grooves in the bottom layer, given their narrow dimensions. For the same reason, compression of the upper layer (the 'roof') will not have detrimental effect on the dimensions of the underlying grooves. Spaces between the grooves will ensure interlayer connection due to integration of the upper and lower layers by mechanisms discussed in the previous chapter. To test this hypothesis, two layered constructs, made of the 10.6 mm gels in each layer were made as shown schematically in figure 2. The base layer was micro-moulded with the templates of 25, 50 and 100 µm width and uniform 75µm height. The resulting collagen constructs were incubated with PBS for 5 minutes without removing the template to avoid pattern deformation. After the template was taken, liquid was removed from the wells and a second gel was set and compressed on top of the first, patterned, layer. The dimensions of the resulting channels were measured from the histological images. Formation of continuous channels was confirmed by examination of the constructs using SEM.

Histological and SEM examination of the resulting constructs confirmed formation of the open channels made using this technique with the base, patterned layer retaining the grooves following compression of the second layer on top. Width of the channels was measured in the widest part of the channel. Depth was measured

as a distance from the bottom of the groove to the top layer of collagen. The dimensions of the channels were compared with the respective width and depth of the grooves in the single patterned construct made of 10.6 mm gels as described earlier in the Results section of this chapter.

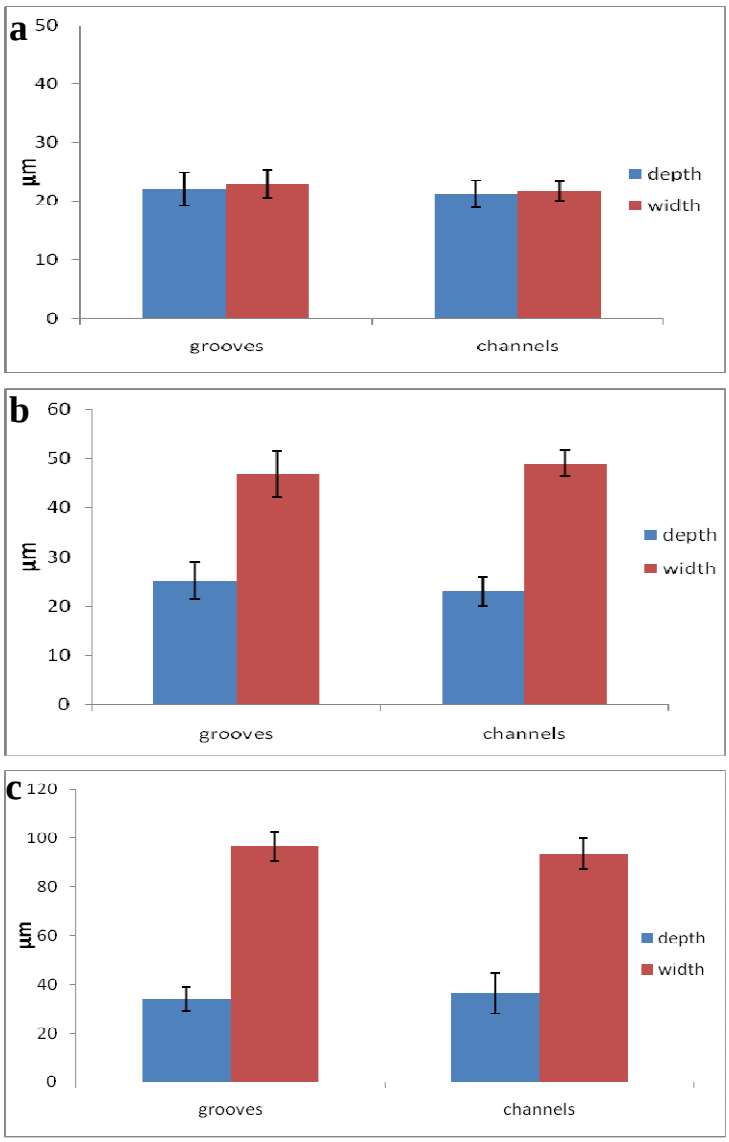

Fig. 10 Bar charts showing the dimensions of the channels (depth and width), made by micro-moulding 10.6 mm gels (base layer) and casting and compressing fresh gel of the same height on top (upper layer, roof of the channel). The dimensions of the grooves in the single layer are plotted for comparison. (a) 25x75 µm template, (b) 50x75 µm template, (c) 100x75 µm template.

Use of the 25x75 µm template resulted in the formation of square channels which were 21.7±1.7 µm wide (compared to 22.9±2.3 µm in the single layer) and 22.9±2.9 µm (compared to 22.1±2.8 µm in the single layer) deep. Dimensions of the channels did not differ from the dimensions of the grooves in the single layer.

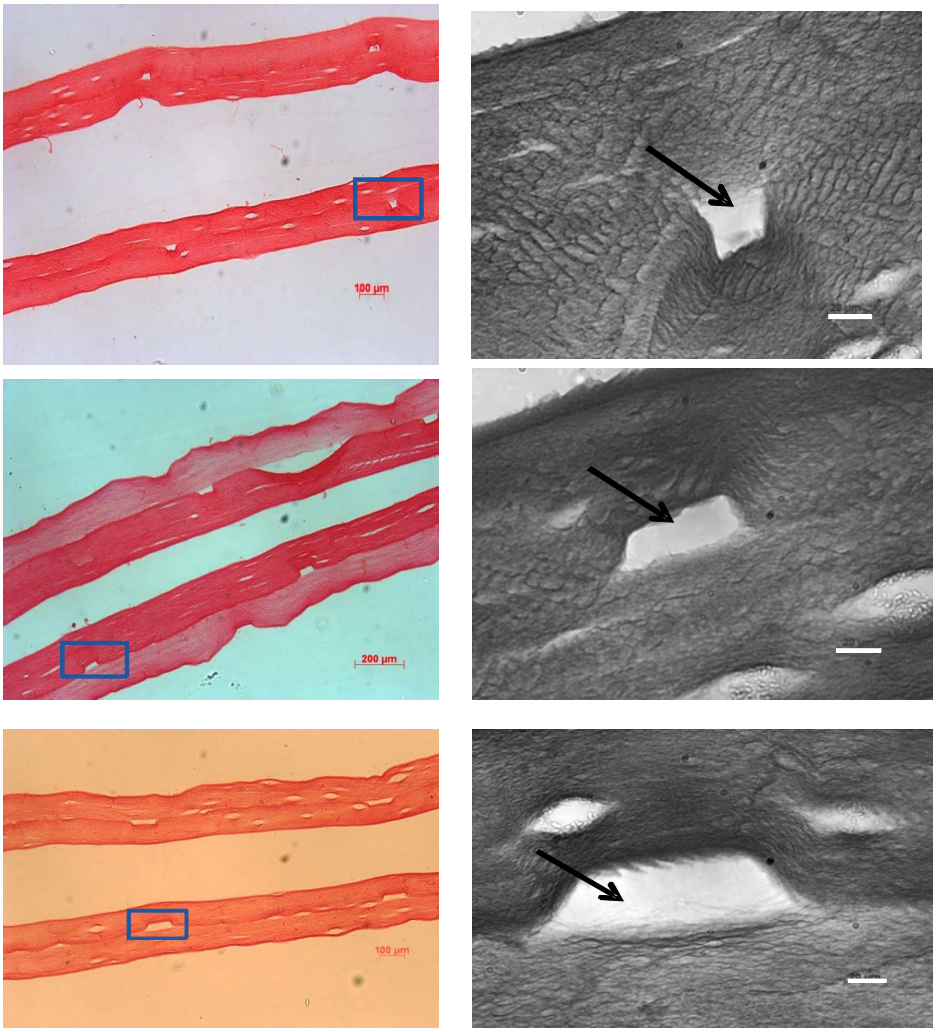

Fig. 11 Representative histological images (low and high magnification, inserts) of the open channels (transverse view, SiriusRed staining) made by micro-moulding 10.6 mm gels (base layer) and casting and compressing fresh gel of the same height on top (upper layer, roof of the channel). (a) 25x75 µm template, (b) 50x75 µm template, (c) 100x75 µm template. Solid arrows indicate the open area of the channel, arrow heads point at the collagen fibrils, protruding into the channels from the upper layer (the 'roof').

When the template of 50x75 µm was used to pattern the base layer, channels of the following dimensions were achieved. The mean width of the channels was 47.8±2.6 µm (not different from those in the single layer of 46.7±4.7 µm). The depth of the channels was 22.9±2.9 µm (compared to 25.1±3.8 µm in the single layer). The differences were not significant.

Width of the channels, made with the use of 100x75 µm template was 93.7±6.4 µm (value for the single layer was 96.6±5.9 µm). Depth of these was 36.4±8.3 µm (value for the single layer was34.3±4.8 µm). Again differences between the dimensions of the grooves in the single layer did not differ significantly from the dimensions of the two-part channels. These results show that pattern, formed by micro-moulding of the fluid leaving surface of the collagen gels in the multi-well format is stable enough to withstand pressures created by the compression of the second collagen gel. Possible mechanisms will be proposed in the Discussion section of this chapter

Effect of the embedded cells on the dimensions of the grooves in culture

It has been shown in Chapter 4 that grooves, micro-moulded into the fluid leaving surface of the plastic compressed cell-seeded collagen constructs are stable over 2 weeks in culture. The question asked here was if the same applies to cell-seeded collagen gels, which were micro-moulded in a multi-well plate format and using rectangular cross-section template. Gels of the 10.6 mm initial height, with the cells seeded *in situ* were compressed with the 100x75 µm template and cultured under standard tissue culture conditions for two weeks. Constructs were fixed at 1 and 2 weeks and the dimensions of the grooves assessed using image analysis. Resulting data were compared to that for the grooves in the acellular constructs patterned with the template of the same dimensions. The dimensions of the grooves after one week in

culture did not differ from those in the acellular constructs (Figure 12 a). The mean width of the grooves was 96.7±5 µm (compared to 96.6±5.9 µm in the acellular constructs), the mean depth of the grooves was 36.6±3.4 µm (compared to the 34.3±4.8 µm in the acellular constructs).

After two weeks in culture, the mean width of the grooves remained unchanged with the value of 96.2±6.2 µm. However, the mean depth of the grooves in the cellular constructs after two weeks decreased slightly from 36.6±3.4 µm to 30.3±3.1 µm. This was not significant compared to the value at week one or to the acellular constructs.

As can be seen from the histological images in the Figure 14 b and c, topological features were present in the cell-seeded constructs after both one and two weeks in culture. Clear signs of cell-matrix remodelling were evident (indicated by dashed ovals on the Figure 14 based on the characteristic 'lacy' appearance of the construct, which developed over time in culture. This indicates that cells were active and viable deep in the construct over prolonged periods.

These results show that micro-moulding of the topological features into the fluid leaving surface of the cell-seeded collagen gels in the 12 well plate format results in the grooves stable for at least two weeks in culture conditions, confirming results reported in Chapter 4.

a

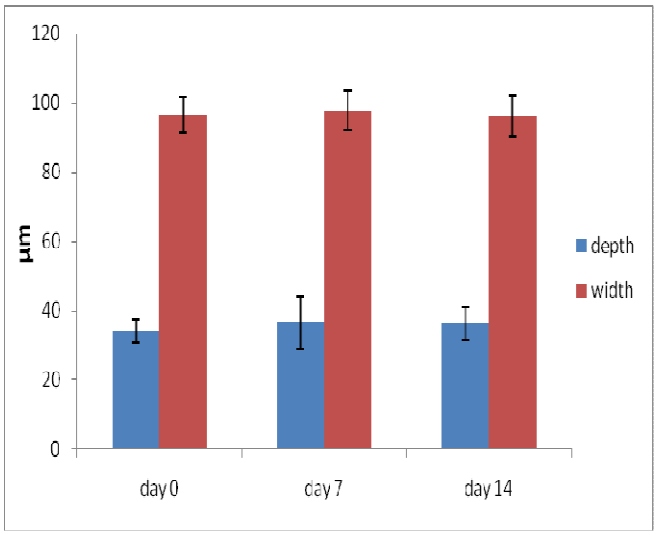

b

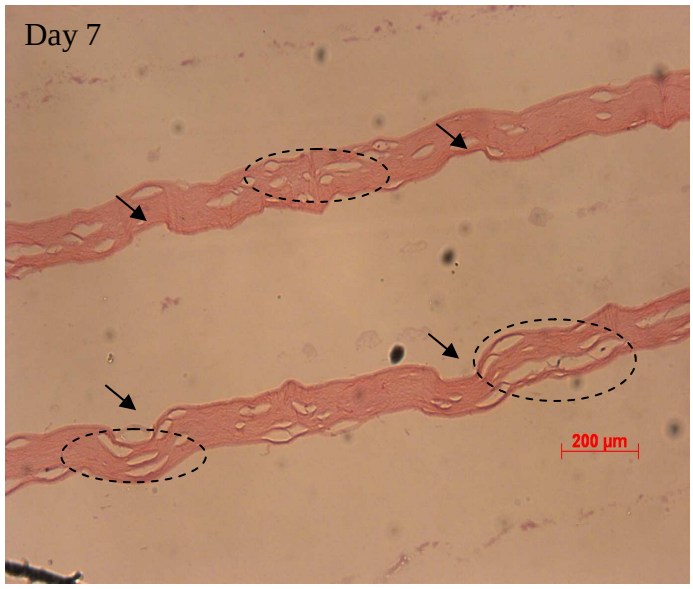

c

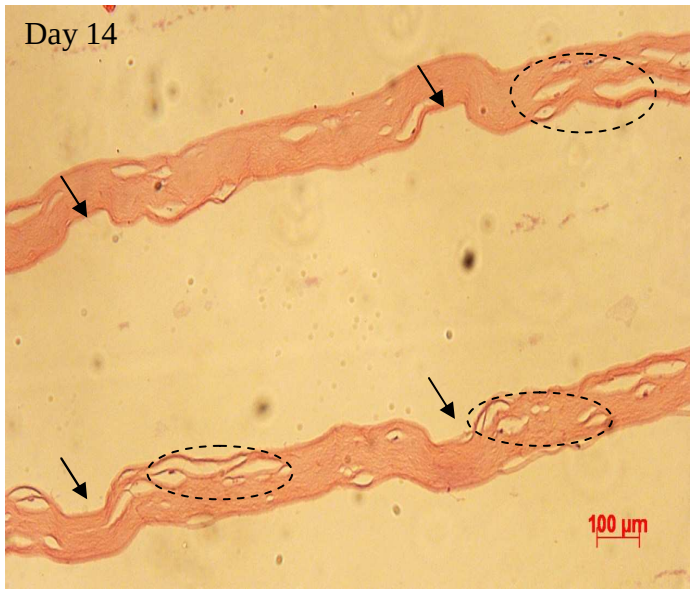

Fig.12 (a) Bar chart showing the dimensions (depth and width) of the grooves, made in the single-layered constructs using 100x75µm template. Dimensions of

the grooves in the cell-seeded constructs, cultured for 1 week and 2 weeks are compared with the dimensions of the grooves in the acellular constructs at time 0. (b) Representative histological images (H&E staining) of the patterned cellular constructs at week 1 and 2. Dashed ovals indicate areas of cellular matrix remodelling, arrows point at the grooves in the constructs surface.

Efficiency of the cell delivery into the grooves during the micro-moulding of the gels.

Direct delivery of the cells into the micro-channels or micro-grooves in the collagen constructs is of potential benefit for engineering of construct with micro-vasculature. It is also an important step in the study of the effects of surface topology on cell behaviour in soft native materials. To this end, the efficiency of novel cell-delivery technique has been investigated. In this method, the cells were seeded on the micro-moulding template.

After micro-moulding process was completed and the pattern formed, the template was left on the construct for 2 hours to enable cells to transfer attachment to the collagen substrate. The hypothesis was that, as collagen is a natural extracellular matrix polymer rich in RGD (Arg-Gly-Asp) sequences cells will over time preferentially attach to the collagen and not to the synthetic template. To test this, the number of the cells, collected on the template per rung was counted using live-dead assay. This value was compared to the number of cells in the grooves following the micro-moulding. The template of 100x75 μm was used for cell delivery and patterning, as larger surface area would result in higher number of captured cells.

To assess the efficiency of the delivery method, firstly mean number of cells, seeded onto the rungs of the template was established using live-dead staining assay (see Chapter 2). The mean number of cells, seeded on the rungs (n=20 rungs, 3 templates) after 2 hours of incubation with the cell suspension was 27±5 cells per rung. This was not surprising given that template occupied only 11.6% of the surface area of the well. Indeed, examination of the well, where templates were incubated

with the cells showed that cells mostly settled at the bottom of the well. First image in the Figure 13 (a) shows HaCat cells (green), seeded on the rungs of the template prior to delivery, and it can be seen from the cell-shape (round) that the cells did not firmly attach to the template yet, making it more possible to for them to preferentially attach to collagen surface after delivery into the grooves.

Following the micro-moulding and two hours of transfer from the template (cell side facing the grooves) to the patterned collagen construct, the mean number of cells in each groove of the construct was 5±2 cells/groove (n=20 grooves, 3 collagen constructs). Based on the mean number of cells on the rungs prior to delivery it gives approximately 18.5% efficiency of the delivery method. Middle image in Figure 13 (a) shows representative photograph of the live HaCat cells in the groove immediately following the delivery procedure. As can be seen from the image, cells are confined to the groove and still retain round shape. The same can be seen from the SEM images of the cells in the grooves in Figure 13 b. Also, from the SEM images in Figure 13 b it is clear that following two hours transfer period (from the template onto the collagen), cells start to extend processes and attach to the collagen surface. This suggest active (‘crawl’ from the rung), rather than passive (i.e. drop from the rung) mode of cell delivery.

At day 1 of culture (Figure 13a, last image), these cells changed shape from round to slightly elongated with some cells detected beyond the boundary of the groove. This was expected, as it is known that HaCat cells are highly motile (Kehe et al., 1999) and the depth of the grooves (approximately 30 μm) was evidently not enough to prevent these cells from leaving it.

The results indicate that it is possible in the process of micro-moulding to deliver live cells into the grooves. Indeed, live-dead assay showed no dead cells in the

grooves following the micro-moulding suggesting that the process was cell-friendly. Therefore, this technique merits further investigation. Several ways to improve the efficiency of the direct delivery method will be proposed in the discussion section of this chapter.

With regards to the fabrication of the cell seeded micro-channels, a small pilot study has been conducted, where cells were delivered as described before and a two-part channel was formed by adding top layer of compressed collagen. Constructs were cultured for 1 week, fixed, sectioned and stained (H&E method, see Chapter 2). Reflecting low number of cells in the grooves, majority of the observed channels did not contain cells. However, some channels contained cells at high density, as shown in Figure 14. Cells were contained in the channel, i.e. did not migrate out of the groove and between the layers after 1 week in culture. This was in stark contrast with the behaviour of these cells in the grooves.

As shown on the last image in Figure 13 a, after only 24 hrs culture period some cells migrated out of the grooves.

Evidently, interlayer connection (as discussed in Chapter 6) created a tight seal between layers 1 and 2 (between groove and roof), and this bond prevented cells from leaving the confinement of the channels even after 1 week in culture. There were no obvious signs of cell remodelling of the collagen matrix, and based on the morphological images, cells were proliferating and forming lining of the channel. This behaviour of epithelial cells in tubes (channels) has been described previously by Riehle et al. (1998). These promising preliminary results indicate that with the further development of the technique it can be used to provide cellular (endothelial cells) lining to the micro-channels as a first step to engineer primitive micro-vasculature in the collagen constructs.

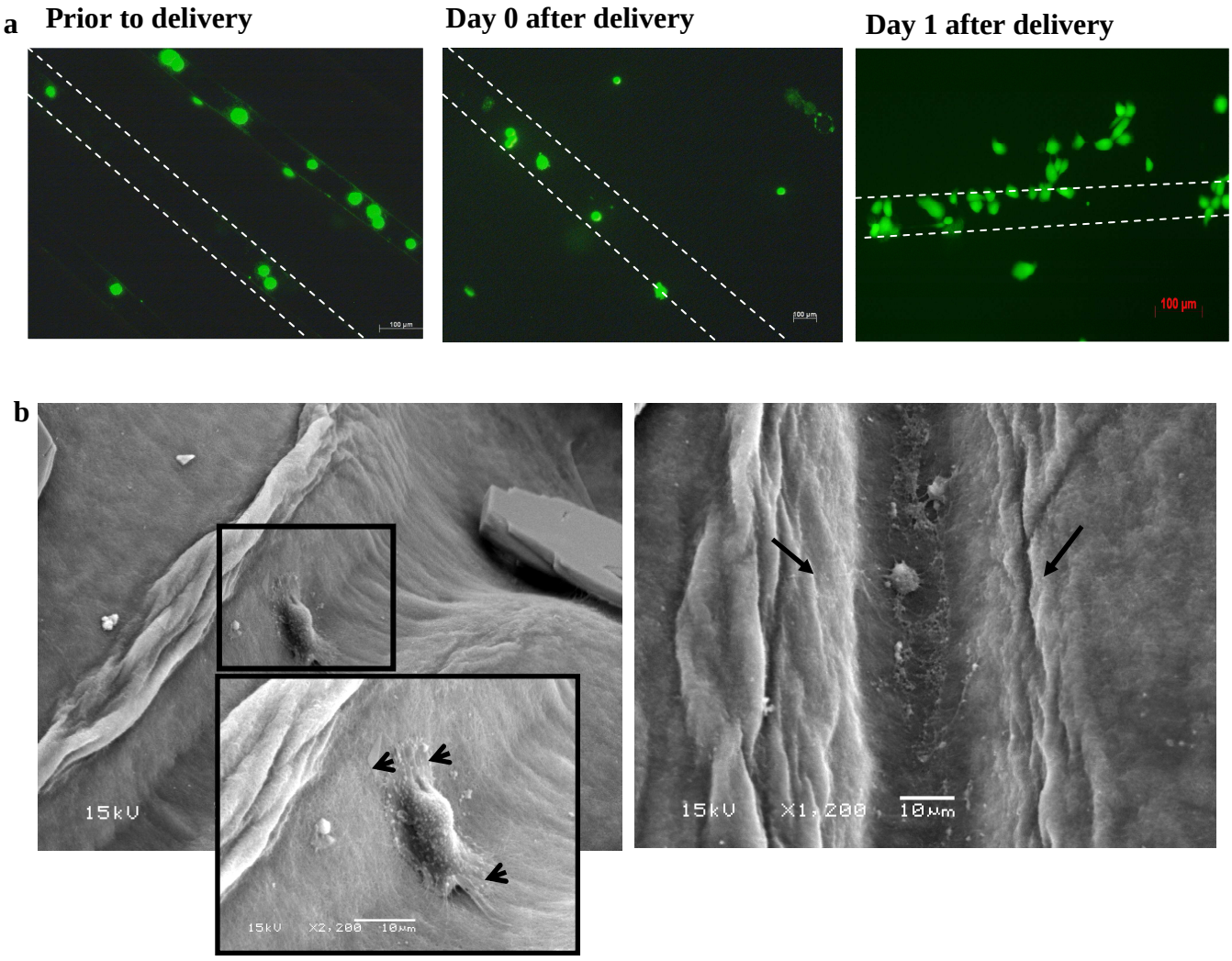

Fig. 13 (a) Images of the live HaCat cells (green), stained using live-dead protocol. Left – cells on the rungs of the template, following 2 hrs incubation with the cell suspension. Middle and right are images of the cells in the grooves, taken at time 0 and 24 hrs of culture period. Dashed lines indicate the rung of the template (left image), and grooves (centre and right images). (b) SEM images of the cells, delivered in the grooves following direct cell delivery protocol at time 0. Insert – higher magnification of the cell in the groove showing cell, attached to the collagen surface. Arrows on the image on the right point at the groove borders. Open arrows show cell filopodia attached to the collagen fibres.

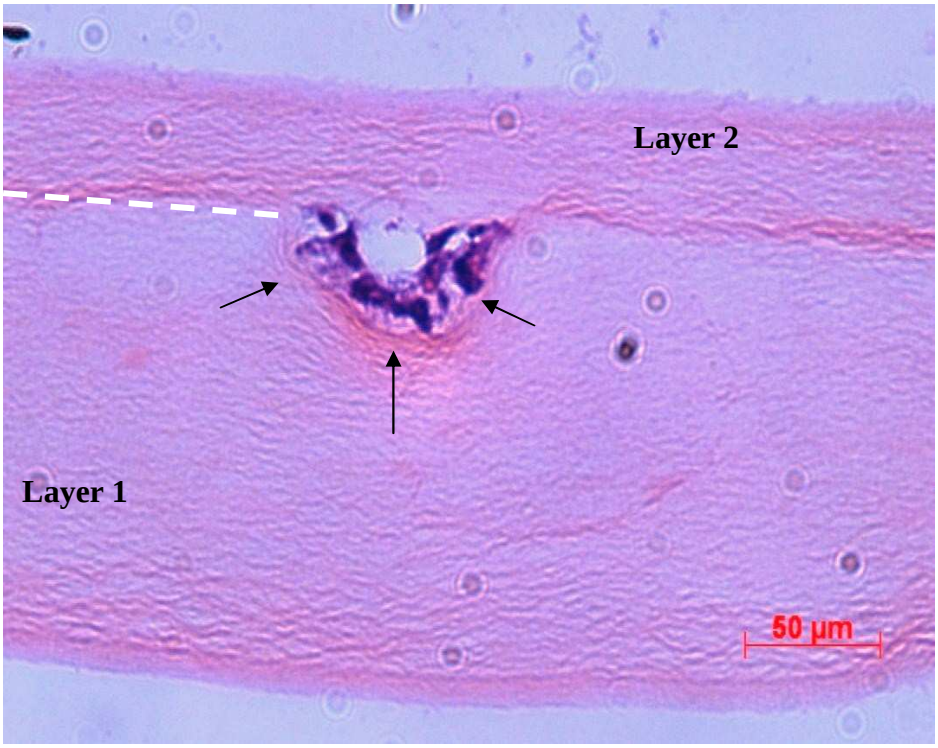

Fig. 14 Histological image of the channel in the double-layered collagen construct, with the cells (HaCat), delivered using the direct cell delivery protocol, and cultured for 1 week. Layer 1 (patterned layer) was made of 10.6 mm gel, layer 2 (roof of the channel) was made of 5.3 mm gel. Dashed line indicates interface between layers, arrows point at the channel lumen.

Discussion

The importance of the surface patterning in the natural polymer constructs has been discussed in Chapter 4. Also, methods of patterning the fluid leaving surface of the PC collagen construct have, compressed using original method, been developed and discussed (see Chapter 4) Mechanisms of the pattern formation in this system (i.e. on the single FLS) have been proposed in the same chapter. In this study, pattern formation on the primary FLS of the collagen gels, compressed using multi-well plastic compression system (see Chapter 5) has been evaluated. In addition, the possibility of fabricating two and three layered constructs (see Chapter 6) with incorporated channels has been explored.

We have hypothesized that use of the impermeable template in the multi-well compression format will affect the fluid flow patterns of the compressed gels. To test this hypothesis following parameters have been investigated: (i) average fluid loss against time of compression from the collagen gels with the templates of different dimension, end time-point of full compression with the templates of the same dimensions and effect of micro-moulding on the dynamics of fluid loss from the compressed gels compared with the non-moulded gels.

Another unknown was the effect of the template dimensions and of collagen gel height on the resulting pattern fidelity. To answer this question, width and depth of the grooves, made using the templates of different dimensions in the gels of the same height and width and depth of the grooves made using template of one dimension in the gels of different heights was assessed. These were than compared to the dimensions of the 'roofed' channels, produced by micro-moulding double and triple-layered collagen gels to answer the question of channel survival after setting and compressing of the 'roof' layer.

Additionally, stability of the in the constructs with the embedded cells in culture was assessed. Finally, we have developed and tested new method of direct cell delivery and tested its performance both in the grooves and in the 'roofed' channels.

As discussed previously, the stable patterns on the single FLS are formed as a result of fluid flow from the collagen gels around an impermeable template. This seems to lead to the re-moulding of collagen fibrils around the template as the gels shrinks, eventually creating a stable topology in the construct. However, this was true in the system where single FLS is formed, whereas in the multi-well format multiple fluid leaving surfaces are potentially created due to the small surface area of the gels

and resulting pressure build-up (Chapter 5). Therefore, the effect of the secondary FLS formation on the patterning of the gels was investigated here.

As the templates were impermeable, therefore reducing the fluid leaving surface area, it has been hypothesised that micro-moulding will affect fluid flow from the collagen gels, as permeability of the FLS will decrease faster compared to the non-moulded gels. To test this theory, gels (of the 10.6 mm height) were used as their compression curve has a distinct feature ('jump'). This probably corresponding with the formation of the secondary FLS at the bottom of the gel at minute 2 (see Chapter 5, discussion). Therefore, this 'jump' in the curve was used as a reference point in comparing with compression curves of moulded gels.

It was shown in this study that use of the impermeable templates of all dimensions led to disappearance of the 'jump' from the compression curves of the gels compressed with the templates. It appears that by reducing the surface area of the primary FLS by approximately 10% secondary FLS formation was triggered earlier, probably during the first minute of compression. This is supported by the fact that fluid loss from the micro-moulded gels was greater than that from non- moulded gels during first minutes of compression. Formation of the secondary FLS so early in the process was probably also the reason for faster compression of the moulded gels. Therefore, the crucial time-period for pattern formation on the primary FLS was the first minute of compression. However, it is not possible to determine if during the rest of the process fluid flow is confined solely to the secondary FLS or distributed between the two, in other words if patterned features undergo further remodelling or are fully formed in the first minute of the process, rendering the primary FLS virtually impermeable. However, the fact that micro-moulding of the 5.3 mm gels led to formation of the secondary FLS, evident from the histological images seem to support

the first theory, as gels of this height do not form secondary FLS when compressed without the template (see Chapter5).

Further investigation supported the theory of the instant formation of the grooves, when using the multi-well compression system. Analysis of the dimensions of the grooves showed that neither dimensions of the template nor the height of the gel (i.e. the total amount of protein present) had an effect on the resulting features. Therefore, the dimensions of the grooved are determined during the first minute, when the open (between rungs) area of the primary FLS had become impermeable.

In all cases, the width of the grooves closely resembled the width of the template; however the depth of the grooves was considerably less than expected. This is in a contrast with the pattern fidelity reported in Chapter 4. In this study grooves produced by 25, 50 and 100 µm wide rungs, had in the best case half of the depth (template – 75 µm). When glass fibres were used to pattern single FLS in Chapter 4, an excellent degree of pattern fidelity was achieved. The differences in pattern fidelity in two studies could be due two reasons – different cross-section of the template and multiple fluid flow directions in the multi-well format.

The patterning mask, used in Chapter 4, had a circular cross-section, whereas in this study the cross-section of the template was rectangular. It is possible that the fluid movement around a cylinder will differ from the flow around a parallelepiped at the micron level. The difference in the fluid flow around a cylinder with the circular and rectangular cross-section is well documented and modelled in literature. However, these models are based on a steady fluid flow in an ideal system and so difficult to apply here.

Plastic compression is a dynamic process, with added complexity of accumulation of collagen fibres on the FLS and the fact that fluid is essentially

flowing through a mesh of nano-fibres that compacts over time. Therefore, it is challenging to mathematically model the fluid flow around a template in this system, where all these factors will need to be taken into account. However, it seems to be possible to propose at least three consecutive directions of fluid flow, which could explain why the depth of the grooves was less than expected. The proposed mechanism is shows as a diagram in Figure 15.

Firstly, it seems reasonable to predict that at the beginning of the compression, when templates are placed on the gels and load is applied, full depth of the grooves is achieved. At this point the thickness of the template is irrelevant compared to the initial height of gel (e.g. 75 µm thick templates compared to 5300 µm (minimum) high gels).

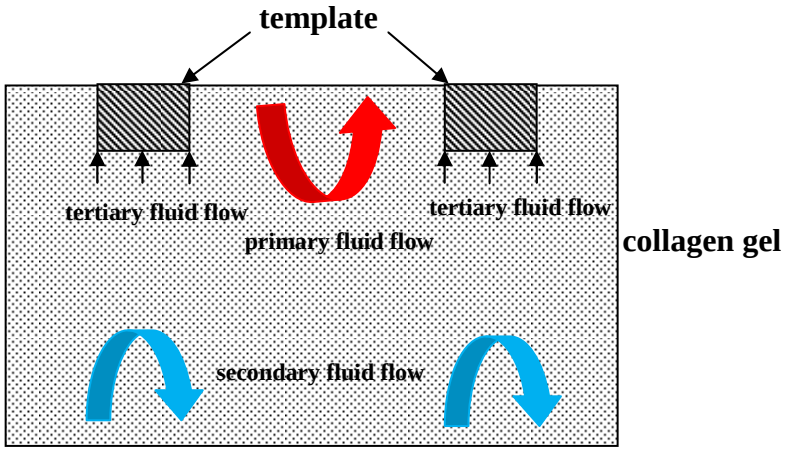

Fig. 15 Diagram, showing proposed mechanism of pattern formation in the multi-well format. Immediately after contact with absorbent and loading, fluid starts to flow out of the gel towards the absorbent (primary flow). However, presence of the impermeable template results in faster blockage of the primary FLS due t the process of ultrafiltration. Following that event, fluid starts to leave the gel through the bottom part (secondary flow), creating secondary FLS. This is blocked as well due to the same ultrafiltration process. Fluid, still left in the gel by this point can leave through the only unblocked surface – bottom of the grooves (tertiary flow). This potentially leads to slight lift off of the template and possibly collapse of the walls of the grooves, resulting in shallower than expected features.

The primary fluid flow (primary FLS) is formed, as described before, at the surface in contact with absorber, and because the templates are impermeable, water

will initially flow through the inter-rung intervals. This will continue, until these spaces become blocked by the collagen fibrils (as discussed in Chapter 5), and, as already has been proposed, will happen within the first minute of the process. At this point, primary FLS is formed.

The rest of the fluid in the gels will flow through the bottom of the gel, forming a secondary FLS, as proposed in Chapter 5. However, when this exit route becomes blocked, an additional, tertiary fluid leaving direction can be hypothesised, through the bottom of the grooves (evidence of which can be seen from the histological images). This event can lead to two possible outcomes, which may lead to reduced depth of the grooves. First, lift of the bottom part of the groove as collagen fibrils accumulate there and second collapse of the overstretched walls as liquid leaves around the template. This last could also explain occurrence of trapezoid-shaped grooves in some cases (as opposed to the expected rectangular cross-section).

Dimensions of the grooves tested in the presence of matrix-remodelling cells in culture conditions did not change compared to the initial, which was in agreement with the results, reported in Chapter 4. Therefore, although mechanisms of pattern formation in the multi-well format are somewhat different (multiple fluid exit points compared to single in the original method) from those using the original method of PC, the resulting features were stable in culture conditions making it a useful tool, in particular to study cell-pattern interactions on the natural polymer.

The stability of the pattern and possibility of fabrication of multilayered constructs in the multi-well format created an exciting opportunity to make multilayered constructs with predetermined channels. Each channel consisted of the bottom and side walls (groove in the base, templated layer) and the roof (top layer of collagen). The hypothesis was that viscosity of the collagen in the upper layer and

micron width of the grooves in the bottom layer would prevent occlusion of the lumen of the channel. Indeed, open channels were produced using all template dimensions on the base layer. More importantly, the dimensions of the produced channels did not differ from those of the grooves in the single-layered constructs, suggesting considerable mechanical strength of the supporting side walls of the grooves.

Formation of the open channels using this technique can serve as an alternative to the method, described in Chapter 3, where channels were formed by incorporation of soluble fibres in the bulk of the construct. It has been shown that incorporation of such channels into the PC collagen constructs leads to the increased oxygen perfusion through the layers of a spirally assembled scaffold (Cheema et al., 2010). Although this method is useful, there are a few disadvantages. Firstly, the thickness of the resulting construct is determined by the FLS area, and therefore limited. Secondly, although the phosphate based glass fibres chemistry can be modified to have little detrimental effect on the resident cells; there are still concerns about their use *in vivo* (Skelton et al., 2007). Therefore, formation of the stable channels in the collagen constructs, ultimately with embedded cells, that do not require any additional treatment (eg. cross-linking or dissolution) is advantageous.

Several methods have been reported by other groups to create controllable micro-channels is to layer micro-patterned sheets, so that pattern in the underlying layer is covered by the next layer of biomaterial, creating open channels. However, this approach has been generally used for synthetic polymers, such as poly-(glycerol sebacate) (Fidkowski C. et al., 2005), polydimethylsiloxane (Shin M. et al., 2004, Mata et al., 2009), poly(L-lactic acid) (Pappenburg et al., 2009), poly (lactide-co-glycolide), poly(ε-caprolactone-co-glicolide), poly(dioxanone) and Monocril® (Ryu et al., 2006). The two parts of the channels (the patterned layer and the upper cover)

are held together by uncured polymer (PMDS, Mata et al., 2009), treatment of the interface by oxygen plasma (Fidkowski C. et al., 2005, Shin M. et al., 2004), solvent vapour bonding (Ryu et al., 2006) or by physically rolling patterned stacted sheets in a tube (Pappenburg et al., 2009). Although, these methods successfully create open channels, use of synthetic materials and additional steps needed to hold the patterned sheets together make these methods less attractive for engineering living tissue equivalents.

In the method described here, next module is readily attached to the previous one (as discussed in Chapter 6) and assembly of the whole construct is serial as opposed to the parallel reported by other groups. Another advantage of this technology is a possibility to fabricate a 'living' construct, where each layer, the surface of the construct and potentially each channel can be seeded with the different cell type and used as model tissues (eg. replacement of animal experiment). Therefore, this model merits further work is evaluate the mechanical properties of the whole scaffold and the channels as well as stability of the channels in the cell-seeded constructs.

It has been shown that channels in the PC constructs result in increased oxygen diffusion through the construct compared to the constructs without channels (Cheema et al., 2010). As such, channelled multilayered constructs, assembled using multi-well plastic compression system, should provide sufficient degree of oxygen diffusion to the embedded cells in the centre of the constructs. However, for in vivo survival of the deep cell population, inosculation (connection with the blood system of the host) of the construct may be beneficial. To this end, the direct cell delivery method has been tested in the current study as a proof of principle as a first step to creating a primitive micro-vasculature. Cells survived the process, and were confined

to the grooves after process was completed. We had also demonstrated that cells can be trapped in the channels and successfully cultured, although further experimental work is needed to test these data.

Greater delivery efficiency can be achieved by coating the carrier masks with the thermo-responsive polymer (e.g. poly(N-isopropylacrylamide (Hannachi, Yamato and Okano, 2009) and culturing the cells to confluence on the masks prior to delivery. When cell-sheet is ready, the process of delivery can be performed as reported in this chapter with the temperature drop at the end of compression so that the sheet of cells will be deposited directly at the bottom of the grooves. Second layer of collagen (the roof) can be added at this stage, so that cells are confined to the channel.

The main advantage of this technique is that cell delivery and constructs fabrication happen simultaneously and cell-independently, offering great saving on time and high degree of control over the resulting pattern compared to other conventional methods of cell patterning. Among the other methods of cell patterning is use of patterned extracellular matrix proteins (Bhatia et al., 1997), ink-jet printing (Roth et al., 2004) and use of stencils (Folch et al., 2000, Wright et al., 2007).

Although useful, these methods have certain disadvantages. Patterning of the ECM proteins usually used for patterning cells on the synthetic constructs. The rationale behind this approach is that by controlling the adhesive pattern one can create patterns of cells, as they will adhere to the predetermined areas on the surface of the construct. However, this method is highly dependent on cells adhesion, coupled with the protein denaturation and synthetic nature of the constructs bulk. Ink-jet printing allows for precise deposition of ECM proteins and cells; however the method is still in the development stage and suffers from clogging by the proteins and inferior cell viability. Use of stencils as a direct cell delivery, although allowing for

controllable cell patterning when stencils are in contact with the surface of the construct, but after stencils are removed cells are no longer confined to the pattern which effectively disappears (Campbel and Weiss, 2007, Hannachi, Yamato and Okano, 2009).

Proposed method can be potentially used for lining the channels with endothelial cells as a model of primitive capillary system, to study stem-cells behaviour and for improvement of nerve repair by lining the channels with Schwann cells. A further investigation into compatibility of the process with these cell-types is needed. In conclusion, the new method of micro-moulding channels and grooves into the multi-layered collagen scaffolds opens new opportunities to engineer complex tissue equivalents, both for *in vitro* and *in vivo* use.

Chapter 8.

Summary, conclusions and further work.

Summary and conclusions

Collagen type I is the main structural protein in the mammalian body. As such this material is the ideal candidate for tissue engineering purposes, providing native structural environment to the embedded cells, as opposed to using synthetic substitutes. However, in the form of hyper-hydrated gel, this material has poor mechanical characteristics, being too weak, indeed unstable, to withstand mechanical loading or manipulations. The ability of plastic compression to produce dense, bio-mimetic collagen structure is valuable for fabrication of the dense tissue-like constructs, with superior mechanical properties, compared to the hyper-hydrated collagen gel.

The main mechanism of PC is the uniaxial removal of fluid under load, which does not return upon load removal, giving the process its name as plastic (irreversible) compression. The major advantages of this are the high viability of the embedded cells, and, at the same time, its complete independence from the cell activity.

Collagen density increases from 0.2% in the hyperhydrated collagen gel to approximately 12% following the compression process (Brown et al., 2005, Cheema et al., 2007). In the cell-containing gels collagen density following compression rose as cells contribute to the liquid content and volume of the initial gel, with final cell densities of 10-20% depending on the initial seeding density and spherical cell shape (i.e. cells are unattached). Generally, it is possible to extrapolate the eventual cell density in the PC scaffold by multiplying the initial cell number by fold volume change, which corresponds to 58 based on the increase in collagen concentration (Brown et al., 2005, Bitar et al., 2007, Cheema et al., 2007, Cheema et al., 2008).

Human dermal fibroblasts, embedded into the PC collagen constructs remained viable for up to 5 weeks in culture. Constructs at this time-point were morphologically compatible to the early connective tissues without signs of considerable cell death or matrix disintegration (Brown et al., 2005).

Material properties of the compressed collagen constructs have been further investigated using mechanical testing. Acellular spirally rolled PC constructs, tested in tensile mode showed typical toe and linear load-bearing regions, yield and maximum break-stress levels. These constructs had functionally useful mean tensile break strength of 0.6±0.11 MPa with a modulus of 1.5±0.36 MPa. Interestingly, cellular constructs, tested in the same mode showed that although there was initial reduction in yield strength and modulus (71 and 34% respectively), after two weeks in culture mechanical properties of these constructs improved to the level of acellular samples. This phenomenon can be taken as a sign of functional collagen remodeling of the matrix by the resident cells (Brown et al., 2005)

Spirally rolled PC collagen sheets, tested under unconfined compressive load, showed typical response of densification behaviour, where strain increases rapidly with the increase in stress. As this test represents in effect further compression, there was an initial linear region in modulus ($0.03MNm^{-2}$), which was replaced by a rapid increase in modulus as constructs became more compressed (Cheema et al., 2007).

This method has already been used for skin, bone, bladder and nerve tissue engineering. The main goal of this study was to further advance the methodology with the particular aim of formation of the stable micro-architecture in the constructs (both external and internal) and to understand the mechanisms of the formation of these features. The hypothesis under test was that controllable deflection of the fluid out flow from the gel, during compression, will result in the permanent and predictable

deformation of the fibril architecture and distribution on the micron-scale, giving stable topological features with predictable dimensions and geometry.

The overarching hypothesis of this project sounded as follows: dense collagen constructs with a viable cell population and engineered microarchitecture (i.e. surface topology, internal microchannels and defined interfaces) will be a valuable tool for clinical and pharmacological applications as well as an easy-to-use model of basic biological processes. The technique described in this work has been already proposed for corneal tissue engineering to fabricate limbal stem cell niches in the PC collagen constructs as well as for peripheral nerve regeneration and microvascularisation of the dense collagen implants.

One of the ways to introduce the internal micro-structures into the compressed collagen matrix is to incorporate soluble glass fibres, of known dissolution time, diameter and direction, into the collagen gel prior to compression. The geometry of these fibres can be reduced along their length by dissolving more of the glass from one end and less at the other. This is achieved by immersing in PBS and gradually reducing the length of the immersed fibre, giving a greater dissolution time at one end than the other (see Appendix 1). Gradual reduction in diameter of the resulting fibres along their length has been confirmed together with the change in shape of the channels in the PC construct compressed with these fibres from cylindrical to conical. Incorporation of such fibres into the PC construct is designed to result in controlled directional ingrowth (both in time and space) of the tissue into the construct, as the thicker end of the fibre will block the ingrowth at one end, whereas on the opposite, thinner end will disappear faster, opening up a channel for ingrowth. This will in time create a permissive channel for cell ingrowth from the thin to thick end. This would be of a particular use for nerve tissue engineering, both peripheral and central, where

timing and direction of axons ingrowth is crucial for successful repair of the damaged tissue.

Formation of the pattern on the surface of the compressed collagen constructs was investigated next. In this study, particular attention has been given to the mechanisms of pattern formation. The plastic compression process creates an internal anisotropy in the construct with the higher density layer of protein on the primary fluid leaving surface compared to the opposite, non-fluid leaving surface. By placing the shaped template between the gel and absorbent, the pattern was formed on the FLS, either simultaneously with compression or following partial fluid removal. In both cases, resulting features (in this case grooves) closely resembled the template (glass fibres of the known diameter). In contrast, when the template was placed on the non-fluid leaving surface, either before compression or at the final stages of the process, the resulting grooves had low fidelity to the template, being much shallower and wider than expected. The discrepancy in the pattern was explained by the different densities of collagen in the two surfaces which may have different pattern-retaining properties. Pattern formation on the FLS was stable over 2 weeks in culture in both cellular and acellular constructs. The process of the pattern formation on the FLS, which is formed by moulding of the collagen fibrils around the impermeable template has been named here micro-moulding.

To further advance the original methodology, a model of scaling-up the PC constructs fabrication has been developed and evaluated. The new technique was based on the same general principle of uniaxial fluid removal from the collagen gels under load. However, gels were set in the multi-well format, using standard tissue-culture grade 12 well-plates. This provided inherent advantages of convenience, speed, economy but particularly reproducibility. The resulting constructs remained in

the wells, reducing handling, which is of a particular benefit when cellular constructs are made, greatly reducing contamination and damage. Moreover, our results show that PC of cell-containing collagen gels in the new system does not affect cell viability or their ability to remodel the matrix. The technique developed here can be used for compression in other formats (6, 24, 96 well plates) in common use. Most importantly, the new system greatly reduces variability between the constructs (as a function of their weight, thickness and total fluid loss) whilst effectively multiplying the speed of production dramatically. This in turn adds to the reproducibility of the results of this and subsequent studies, based on plastic compression of collagen.

Here, the absorbent and the load were placed on top of the gels, inverting the position of the FLS, compared to the original method (Brown et al, 2005), so that it is on top of the newly cast gel.

It has been shown previously that the ratio of FLS to the height of the gel can affect the process of plastic compression (Hadjipanayi et al., 2010), where a single FLS was formed at the bottom of the gel. To test if same was true for the new system collagen gels of different volume to surface area ratio (height) have been compared. We have shown that increasing the height of gels significantly changes the dynamics of the compression process and affects morphology of the resulting constructs.

Based on these results we have proposed a new mechanism of multiple FLS formation during collagen gels compression in the new format. According to this theory the gel which is set in a non-permeable well and placed under load can be considered as a column of fluid under pressure. In the first instance, fluid will leave predominantly through the primary FLS (upper surface), which is in contact with the absorber. However, this FLS becomes blocked by high density of collagen fibrils in the course of compression (Hadjipanayi et al., 2010). The rest of the fluid in the gel

remains under pressure. This makes it increasingly likely that alternative exit points (i.e. bottom of the gel and/or its sides) will become secondary/tertiary FLSs

The dynamics of fluid flow from the gels and growing resistance of the fluid leaving surface also allowed for calculation of the critical collagen concentration per surface area. This allowed us to estimate the collagen density which triggers slowing down of the fluid outflow, and so the PC end-point. This approach has added significantly to understanding of the PC process and allows mechanistic prediction and design of the effects of the gels dimensions on the properties of the resulting constructs.

The described method was used to design and build a semi-automated machine by an industrial partner (TAP Biosciences, Royston, UK; see Appendix 2). The machine allows automated setting and compressing of collagen gels in a selection of standard multi-well formats (currently 96 and 12-well plates).

The described methodology has been used for fabrication of the multilayered constructs, which is not possible using the original methodology. In the new system, upward direction of the principle fluid flow means that after the process is completed, a new gel can be cast and compressed on top of the previous, with its new FLS open to the absorbent so that each layer is compresses freshly and predictably in highly repetitive manner. In this manner process can be repeated indefinitely, making it possible to fabricate thick multilayered collagen constructs. In the original method, where fluid was removed downwards, a new gel is cast and compressed on top, fluid needed to be forced though its own forming FLS *and* through the previous layer's fluid leaving surface. In the multi-well compression format, this obstacle is easily avoided.

Moreover, this way of multi-layering leads to stable integration between the layers, probably due to the reswelling of the dehydrated FLS in the previous layer during and with fibril aggregation as the upper, fresh collagen gel is set. This leads to the formation of a tight bond between layers, with collagen fibrils knitting the two together. Examination of the compression profiles of the gels, which are set and compressed on top of the previously compressed ones, led to the conclusion that multilayering affects the progression of the process. In particular, it appears that secondary fluid leaving surface was formed earlier in the upper gels than in the base ones. This could be attributed to the reswelling of the primary FLS of the base layer which triggers earlier fluid outflow from the upper layer and also suggest certain degree of interlayer fluid exchange. This, however, had no obvious effect on the overall construct morphology and up to ten layered constructs can be fabricated with the proportionally increased thickness.

Multilayered cellular constructs can be fabricated in this system and cultured up to 3 weeks without layer separation and obvious detrimental effect on cell activity. The developed method of multilayered collagen-based constructs is therefore a valuable tool for fabrication of thick tissues in a standardised and controlled manner.

Finally, it has been shown that micro-moulding of the stable topographical feature is possible in the new multi-well format. It has been anticipated that the mechanisms of topography formation will differ from those using the original method due to the formation of primary and secondary FLS and probably shape of the template (rectangular as opposed to circular cross-section).

The width of the grooves showed good fidelity to the templates in all cases; however depth of the grooves was less than expected regardless of the widths of the template of the total protein content of the gels (height). These data allowed proposing

following mechanism of the pattern formation. At least three subsequent fluid flow directions were formed during patterning. Firstly, through the primary FLS, which becomes blocked faster than without a template, as indicated by the compression profiles of the templated gels. Therefore, a secondary FLS was formed earlier in the process and becomes blocked in turn, as greater amount of fluid needed to be forced through it.

By that time in the process the width of the template bars was already permanently moulded into the constructs. The rest of the fluid, still trapped in the gel remains under pressure. The easiest way for it to leave appeared to be from under the template, forming tertiary FLS. That would rise up the base of the grooves. As a result, walls of the grooves would collapse, resulting in less than expected depth.

Patterned collagen constructs were used as a base layer when fabricating ‘roofed’ channels. Channels between the layers were formed by compressing collagen gels on top of the patterned base layers, creating a ‘roof’ over the grooves.

Additionally, cell delivery into the grooves during micro-moulding was tested. The cells survived this process and were confined to the bottom of the grooves immediately after process completion. However later in the culture period some cells escaped confinement of the grooves probably due to the motile nature of the cell-type used (HaCat cell line) and shallowness of the grooves. This was not seen when cells-seeded grooves were covered by the roof. Indeed cells were confined to the channel even after 1 week in culture, showing signs of proliferation and possible lining of the channels. These findings make this technology worth further investigation and development, in particular for creating cell-lined channels for micro-vascular tissue engineering.

In conclusion, the starting hypothesis partially survived in the course of this study. By controllably deflecting fluid flow from the collagen gels during the process of plastic compression stable and predictable internal and external topological features can be introduced into the PC collagen constructs in a controllable manner. However, formation of the additional FLS was not taken into account when starting hypothesis was developed. That new factor offers new questions and avenues for further development, in particular with regard to the formation of the pattern on this additional surface. By understanding the mechanisms and limitations of these processes it is possible to fabricate living tissue equivalents with the complex micro-architecture, closely mimicking that of the native tissues. Current study outlined basic characteristics and mechanisms of the formation of these topological features and following directions for the future work can be suggested to further progress the knowledge, gained up to date.

Recommendations for further work.

1) **Does conical shape of the soluble fibres translates into directional opening of the channel?**
    1. Determine the rate of dissolution of the conical fibres included in the compressed collagen at set time-points to monitor opening of the channels.
    2. Test the dynamics of tissue ingrowth into the channels at both thick and thin end *in vitro* using dorsal root ganglia as a model tissue.
2) **How does cross-section of the template affects the dimensions of the topology in the PC constructs with single FLS?**
    1. Test the effect of the cross-section of the template on the resulting features with the rectangular template.
3) **How formation of the additional FLS affects mechanical properties of the PC constructs?**

1. Test mechanical properties of the resulting constructs and compare to those, made using the original method. It is possible, that formation of the secondary FLS will have an effect on this parameter.
2. Test the possibility of pattern formation on the secondary FLS.

4) What are the precise mechanisms of interlayer bond formation and their effect on the construct mechanical properties and behaviour of the embedded cells?

1. Investigate interlayer fluid movement.
2. Test the migration of cells between layers.
3. Test the mechanical strength of the interlayer connection.

5) What are the mechanical properties of the roofed channels and their stability in the presence of the embedded, matrix-remodelling cells and epithelial cells?

1. Test mechanical (burst) strength of the channels.
2. Test stability of the channels made in the cellular constructs.
3. Further development of the cell-delivery technique.

List of references:

Abou Neel E. (2006) Collagen-Phosphate Glass Fibres for Biomedical and Tissue Engineering Applications. PhD thesis, University College London, UK.

Abou Neel EA, Ahmed I, Blaker JJ, Bismarck A, Boccaccini AR, Lewis MP (2005) Effect of iron on the surface, degradation and ion release properties of phosphate-based glass fibres. Acta Biomaterialia. 1(5):553-63.

Ahmed I, Lewis M, Olsen I, Knowles JC. (2004) Phosphate glasses for tissue engineering: Part 2. Processing and characterisation of a ternary-based P2O5-CaO-Na2O glass fibre system. Biomaterials. 25(3):501-7.

Ahn G, Park JH, Kang T, Lee JW, Kang HW, Cho DW. (2010) Effect of pore architecture on oxygen diffusion in 3D scaffolds for tissue engineering. J Biomech Eng. 132(10):104506.

Akiyama H, Ito A, Kawabe Y, Kamihira M (2009) Fabrication of complex three-dimensional tissue architectures using a magnetic force-based cell patterning technique. Biomed Microdevices. 11(4):713-21.

Allmeling C, Jokuszies A, Reimers K, Kall S, Choi CY, Brandes G (2008) Spider silk fibres in artificial nerve constructs promote peripheral nerve regeneration. Cell Proliferation. 41(3):408-20.

Ananta M, Aulin CE, Hilborn J, Aibibu D, Houis S, Brown RA, Mudera V. (2009) A poly(lactic acid-co-caprolactone)-collagen hybrid for tissue engineering applications. Tissue Eng Part A. 15(7):1667-75.

Annabi N, Nichol JW, Zhong X, Ji C, Koshy S, Khademhosseini A, Dehghani F. (2010) Controlling the porosity and microarchitecture of hydrogels for tissue engineering. Tissue Eng Part B Rev. 16(4):371-83.

Aviss KJ, Gough JE, Downes S. (2010) Aligned electrospun polymer fibres for sceletal muscle regeneration. European Cells & Materials., 19:193-204.

Bell E, Ivarsson B, Merrill C. (1979) Production of a tissue-like structure by contraction of collagen lattices by human fibroblasts of different proliferative potential in vitro. Proc Natl Acad Sci U S A. 76(3):1274-8.

Ber S., Koese G.T., Hasirci V. (2005) Bone tissue engineering on patterned collagen films: an in vitro study. Biomaterials 26: 1977-1986

Bhatia S N, Yarmush M L and Toner M (1997) Controlling cell interactions by micropatterning in co-cultures: hepatocytes and 3T3 fibroblasts J. Biomed. Mater. Res. 34 189–99

Bitar M, Brown RA, Salih V, Kidane AG, Knowles JC, Nazhat SN. (2008) Effect of cell density on osteoblastic differentiation and matrix degradation of biomimetic dense collagen scaffolds. Biomacromolecules. 9(1):129-35.

Bitar M, Knowles JC, Lewis MP, Salih V. (2005) Soluble phosphate glass fibres for repair of bone-ligament interface. J Mater Sci Mater Med., 16(12):1131-6.

Bitar M, Salih V, Brown RA, Nazhat SN. (2007) Effect of multiple unconfined compression on cellular dense collagen scaffolds for bone tissue engineering. J Mater Sci Mater Med. 18(2):237-44.

Bitar M, Salih V, Mudera V, Knowles JC, Lewis MP. (2004) Soluble phosphate glasses: in vitro studies using human cells of hard and soft tissue origin. Biomaterials, 25(12):2283-92.

Bozkurt A, Brook GA, Moellers S, Lassner F, Sellhaus B, Weis J, (2007) In vitro assessment of axonal growth using dorsal root ganglia explants in a novel three-dimensional collagen matrix. Tissue Engineering., 13(12):2971-9.

Brouwer KM, van Rensch P, Harbers VE, et al., (2011) Evaluation of methods for the construction of collagenous scaffolds with a radial pore structure for tissue engineering J Tissue Eng Regen Med. 5(6):501-4

Brown R.A. (2000) Bioartificial implants: design and tissue engineering. In: Structural Biological Materials (Elices M, ed), Vol 4. Elsevier, Oxford, UK. pp 107-157

Brown RA, Wiseman M, Chuo CB, Cheema U, Nazhat SN. (2005) Ultrarapid engineering of biomimetic materials and tissues: Fabrication of nano- and microstructures by plastic compression. Advanced Functional Materials., 15(11):1762-70.

Bruder J.M., Monu N.C., Harrison M.W., Hoffman-Kim D. Fabrication of polymeric replicas of cell surfaces with nanoscale resolution. (2006) Langmuir 22: 8266-8270

Brunette DM. (1986) Spreading and orientation of epithelial cells on grooved substrata. Exp Cell Res. 167(1):203-17.

Bunting S, Di Silvio L, Deb S, Hall S. (2005) Bioresorbable glass fibres facilitate peripheral nerve regeneration. Journal of Hand Surgery-British and European Volume, 30B(3):242-7.

Buxton PG, Bitar M, Gellynck K, Parkar M, Brown RA, Young AM, Knowles JC, Nazhat SN. (2008) Dense collagen matrix accelerates osteogenic differentiation and rescues the apoptotic response to MMP inhibition. Bone. 43(2):377-85

Cai J, Peng XJ, Nelson KD, Eberhart R, Smith GM. (2005) Permeable guidance channels containing microfilament scaffolds enhance axon growth and maturation. Journal of Biomedical Materials Research Part A., 75A(2):374-86.

Campbell PG, Weiss LE. (2007) Tissue engineering with the aid of inkjet printers. Expert Opin Biol Ther.7(8):1123-7.

Cao Y., Poon Y.F., Feng J., Rayatpisheh S., Chan V., Chan-Park M.B. (2010) Regulating orientation and phenotype of primary vascular smooth muscle cells by biodegradable films patterned with arrays of microchannels and discontinuous microwalls. Biomaterials. 31(24):6228-38.

Chan B.P., Leong K.W. (2008) Scaffolding in tissue engineering: general approaches and tissue-specific considerations. Eur Spine J. 17 (4): 467-79.

Chan BP, So KF. (2005) Photochemical crosslinking improves the physicochemical properties of collagen scaffolds. J Biomed Mater Res A. 75(3):689-701.

Cheema U, Alekseeva T, Abou-Neel EA, Brown RA. (2010) Switching off angiogenic signalling: creating channelled constructs for adequate oxygen delivery in tissue engineered constructs. Eur Cell Mater. 20:274-80.

Cheema U, Brown R, Alp B, MacRobert A. (2008) Spatially defined oxygen gradients and vascular endothelial growth factor expression in an engineered 3D cell model. Cell Mol Life Sci., 65(1):177-86.

Cheema U, Hadjipanayi E, Tammi N, Alp B, Mudera V, Brown RA. (2009) Identification of key factors in deep O2 cell perfusion for vascular tissue engineering. Int J Artif Organs. 32(6):318-28.

Cheema, U Chuo, CB , Sarathchandra, P Nazhat, SN Brown, RA (2007) Engineering functional collagen scaffolds: Cyclical loading increases material strength and fibril aggregation. Advanced Functional Materials, 17(14): 2426-2431

Chehroudi B, Gould TR, Brunette DM. (1990) Titanium-coated micromachined grooves of different dimensions affect epithelial and connective-tissue cells differently in vivo. J Biomed Mater Res. 24(9):1203-19.

Chehroudi B, Gould TR, Brunette DM. (1989) Effects of a grooved titanium-coated implant surface on epithelial cell behavior in vitro and in vivo. J Biomed Mater Res. 23(9):1067-85.

Chen S, Hirota N, Okuda M, Takeguchi M, Kobayashi H, Hanagata N, Ikoma T. (2011) Microstructures and rheological properties of tilapia fish-scale collagen

hydrogels with aligned fibrils fabricated under magnetic fields. Acta Biomater 7(2):644-52.

Chiu LL, Weisel RD, Li RK, Radisic M. (2011) Defining conditions for covalent immobilization of angiogenic growth factors onto scaffolds for tissue engineering. J Tissue Eng Regen Med. 5(1):69-84.

Chow WN, Simpson DG, Bigbee JW, Colello RJ. (2007) Evaluating neuronal and glial growth on electrospun polarized matrices: bridging the gap in percussive spinal cord injuries. Neuron Glia Biology., 3:119-26.

Chunga H.J., Park T.G. (2007) Surface engineered and drug releasing pre-fabricated scaffolds for tissue engineering. Matrices and Scaffolds for Drug Delivery in Tissue Engineering. 59(4-5):249-262.

Chunga H.J., Park T.G. (2007) Surface engineered and drug releasing pre-fabricated scaffolds for tissue engineering. Matrices and Scaffolds for Drug Delivery in Tissue Engineering. 59(4-5):249-262.

Clark P., Connoly P., Curtis A.S.G., Dow J.A.T., Wilkinson C.D.W. (1987) Topographical control of cell behaviour I. Simple step cues. Development 99: 439-448

Clark P., Connoly P., Curtis A.S.G., Dow J.A.T., Wilkinson C.D.W. (1990) Topographical control of cell behaviour: II. multiple grooved substrata. Development 108: 635-644

Comper WD, Veis A. (1977) The mechanism of nucleation for in vitro collagen fibril formation. Biopolymers. 16(10):2113-2131.

Cornwell KG, Downing BR, Pins GD. (2004) Characterizing fibroblast migration on discrete collagen threads for applications in tissue regeneration. J Biomed Mater Res A. , 71(1):55-62.

Curtis A, Riehle M. (2001) Tissue engineering: the biophysical background. Phys Med Biol. 46(4):R47-65.

Dalby MJ, Riehle MO, Yarwood SJ, Wilkinson CD, Curtis AS (2003) Nucleus alignment and cell signaling in fibroblasts: response to a micro-grooved topography. Exp Cell Res. 284(2):274-82.

Dalby MJ. (2005) Topographically induced direct cell mechanotransduction. Med Eng Phys. 27(9):730-42.

Devauchelle N, Badet L, Lengele B, et al. (2006) First human face allograft: early report. Lancet.;368:203–209

Dittrich R, Tomandl G, Despang F, Bernhardt A, Hanke T, Pompe W, et al. (2007) Scaffolds for hard tissue engineering by ionotropic gelation of alginate-influence of selected preparation parameters. Journal of the American Ceramic Society., 90(6):1703-8.

Downing B.R., Cornwell K., Toner M., Pins G.D. (2005) The influence of microtextured basal lamina analog topography on keratinocyte function and epidermal organization. J Biomed Mater Res A. 72(1):47-56.

Du Y, Ghodousi M, Lo E, Vidula MK, Emiroglu O, Khademhosseini A. (2010) Surface-directed assembly of cell-laden microgels. Biotechnol Bioeng. 105(3):655-62.

Du Y, Lo E, Vidula MK, Khabiry M, Khademhosseini A. 2008Method of Bottom-Up Directed Assembly of Cell-Laden Microgels. Cell Mol Bioeng.; 1(2):157-162.

Dunn GA, Heath JP (1976). A new hypothesis of contact guidance in tissue cells. Exp Cell Res. 101(1):1-14.

East E, de Oliveira DB, Golding JP, Phillips JB. (2010) Alignment of astrocytes increases neuronal growth in three-dimensional collagen gels and is maintained following plastic compression to form a spinal cord repair conduit. Tissue Eng Part A. 16(10):3173-84

Ejim OS, Blunn GW, Brown RA. (1993) Production of artificial-orientated mats and strands from plasma fibronectin: a morphological study. Biomaterials. 14(10):743-8.

Falconnet D, Csucs G, Grandin HM, Textor M. (2006) Surface engineering approaches to micropattern surfaces for cell-based assays. Biomaterials. 27(16):3044-63

Feng J., Chan-Park M.B., Shen J., Chan V. (2007) Quick layer-by-layer assembly of vascular smooth muscle cells in deep microchannels. Tissue Eng 13:1003-1012

Fidkowski C., Kaazempur-Mofrad MR., Borenstein J, Vacanti JP., Langer R, Wang Y.(2005) Endothelialized microvasculature based on biodegradable elastomer. Tissue Eng 11 (1-2): 302-309

Finkenzeller G, Graner S, Kirkpatrick CJ, Fuchs S, Stark GB. (2009) Impaired in vivo vasculogenic potential of endothelial progenitor cells in comparison to human umbilical vein endothelial cells in a spheroid-based implantation model. Cell Prolif. 42(4):498-505

Flemming RG, Murphy CJ, Abrams GA, Goodman SL, Nealey PF. (1999) Effects of synthetic micro- and nano-structured surfaces on cell behavior. Biomaterials. 20(6):573-88.

Folch A, Jo B H, Hurtado O, Beebe D J and Toner M (2000) Microfabricated elastomeric stencils for micropatterning cell cultures J. Biomed. Mater. Res. 52 346–53

Folch A, Toner M. (2000) Microengineering of cellular interactions. Annu Rev Biomed Eng 2:227-56

Francis R.J. (1990) Amyloid. Chapter 10 in Theory and Practice of Histological Techniques (Bancroft J.D. and Stevens A., ed.) Churhill Livingstone, UK, pp:155-175.

Francis R.J. (1990) Amyloid. Chapter 10 in Theory and Practice of Histological Techniques (Bancroft J.D. and Stevens A., ed.) Churhill Livingstone, UK, pp:155-175.

Freed LE, Guilak F, Guo XE, Gray ML, Tranquillo R, Holmes JW, Radisic M, Sefton MV, Kaplan D, Vunjak-Novakovic G. (2006) Advanced tools for tissue engineering: scaffolds, bioreactors, and signaling. Tissue Eng. 12(12):3285-305.

Gafni Y, Zilberman Y, Ophir Z, Abramovitch R, Jaffe M, Gazit Z, Domb A, Gazit D. (2006) Design of a filamentous polymeric scaffold for in vivo guided angiogenesis. Tissue Eng. 12(11):3021-34.

Ghanaati S, Fuchs S, Webber MJ, Orth C, Barbeck M, Gomes ME, Reis RL, James Kirkpatrick C. (2010) Rapid vascularization of starch-poly(caprolactone) in vivo by outgrowth endothelial cells in co-culture with primary osteoblasts. J Tissue Eng Regen Med. DOI: 10.1002/term.373

Golden AP, Tien J. (2007) Fabrication of microfluidic hydrogels using molded gelatin as a sacrificial element. Lab Chip. 7(6):720-5.

Grinnell F, Lamke CR. (1984) Reorganization of hydrated collagen lattices by human skin fibroblasts. J Cell Sci. 66:51-63.

Groeber F, Holeiter M, Hampel M, Hinderer S, Schenke-Layland K. (2011) Skin tissue engineering--in vivo and in vitro applications. Adv Drug Deliv Rev. 63(4-5):352-66.

Gross J, Kirk D. (1958) The heat precipitation of collagen from neutral salt solutions: some rate-regulating factors. J Biol Chem. 233(2):355-60.

Guillemette M.D., Cui B., Roy E., Gauvin R. et al. (2009) Surface topography induces 3D self-orientation of cells and extracellular matrix resulting in improved tissue function. Integr Biol 1: 196-204.

Guillemette MD, Park H, Hsiao JC, Jain SR, Larson BL, Langer R, et al. Combined technologies for microfabricating elastomeric cardiac tissue engineering scaffolds. Macromol Biosci. 2010, 10(11):1330-7.

Habraken WJ, Wolke JG, Jansen JA. (2007) Ceramic composites as matrices and scaffolds for drug delivery in tissue engineering. Adv Drug Deliv Rev. 59(4-5):234-48.

Hadjipanayi E, Ananta M, Binkowski M, Streeter I, Lu Z, Cui ZF, Brown RA, Mudera V. (2010) Mechanisms of structure generation during plastic compression of nanofibrillar collagen hydrogel scaffolds: towards engineering of collagen. J Tissue Eng Regen Med DOI: 10.1002/term.343

Hadjipanayi E, Brown RA, Mudera V. (2009) Interface integration of layered collagen scaffolds with defined matrix stiffness: implications for sheet-based tissue engineering. J Tissue Eng Regen Med. (3):230-41.

Hadjipanayi E, Mudera V, Brown RA. (2009) Close dependence of fibroblast proliferation on collagen scaffold matrix stiffness. Tissue Eng Regen Med. 3(2):77-84.

Hadjipanayi E, Mudera V, Brown RA. (2009) Guiding cell migration in 3D: a collagen matrix with graded directional stiffness. Cell Motil Cytoskeleton. 66(3):121-8.

Hadjipanayi E., (2010) Engineering physical structure in biomimetic collagen scaffolds: strategies for regulating cell behaviour, PhD Thesis, University College London, UK

Hadjizadeh A, Doillon C. Directional migration of endothelial cells towards angiogenesis using polymer fibres in a 3D co-culture system. J Tissue Eng Regen Med. 2010, 4(7):524-31.

Hamilton DW, Oakley C, Jaeger NA, Brunette DM. 2009. Directional change produced by perpendicularly-oriented microgrooves is microtubule-dependent for fibroblasts and epithelium. Cell Motil. Cytoskelet. 66(5):260–71

Hannachi IE, Yamato M, Okano T. (2009) Cell sheet technology and cell patterning for biofabrication. Biofabrication. 1(2):022002

He Q, Zhao Y, Chen B, Xiao Z, Zhang J, Chen L, Chen W, Deng F, Dai J. (2011) Improved cellularization and angiogenesis using collagen scaffolds chemically conjugated with vascular endothelial growth factor. Acta Biomater. 7(3):1084-93.

Helary C, Abed A, Mosser G, Louedec L, Meddahi-Pellé A, Giraud-Guille MM. (2011) Synthesis and in vivo integration of improved concentrated collagen hydrogels. J Tissue Eng Regen Med. 5(3):248-52

Helary C, Bataille I, Abed A, Illoul C, Anglo A, Louedec L, Letourneur D, Meddahi-Pellé A, Giraud-Guille MM. (2010) Concentrated collagen hydrogels as dermal substitutes. Biomaterials. 31(3):481-90.

Hoffman-Kim D., Mitchel J.A., Bellamkonda R.V. (2010) Topography, cell response, and nerve regeneration. Annu Rev Biomed Eng. 12:203-31

Hollister S.J. (2005) Porous scaffold design for tissue engineering Nat Mater. 4: 518-524

Holmes A, Brown R., Shakesheff K. (2009) Engineering tissue alternatives to animals: applying tissue engineering to basic research and safety testing. Regen Med. 4(4):579-92.

Hu K, Shi H, Zhu J, Deng D, Zhou G, Zhang W, Cao Y, Liu W. (2010) Compressed collagen gel as the scaffold for skin engineering. Biomed Microdevices. 12(4):627-35.

Huang S, Fu X. (2010) Naturally derived materials-based cell and drug delivery systems in skin regeneration. J Control Release. 142(2):149-59.

Huang WL, Begum R, Yang Q, Gheysens T, Skaer N, King V, et al. Regenerative potential of silk conduits following peripheral nerve injury. Tissue Engineering. 2007, 13(7):349.

Hulmes (2008) Collagen diversity, synthesis and assembly. Chapter 2 in Collagen :Structure and Mechanics, Fratzl P. (ed.) pp: 15-47

Hulmes D.J.S. (2002) Building collagen molecules, fibrils, and suprafibrillar structures. J Struct Biol. 137(1-2):2-10.

Hutmacher D.W. (2001) Scaffold design and fabrication technologies for engineering tissues – state of the art and future perspectives. J Biomater Sci Polym Ed. 12: 107-124

Hynes RO. (2009) The extracellular matrix: not just pretty fibrils. Science. 326(5957):1216-9.

Ingber D.E. (2005) Mechanical control of tissue growth: function follows form. PNAS 102(33): 11571-11572

Isenberg B C, Tsuda Y, Williams C, Shimizu T, Yamato M, Okano T and Wong J Y (2008) A thermoresponsive, microtextured substrate for cell sheet engineering with defined structural organization Biomaterials 29 2565–72

Ito A, Shinkai M, Honda H, Kobayashi T. (2005) Medical application of functionalized magnetic nanoparticles. J Biosci Bioeng. 100(1):1-11.

Janakiraman V., Kienitz B.L., Baskaran H. (2007) Lithography technique for topographical micropatterning of collagen-glycosaminglycan membranes for tissue engineering applications. J Med Device 1(3): 233-237

Janakiraman V., Kienitz B.L., Baskaran H. (2007) Lithography technique for topographical micropatterning of collagen-glycosaminglycan membranes for tissue engineering applications. J Med Device 1(3): 233-237

Kapoor A., Caporali E.H.G., Kenis P.J.A., Stewart M.C. (2010) Micropographically patterned surfaces promote the alignment of tenocytes and extracellular collagen. Acta Biomaterialia 6: 2580-2589

Karamichos D, Brown RA, Mudera V (2006) Complex dependence of substrate stiffness and serum concentration on cell-force generation. J Biomed Mater Res A. 78(2):407-15

Kehe K, Abend M, Kehe K, Ridi R, Peter RU, van Beuningen D. (1999) Tissue engineering with HaCaT cells and a fibroblast cell line. Arch Dermatol Res. 291(11):600-5.

Kehe K, Abend M, Kehe K, Ridi R, Peter RU, van Beuningen D. (1999) Tissue engineering with HaCaT cells and a fibroblast cell line. Arch Dermatol Res. 291(11):600-5.

Kelm JM, Fussenegger M. (2010) Scaffold-free cell delivery for use in regenerative medicine. Adv Drug Deliv Rev. 62(7-8):753-64.

Keung A.J., Kumar S., Schaffer D.V. (2010) Presentation counts: microenvironmental regulation of stem cells by biophysical and material cues. Annu Rev Cell Dev Biol. 26:533-56

Kobel S., Limacher M., Gobaa S., Laroche T., Lutolf M.P. (2009) Micropatterning of hydrogels by soft embossing. Langmuir 25 (15): 8774-8779.

Krych AJ, Rooney GE, Chen B, Schermerhorn TC, Ameenuddin S, Gross L, et al. Relationship between scaffold channel diameter and number of regenerating axons in the transected rat spinal cord. Acta Biomaterialia. 2009, 5(7):2551-9.

Kureshi A, Cheema U, Alekseeva T, Cambrey A, Brown R. (2010) Alignment hierarchies: engineering architecture from the nanometre to the micrometre scale. J R Soc Interface 7 Suppl 6:S707-16.

Langer R, Vacanti JP. (1993) Tissue engineering. Science. 260(5110):920-6.

Le Gros Clark W.E. (1975) The tissues of the body, sixth edition. Oxford University Press, Oxford, Great Britain.

Lee H.J., Nam S.H., Son K.J., Koh W-G. (2010) Micropatterned fibrous scaffolds fabricated using elecrospinning and hydrogel lithography: new platform to create cellular micropatterns. Sensors and Actuators B. 148:504-510

Leong K.F., Chua C.K., Sudarmadji N., Yeong W.Y. (2008) Engineering functionally graded tissue engineering scaffolds Journal of the Mechanical Behavior of Biomedical Materials 1(2): 140-152

Levis HJ, Brown RA, Daniels JT. (2010) Plastic compressed collagen as a biomimetic substrate for human limbal epithelial cell culture. Biomaterials. 31(30):7726-37.

Li J., Rickett TA, Shi R. (2009) Biomimetic nerve scaffolds with aligned intraluminal microchannels: a "sweet" approach to tissue engineering. Langmuir. 25(3):1813-7.

Liu X, Lim JY, Donahue HJ, Dhurjati R, Mastro AM, Vogler EA. (2007) Influence of substratum surface chemistry/energy and topography on the human fetal osteoblastic cell line hFOB 1.19: Phenotypic and genotypic responses observed in vitro. Biomaterials. 28(31):4535-50.

Macchiarini P, Jungebluth P, Go T, Asnaghi MA, et al., (2008) Clinical transplantation of a tissue-engineered airway. Lancet. 372(9655):2023-30.

Madaghiele M, Sannino A, Yannas IV, Spector M. (2008) Collagen-based matrices with axially oriented pores. J Biomed Mater Res A. 85(3):757-67.

Madden LR, Mortisen DJ, Sussman EM, Dupras SK, Fugate JA, Cuy JL, et al. Proangiogenic scaffolds as functional templates for cardiac tissue engineering. Proceedings of the National Academy of Sciences of the United States of America. 2010, 107(34):15211-6.

Malafaya PB, Silva GA, Reis RL. (2007) Natural-origin polymers as carriers and scaffolds for biomolecules and cell delivery in tissue engineering applications. Adv Drug Deliv Rev. 59(4-5):207-33.

Martínez E, Engel E, Planell JA, Samitier J. (2009) Effects of artificial micro- and nano-structured surfaces on cell behaviour. Ann Anat. 191(1):126-35.

Mata A., Kim E.J., Boehm C.A., Fleischman A.J., Muschler G.F., Roy S. (2009) A three-dimensional scaffold with precise micro-architecture and surface microtextures. Biomaterials. 30:4610-4617

Mazzoccoli JP, Feke DL, Baskaran H, Pintauro PN (2010) Development of multilayered cell-hydrogel composites using an acoustic focusing technique. Biotechnol Prog. 26(2):600-5.

Micol LA, Ananta M, Engelhardt EM, Mudera VC, Brown RA, Hubbell JA, Frey P. (2011) High-density collagen gel tubes as a matrix for primary human bladder smooth muscle cells. Biomaterials. 32(6):1543-8.

Mironov V, Kasyanov V, Markwald RR, Prestwich GD. (2008) Bioreactor-free tissue engineering: directed tissue assembly by centrifugal casting. Expert Opin Biol Ther. 8(2):143-52.

Moon S, Hasan SK, Song YS, Xu F, Keles HO, Manzur F, Mikkilineni S, Hong JW, Nagatomi J, Haeggstrom E, Khademhosseini A, Demirci U. (2010) Layer by layer three- dimensional tissue epitaxy by cell-laden hydrogel droplets. Tissue Eng Part C Methods.16(1):157-66.

Mudera VC, Pleass R, Eastwood M, Tarnuzzer R, Schultz G, Khaw P, McGrouther DA, Brown RA. (2000) Molecular responses of human dermal fibroblasts to dual cues: contact guidance and mechanical load. Cell Motil Cytoskeleton. 45(1):1-9.

Nakagami H, Maeda K, Morishita R, Iguchi S, Nishikawa T, Takami Y. (2005) Novel autologous cell therapy in ischemic limb disease through growth factor secretion by cultured adipose tissue-derived stromal cells. Arterioscler Thromb Vasc Biol. 25(12):2542-7.

Nazhat S.N., Neel EA, Kidane A, Ahmed I, et al. (2007) Controlled microchannelling in dense collagen scaffolds by soluble phosphate glass fibers. Biomacromolecules. 8(2):543-51.

Nelson C.M., Inman J.L., Bissell M.J. (2008) Three-dimensional lithographically defined organotypic tissue arrays for quantitative analysis of morphogenesis and neoplastic progression. Nat Protoc 3(4): 674-678

Nelson C.M., Tien J. (2006) Microstructured extracellular matrices in tissue engineering and development. Current Opinion in Biotechnology 17: 518-523

Norman J.J., Desai T.A. (2005) Control of cellular organization in three dimensions using a microfabricated polydimethylsiloxane-collagen composite tissue scaffold. Tissue Eng. 11(3-4):378-86.

Ohashi K, Yokoyama T, Yamato M, Kuge H, Kanehiro H, Tsutsumi M, Amanuma T, Iwata H, Yang J, Okano T, Nakajima Y. (2007) Engineering functional two- and three-dimensional liver systems in vivo using hepatic tissue sheets. Nat Med. 13(7):880-5.

orientation and phenotype of primary vascular smooth muscle cells by biodegradable films patterned with arrays of microchannels and discontinuous microwalls. Biomaterials 31: 6228-6238

Pampaloni F, Reynaud EG, Stelzer EH. (2007) The third dimension bridges the gap between cell culture and live tissue. Nat Rev Mol Cell Biol. 8(10):839-45.

Papenburg BJ, Liu J, Higuera GA, Barradas AM, de Boer J, van Blitterswijk CA, Wessling M, Stamatialis D. (2009) Development and analysis of multi-layer scaffolds for tissue engineering. Biomaterials. 30(31):6228-39

Papenburg BJ, Vogelaar L, Bolhuis-Versteeg LA, Lammertink RG, Stamatialis D, Wessling M. (2007) One-step fabrication of porous micropatterned scaffolds to control cell behavior. Biomaterials. 28(11):1998-2009.

Park J., Bertiaume F., Toner M., Yarmush M.l., Tilles A.W. (2005) Microfabricated grooved substrates as platforms for bioartificial liver reactors. Biotechnology and Bioengineering. 90(5): 632-644

Pedraza CE, Marelli B, Chicatun F, McKee MD, Nazhat SN. (2010) An in vitro assessment of a cell-containing collagenous extracellular matrix-like scaffold for bone tissue engineering. Tissue Eng Part A. 16(3):781-93.

Perry H, Greiner C, Georgakoudi I, Cronin-Golomb M, Omenetto FG (2007) Simple fabrication technique for rapid prototyping of seamless cylindrical microchannels in polymer substrates Rev Sci Instrum. 78(4):044302.

Pietak A., McGregor A., Gauthier S., Oleschuk R., Waldman S.D. (2008) Are micropatterned substrates for directed cell organisation an effective method to create ordered 3D tissue constructs? J Tissue Eng Regen Med. 2: 450-453

Pins G.D., Toner M., Morgan J.R. (2000) Microfabrication of an analog of the basal lamina: biocompatible membranes with complex topographies. The FASEB J 14: 593-603.

Place ES, George JH, Williams CK, Stevens MM. (2009) Synthetic polymer scaffolds for tissue engineering. Chem Soc Rev. 38(4):1139-51.

Prichard H. L., Reichert W. M., Klitzman B. 2007 Adult adipose-derived stem cell attachment to biomaterials Biomaterials, 28(6): 936-946

Ramshaw JA, Peng YY, Glattauer V, Werkmeister JA. (2009) Collagens as biomaterials. J Mater Sci Mater Med. 20 Suppl 1:S3-8.

Reckhenrich AK, Hopfner U, Krötz F, Zhang Z, Koch C, Kremer M, Machens HG, Plank C, Egaña JT. (2011) Bioactivation of dermal scaffolds with a non-viral copolymer-protected gene vector. Biomaterials. 32(7):1996-2003

Reichl S, Bednarz J, Müller-Goymann CC. (2004) Human corneal equivalent as cell culture model for in vitro drug permeation studies. Br J Ophthalmol. 88(4):560-5.

Riehle M, Ferris D, Hamilton D and Curtis A S G (1998) Cell behaviour in tubes. Exp. Biol. Online (http://link.springer.de/link/service/journals/00898/index.htm)

Roth EA, Xu T, Das M, Gregory C, Hickman JJ, Boland T (2004) Inkjet printing for high-throughput cell patterning. Biomaterials. 25(17):3707-15.

Ryu W, Min SW, Hammerick KE, Vyakarnam M, Greco RS, Prinz FB, Fasching RJ. (2007) The construction of three-dimensional micro-fluidic scaffolds of biodegradable polymers by solvent vapor based bonding of micro-molded layers. Biomaterials. Feb;28(6):1174-84.

Serpooshan V, Muja N, Marelli B, Nazhat SN. (2011) Fibroblast contractility and growth in plastic compressed collagen gel scaffolds with microstructures correlated with hydraulic permeability. J Biomed Mater Res A. 96(4):609-20

Shah R, Sinanan AC, Knowles JC, Hunt NP, Lewis MP. (2005) Craniofacial muscle engineering using a 3-dimensional phosphate glass fibre construct. Biomaterials, 26(13):1497-505.

Shen JY., Chan-Park M.B., He B., Zhu A.P., Zhu X., Beuerman R.W. et al. (2006) Three-dimensional microchannels in biodegradable polymeric films for control orientation and phenotype of vascular smooth muscle cells. Tissue Eng 12: 2229-2240

Shevchenko RV, James SL, James SE. (2010) A review of tissue-engineered skin bioconstructs available for skin reconstruction. J R Soc Interface. 7(43):229-58.

Shin M, Matsuda K, Ishii O, Terai H, Kaazempur-Mofrad M, Borenstein J, Detmar M, Vacanti JP. (2004) Endothelialized networks with a vascular geometry in microfabricated poly(dimethyl siloxane). Biomed Microdevices. 6(4): 269-78.

Silva M, Cyster LA, Barry JJA, Yang XB, Oreffo ROC, Grant DM (2006) The effect of anisotropic architecture on cell and tissue infiltration into tissue engineering scaffolds. Biomaterials. 27(35):5909-17.

Skelton KL, Glenn JV, Clarke SA, Georgiou G, Valappil SP, Knowles JC, Nazhat SN, Jordan GR. (2007). Effect of ternary phosphate-based glass compositions on osteoblast and osteoblast-like proliferation, differentiation and death in vitro. Acta Biomater 3(4): 563-72.

Sørensen A, Alekseeva T, Katechia K, Robertson M, Riehle MO, Barnett SC. (2007) Long-term neurite orientation on astrocyte monolayers aligned by microtopography. Biomaterials. 28(36):5498-508

Srouji S, Kizhner T, Suss-Tobi E, Livne E, Zussman E. (2008) 3-D Nanofibrous electrospun multilayered construct is an alternative ECM mimicking scaffold. J Mater Sci Mater Med. 19(3):1249-55.

Stokols S, Sakamoto J, Breckon C, Holt T, Weiss J, Tuszynski M. (2006) Templated agarose scaffolds support linear axonal regeneration. Tissue Engineering. 12(10):2777-87.

Stokols S, Tuszynski M. (2004) The fabrication and characterization of linearly oriented nerve guidance scaffolds for spinal cord injury. Biomaterials. 25(27):5839-46.

Sundback C, Hadlock T, Cheney M, Vacanti J.(2003) Manufacture of porous polymer nerve conduits by a novel low-pressure injection molding process. Biomaterials. 24(5):819-30.

Teixeira AI, Abrams GA, Bertics PJ, Murphy CJ, Nealey PF. J Cell Sci. (2003) Epithelial contact guidance on well-defined micro- and nanostructured substrates. 116(Pt 10):1881-92.

Teixeira AI, Nealey PF, Murphy CJ. (2004) Responses of human keratocytes to micro- and nanostructured substrates. J Biomed Mater Res A. 71(3):369-76.

Then KY, Yang Y, Ahearne M, El Haj AJ. (2011) Effect of microtopographical cues on human keratocyte orientation and gene expression. Curr Eye Res. 36(2):88-93.

Tsuda Y, Shimizu T, Yamato M, Kikuchi A, Sasagawa T, Sekiya S, Kobayashi J, Chen G, Okano T. (2007) Cellular control of tissue architectures using a three-dimensional tissue fabrication technique. Biomaterials. 28(33):4939-46.

Uriarte-Montoya MH, Arias-Moscoso JL, Plascencia-Jatomea M, Santacruz-Ortega H (2010) Jumbo squid (Dosidicus gigas) mantle collagen: extraction, characterization, and potential application in the preparation of chitosan-collagen biofilms. Bioresour Technol. 101(11):4212-9.

Van Vlierberghe S, Dubruel P, Lippens E, Masschaele B, Van Hoorebeke L, Cornelissen M (2008). Toward modulating the architecture of hydrogel scaffolds: curtains versus channels. Journal of Materials Science-Materials in Medicine. 19(4):1459-66.

Vazin T., Schaffer D.V. (2010) Engineering strategies to emulate the stem cell niche. Trends in Biotech 28(3): 117-124

Verma MK, Majumder A, Ghatak A. (2006) Embedded template-assisted fabrication of complex microchannels in PDMS and design of a microfluidic adhesive. Langmuir. 22(24):10291-5.

Vernon R.B., Gooden M.D., Lara S.L., Wight T.N. (2005) Microgrooved fibrillar collagen membranes as scaffolds for cell support and alignment. Biomater 26: 3131-3140

Vernon RB, Gooden MD, Lara SL, Wight TN (2005) Native fibrillar collagen membranes of micron-scale and submicron thicknesses for cell support and perfusion. Biomaterials. 26(10):1109-17.

Walboomers XF, Croes HJ, Ginsel LA, Jansen JA. (1998) Growth behavior of fibroblasts on microgrooved polystyrene. Biomaterials. 19(20):1861-8.

Wang L, Murthy SK, Barabino GA, Carrier RL. (2010) Synergic effects of crypt-like topography and ECM proteins on intestinal cell behavior in collagen based membranes. Biomaterials. 31(29):7586-98

Wang Y.C., Ho C-C. (2004) Micropatterning of proteins and mammalian cells on biomaterials. The FASEB J. 18(3):525-527

Weiss P. (1945) Experiments on cell and axon orientation in vitro: the role of colloidal exudates in tissue organisation. J exp Zool. 100: 353-386

Wojciak-Stothard B, Curtis AS, Monaghan W, McGrath M, Sommer I, Wilkinson CD. 1995. Role of the cytoskeleton in the reaction of fibroblasts to multiple grooved substrata. Cell Motil. Cytoskelet.31(2):147–58

Wood GC, Keech MK. (1960) The formation of fibrils from collagen solutions. 1. The effect of experimental conditions: kinetic and electron-microscope studies. Biochem J. 75:588-98.

Wright D, Rajalingam B, Selvarasah S, Dokmeci M R and Khademhosseini A (2007) Generation of static and dynamic patterned co-cultures using microfabricated parylene-C stencils Lab Chip 7 1272–9.

Yang F, Both SK, Yang X, Walboomers XF, Jansen JA. (2009)Development of an electrospun nano-apatite/PCL composite membrane for GTR/GBR application. Acta Biomater. 5(9):3295-304.

Yang J, Yamato M, Kohno C, Nishimoto A, Sekine H, Fukai F, Okano T. (2005) Cell sheet engineering: recreating tissues without biodegradable scaffolds. Biomaterials. 26(33):6415-22.

Yang Y, El Haj AJ. (2006) Biodegradable scaffolds--delivery systems for cell therapies. Expert Opin Biol Ther. 6(5):485-98.

Yeh J, Ling Y, Karp JM, Gantz J, Chandawarkar A, Eng G, Blumling J 3rd, Langer R, Khademhosseini A. (2006) Micromolding of shape-controlled, harvestable cell-laden hydrogels. Biomaterials. 27(31):5391-8.

List of conference abstracts

1. Alekseeva T., Allovskaya A., Abou Neel E.A., Knowles J.C., Engineering microchannels into collagen constructs with soluble phosphate glass fibres for neural tissue repair. Oral presentation, Tissue Engineering and Regenerative Medicine International Society meeting, London, UK, 2007

2. Alekseeva T., Tully F., Abou Neel E. A., Knowles J.C., Brown R. A. Development of conical soluble phosphate glass fibres for directional generation of microchannels in dense collagen implants. The Tissue and Cell Engineering Society meeting, Nottingham, UK, 2008

3. Alekseeva T., Jawad H., Purser M., Brown R. A. New improved technique of plastic compression of collagen using upward fluid flow. Oral presentation, 8th International Conference on Cell & Stem Cell Engineering (ICCE), 2010

4. Alekseeva T., Tully F., Knowles J. C., Brown R. A. Embossing stable features onto the plastic compressed collagen, Tissue Engineering and Regenerative Medicine International Society meeting, Galway, Ireland, 2010

5. Alekseeva T., Tully F., Knowles J. C., Brown R. A. Surface anisotropyaffects embossing in plastic compressed collagen, Tissue Engineering and Regenerative Medicine International Society meeting, Galway, Ireland, 2010

6. Alekseeva T., Tan N. S., purser M. H., Brown R. A. Multi-layered collagen scaffolds with engineered microchannels for skin tissue engineering applications. The Tissue and Cell Engineering Society (TCES) meeting, Leeds, UK, 2011

7. Alekseeva T., Tan N. S., Purser M. H., Brown R. A. Engineering a vascular bed for implant perfusion: 'roofed-micro-channels' within dense collagen scaffolds. Oral presentation, Tissue Engineering and Regenerative Medicine International Society meeting, Granada, Spain, 2011

List of publications

1. Alekseeva T, Hadjipanayi E., Neel EA, Brown RA. (2011) Engineering stable topography in dense bio-mimetic 3D collagen scaffolds. Accepted for publication ECells and Materials Journal
2. Alekseeva T, Neel EA, Knowles JC, Brown RA. (2011) Development of conical soluble phosphate glass fibers for directional tissue growth. J Biomater Appl. doi: 10.1177/0885328210394396
3. Alekseeva T., Jawad H., Purser M., Brown R.A. (2011) New improved technique of plastic compression of collagen using upward fluid flow. 8th International Conference on Cell & Stem Cell Engineering (ICCE), IFMBE Proceedings, Vol. 30: 5-9

4. Kureshi A, Cheema U., Alekseeva T., Cambrey A., Brown R. (2010) Alignment hierarchies: engineering architecture from the nanometre to the micrometre scale. J R Soc Interface. 7 (6):S707-16.
5. Cheema U., Alekseeva T., Abou-Neel E.A., Brown R.A. (2010) Switching off angiogenic signalling: creating channelled constructs for adequate oxygen delivery in tissue engineered constructs. Eur Cell Mater. 20:274-80.

MewburnEllis

LLP

For the attention of Ned Grace
The Automation Partnership
York Way
Royston
Hertfordshire
SG8 5WY

BY EMAIL

09 August 2011

Dear Sirs

European Patent Application No. 06788520.8
Applicant : JCL BUSINESS PLC
Your ref: RAFT-003(EP)(JCL Bus:66-052)
Our ref: 666C21.EPG
Title: BIOMATERIAL SCAFFOLDS FOR CONTROLLED TISSUE GROWTH

We now inform you that the mention of grant of this patent will be published in the European Bulletin of 31 August 2011.

We enclose a copy of the decision to grant.

We will write again about the necessary steps to achieve effect of the European Patent in the countries wanted.

Yours faithfully

Lee Mundy
European Grant
For MEWBURN ELLIS LLP
lee.mundy@mewburn.com

C.C. Grant Cameron
C.C. Derek Reay
C.C. Adelaida Prieto Edo

Europäisches Patentamt
European Patent Office
Office européen des brevets

European Patent Office
Postbus 5818
2280 HV RIJSWIJK
NETHERLANDS
Tel. +31 (0)70 340-2040
Fax +31 (0)70 340-3016

Sutcliffe, Nicholas Robert
Mewburn Ellis LLP
33 Gutter Lane
London
EC2V 8AS
ROYAUME UNI

08 AUG 2011
MEWBURN ELLIS LLP

For any questions about this communication:
Tel.:+31 (0)70 340 45 00

Date: 04.08.11

Reference	Application No./Patent No.
NRS/CP6684021	08788520.8 - 1219 / 2197504

Applicant/Proprietor: UCL Business PLC

Decision to grant a European patent pursuant to Article 97(1) EPC

Following examination of European patent application No. 08788520.8 a European patent with the title and the supporting documents indicated in the communication pursuant to Rule 71(3) EPC dated 06.04.11 is hereby granted in respect of the designated Contracting States.

Patent No. : 2197504
Date of filing : 03.09.08
Priority claimed : 04.09.07/GBA 0717168

Designated Contracting States and Proprietor(s) : AT BE BG CH CY CZ DE DK EE ES FI FR GB GR HR HU IE IS IT LI LT LU LV MC MT NL NO PL PT RO SE SI SK TR
UCL Business PLC
The Network Building, 2nd Floor
97 Tottenham Court Road
London W1T 4TP/GB

This decision will take effect on the date on which the European Patent Bulletin mentions the grant (Art. 97(3) EPC).

The mention of the grant will be published in European Patent Bulletin 11/35 of 31.08.11.

Examining Division

Schneider A Espinosa Y Carretero Lamers W

Europäisches Patentamt • European Patent Office • Office européen des brevets

Registered letter
EPO Form 2006A 12.07 (28/07/11)

to EPO postal service: 29.07.11

RAFT™

Real Architecture For 3D Tissue

New system for creating realistic 3D tissue models for drug discovery research.

TAP
Biosystems

Real Architecture For **3D** Tissue

New system for creating realistic 3D tissue models for drug discovery research.

RAFT™

Introduction

There are striking differences in the morphology and biological response of cells in a 3D environment compared to standard 2D culture, including differentiation, proliferation and drug metabolism. Adoption of 3D technologies into routine use has been slow because they are technically demanding, labour intensive and can give variable results.

TAP Biosystems has recognised this need and RAFT – Real Architecture For 3D Tissue – is designed to address these specific problems, and enables researchers to produce truly biomimetic tissue models simply and conveniently.

The RAFT System is based on a novel, patented process using collagen to mimic closely an *in vivo* environment. The RAFT workstation, consumables and reagents together allow multi-cellular 3D tissue models to be made rapidly and consistently in standard plate formats.

RAFT process

Cells and neutralised collagen are mixed and incubated to create a cell seeded hydrogel. Some of the liquid in the hydrogel is then removed gently by absorption which results in a strong transparent tissue model made of cells encapsulated in a biomimetic fibrillar matrix of collagen.

The RAFT System provides scientists with an extremely flexible way to make well defined 3D tissue models. Complex multilayer tissue models can be formed with different cell types or seeding densities in each layer.

Up to 96 tissue models can be made in a standard plate format with minimal hands on time. The tissue remains in the same well from creation until the end of the experiment, and can be analysed using a wide variety of standard imaging, biochemical, histological and 'omics techniques.

RAFT functions

• Rapidly produces 3D tissue models
• Uses collagen – the ideal material for forming 3d tissue models
• Enables up to 96 tissue models to be made simultaneously
• Tissue models can be made in standard well plates or permeable membrane inserts for barrier assays or culture at the air / liquid interface
• Supports complex cell co-culture – the user has full control of cell type(s) and cell densities

RAFT benefits

• Realistic – provides the cells with a more natural environment

• Flexible – supports a wide range of assay models and analytical techniques
• Reproducible – create consistent 3D tissue models
• Rapid – no cross linking agents are used, and cells are present from the start so can be used immediately

Applications include

• Cell based screening
• Target validation
• Lead Optimisation
• Cell biology
• Safety pharmacology

To learn more about the RAFT system contact:

Dr Grant Cameron, RAFT Development Director,
TAP Biosystems
York Way, Royston, Herts, SG8 5WY
United Kingdom
Telephone
+44 1763 227200
Email
info@tapbiosystems.com
Visit
www.tapbiosystems.com

April 2011

Real Architecture For **3D** Tissue

RAFT 96-well workstation